

**The Briançonnais units along the ECORS-CROP
transect (Italian-French Alps):
structures, metamorphism and geochronology**

Inauguraldissertation

zur

Erlangung der Würde eines Doktors der Philosophie

vorgelegt der

Philosophisch-Naturwissenschaftlichen Fakultät

der Universität Basel

von

Stefan Bucher

aus Kerns (OW)

Basel, 2003

Genehmigt von der Philosophisch –Naturwissenschaftlichen Fakultät

auf Antrag von

Prof. Dr. S. M. Schmid

Basel, den 18. Dezember 2003

Prof. Dr. M. Tanner
Dekan

Abstract

This study analyses the tectono-metamorphic evolution of the Briançonnais units in Italian-French Western Alps. Along the ECORS-CROP transect detailed structural fieldwork together with petrological investigations were carried out in order to study the tectono-metamorphic evolution on a larger scale. Furthermore the different deformation phases were dated by the ^{39}Ar - ^{40}Ar incremental heating technique and by the Lu-Hf isotope system.

From the west to the east, the Zone Houillère unit, the Ruitor unit, the Internal unit and the Piemonte-Liguria oceanic unit underwent a common structural evolution. Three ductile deformation phases (D1-D3) are distinguished.

During D1 all units reached peak pressure conditions. Evidently D1 structures have been largely overprinted by subsequent deformation. On macroscopical scale a first foliation S1 is preserved in D2 fold hinges only. Microstructural observations, however, also indicated the existence of the S1 foliation. Mineral assemblages corresponding to D1 indicate a clear metamorphic grade from (sub)greenschist facies conditions in the most external unit (i.e. NW), the Zone Houillère unit, to eclogite facies conditions in Piemonte Liguria oceanic unit, the most internal unit (i.e. SE). In the units in between P-T estimates indicate a continuous increase of the metamorphic grade towards more internal units. While in the Permo-Triassic cover of the Ruitor unit P-T estimates point to pressures of around 12 kbar at temperatures of 450-480° C, pressures of about 16 kbar at temperatures around 500° C are obtained for the Internal unit. This metamorphic gradient is in agreement with the paleogeographic position of the units and allows the conclusion that paleogeographic more internal units were deeper subducted than more external units. Lu-Hf dating of the HP mineral assemblage suggests that maximum depths were reached between 64-56 Ma ago. ^{39}Ar - ^{40}Ar dating of white mica in an eclogitic boudin yields an age of 47 ± 1 Ma. Because mica formation postdates garnet growth, but clearly predate the D2 deformation, the mica ages are interpreted to date the latest stages during D1.

D2 represents the main deformation event, characterised by isoclinal folding on all scales. Owing to the intense transposition, the main foliation is a composite between D1 and D2. F2 folds axis show a wide spread in plunge azimuth from ESE to WNW between the Houiller Front and the Valgrisenche. In the rest of the study area F2 fold axis plunge to the WNW. The orientation of L2 stretching lineations is parallel to the F2 folds axis. The transport direction during D2 is consistently top-to-the-WNW, which is indicated by shear bands and asymmetric porphyroblasts. P-T estimates indicate that D2 is associated with decompression from peak pressures to about 5 kbar at temperatures around 400° C.

In conclusion these observations allow the interpretation that nappe stacking takes place during exhumation parallel and within the subduction channel. ^{39}Ar - ^{40}Ar dating of D2 mylonites indicates an age of 40 Ma for the activity of the tectonic contact between the Piemonte-Liguria oceanic unit and the Internal unit. In contrary at the most external tectonic contact between the Ruitor unit and the Zone Houillère unit an age of 35 Ma is obtained. These data are in line with structural observations indicating a westward migration of the deformation during D2, whereby the Zone Houillère unit is incorporated into the nappe stack during a late stage of D2.

D3 is characterised by open mesoscale parasitic folds, which refold the main S1/S2 foliation, and of L2 stretching lineations causing the wide range of orientations. D3 fold axis plunge moderately to the NE or SW and they have a gently SE-dipping axial planes. Mapping the vergency of mesoscopic

D3 folds indicates two D3 megafolds. The first and W-closing megafold (Ruitor mega-fold) affects all previous structures, including former nappe contacts. The second and tectonically higher D3 megafold (Valsavaranche mega-fold) closes towards the east. This D3 megafold crops out in the uppermost Valgrisenche and Val di Rêhmes and refolds the entire nappe stack back into an upright position. In the area of the Grande Sassièra, for example, a Piemonte–Liguria klippe lies above the Internal unit and the axial plane of the Valsavaranche mega-fold. This hitherto undetected D3 megafold can be correlated with the well-known Valsavaranche-backfold found and described by Argand (1911).

In conclusion the combined investigations of nappe-stack polarity, kinematics of shearing and metamorphic field gradients reveal that rather nappe refolding than normal faulting or back-thrusting led to the present day geometry of the nappe stack in the internal parts of the ECORS-CROP transect.

Table of content

Abstract

Introduction

Introduction and aim of the study 1

Chapter 1:

Tectonic evolution of the Briançonnais units along a transect (ECORS-CROP) through the Italian- French Western Alps

Abstract 9

Introduction 9

Geological setting 10

 Zone Houillère unit 11

 Ruitor unit 11

 Internal unit 11

 Piemont-Ligurian oceanic unit 11

 Gran Paradiso massif 11

Deformation history 18

 Pre-alpine structures 19

 D1 structures 19

 D2 structures 19

 D3 structures 22

Discussion of the regional variability in orientation and strain intensity of D2 and D3 structures 22

Sense of movement inferred for individual tectonic contacts

D1 and D2 22

Transport directions associated with D3 24

 Cross sections and regional structures 24

 Combined cross sections A-A', A''-A''' and B-B' 24

 Combined cross sections C-C' and D-D' 25

 Combined cross sections D-D'' and E-E' 26

 Summary an interpretation of the large-scale structures 26

Discussion 27

Conclusion and summary 31

Chapter 2:

Metamorphic evolution of the Briançonnais unit in the Western Alps: New data on metasedimentary rocks

Abstract 37

Introduction 38

Geological setting 39

 Zone Houillère unit 40

 Ruitor unit 40

 Internal unit 40

Mineral and whole rock chemistry 42

Methods of investigation 42

Sample selection and whole rock chemistry	42
Sample description and microstructures	42
Sample Rui9906	42
Sample Cere0035	44
Sample Vag0139	45
Sample Cret006 and SB 1.38.2	45
P-T estimates	47
Methods used	47
Sample Rui9906	48
Sample Cere0035	48
Sample Vag0139	49
Sample Cret006	49
Interpretation	49
Correlation between Petrology and deformation	51
P-T-d paths	52
Conclusions	54
Chapter 3:	
Late stage Deformation in a collisional orogen (Western Alps): Nappe refolding, back-thrusting or normal faulting?	
Abstract	63
Introduction	63
Criteria to distinguish between back-thrusting, normal faulting and nappe refolding	63
Nappe stack polarity and palaeogeography	63
Sense of shearing	63
Changes of metamorphic grade	64
Regional setting of the study area	64
New structural and petrological data	64
Interpretation	65
Discussion	69
Conclusions	69
Chapter 4:	
From HP to late stage deformation: Dating the tectonometamorphic evolution along a transect (ECORS-CROP) through the Italian-French Western Alps	
Abstract	73
Introduction	74
Geological setting	75
Tectono-metamorphic evolution	77
Analytical techniques	78
Microstructural observations and Microchemistry of multiple mica generations	79
Introductory sample and theoretical foundation	83
The classical approach	83
The role of diffusion	85

Deformation induced resetting: an example from the Monte Rosa	86
Influence of the purity of the samples for $^{39}\text{Ar}/^{40}\text{Ar}$	87
Influence of grain size on ages	89
Results	90
Zone Houillère unit	90
Ruitor unit	91
Internal unit	95
Piemont-Liguria oceanic unit (Schistes lustrés)	96
Summary and Interpretation	97
Tectonic interpretation	101
Conclusion	102
Chapter 5:	
Lu-Hf and Sm-Nd systematic in HP metamorphic rocks: preliminary results of a case study from the Piemont-Liguria oceanic unit (Italian-French Alps)	
Introduction	107
Petrology	
Metasediment sample Lan003	108
Metabasite sample Vaud003	109
Metasediment sample Lev008	109
Analytical Methods	110
Results	110
Lu-Hf and Sm-Nd isotope geochemistry	110
Introductory remark and the ^{176}Lu decay constant	110
Metasediment sample Lan003	110
Metabasite sample Vaud003	111
Metasediment sample Lev008	113
Discussion and Interpretation	114
Summary and Conclusions	117
Synthesis	123
References	127
Appendix	
Appendix I: Structural data	141
Appendix II: Deformation table	155
Appendix III: Ar-Ar geochronology	159

Introduction

Introduction and aim of the Study

The present study deals with the structural evolution of the Briançonnais domain in the Italian-French Western Alps. The combined structural, petrological and geochronological investigations along the ECORS-CROP seismic transect (Roure et al. 1996, Schmid and Kissling 2000) contribute to a better understanding of the geodynamic evolution of the Western Alps.

The ECORS-CROP transect is one of the main seismic transects crossing the Alps and runs NW-SE through the French-Italian Alps. Investigating the tectono-metamorphic evolution of the various units is of importance for interpreting the seismic data from depth to surface, and for understanding the evolution of the Alps in general. Together with the results of two other seismic transects in Switzerland (NFP 20) it became clear that style of the deformation and dating of individual tectonic and metamorphic events substantially differ between the western and central Swiss Alps (e.g. Pfiffner et al. 1997, Schmid et al. 1996, Escher et al. 1997). In this sense, the investigations along the ECORS-CROP seismic transect presented here may also contribute to the understanding of the evolution of the Alps on the scale of the orogen. The most striking differences between the Swiss Alps and the Italian-French Alps crossed by the ECORS-CROP transect are the absence of the amphibolite facies “Leponitic” metamorphic overprint and the change in strike along the “Arc of the Western Alps”.

However, the lack of a consistent tectonic model for the Briançonnais domain of the Italian-French part of the Western Alps makes comprehensive structural and kinematic interpretations on the scale of the orogen impossible. While a good summary of the geophysical data is available (Roure et al. 1996), the recent geological field data (e.g. Caby 1996, Butler et al. 1997) are inconsistent and even in contradiction to the geophysical results. What turned out to be an overturned nappe stacks according to this study was interpreted to be either due to back-thrusting (Butler et al. 1997) or normal faulting (Caby 1996). All three models are based on the interpretation of the kinematics observed at the same tectonic contact. The interpretation in terms of normal faulting seems unlikely in the light of the seismic results obtained along the ECORS-CROP transect, while the postulate for back-thrusting is based on a different interpretation of the sense of shearing. The studies of Baudin (1987) and Cigolini (1995) remained on local and limited scale. Geochronological constraints are rare, and the few existing data are linked to questionable tectonic interpretations (Butler and Freeman 1997). The interpretation of the data by Butler and Freeman (1997) is also hampered by the fact that their samples contained two chemically distinct populations. However, the external parts of the ECORS-CROPS transect have recently been well investigated by Fügenschuh et al. (1999), Loprieno (2000), Ceriani (2001), Ceriani et al. (2001), Ceriani et al. (2003) and Fügenschuh and Schmid (2003), also within the framework of the Western-Alps project at the Departement of Earth Sciences of the University of Basel. Furthermore, Schmid and Kissling (2000) presented a first synthesis between the geometry of the deep structures and that of the surface geology along the ECORS-CROP transect.

This study particularly addresses the following topics: (i) the polydeformational tectonic evolution of the different tectonic units based on detailed structural mapping (scale 1:10'000, topographic maps of the “Regione autonoma di Val d’Aosta”), (ii) determination of the P-T conditions of the alpine metamorphic events in the different tectonic units, and (iii) dating of the deformation phases and HP conditions derived from ^{39}Ar - ^{40}Ar white mica analyses and from the Lu-Hf and the Sm-Nd analyses on garnet, respectively.

The present study was part of and supported by the Swiss National Science Foundation projects 20-63391.00 and 20-55559.98 titled: The Penninic units of the Western Alps along the ECORS-CROP transect and the formation of the arc of the Western Alps. In this project carried out at the Department of Earth Sciences at the University Basel and also at the Institut für Geologie at the University Berne (age dating) many other persons were involved: these are Romain Bousquet, Stefano Ceriani, Christian de Capitani, Martin Frey, Bernhard Fügenschuh, Lukas Keller, Ilka Kleinhanns, Jan Kramers, Andrea Loprieno, Christina Ulardic, Igor Villa and Stefan Schmid.

Geography and geological framework

The investigations were carried out within a 20 km long corridor along the ECORS-CROP transect, between the Pt. S. Bernard pass in the northwest and the Val di Rhêmes in the southeast (Fig. 1.1). Perpendicular to the strike of the Alps the study area extends from the Aosta Valley in Italy all the way across the French-Italian border to the northern side of Val d'Isère (Fig. 1.1). Elevation varies between 700 meters a.s.l. in the main valleys to 3500 meters a.s.l. in the area of the Ruitor summit.

Geologically, the northwestern boundary of the study area is represented by the Houiller Front, which separates the Valaisan oceanic domain in the NW from the Zone Houillère unit in the SE (Fig. 1.2). The Zone Houillère unit, consisting mainly of a Paleozoic sedimentary sequence, is the most external unit of the Briançonnais paleogeographic domain in the study area (Fig. 1.2). Further in the SE the Ruitor unit, the Internal unit (Briançonnais terrane) and the Piedmont-Liguria (PL) oceanic unit are cropping out. Ruitor unit and Internal unit are characterised by pre-alpine basement

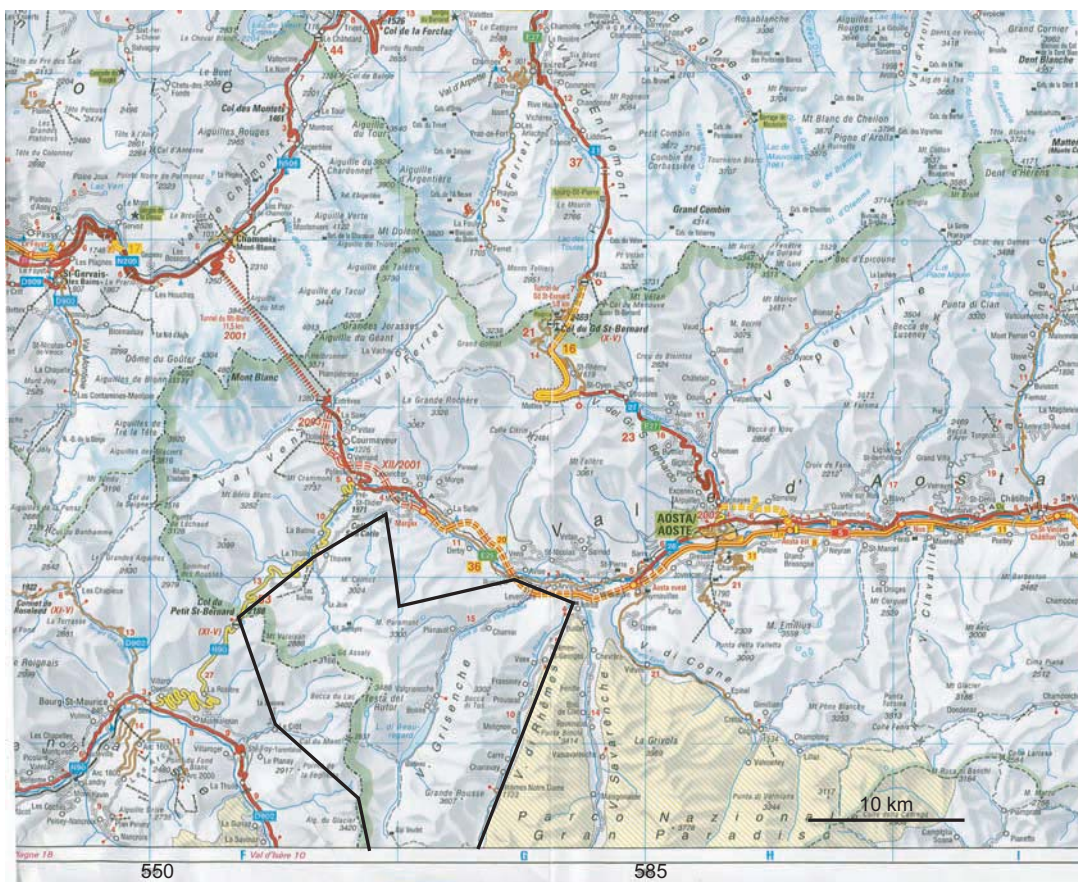


Fig. 1: Topographic map of the Aosta valley. The study area is outlined by the black line. Note coordinates correspond to the Swiss projection

with a thin Permo-Mesozoic cover. The PL oceanic unit predominantly consists of calcschists, which are interlayered with different amounts of metabasites. In the SE the Gran Paradiso “internal” massif,

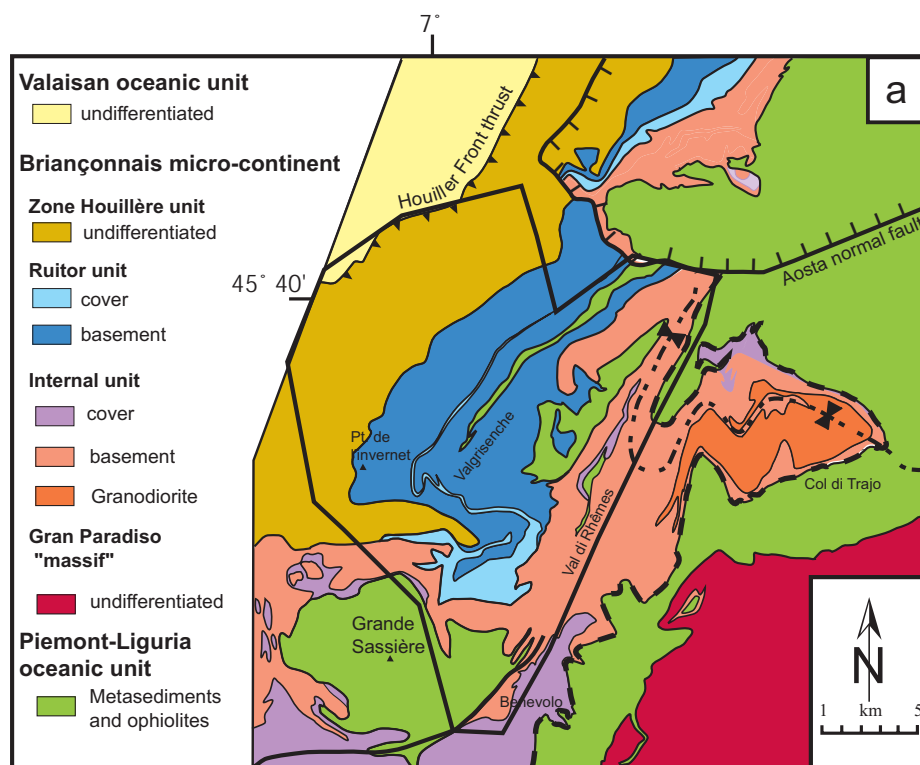


Fig. 2: Geological map of the area between the Pt. St. Bernard pass and Grand Paradiso massif showing the different tectono-metamorphic units outcropping in the study area (after Bucher et al., 2003). The study area is outlined by the black line.

also part of the Briançonnais terrane, delimits the study area.

Organisation of thesis

The present thesis is organised as a “cumulative thesis”, consisting of introduction, five main chapters and a summarizing synthesis. In the following a brief outline of the different chapters, and the role of the author of this thesis, is given. Chapters 1-5 are all manuscripts, which are published, submitted or prepared for submission in journals. The synthesis combines the conclusions of the chapters 2-5 and synthesizes the timing of the tectono-metamorphic evolution.

Chapter 1: Tectonic evolution of the Briançonnais units along a transect (ECORS-CROP) through the Italian-French Western Alps

By Stefan Bucher, Stefan M. Schmid, Stefano Ceriani, Romain Bousquet, Christina Ulardic and Bernhard Fügenschuh; submitted for publication to “*Eclogae Geologicae Helvetiae*”.

This Chapter provides an introduction to the regional geology of the northern Western Alps and the tectono-metamorphic units of the Briançonnais paleogeographic domain in particular. On the base of new field data, collected by the first author, the spatial relationship of the different tectonic units is unravelled. This manuscript focuses on the large-scale structures, the kinematics and the relative timing of the different tectonic contacts. The observations allow for a revised interpretation of the ECORS-CROP profile and for a new tectonic evolution of the Western Alps.

Structural data from the Houiller Front to the Valgrisenche and the data south of the Rifugio Benevolo were collected by the first author. Romain Bousquet contributed data from the Valsavaranche towards the east. Additional data from the Valgrisenche are taken from the master thesis of Christina Ulardic, who was co-supervised by the first author.

Chapter 2: Metamorphic evolution of the Briançonnais units in the Western Alps: New data on metasedimentary cover rocks

By Stefan Bucher and Romain Bousquet; manuscript to be submitted

The metamorphic gradient from eclogite facies conditions in the Piemont-Liguria oceanic unit to subgreenschist facies conditions in the external part of the Zone Houillère unit is known since a long time. However, the alpine metamorphic evolution in the intervening Briançonnais units is still poorly known and in discussion. Because the distinction between alpine and pre-alpine minerals is difficult in basement rocks, only samples from the Permo-Mesozoic cover were analysed in this study. Due to the strong greenschist facies overprint only few samples retained the original HP-mineral assemblage. Samples from the Zone Houillère unit, the Ruitor unit and the Internal unit, which display the HP-mineral assemblage Grt, Ctd, Phg, Chl, Pg, and Grt, Gln, Phg, Pg respectively, were selected for detailed petrological analysis. P-T conditions were calculated by the computer programs DOMINO (De Capitani 1994) and TWQ (Berman 1991). In the Zone Houillère unit pressures of ~5 kbar at 375°C are indicated. Pressures between 11 kbar and 13.5 kbar at temperatures of ~450°C are derived for the Ruitor unit. Slightly higher pressures and temperatures are estimated for the Internal unit. This chapter is the result of a collaboration between the first author and Romain Bousquet. The first author contributed data from the Zone Houillère unit, the Ruitor unit and the Internal unit including the microprobe analyses and he performed thermo-barometric calculations.

Chapter 3: Late stage deformation in a collisional orogen (Western Alps): Nappe refolding, back-thrusting or normal faulting?

By Stefan Bucher, Stefan M. Schmid, Romain Bousquet, Bernhard Fügenschuh; published in *Terra Nova*, 2003, 15, 109-117

This chapter published in “Terra Nova” discusses the role of late stage deformations in orogens. The Western Alps serve as a case study for demonstrating criteria, which allow a distinction between the different modes of late stage deformation. On the one hand this chapter represents a summary of the structural and petrological data of chapter 1 and 2. On the other hand it presents a new geodynamic model for the evolution of the Western.

Stefan M. Schmid, Romain Bousquet and Bernhard Fügenschuh substantially contributed towards the discussions presented in this publication and in the improvement of the manuscript.

Chapter 4: From HP to late stage deformation: Dating the tectono-metamorphic evolution along a transect (ECORS-CROP) through the Italian-French Western Alps

By Stefan Bucher, Igor M. Villa, Ilka Kleinhanns, Lukas Keller, Romain Bousquet, Stefan M. Schmid; manuscript prepared for submission to the “Journal of Metamorphic Geology”.

Based on 15 samples collected across the entire Briançonnais paleogeographic domain and the Piemont-Liguria oceanic unit of the Italian-French Western Alps the first two deformation phases (D1 & D2) are dated by ^{39}Ar - ^{40}Ar incremental heating on white micas. D1-micas taken from an eclogitic boudin, which was overprinted by D2, show a plateau age of 47 ± 1 Ma. D2 mylonites, on the other hand, show a plateau age of 40 ± 1 Ma. Most of the samples display mixed ages. Only a careful chemical and petrological analysis of the minerals allows for an age interpretation of the

different populations that represent different deformation phases, as is indicated by microstructural and electron microprobe analysis.

This chapter comprises the ^{39}Ar - ^{40}Ar geochronological analyses carried out for this thesis in collaboration with Igor M. Villa from the Institut für Geologie at the University Berne. The first author selected the samples, performed the mineral separation and the ^{39}Ar - ^{40}Ar measurements on white micas. Igor M. Villa helped in the interpretation of the data and he improved the first version of the manuscript. In addition to the samples collected by the first author, Romain Bousquet provided further samples from the study area and Lukas Keller samples from the Monte Rosa unit, which also have been analysed for this study.

Chapter 5: Lu-Hf and Sm-Nd systematics in HP metamorphic rocks: preliminary results of a case study from the Piemont-Liguria oceanic unit (Northern Western Alps)

By Stefan Bucher, Romain Bousquet and Ilka Kleinhanns; manuscript prepared for submission

This manuscript presents the results of Lu-Hf and Sm-Nd geochronology on garnet are presented. Three samples from the PL-oceanic unit were analysed in terms of Lu-Hf and Sm-Nd isotopic systems for dating the HP-conditions. Weakly retrogressed mafic and pelitic samples show ages ranging between 55 and 60 Ma, interpreted to represent the HP conditions. A sample with abundant indications for retrogression shows an age of 48 ± 4.7 Ma, consistent with the ^{39}Ar - ^{40}Ar ages. However, all samples show isotopic disequilibrium between HP minerals and whole rock, suggesting a (partial) reequilibration during the retrograde part of the alpine metamorphic cycle.

This section results from a collaboration of the first author with Ilka Kleinhanns from the Institut für Geologie at the University Berne, who carried out the measurements and substantially contributed to the interpretation. Samples were collected by Romain Bousquet.

Synthesis

This section summarises the discussions and conclusions presented in the individual chapters. The structural, petrological and geochronological data will be summarised in chronological order and embedded in the tectonic as inferred from the results of the structural analysis.

Appendix

APPENDIX I presents all the structural data.

APPENDIX II includes a table, which attempts to correlate the deformation across the entire Western Alps.

Geochronological data not included in the manuscript of Chapter 4 are found in **APPENDIX III**.

This thesis contains information and data not intended for publication (Appendices I), or not yet prepared for submission (Appendix II)

Chapter 1

Tectonic evolution of the Briançonnais units along a transect
(ECORS-CROP) through the Italian- French Western Alps

By Stefan Bucher, Christina Ulardic, Romain Bousquet, Stefano Ceriani,
Bernhard Fügenschuh, Yves Gouffon & Stefan M. Schmid
Paper published in "Eclogae geologicae Helvetiae", 2004, Volume 97/3, pages 321-346.

0012-9402/04/030321-25
 DOI 10.1007/s00015-004-1139-0
 Birkhäuser Verlag, Basel, 2004

Eclogae geol. Helv. 97 (2004) 321–345

Tectonic evolution of the Briançonnais units along a transect (ECORS-CROP) through the Italian-French Western Alps

STEFAN BUCHER^{1*}, CHRISTINA ULARDIC², ROMAIN BOUSQUET¹, STEFANO CERIANI¹,
 BERNHARD FÜGENSCHUH¹, YVES GOUFFON³, & STEFAN M. SCHMID¹

Key words: Western Alps, Briançonnais, ECORS-CROP, deformation, post-nappe folding, exhumation, nappe stacking

ABSTRACT

Based on new structural data from an area in the Italian-French Western Alps, situated between the Petit Saint Bernard pass and the Gran Paradiso massif, the large-scale geometry of the tectonic features is established for the tectonic units derived from the Briançonnais paleogeographic domain. Based on this, and other new data on the metamorphic evolution and geochronology of the area, a consistent model for the tectonic evolution for the Briançonnais domain is proposed. A nappe stack consisting of, from bottom to top, Zone Houillère unit, Ruitor unit, Internal unit and Piemont-Ligurian oceanic unit, was affected by three deformation phases. The third phase of deformation (35–31 Ma), referred to as post-nappe folding, is responsible for the formation of two large-scale folds: the Ruitor and Valsavaranche mega-folds. An overturned nappe stack, characterized by foreland-dipping foliations, is found between the axial planes of these two mega-folds. No evidence was found for back-thrusting, postulated by many previous authors. The individual thrusts between the tectonic units were active during a second phase of deformation (43–35 Ma), characterized by top-NW to -NNW shearing. This D2 is related to nappe stacking and accompanied by substantial exhumation. Thrusting becomes relatively younger towards the external parts of the study area. We emphasize that extension played no significant role in the exhumation of the high-pressure units of the Italian-French Alps. The contacts between the tectonic units were already active during the first phase of deformation (50–43 Ma), which is related to subduction and peak pressures.

ZUSAMMENFASSUNG

Anhand neuer strukturgeologischer Untersuchungen zwischen dem Col du Petit Saint Bernard und dem Gran Paradiso Massiv, entlang der Grenze zwischen Italien und Frankreich, werden die Grossstrukturen der vom Briançonnais Mikrokontinent abgeleiteten tektonischen Einheiten aufgezeigt. Zusätzliche, neue geochronologische sowie petrologische Daten führen zu einem neuen, konsistenten tektonischen Modell für die paleogeographische Domäne des Briançonnais. Der Deckenstapel im untersuchten Gebiet besteht, vom Liegenden zum Hangenden, aus Zone Houillère Unit, Ruitor Unit, Internal Unit und Piemont-Liguria oceanic Unit. Dieser Deckenstapel wurde von drei Deformationsphasen überprägt. Während der dritten Deformationsphase (31–35 Ma), welche durch die Verfaltung dieses Deckenstapels charakterisiert wird, entstehen zwei Grossfalten: Ruitor und Valsavaranche Mega-Falte. Zwischen den Achsenebenen dieser beiden Mega-Falten ist ein überkippter Deckenstapel mit zum Vorland einfallenden Foliationen zu beobachten. Für die von einigen früheren Autoren postulierten Rücküberschiebungen konnten keine Evidenzen gefunden werden. Die verschiedenen Überschiebungen zwischen den tektonischen Einheiten waren während der zweiten Deformationsphase (43–35 Ma) aktiv und zeigen eine top-NW bis top-NNW Kinematik. D2 steht im Zusammenhang mit der Deckenstapelung, welche gleichzeitig zu substantieller Exhumation der Hochdruckeinheiten führte. Die Überschiebungen werden zu den externen Teilen des Untersuchungsgebietes hin zunehmend jünger. Extension spielte während der Exhumation nur eine untergeordnete Rolle. Die Kontakte zwischen den verschiedenen tektonischen Einheiten waren schon während der ersten Deformationsphase (50–43 Ma), d.h. während der Subduktion und des Hochdrucks aktiv.

Introduction

Two oceanic suture zones bound the tectonic units derived from the Briançonnais paleogeographical domain: the Valaisan suture and the more internal Piemont-Ligurian suture. Prior to Tertiary collision between the Apulian and the European plates, responsible for the forming of the Alps (e.g. Argand 1916, Schmid et al. 2004), the Briançonnais paleoge-

graphic domain was part of a micro-continent, situated between the above-mentioned oceanic units (Trümpy 1955, Frisch 1979, Stampfli 1993, Froitzheim et al. 1996).

In the northern part of the Italian-French Western Alps, the ECORS-CROP seismic traverse (Nicolas et al. 1990, Roure et al. 1996) crosses the following four major tectonic units, derived from the Briançonnais domain (Fig. 1): Zone Houillère unit, Ruitor unit, Internal unit and Gran Paradiso

¹ Geologisch-Paläontologisches Institut, Bernoullistr. 32, 4056 Basel, Switzerland

² Swiss Re, Centre for Global Dialogue, Gheistrasse 37, Rüschlikon, Switzerland

³ Bundesamt für Wasser und Geologie BWG, 3003 Bern-Ittigen, Switzerland

* Correspondence: Stefan Bucher, Muséum d'histoire naturelle, rue des Terreaux 14 2000 Neuchâtel, Switzerland. E-mail: Stefan.Bucher@unine.ch

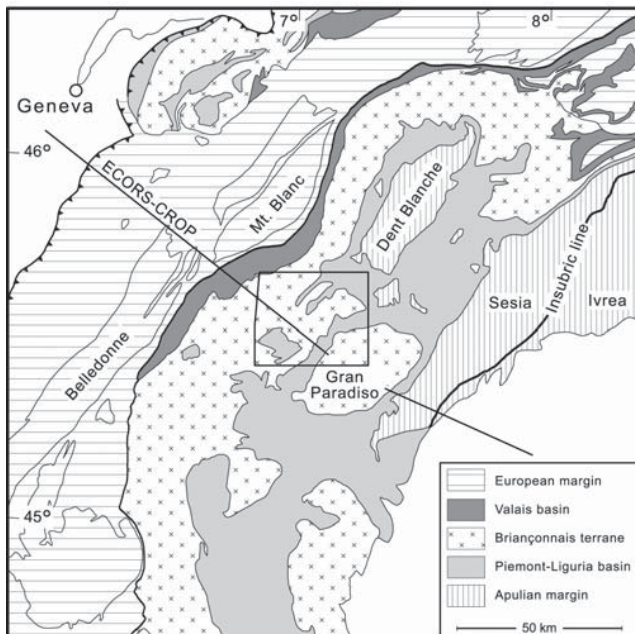


Fig. 1. Paleogeographic domains of the Western Alps, after Bucher et al. (2003). The rectangle shows the location of the study area.

massif (Fig. 2). Despite of the impressive works of many Alpine Geologists (Argand 1911, 1912, Ellenberger 1958, Elter 1960, Fabre 1961, Lemoine 1961, Dal Piaz 1965, Dal Piaz & Govi 1965, Elter & Elter 1965, Bertrand 1968, Caby 1968, Elter 1972, Marion 1984, Baudin 1987, Mercier & Beaudoin 1987, Cigolini 1995, Caby 1996) there still is no consistent picture regarding the large-scale structure, nor regarding the tectonic evolution of the Briançonnais units in the Italian-French Alps. During Alpine orogeny the Briançonnais units underwent a complex tectono-metamorphic evolution, resulting in a field metamorphic gradient that ranges from eclogitic conditions in the internal parts (Gran Paradiso; Chopin 1977, Dal Piaz & Lombardo 1986) to sub-greenschist facies conditions in the external parts of the Zone Houillère unit (Desmons et al. 1999). This gradual change points to a difference in the tectono-metamorphic evolution of the individual tectonic units of the Briançonnais. It also allows for investigating the processes responsible for such differences between the internal Penninic units and the more external Valais and European margin (Dauphinois) units. The Briançonnais is a key area in that it occupies an intermediate position, being situated between the most internal HP units and a second more external belt of high-pressure rocks (Valaisian; Goffé & Bousquet 1997, Bousquet et al. 2002), and/or the low-grade units of the European domain (Aprahamian 1988, Frey et al. 1999). These more external units are characterized by a different metamorphic evolution in terms of timing and P-T conditions.

In order to establish the structure and the tectonic evolution of the Briançonnais domain, the superposition of the different tectono-metamorphic events within the Briançonnais units and their kinematics during the Alpine cycle must be unraveled. Thereby the understanding of the geometry and the large-scale structures is of primary importance, as has been discussed since a long time (Milnes 1974, Müller 1983, Ring 1995, see also Bucher et al. 2003 and references therein). The retro-deformation of such large-scale structures, formed during the late stage deformation, is a prerequisite for unraveling the main stages of the tectonic and metamorphic evolution of an orogen (Dewey 1988, Platt et al. 1989, Escher et al. 1993).

The main schistosity along the ECORS-CROP profile changes from a SE-dip in the external part of the Briançonnais (Houiller Front) to a dominant NW-dip in the southeastern part (Gran Paradiso), a feature that is often referred to as “fan structure of the Briançonnais” (Fabre 1961, Lemoine 1961). It is classically explained by outward directed displacement, followed by inward directed back-thrusting (Butler & Freeman 1996). However, Caby (1996) already stated that the kinematics along the various tectonic contacts only show evidence for outward directed displacement.

It is the aim of this contribution to examine the large-scale structure of the Briançonnais domain in the Western Alps. The new structural data will be presented and used to constrain the present-day geometry, characterized by large-scale post-nappe folding, and to analyze the tectonic evolution of these dominant large-scale structures within the Briançonnais nappe stack. Based on this we will propose a new interpretation of the tectonic evolution of the internal part of the northern part of the Western Alps, and we will point out the geodynamic implications of the different deformation phases at the scale of the orogen.

Geological setting

The investigated area, extending along the ECORS-CROP seismic line from the Pt. St. Bernard pass in the NW to the border of the Gran Paradiso massif in the SE (Fig. 2), traverses most of the Briançonnais units of the Italian-French Western Alps. In the NW the Zone Houillère unit, representing the most external part of the Briançonnais paleogeographic domain, is separated by the Houiller Front (Bertrand et al. 1996, Fügenschuh et al. 1999) from the Valaisian units (Antoine 1971, Loprieno 2001). The more internal Ruitor unit to the SE is classically separated into an external (“Ruitor externe”) and an internal part (“Ruitor interne”), respectively (Caby 1996). The Internal unit, still further to the SE, is tectonically separated from the Piemont-Liguria (P-L) oceanic unit by a contact much discussed in the literature and referred to as the “Entrelor tectonic contact” (ETC) by Bucher et al. (2003). The P-L oceanic unit is the only tectonic unit of the investigated area that does not belong to the Briançonnais paleogeographic domain. The Gran Paradiso

massif, outcropping to the SE of the P-L oceanic unit, again belongs to the Briançonnais domain and represents the internal basement massif situated in our study area (Brouwer et al. 2002). The “Internal Massifs” are interpreted to paleogeographically represent the most internal basement units, situated next to the P-L oceanic unit. Some authors therefore classify them as “External Piemont” and assign them to the “Piemontais” paleogeographical domain. The paleogeographic position, however, remains the same for either attribution.

Zone Houillère unit

This unit is characterized by a Paleozoic sequence of continental deposits (Fabre 1961). The lower part of this sequence consists of black schists with anthracitic lenses and arkoses (Namurian to Stephanian in age; Feys 1963, Gréber 1965). The upper part is dominated by arkoses and conglomerates, probably of Stephano-Autunian age (Fabre 1961). The clasts mainly consist of polycrystalline quartz, micaschist and paragneiss. The latter display a polyphase metamorphic imprint (Desmons & Mercier 1993). A Permo-Triassic sequence discordantly overlies this Carboniferous sequence (Ellenberger 1958, Elter 1960). During the Alpine deformation the Zone Houillère unit was decoupled from its former basement, whose present-day position remains unknown, since it does not outcrop at the earth's surface (Desmons & Mercier 1993).

Ruitor unit

The Ruitor unit dominantly consists of pre-Permian (450–480 Ma, Guillot et al. 2002) garnet micaschists and paragneisses with abundant intercalated metabasites (Baudin 1987). There is definitely an Alpine metamorphic overprint (Caby 1996), but some relicts of pre-Alpine metamorphism survived the Alpine cycle (Bocquet [Desmons] 1974). Its sedimentary cover is made up by a thin Permo-Triassic sequence, consisting of “Verrucano”-type conglomerates (Trümpy 1966) at the base, followed by lower Triassic meta-arkoses, which are stratigraphically overlain by quartz-phyllites and ankerite-bearing micaschists (Ulardic 2001). This sequence crops out all along Valgrisenche (Fig. 2).

The separation of the Ruitor unit into an external and an internal part is still a matter of debate since it is not marked by an unequivocal tectonic surface. Desmons & Mercier (1993) question this separation. Some authors made a separation based on the dominant mineral assemblage (Alpine vs. pre-Alpine; i.e. Caby in Debelmas et al. 1991a) while others used intensity of Alpine deformation as a criterion (i.e. Gouffon 1993) for defining such a boundary between two parts of the Ruitor unit. Further south, the Sapey gneiss occurs (Isère Valley) in the same tectonic position as the Ruitor unit (Fig. 2, Bertrand et al. 1998) and is interpreted to be the continuation of the latter. Bertrand et al. (1998) interpret the Sapey gneiss to be the basement of the Zone Houillère unit. This interpre-

tation is debated since a long time and will be discussed later in this text.

Internal unit

The Internal unit (“Zona Interna”) of the Italian authors (Cigolini 1995 and references therein) corresponds to the “Briançonnais interne” of the French authors, found further south in the Vanoise-Mont Pourri area (i.e. Caby, 1996). Northwards the Internal unit was correlated with the Mont Fort unit (Gouffon 1993). The Internal unit is made up of a lower part, formed by paragneisses and micaschists with a polymetamorphic history (Bocquet 1974, Cigolini 1995), and of a mono-metamorphic upper part, consisting of lower Permian to Mesozoic formations. According to Amstuz (1955, 1962), the lower part is mainly of volcano-clastic origin. This succession is intruded by Paleozoic granitic and granodioritic bodies of variable size (i.e. the Cogne granodiorite, Bertrand et al. 2000).

Leucocratic gneisses define the base of the mono-metamorphic upper part. These are followed by a typical Permo-Triassic sequence consisting of conglomerates (“Verrucano”), quartzitic meta-sandstones, impure quartzites and ankerite-bearing micaschists. The younger Mesozoic cover is only preserved in the southern part of the study area. Multiple erosion events characterize the Mesozoic sequence, as is discussed by Jaillard (1989, 1990), Adatte et al. (1992) and Saadi (1992). For the purposes of this study, the data of the latter mentioned authors were completed with structural data.

Piemont-Liguria oceanic unit

The P-L oceanic unit predominantly consists of calc-schists. These are interlayered with different amounts of metabasites (Elter 1972, Cigolini 1995). Two types of metabasites do occur: mostly retrogressed eclogites and prasinites. While some authors proposed a subdivision of the Piemont-Liguria oceanic unit within our working area into an eclogitic (“Zermatt-Saas Fee”) and a non-eclogitic (“Combin”) part (Droop et al. 1990, Ballèvre and Merle 1993, Dal Piaz 1999), our observations indicate a mélange consisting of eclogitic and blueschist mafic boudins, embedded in a matrix of HP metasediments (Bucher et al. 2003).

Gran Paradiso massif

The Gran Paradiso massif comprises mainly Hercynian granitoids with an intrusion age of 350–270 Ma (Bertrand et al. 2000). These intruded meta-sedimentary rocks (Gneiss Minuti) that contain eclogite pods metamorphosed during the Alpine cycle (Compagnoni and Lombardo 1974, Ballèvre 1990, Borghi et al. 1996). Evidence for HP metamorphic conditions is also found within the orthogneisses (Brouwer et al. 2002). Paleogeographically the Gran Paradiso massif represents the most internal unit of the Briançonnais domain, adjacent to the Piemont-Liguria Ocean.

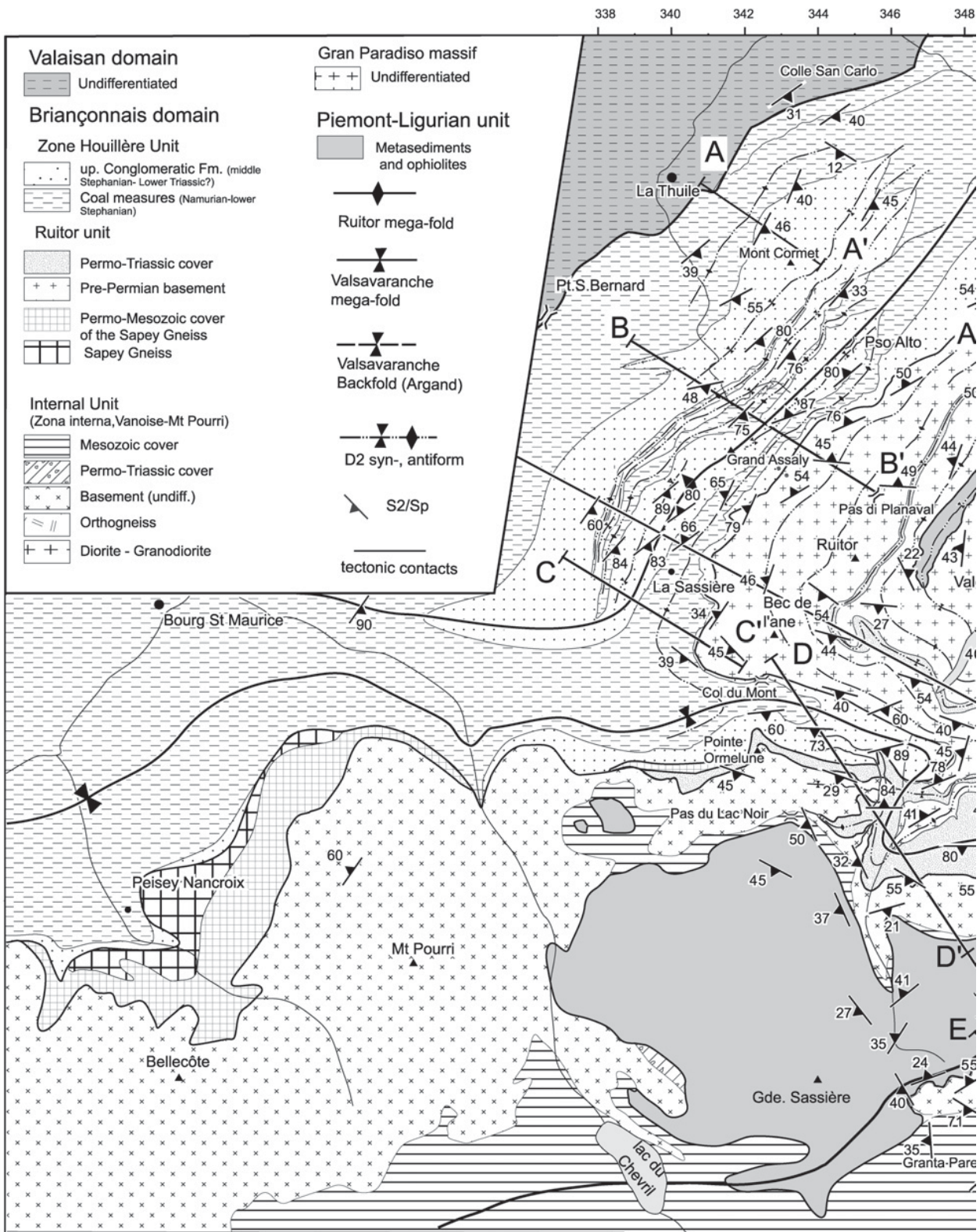
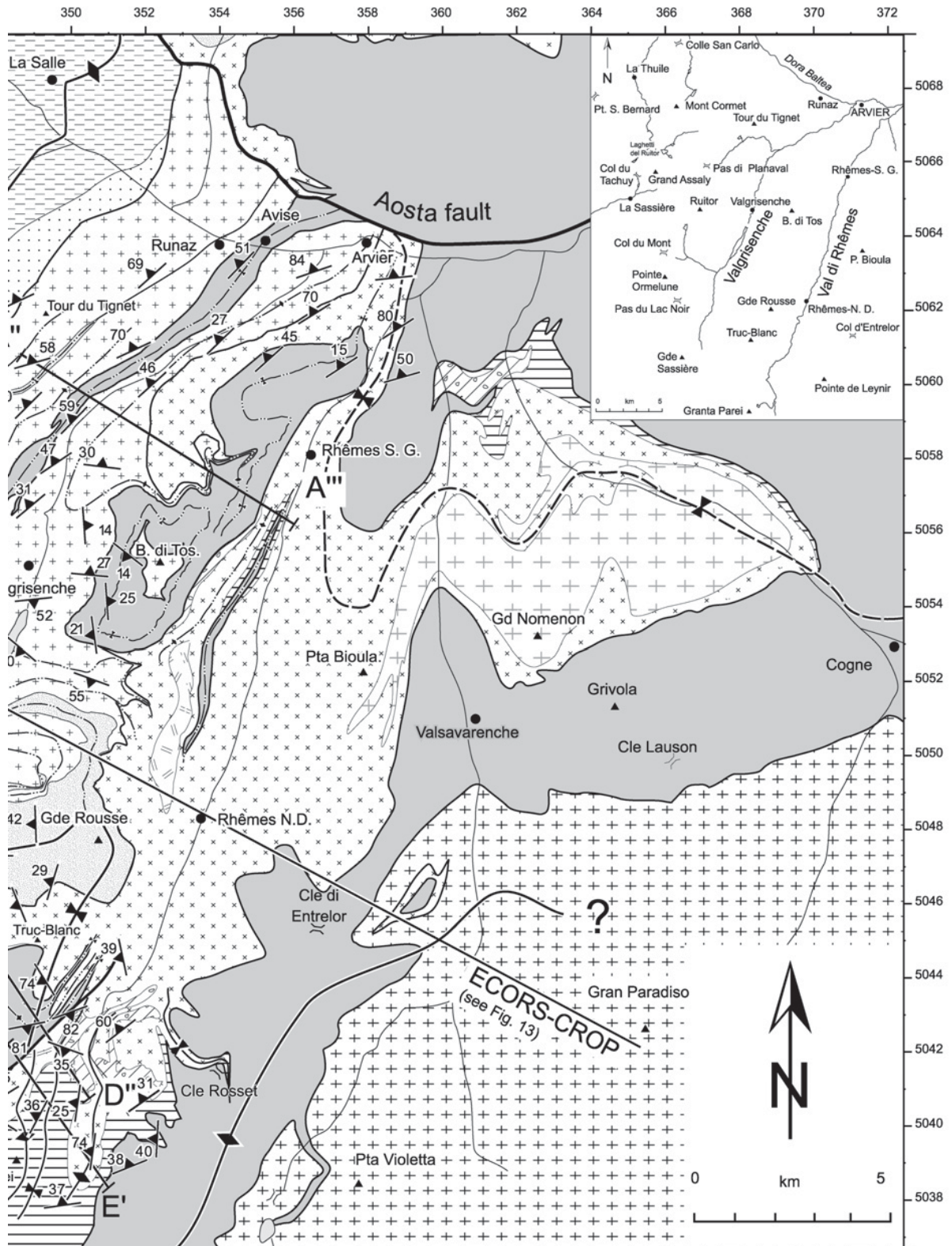


Fig. 2. Geological and structural map of the study area. Letters A-A' to E-E' mark the traces of the detailed cross sections shown in Figure 12.



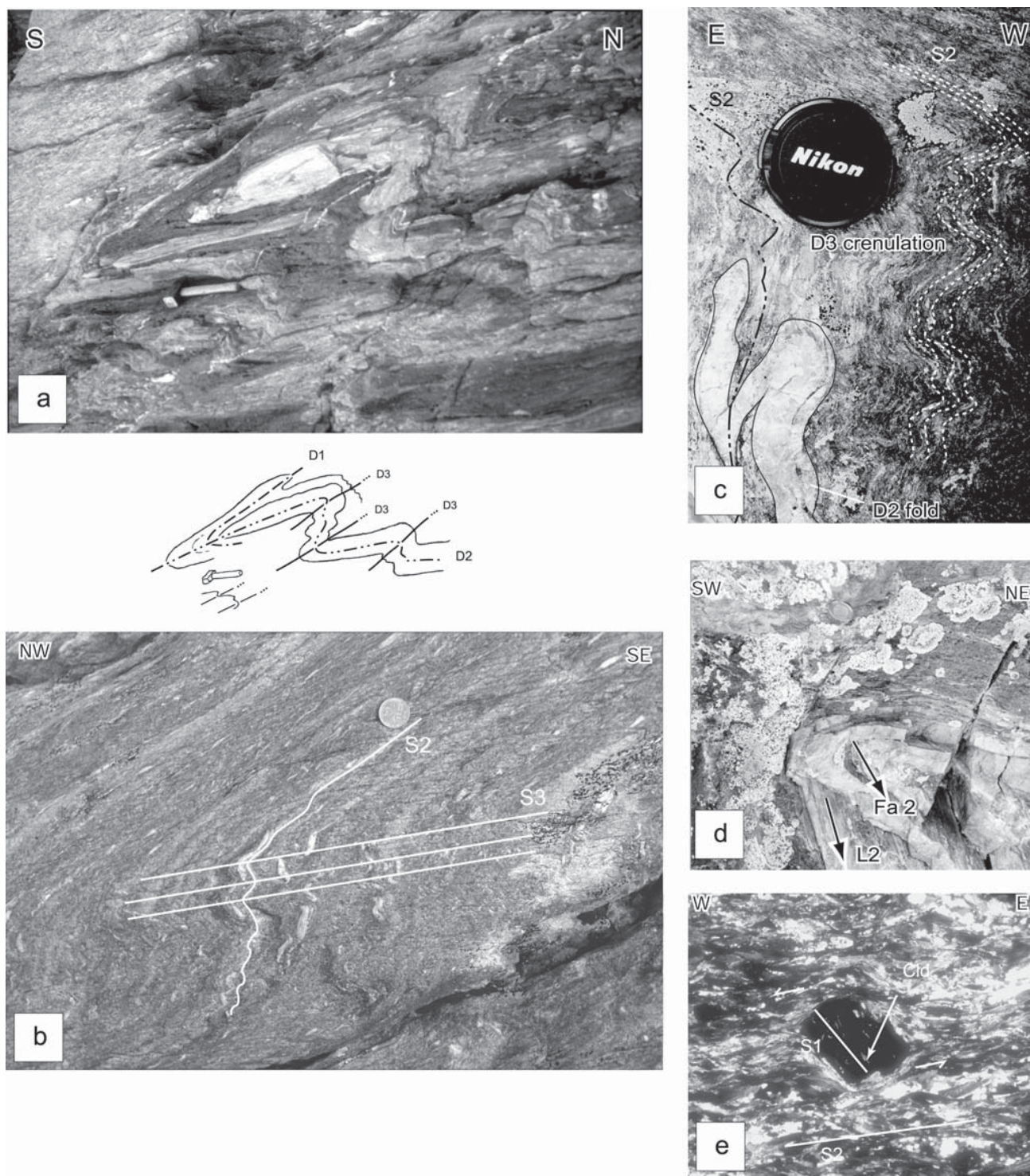


Fig. 3. Meso- and microscopic structures. a) Superposed D1-, D2 and D3-folds in the P-L oceanic sediments from the Valgrisenche; b) asymmetric D3 folds in the Upper Conglomeratic Formation of the Houiller unit from the upper limb of the Ruitor mega-fold; c) D2 fold, overprinted by open D3 folds with a subhorizontal axial plane, in the Permo-Triassic cover from the uppermost Valgrisenche; d) characteristic D2 fold in the Permo-Triassic cover of the Internal unit, showing parallelism between F2 fold axis and stretching lineation, from the uppermost Val di Rhêmes; e) Garnet porphyroblast, preserving a relict internal S1 foliation, defined by chloritoid and phengite, embedded in the S2 foliation; thin section from the Cogne area (micrograph with crossed polarizers).

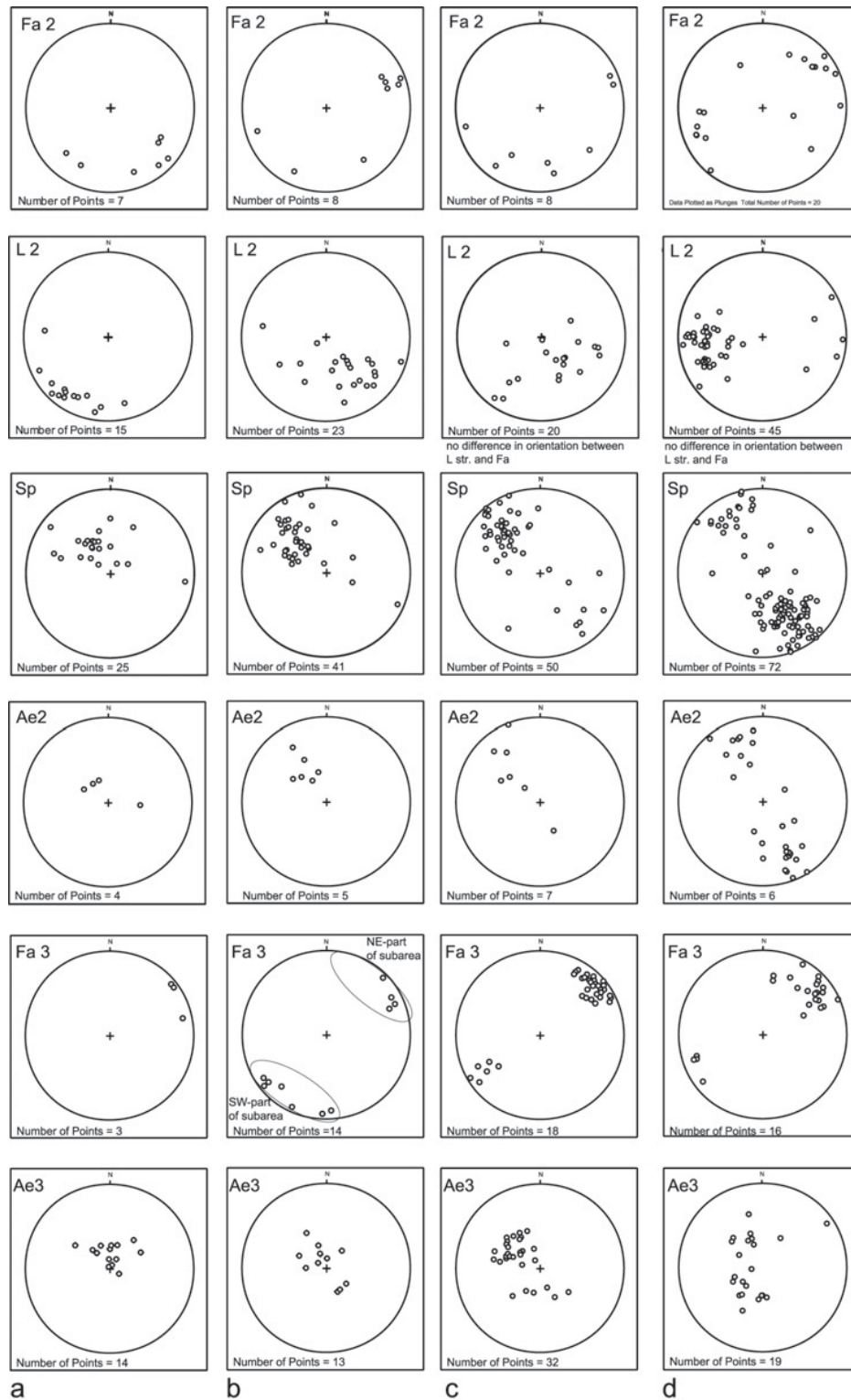


Fig. 4. Structural data from Area I, i.e. the external part of the Zone Houillère unit. Stereoplots (equal area, lower hemisphere) in columns a, b, c and d show data from sub-areas a to d within Area I, as defined in Fig. 5. Abbreviations are: Fa2: fold axis of D2; L2: stretching lineation of D2; Sp: composite foliation S0/S1/S2; Ae2: axial plane of D2 folds; Fa3: fold axis of D3; Ae3: axial plane of D3 folds.

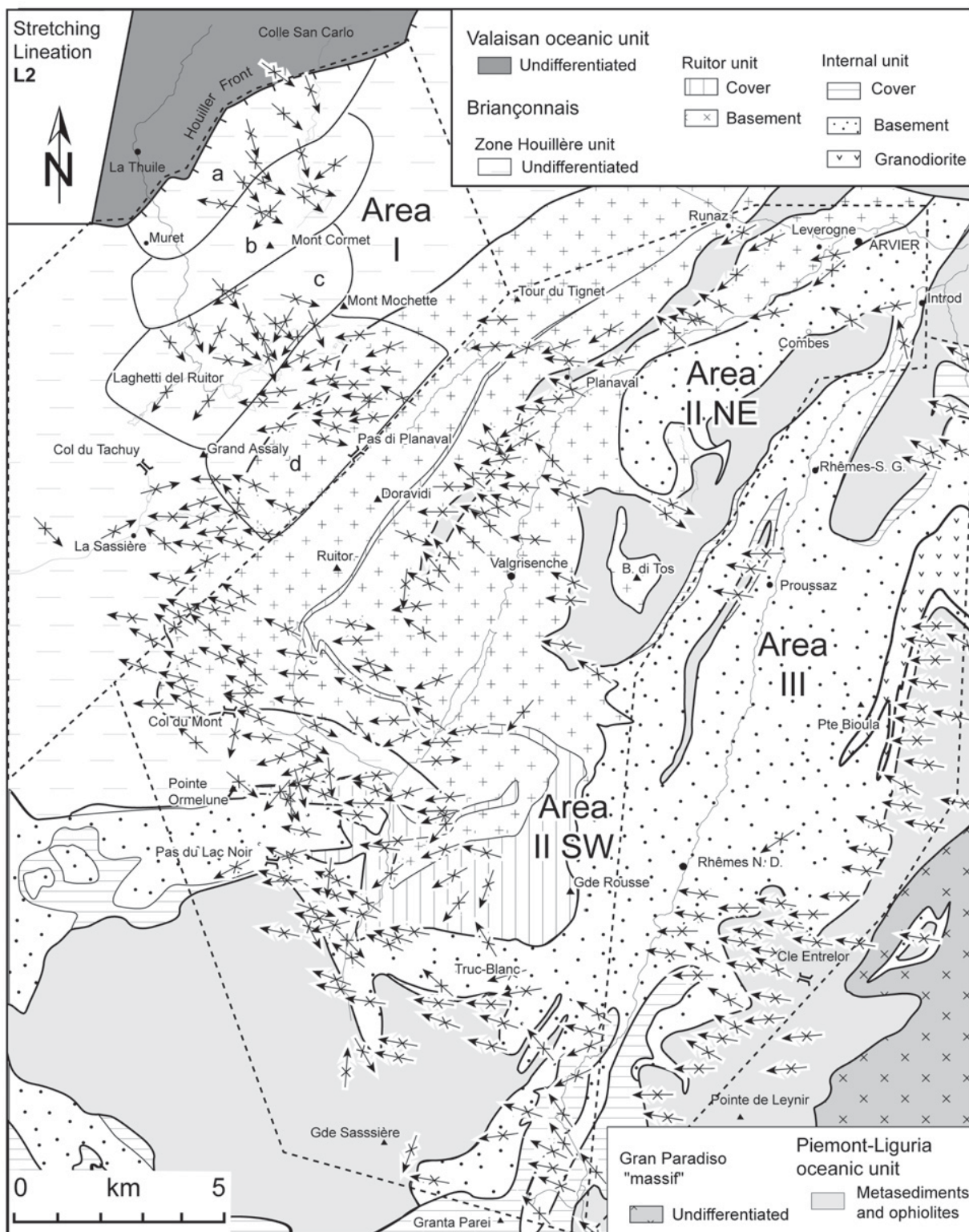


Fig. 5. Map of L2 stretching lineations. Dashed lines indicate the outlines of the Areas I to III and their sub-areas, respectively, from which the structural data shown in Figs. 4 and 6 have been collected.

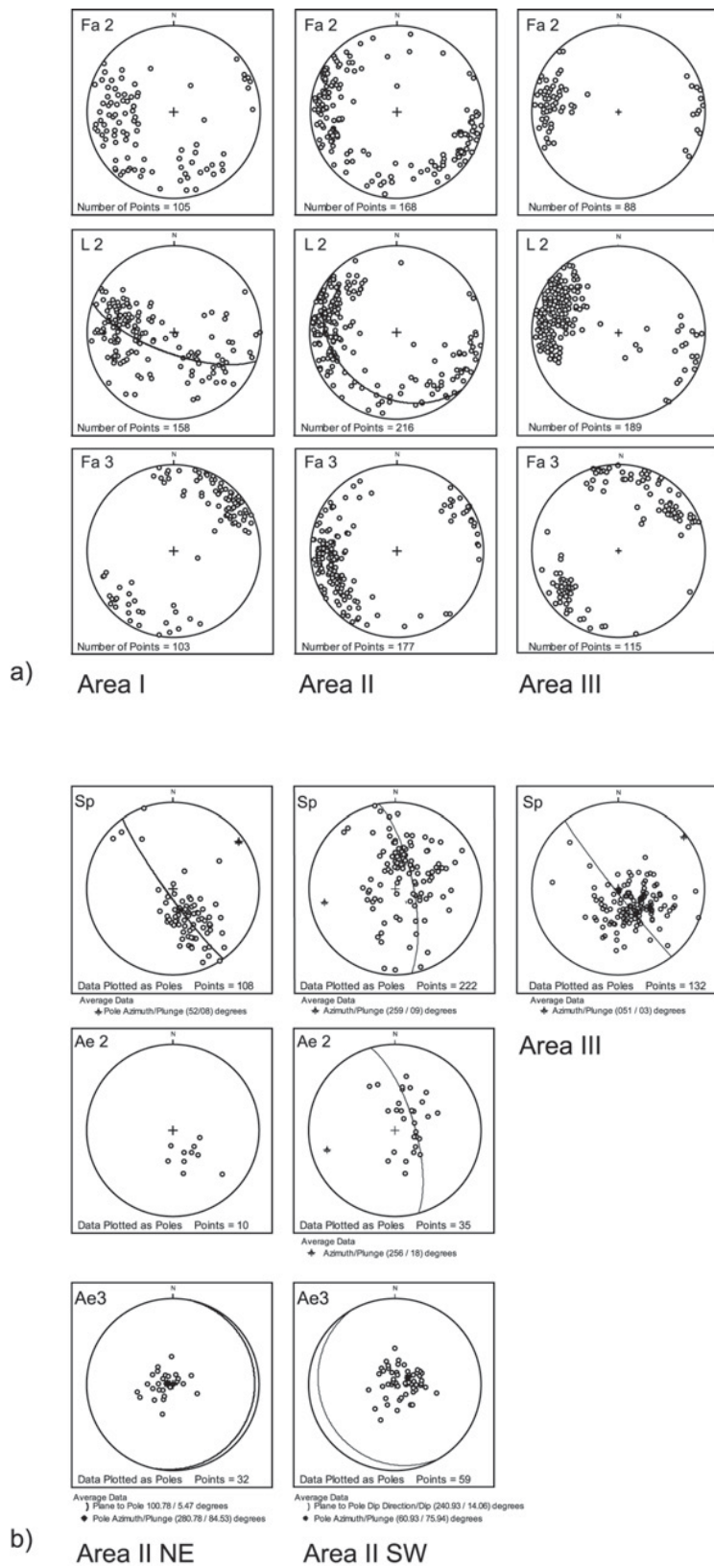


Fig. 6. Structural data from the study area, grouped in three areas. Area I: external part; Area II: central part; Area III: internal part; for locations see Fig. 5. a) Linear features Fa2, L2 and FA3; b) planar features Sp, Ae2 and Ae3; see Fig. 4 for abbreviations. Areas I, II and III, as well as the NW and SE part of Area II, are outlined in Fig. 5. Note that all the planar features from Area I are shown separately in Figure 4.

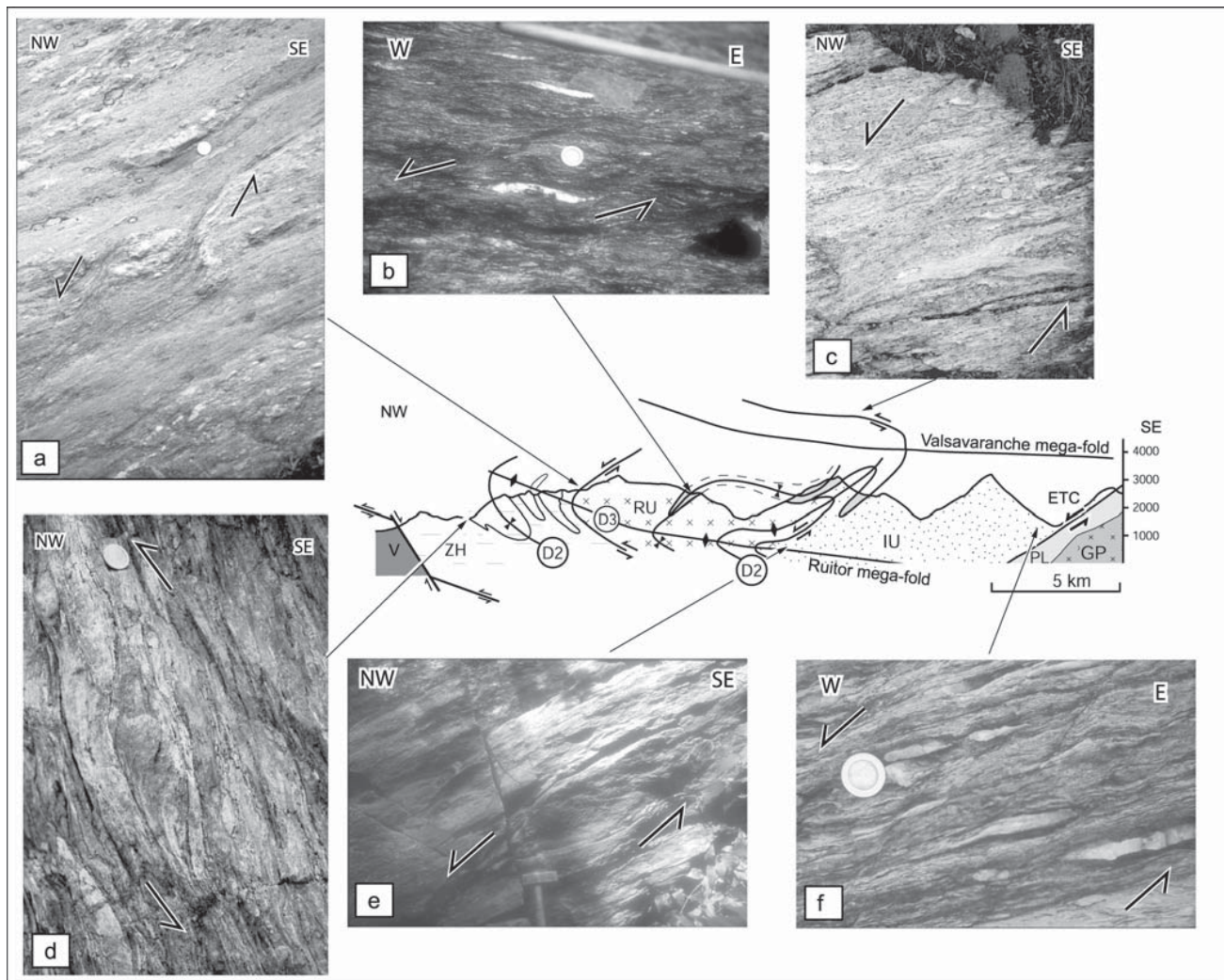


Fig. 7. Photographs illustrating kinematic indicators from different tectonic contacts: a) Top-W sense of shear in the Zone Houillère unit, at the contact with the Rutor unit (Glacier de l'Invernet); b) top-W sense of shear at the tectonic contact between the Piemont-Liguria Schistes Lustrés and the Rutor unit in the Avisa synform; c) top-W sense of shear in the uppermost Valgrisenche (Permo-Triassic cover of the Internal unit); d) top-W sense of shear in the Zone Houillère unit; note that the foliation is SE-dipping and hence schistosity and related senses of shear remained in their original orientation; e) tectonic contact between Rutor unit and Internal unit, also showing top-NW sense of shear (in the Rutor unit above Arvier); f) shear bands within the Internal unit in the Val di Rhêmes, near the Rifugio Benevolo (Permo-Triassic cover). Center: Cross section, modified after Bucher et al. (2003); V: Valaisan domain; ZH: Zone Houillère unit; RU: Rutor unit; IU: Internal unit; PL: Piemont-Liguria unit; GP: Gran Paradiso unit; ETC: Entrelor tectonic contact. See Bucher et al. 2003 for photographs of top-W sense of shear indicators from the ETC.

Deformation history

Overprinting patterns observed on the macroscopic (large-scale), mesoscopic (outcrop scale) and microscopic (large-scale), mesoscopic (outcrop scale) and microscopic scales (Fig. 3) indicate the existence of three major ductile deformation phases (D1 to D3). All three deformation phases are present in all investigated tectonic units. First order large-scale structures were mapped by using second order fold asymmetries of parasitic folds, and additionally, bedding-cleavage relationships. Transport directions were inferred

from mesoscopic or microscopic sense of shear criteria (Simpson & Schmid 1983).

While the separation into three mesoscopically and microscopically visible deformation phases is generally in agreement with the observations of other workers, who carried out detailed investigations on parts of the study area (Caby 1968, Baudin 1987, Cigolini 1995, Caby 1996), the significance of these different deformation phases on a macroscopic scale remains disputed. Hence the present-day overall geometry of the nappe stack is still in discussion (Bucher et al. 2003). Local

variations in the orientation of these structures and changes in the strain magnitude associated with the various deformation phases will be discussed later.

Pre-Alpine structures

The strong Alpine blueschist, and especially, a subsequent greenschist overprint (Baudin 1987), transposed most of the pre-Alpine planar features. Despite of this, two or three pre-Alpine amphibolite facies metamorphic events have so far been recognized within relict fold hinges found in the Ruitor unit (Desmons et al. 1999). While most other pre-Alpine minerals were destroyed during Alpine deformation, pre-Alpine garnet is often preserved, especially in the western and central parts of the Ruitor unit. Based on this observation it appears that Alpine deformation is weaker in the western and central parts of the Ruitor unit. Relics of a pre-Alpine metamorphic event were also preserved in the Internal unit (Cigolini 1981, 1995).

D1 structures

D1, the first Alpine deformation feature present in all the studied tectonic units, has largely been overprinted by subsequent deformations. On a mesoscopic scale the first foliation S1 is only preserved in F2 fold hinges (Fig. 3a). In thin section S1 is either defined by a relict foliation formed by chloritoid, phengite and garnet, preserved within D2 microlithons, or, as an internal foliation within garnet formed by phengite or chloritoid (Fig. 3e). This D1 mineral assemblage is associated with peak pressure conditions. Pressures range from 10–14 kbar (at temperatures around 400–450°C), as found in the Internal unit and the Ruitor unit, down to 5 kbar (at around 350–400°C), as described for the Zone Houillère unit (Bucher et al. 2003). However, no major D1 fold structures were observed at the large-scale in the study area.

D2 structures

D2 represents the major phase of deformation observed within the study area. The very penetrative D2 structures are characterized by tight to isoclinal folds, observable at all scales (Fig. 3a, c). While an older schistosity S1 is sometimes recognizable in D2-fold hinges, S1 becomes sub-parallel to the strong axial plane cleavage S2 in the F2 fold limbs (Fig. 3c). Hence, the main foliation in the area is a composite between S1 and S2 (Figs. 2, 4, 6). In the Internal unit the mineral assemblage garnet, phengite, epidote, chlorite and plagioclase is stable in the second schistosity, replacing the peak-pressure mineral assemblage. P-T estimates indicate that D2 is contemporaneous with decompression from 14 to 5 kbar at temperatures around 450–500°C (Bucher et al. 2003).

Plunging angle and azimuth of F2 fold axes are variable. A plunge from E-SE to W-NW is observed between the Houiller Front and the Valgrisenche, while F2 predominantly plunges to the W-NW in rest of the study area (Figs. 4, 5, 6). A strong

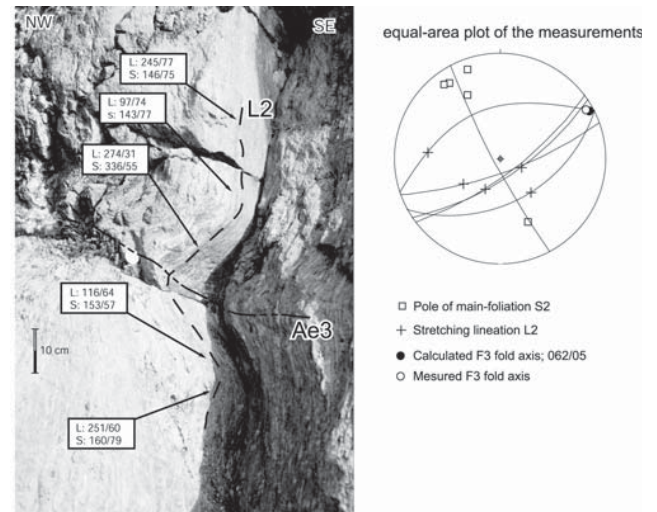


Fig. 8. D2 stretching lineation, refolded by M-type parasitic D3 folds, from the hinge of the Ruitor mega-fold in the Upper Conglomeratic Formation of the Houiller unit. Photograph and stereonet illustrate the variability of the plunge of L2 (between a SE- and a W-plunge, respectively), due to the overprinting by D3.

stretching lineation, defined by quartz and mica, is often observed to be oriented parallel to these fold axes (Fig. 3d). The transport direction, including that observed along the contact referred to as “Entrelor tectonic contact” (Bucher et al. 2003) or “Entrelor shear zone” (Butler & Freeman 1996), is consistently top-W-NW, as is indicated by shear bands and asymmetric porphyroclasts (Fig. 7a–f). The observed parallelism between fold axes and stretching lineations (Fa2 and L2 depicted in Fig. 3d, see also orientation data from Areas I to III in Fig. 6) indicates pervasive top-W-NW shearing during D2. Where fold axes and stretching lineations related to D2 are parallel, no inversion of the sense of shear occurs across D2 folds. Figure 4 shows the progressive change in orientation of the composite main foliation (Sp) from a SE-dip (sub-area a) to a predominate dip to the NW (sub-area d). This, together with the data given in Figure 6b, particularly the best fit great circle of the folded composite foliation (Sp), as well as the folding of axial planes of D2 (Ae2), points to overprinting during D3 folding around a NE-SW striking D3 fold axis (see also data on Fa3 given in Figure 6a). This is a clear indication that D3 folding strongly overprints the D2 structures.

The wide range in the orientation of L2 and F2 resulted from this overprinting by the third phase of deformation. The overprint manifests itself by the observation that L2 stretching lineations often plot on a great circle (Fig. 6a, Areas I and II). Direct observations, such as those pictured in Figure 8, show that the variation of the L2 stretching lineation within the hinge zone of a D3 fold is indeed due to D3 overprinting. Locally the variations in the orientation of Fa2 and L2 can be large (Figs. 4, 6), but a systematic variation is superimposed at a larger scale, as will be discussed later.

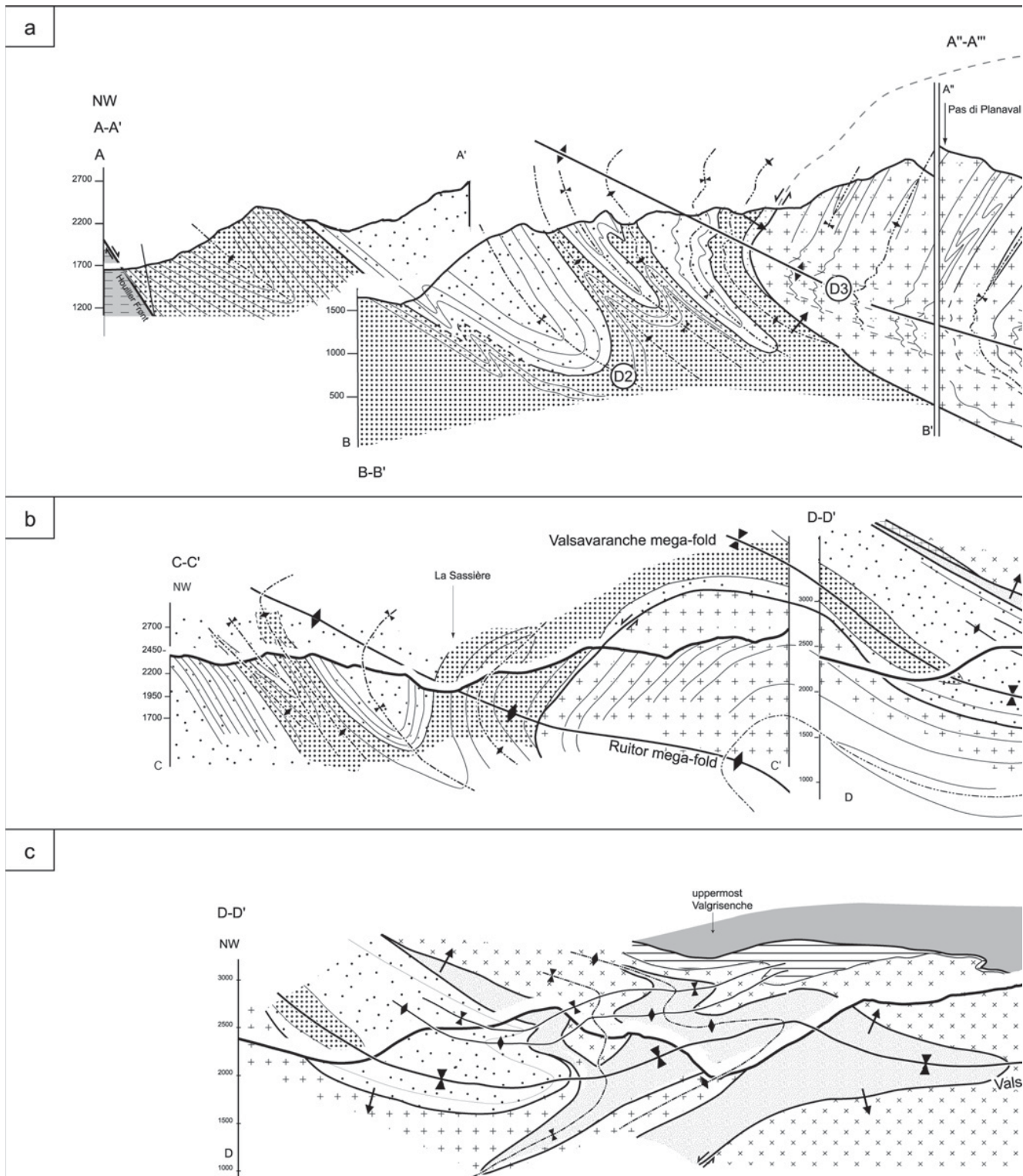
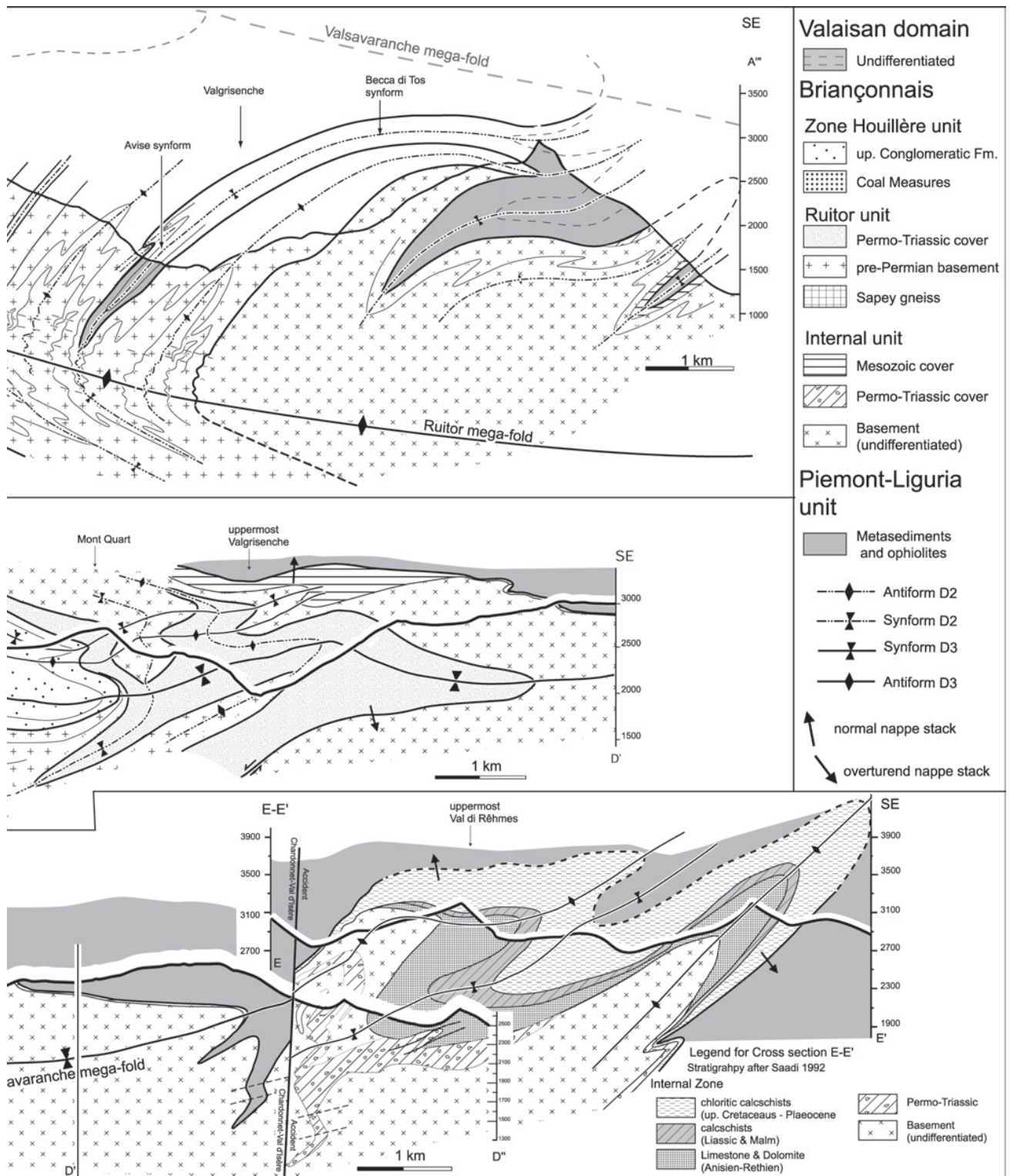


Fig. 9. Detailed cross sections (see Fig. 2 for traces of profiles). The detailed profiles were projected into a joint vertical plane, oriented perpendicular to the mean azimuth of the F3 fold axis (030, 055 respectively) and using an angle of projection given by the plunge of the F3 fold axes. Note that the post-D3 doming is taken into account by contouring the plunge of the F3 fold axes. All the individual cross sections were constructed by using the same procedure. The difference in the



orientation between the cross section A-A' to C-C' and D-D'' to E-E' is due to the changing orientation of the D3 fold axes. a) Cross section A-A', A''-A''' a B-B'; b) cross section C-C' and D-D'; c) cross section D-D', D-D'' and E-E'.

D3 structures

D3 is characterized by open parasitic folds that re-fold the composite S1/S2 main foliation (Fig. 3b–c). The fold axes related to D3 (Fa3) are generally NE-SW oriented and plunge moderately either to the NE or to the SW (Fig. 6a, Fig. 10). In general, the D3 axial planes gently dip to the SE with 5 to 20°, but dips to the SW or NE are also observed locally (Ae3 in Figs. 4, 6). An axial plane pressure solution cleavage is only locally established. Towards tectonically higher positions D3 folds become progressively tighter. The transport direction associated with D3 will be discussed later.

Discussion of the regional variability regarding orientation and strain intensity of D2 and D3 structures

In order to visualize the regional variation in the orientation of L2, Fa2 and Fa3, the study area was subdivided into the sub-areas indicated in Fig. 5.

Area I exhibits the largest variation in the orientation of L2 (Fig. 5). Note, however, that the external parts of Area I (see areas labeled a, b and c in Fig. 5) differ from the rest of the study area in that a large angle between the orientations of L2 stretching lineations and F2 fold axes (Fa2), respectively, is observed. While L2 and Fa2 are parallel in Areas II and III (see Fig. 6), they are often nearly perpendicular to each other in Area I (Fig. 4), particularly in the external parts (Zone Houillère near the Houiller Front. This difference is interpreted to be due to increasing D2-straining toward the SE. In fact, D2-folds become much tighter in this same direction (see cross section depicted in Fig. 9a). It is suggested that the amount of strain during D2 was not sufficient to parallelize F2 fold axes and L2 stretching lineations in the very external parts of the study area.

Apart from the variation regarding non-parallelism vs. parallelism between L2 and Fa2 discussed above, a systematic variation is observable over the entire study area regarding the orientations of L2 stretching lineations and F3 fold axes (Figs. 5 & 10). In the external part of the Zone Houillère unit, where the main foliation dips to the SE (Figs. 2, sub-areas a and b in Fig. 4), L2 stretching lineations scatter and mostly plunge to the SW or to the SE (Fig. 4, 5). In the internal part of the Zone Houillère unit, in the Ruitor unit and the Internal unit of the Valgrisenche, the main foliation generally dips to the NW (sub-area d in Fig. 4, Fig. 6). The L2 stretching lineations, which are here parallel to Fa2, change to a predominant plunge to the WNW (Fig. 5). Nevertheless, local variations interpreted to be due to the effects of D3 straining, are still observed as is seen from the stereoplot in Fig. 6a (Area II), which indicates a spread of L2 within a great circle. Closer to the Gran Paradiso massif, however, where the main foliation still dips to the NW, L2 is very predominantly ENE-WSW oriented (Fig. 6a, Area III), hence the great circle distribution disappears. This systematic variation is interpreted to be due to the fact that strain intensity associated with the third phase of

deformation, increases towards higher tectonic levels, i.e. towards the SE. Hence, increasing D3-strain led to an increasing amount of reorientation of L2 and F2 towards the ESE.

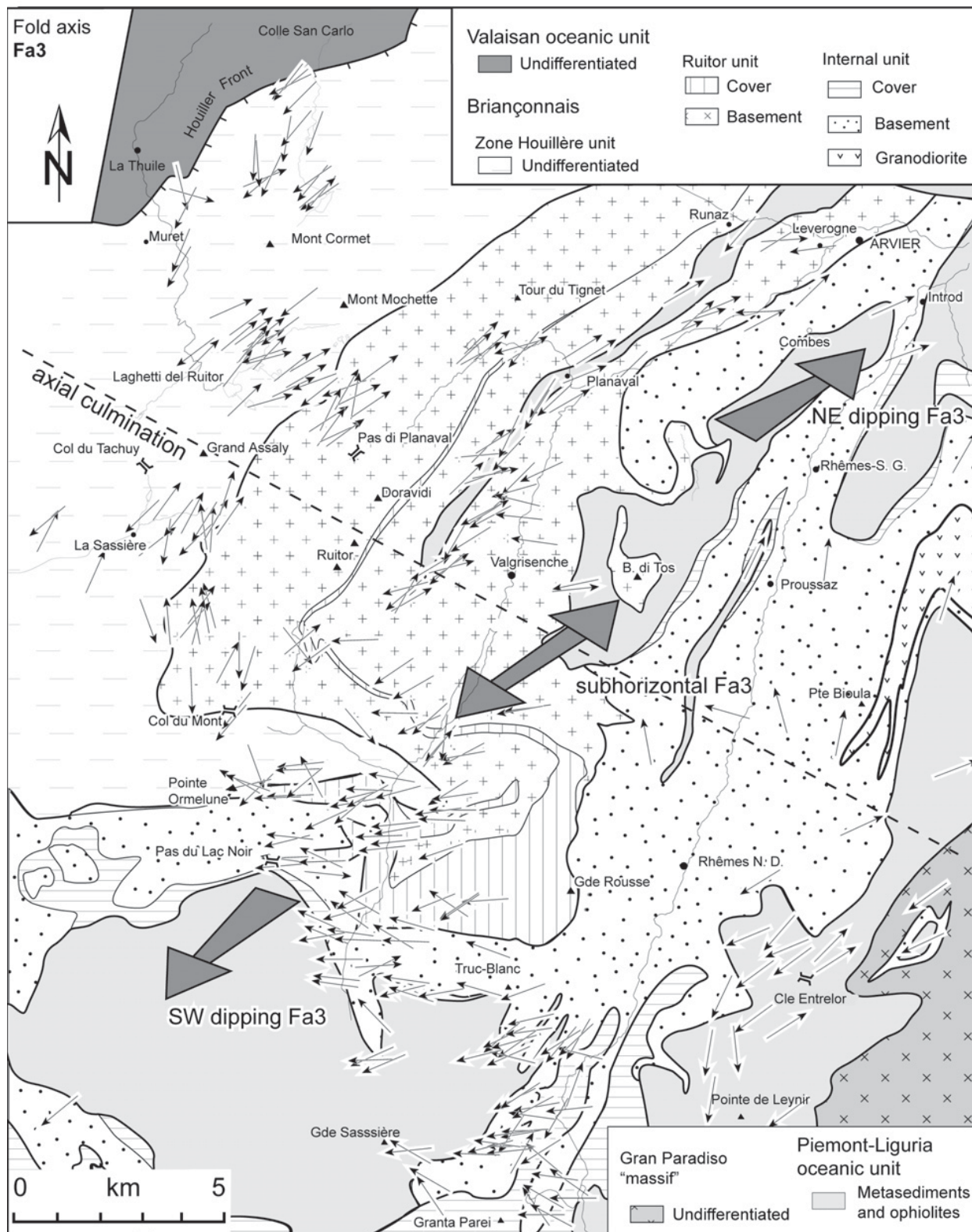
D3 fold axes (Fa3) either plunge to the NE or to the SW (Fig. 6a, Areas I to III; Fig. 10). This variation occurs along strike, rather than across strike, as was observed for D2 structures. In the northeastern part of the study area F3 fold axes plunge to the NE, while they plunge to the SW in the southwest (Fig. 10). A central region, within which D3 fold axes are sub-horizontal, separates these areas. This reflects late-stage (post-D3) doming on a kilometric scale, the Ruitor area forming an axial culmination. Doming can also be inferred from the variability of the D3 axial planes (Ae3), as is shown in Fig. 6b.

Sense of movement inferred for individual tectonic contacts during D1 and D2

The kinematics of movement along the tectonic contacts and the attribution of these kinematics to a specific deformation phase are crucial for understanding the evolution of the study area. Concerning the attribution to particular phases of deformation, field evidence clearly shows that all tectonic contacts outcropping in the study area were overprinted by the third deformation phase after their formation; hence they are either syn-D1 or syn-D2. The tectonic contacts analyzed in terms of kinematics are, from external to internal: contact between Zone Houillère unit and external Ruitor unit, contact between Ruitor unit and Internal unit, and the contacts between Piemonte-Liguria oceanic unit and Ruitor or Internal unit, respectively (Fig. 2).

Mesoscopic shear sense indicators are well preserved where overprinting by D3 folds is not too intense. Shear bands and rotated clasts consistently show top-WNW to top-NW kinematics (Fig. 7a–f). In such cases the senses of shear associated to the L2 stretching lineations characterize the kinematics of movement during D2. In case of the mylonites formed at tectonic contacts their foliation is parallel to the main foliation S2, and the stretching lineations define the kinematics of movement. Hence the kinematics of the tectonic contacts, indicating a top-NW sense of shear, can unequivocally be attributed to the second phase of deformation. Also note that D2 folding and shearing sub-parallel to L2 is contemporaneous, hence this D2 folding could not re-orient the sense of shear.

While all tectonic contacts in the study area were active during D2, relict D1 senses of shear were, however, identified at the tectonic contact between Ruitor unit and Internal unit. Microfabric analysis of preferred quartz c-axis orientation revealed different senses of shear for different layers within one and the same thin section (Fig. 11a shows a relict top-E shear sense). Top-WNW sense of shear, also deduced by quartz c-axis analysis, could be correlated with other criteria such as shear bands and sigma clasts, that are microscopically (Figure 11b) as well as mesoscopically visible and easily attributed to D2. Note that there is an independent observation indicating a pre- or early-D2 activity along the same tectonic



10. Map of F3 fold axis. Grey arrows display the geographic distribution of the dominant orientation of the F3 fold axes, evidencing late doming (D4).

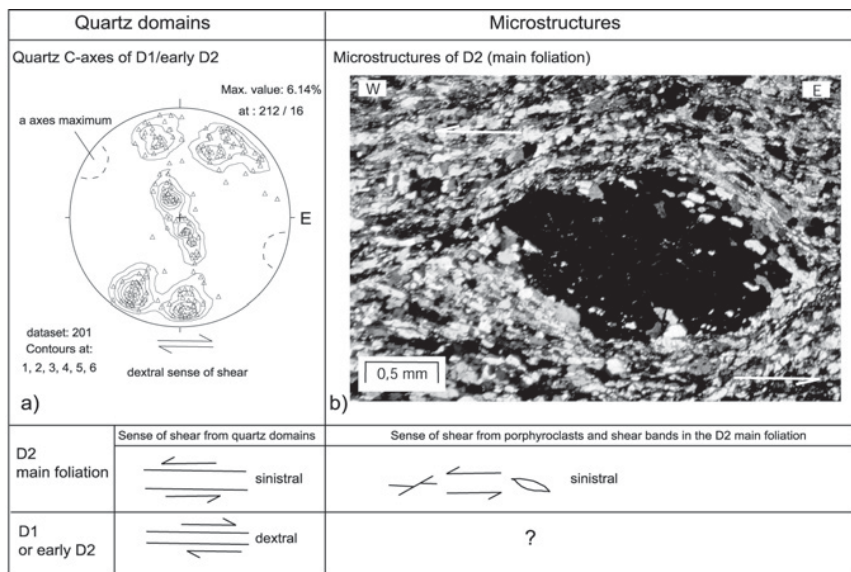


Fig. 11. a) Quartz C-axis preferred orientation, showing a relict D1 top-E sense of shear; b) sigma clast showing D2 top-NW transport direction along the tectonic contact between Ruitor unit and Internal unit (garnet-micaschists of the Ruitor unit from uppermost Valgrisenche).

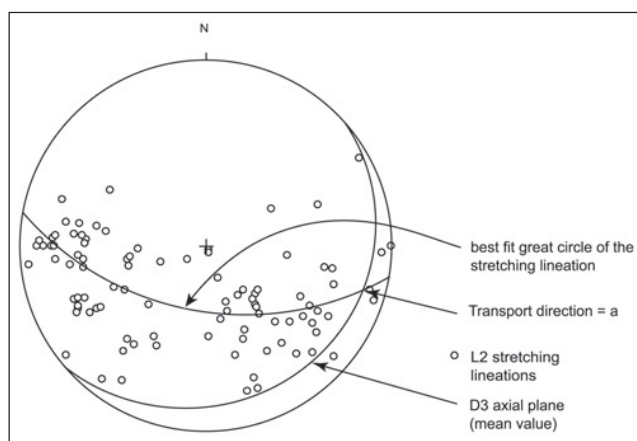


Fig. 12. Construction of transport direction for D3 using a fold in the Upper Conglomeratic Formation of the Houiller unit (after Ramsay & Huber 1987, their Fig. 22.7). Data cover the northeastern part of Area I shown in figure 5.

contacts: D2 folds, except for the contact between Ruitor unit and Zone Houillère unit, locally reformed all of them.

In summary, the studied tectonic contacts could have been already active during D1, or alternatively, during an early stage of D2. Since no L1 stretching lineations are preserved no conclusions can be made regarding the kinematics during D1. With respect to D2, the kinematics of movement is presently found to be top-WNW to top-NW. However, since L2 was re-oriented by D3 straining, as described earlier, the related syn-D2 kinematics must also have been systematically reoriented. The observed progressive reorientation towards the WNW, with increasing amounts of D3-strain, suggests original top-NW, or even top-NNW, shearing during D2.

Transport directions associated with D3

Since no stretching lineation did form during D3, the transport direction cannot be directly inferred. The simple assumption, that the transport direction is perpendicular to the fold axis is not justified, because D3 folds are shear folds, as is indicated by the observation that L2 lineations plot on a great circle (Fig. 12). However, construction of the slip vector “a” active during D3 folding (Ramsay & Huber 1987; their Fig. 22.7) suggests that the transport direction strikes E-W to ESE-WNW (Fig. 12). Note that the polarity of shearing cannot be deduced by this method. Hence this direction could be compatible with the classical postulate of back-thrusting towards the ESE, (i.e. Butler & Freeman 1996). However no stretching lineations or shear zones connected to D3 were observed and large-scale observations, discussed below, do in fact indicate top-WNW transport during D3.

Cross sections and regional structures

Six detailed cross sections (see Fig. 2 for location) were projected into the three combined cross sections depicted in Fig. 9. These combined cross sections will now be discussed in order to examine the large-scale structure of the Briançonnais in the Italian-French Western Alps.

Combined cross sections A-A', A''-A''' and B-B' (Fig. 9a)

This first set of cross sections (Fig. 9a) runs NW-SE, from the Houiller Front in the area of the Petit Saint Bernard pass to the Val di Rhêmes (Fig. 2). Near the Houiller Front, the main foliation (S2) dips to the SE (Fig. 2, sub-areas a and b in Fig. 4). At the earth's surface S2 gradually gets steeper and finally sub-vertical by going towards the tectonic contact with

the Ruitor unit (Fig. 2, sub-areas c and d in Fig. 4). In the northwestern part of section B-B' (Fig. 9a) D3 fold vergency indicates a large scale, northwestward closing antiform situated further to the SE. Where the main foliation is found in a sub-vertical orientation, M-type D3 folds within the Zone Houillère unit indicate the major hinge of a D3 fold. Still within the Zone Houillère, but close to the contact with the Ruitor massif (southeastern part of the cross section B-B' in Fig. 9a) the main foliation changes into a predominant dip to the NW (Figs. 2, 6b) and D3 fold vergency also changes (Fig. 3b). This change in fold vergency is associated with a mega-fold situated within the Ruitor unit (Fig. 9a, southeastern part of section B-B'): the D3 Ruitor mega-fold. The M-type D3 folds mentioned above represent the hinge zone of this Ruitor mega-fold. It is the gradual change in dip of the S2 foliation from a SE dip towards the internal zone that is referred to as "fan-structure" in the literature. However, this "fan-structure" is simply a geometric effect caused by the large-scale D3 Ruitor mega-fold with its flat-lying, gently SE-dipping axial plane.

Along this profile and within the Zone Houillère unit, several large-scale F2 folds are evidenced (Fig. 9a, profiles A-A', B-B'). The axial plane of the easternmost F2 fold is cut by the contact between the Zone Houillère unit and the Ruitor unit. This indicates that this contact is a tectonic one, and that it was still active after D2 folding, i.e. during a late stage of D2. This tectonic contact is, however, refolded by the D3 Ruitor mega-fold. Sedimentological younging criteria indicating younging of the Zone Houillère unit towards the Ruitor unit (Mercier pers. comm. and own observations) indicate that the internal parts of the Zone Houillère unit are in an overturned position. Hence the tectonic contact on top of the Zone Houillère unit, situated in the lower limb of the Ruitor mega-fold, must represent the late-D2 basal thrust of the Ruitor unit onto the Zone Houillère unit.

The Ruitor unit is characterized by a dominant dip of the main foliation (S2) to the NW at the earth's surface. While the D2 antiform situated immediately NW of the Pas di Planaval (Fig. 9a) was already evidenced by Baudin (1987), the first D2 synform found SE of the Pas di Planaval was recognized as a band of Permo-Triassic cover, pinched within the basement of the Ruitor unit, by Caby (1996) (see Fig. 9a, profile A''-A''').

The sediments in this synform play an important role for understanding the large-scale structure of the area. Firstly they independently indicate, besides the evidence described earlier and derived from the facing of the D2 folds from the Zone Houillère, that the Ruitor unit is not the basement of the Zone Houillère. It is this Permo-Triassic cover, lacking Carboniferous deposits and found within a narrow syncline, that represents the cover of the Ruitor basement. Secondly, while different authors (Gouffon 1993, Caby 1996) interpreted the footwall of this Permo-Triassic cover to represent a tectonic contact between "external" and "internal" Ruitor units, the two are simply separated by a narrow D2 upward- and SW-facing syncline, reoriented in the upper limb of the Ruitor mega-fold by D3. This interpretation was recently confirmed by Ullard

(2001), who mapped a synform along the southern continuation of the same cover sequence in the upper Valgrisenche, based on the litho-stratigraphy of the Permo-Triassic sediments. In summary, external and internal Ruitor unit represent the same tectono-metamorphic unit, refolded by F2. This confirms the view of Desmons & Mercier (1993), who pointed out the important role of the intensity of the D2 retrogression, increasing towards the SE. Note that the cross section confirms the increasing intensity of the deformation during D2, expressed by the tightening of the D2 folds towards the SE (Fig. 9a, B-B').

The structures analyzed further to the SE are those which were previously described by Cigolini (1995) and Caby (1996). The synform formed by a D1-thrust at the base of the P-L oceanic unit, that appears pinched within the Ruitor unit (immediately NW of Valgrisenche in profile of Fig. 9a), corresponds to the D2 "Avisé synform" described by Caby (1996). This D2-structure refolds the D1 thrust of the P-L oceanic unit onto the Briançonnais domain and finds its south-eastern continuation within the flat lying P-L sediments below the klippe of the Becca di Tos (Dal Piaz 1965) at the SE end of the profile of Figure 9a.

The change from steeply NW-dipping main (S2) foliations in the profile of Figure 9a to flat-laying foliations further to the SE is an effect of large-scale folding during the third phase of deformation. D3 large-scale folding is responsible for the right-way up and SE-dipping nappe stack observed in the external part of the cross section. The area with the sub-vertical dip of the S2 main foliation, observed further to the SE, represents the hinge zone of the D3 Ruitor mega-fold. The internal part of this cross section, characterized by a NW-dip of the main foliation, exhibits an overturned nappe stack. In summary, the overturning of the nappe stack is due to the formation of the Ruitor mega-fold during D3.

Note that the Ruitor mega-fold is a backfold with a flat lying axial plane, comparable to the Mischabel backfold (Müller 1983) of the Zermatt area, and analogous to what is observed around the Niemet-Beverin fold of the Briançonnais-type Schams nappes of eastern Switzerland (Schmid et al. 1990, Schreurs 1993). It is, however, not a backfold that is necessarily kinematically linked to backthrusting, such as the Vanzone antiform of western Switzerland that formed later in respect to the Mischabel backfold (Kramer 2002). Furthermore the hinterland-dipping axial plane is not compatible with a classical model of backfolding associated by backthrusting.

Combined cross sections C-C' and D-D' (Fig. 9b)

This combined cross section is situated further to the SW (Fig. 2). Due to an axial plunge to the SW (Area II SW in Fig. 6b), associated with post-D3 doming, the structurally highest levels of the study area are exposed along its trace. The profile, running through the uppermost Valgrisenche (Fig. 2), features a second and structurally higher large-scale D3 fold, the Valsavaranche mega-fold closing to the SE. Note that the

“type locality” of this “Valsavaranche mega-fold” occurs much further to the NE, i.e. in the lowermost Valsavaranche (Fig. 2), as will be discussed later.

The northwestern part of this cross section (C-C' in Fig. 9b) displays structures similar to those discussed in the section of Fig. 9a. In part D-D' of this section, however, the axial trace of the Valsavaranche mega-fold enters the profile, as is evidenced by a synform with the Zone Houillère unit in its core, surrounded by basement and cover of the Ruitor unit (Figs. 2 & 9b).

Note that the Permo-Triassic cover sequence, which crosses the uppermost Valgrisenche, and which is attributed to the Ruitor unit in this study (Figs. 2 & 9b), was classified as the Permo-Triassic cover of the Internal unit in the map by Debelmas et al. (1991b). We did not follow this interpretation since the Internal unit (Vanoise-Mont Pourri unit as defined by French authors) has its own sedimentary cover, including a Permo-Triassic sequence at the base. This cover is however outcropping at a higher structural level in this section (Fig. 9b), i.e. directly below the northern end of the klippe formed by the Piemont-Liguria unit at the Gde Sassièr (Fig. 2). Note also that Debelmas et al. (1991b) interpret the Sapèy gneiss outcropping to the west of the Pointe Ormelune (Fig. 2) to continue eastwards and into the profile trace of section D-D' (Fig. 9c). Own field observations, however, clearly indicate that leucocratic rocks interpreted as Sapèy gneiss are in fact part of the upper Conglomeratic Formation of the Zone Houillère unit (Fig. 2).

Further to the SE along the same profile (SE of uppermost Valgrisenche, Fig. 9b) the large-scale D3 Valsavaranche mega-fold is seen to fold the contact between the Permo-Triassic cover of the Ruitor unit (in agreement with all authors) and the basement of the Internal unit. Between Mont Quart and uppermost Valgrisenche this same tectonic contact between Ruitor unit and Internal unit is also folded by D2 large-scale folds.

Near the southeastern termination of profile D-D' in Figure 9 the Permo-Mesozoic cover of the Internal unit is again overlain by the P-L oceanic unit of the Grande Sassièr klippe. This is clear evidence that the nappe stack is right-way-up in the upper limb of the D3 Valsavaranche megafold. The complete nappe pile formed during D1 and D2 consisted of, from base to top, Zone Houillère unit, Ruitor unit, Internal unit and P-L oceanic unit. It is preserved in this profile in its original orientation in the “normal” upper limb of the Valsavaranche mega-fold only.

Combined cross sections D-D'' and E-E' (Fig. 9c)

At the south-eastern end of cross section D-D'' (Fig. 9c) the axial trace of the Valsavaranche mega-fold is seen to run into the P-L oceanic unit. Immediately further to the SE, however, it is cut by a young vertical tectonic contact already described by Marion (1984). Unfortunately the kinematics of this brittle fault, largely sealed by Quaternary cover, remains unknown.

To the SE of this fault, as shown in cross section E-E' (Fig. 9c), lithologies and structures are changing. Instead of the

relatively thin Permo-Mesozoic cover sequence of the Internal unit found NW of this fault, a thicker Mesozoic sequence is present here, characterized by a well-defined stratigraphy comprising Triassic to Paleocene sediments (Jaillard 1989 & 1990, Saadi 1992). On a larger scale this sedimentary sequence belongs to the “série Val d'Isère – Ambin” defined by Ellenberger (1958).

Laterally and towards the SE this rather complete Triassic to Cretaceous sequence is wedging out, except for the upper Cretaceous-Paleocene sequence that is found to still mark the contact of the basement of the Internal unit with the P-L oceanic unit at the south-eastern end of profile E-E' (Fig. 9c). This reflects a lateral facies change which is well known in the Briançonnais and due to multiple erosion events (Jaillard 1989, 1990) that characterize this paleogeographic domain. The structural map (Fig. 2) is partly based on detailed studies carried out in this particular region by Adatte et al. (1992) and Saadi (1992).

In profile E-E', i.e. SE of the subvertical fault mentioned above, the Valsavaranche mega-fold is defined by an M-shaped fold triple. The pair of antiforms with a synform in the middle indicates that the axial trace of the D3 Valsavaranche mega-fold dips to the NW at the south-eastern end of this cross section. The lower limb of this backfold with a foreland dipping axial plane is formed by the P-L oceanic unit that underlies the Internal unit and hence indicates an overturned nappe stack observable at the south-eastern end of profile E-E'. The overturned cover sequence of the Internal Zone (Fig. 9c) confirms this observation. This overturned D2-thrust of the P-L oceanic unit over the Internal zone (“Entrelor tectonic contact”; Bucher et al. 2003) can be followed along strike to the NW and into the area around the Col d'Entrelor. As discussed in Bucher et al. (2003) the observed top-W-NW sense of shear along this overturned thrust excludes back-thrusting along this contact, referred to as “Entrelor shear zone” by Butler & Freeman (1996) and interpreted as a backthrust by these same authors, in spite of clear evidence for top-W-shearing (Caby 1996).

The Valsavaranche mega-fold found near the south-eastern termination is responsible for the existence of a klippe of P-L oceanic unit in the Grande Sassièr area (Fig. 2). This klippe is connected with the rest of the P-L oceanic unit that underlies the Internal unit around the M-shaped hinge-zone of this backfold (Fig. 9c). The D3 folds, which define the Valsavaranche mega-fold, can be followed southward and are correlated with folds described by Marion (1984) in the Val d'Isère.

Summary and interpretation of the large-scale structures

The cross sections of Figure 9 indicate large-scale refolding of the original D1/D2 nappe stack by two D3 mega-folds. This nappe stack is overturned in an area between the axial planes of these two mega-folds.

The structurally lower of the two mega-folds is the west-closing Ruitor mega-fold, found in the external part of the investigated area, where it affects the composite S1/S2 main foliation. The gradual change in dip of the S1/S2 main schistosity

defines a “fan structure” which is only apparent since it is due to the large-scale D3 Ruitor mega-fold. This fold, characterized by a flat-lying axial plane, overturns the entire nappe stack in its upper limb (Fig. 9a).

We localized a second and structurally higher major D3 mega-fold in the uppermost parts of Valgrisenche and Val di Rhêmes (Fig. 9b, Fig. 2). This second mega-fold closes towards the east and brings the entire nappe stack back into an upright position, such as observed in the uppermost part of the Valgrisenche (i.e. in the Grande Sassiè area). This hitherto undetected D3 mega-fold (Fig. 9b–c) is laterally correlated with the well-known Valsavaranche “backfold” described by Argand (1911), which also is an eastward closing fold, whose axial trace was mapped in the lower Valsavaranche and in the Val di Cogne (Fig. 2). Although the Valsavaranche mega-fold is a backfold in the sense that it locally exhibits a foreland-dipping axial plane, it is by no means kinematically linked to back-thrusting. Basically, it just represents the structurally higher of a pair of flat-lying folds. This fold pair exhibits an asymmetry in the sense of mega-scale vergency. However, fold vergency does not indicate the overall sense of shearing (Ramsay & Huber 1987) and thus top-SE shearing cannot be directly deduced from the observed fold geometry (see later discussion). The dip to the foreland of the axial plane is only pronounced at the SE end of the profile of Fig. 9c and due to the late-stage culmination of the Gran Paradiso massif (D4).

The Valsavaranche mega-fold, evidenced by this study in the profile of Fig. 9c, and the Valsavaranche backfold of Argand (1911) occupy identical structural tectonic positions. This can be seen from the fact that the axial trace of the same east-closing mega-fold visible in the profile of Fig. 9c projects immediately above topography at the SE end of the profile of Fig. 9a (compare also Fig. 2). However, due to post-D3 doming (D4), culminating in the Ruitor-area, the trace of the axial plane of this mega-fold is not continuous along strike (Fig. 2). This is in line with the plunge of the fold axes of the third phase of deformation, as can be inferred from Fig. 10. Because of its position NE of the axial culmination, the axial plane of the Valsavaranche mega-fold of the northern and lower parts of the Val di Rhêmes and Valgrisenche dips to the NE (Fig. 2). The lower parts of these two valleys expose the upper limb of the Valsavaranche mega-fold and therefore a right-way-up nappe stack. This same normal nappe stack, structurally situated above the axial trace of the Valsavaranche mega-fold, is also found north of the Aosta fault, which cuts the axial trace of this mega-fold (Fig. 2 and Gouffon 1993). The change of dip of the axial trace of the Valsavaranche mega-fold into the SW-dip observed SW of the Ruitor axial culmination causes the axial plane of the Valsavaranche mega-fold to crop out again in the uppermost parts of the Val di Rhêmes and Valgrisenche (Fig. 2, Fig. 9c). There, i.e. in the Grande Sassiè area, an upright nappe stack is exposed in the upper limb of this same D3 fold.

All tectonic contacts between the constituents of the D1/D2 nappe stack consisting of, from bottom to top, Zone Houillère unit, Ruitor unit, Internal unit and P-L oceanic unit,

are former thrusts, and none of them are back-thrusts. These thrusts were refolded by a pair of D3 mega-folds. The refolding around a NE-SW-oriented axis, approximately perpendicular to L2, that is associated with top-NW senses of shearing, led to the preservation of the thrust-related kinematic indicators, even where former nappe contacts are overturned.

Occasionally, large-scale folding of the nappe contacts is also observed during D2 (i.e. central part of profile in Fig. 9b). While this D2-folding is pervasive and synchronous with the top-NW kinematics deduced for all D2 tectonic contacts, the kinematics of movement during D1, when these tectonic units constituting the nappe stack were first juxtaposed, remains unknown.

Discussion

Despite numerous previous studies, no consistent picture of the large-scale tectonic structure of the Italian-French Alps was available so far, although the successive deformation phases were recognized and described on a meso- and microscopical scale by most previous workers. Many of these studies only addressed individual tectono-metamorphic units. The structural data presented by this study, however, cover a significant portion of the tectonic units attributed to the Briançonnais domain along a major geological-geophysical transect through the Western Alps: the ECORS-CROP profile (Nicolas et al. 1990, Roure et al. 1996, Schmid & Kissling 2000). Furthermore the individual deformation phases can now be better tied to the metamorphic evolution (Bucher et al. 2003).

The finding that external Ruitor and internal Ruitor (or Zone de Leverogne after Gouffon 1993) are part of the same tectono-metamorphic unit is in agreement with Desmons & Mercier (1993), but contrasts with the interpretation of Gouffon (1993). However, the latter author makes a question mark regarding the attribution of the internal Ruitor (Zone de Leverone) to the Siviez-Mischabel nappe (Thélin et al. 1993). Furthermore the internal Ruitor has no continuation north of the Aosta fault (Fig. 1 of Gouffon 1993). Hence we suggest that there is only one Ruitor unit, and that this unit represents the southern continuation of the Pontis nappe of Western Switzerland (Gouffon & Burri 1997) to the south.

Many aspects of the large-scale geometry of D3 nappe refolding (Ruitor mega-fold and Valsavaranche mega-fold) remained undetected, except for parts of the Valsavaranche backfold, already described by Argand (1911), and parts of the Ruitor fold, described by Baudin (1987). On the other hand, we found no evidence for back-thrusting, claimed to be of major importance for the large-scale structure of the Western Alps by many authors (i.e. Butler & Freeman 1996). Hence, nappe refolding (D3) is the dominant mode of late stage deformation in the Western Alps (Bucher et al. 2003). The significance and origin of nappe refolding and related geodynamics depend on the relation between backthrusting, backmovement and backfolding. Classically, two phases of backfolding are known from the Penninic units of Western

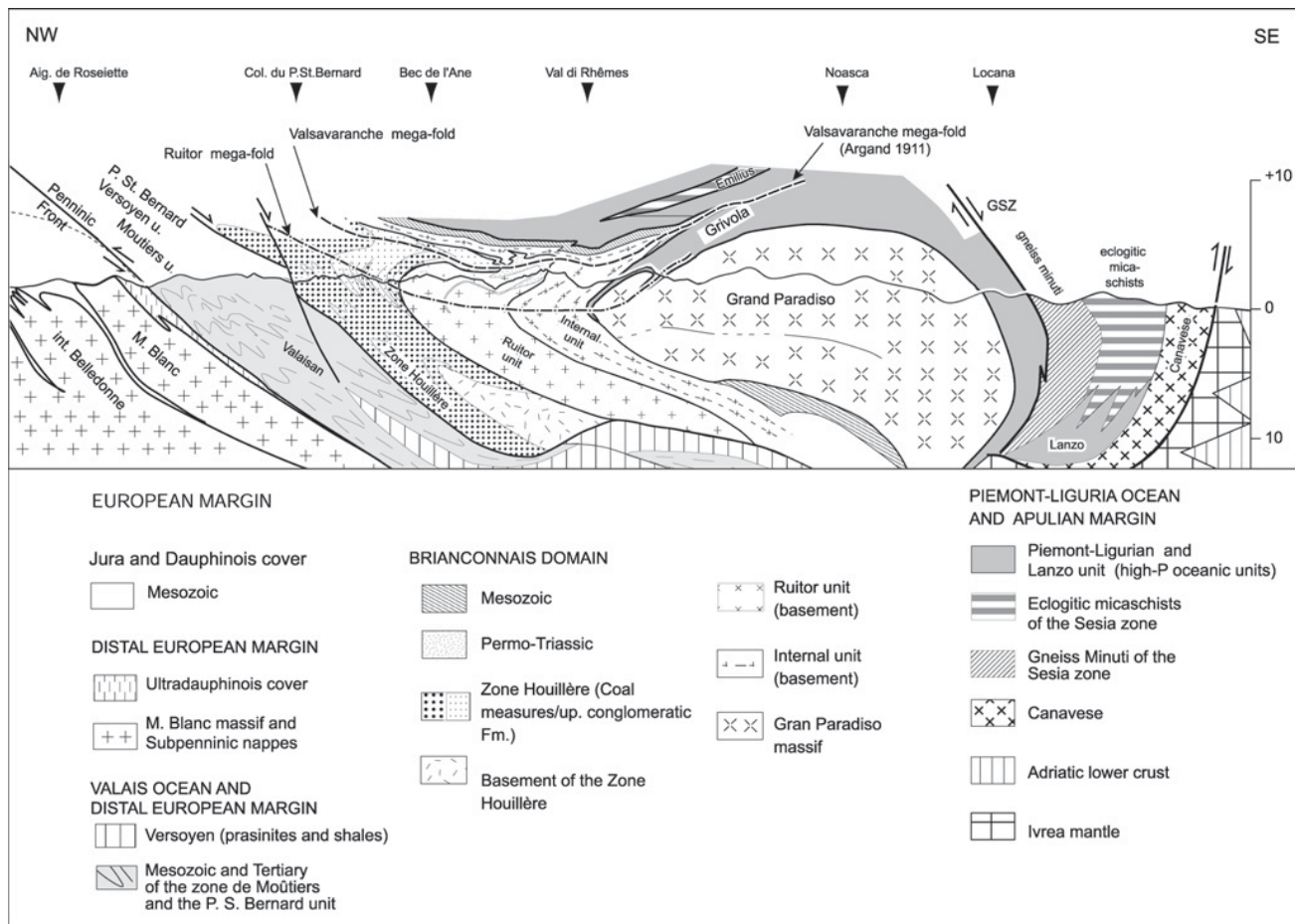


Fig. 13. Cross section along the ECORS-CROP seismic line (profile trace indicated in Figs. 1 & 2), modified after Schmid & Kissling (2000), depicting two large-scale post-nappe folds at the scale of the orogen. GSZ: Gressonney shear zone.

Switzerland and adjacent Aosta valley (e.g. Milnes et al. 1981). During a first phase of backfolding (D3) the Mischabel backfold, characterized by a flat-lying axial plane, develops. The associated sense of shear of D3 structures varies between top-SE and top-SW and parts of this shearing are associated with orogen parallel extension (Keller & Schmid 2001). This is in contrast to the second phase of backfolding, the Vanzone phase (D4), characterized by a steeply foreland-dipping axial plane and directly associated to backthrusting “s. str.” along the Insubric line (Schmid et al. 1987, Kramer 2002). As shown by various authors the first (D3) backfolding phase is not necessarily kinematically linked to back-thrusting or back-movement (Pfiffner et al. 2000, Escher and Beaumont 1997, Ring 1995). However, the question if D3 led to overall backmovement along the ECORS-CROP seismic line still remains. It is argued, that such backmovement is only locally observed. Instead the large scale nappe refolding is interpreted to be due to NW-wards extrusion of the Gran Paradiso in profile view. This extrusion leads to vertical shortening and results in

the relative movement of the overlying units, i.e. the internal Briançonnais, towards the hinterland. The consequences of this relative backmovement are D3 megafolds with flat-lying axial planes. These D3 megafolds are best explained by extrusion induced backfolding in an overall compressional regime. Therefore, although a relative movement towards the hinterland results, the D3 megafolds are not interpreted to have formed in the same geodynamic context as the younger Vanzone phase back-folding and back-thrusting. The latter indicates an overall hinterland directed transport direction of the entire nappe stack.

In conclusion we suggest that the geodynamic context of the two classical backfolding phases is different. The first backfolding phase (D3 mega-folds) develops during the north-(west)ward extrusion of the internal crystalline massifs, which is linked to local, hinterland directed back-movement and vertical shortening. In contrary, the second backfolding phase (Vanzone) results from overall hinterland directed kinematics, directly associated with backthrusting. Similar models are

Tab. 1. Table showing correlation of deformation phases and timing constraints. Strain gradients and inferred geodynamic processes are also shown.

Geodynamic process	Zone Houillère unit	Tectonic contact	Ruitor unit	Tectonic contact	Internal unit	Tectonic contact	P-L oceanic unit	Age (after Bucher et al., sub.)
Late doming	D4		Only evidenced by the changing D3 features (F3, S3) on kilometric scale		Only evidenced by the changing D3 features (F3, S3) on kilometric scale		Only evidenced by the changing D3 features (F3, S3) on kilometric scale	? (< 31 Ma, FT from Hurford & Hunziker, 1989)
Strain gradient		→	Increasing strain towards the SE					→
Large scale nappe refolding	D3		Open folds with a poorly developed, gently dipping (< 25°) axial plane cleavage	folded	Open folds with a poorly developed, gently dipping (< 25°) axial plane cleavage	folded	Open folds with a poorly developed, gently dipping (< 25°) axial plane cleavage	35-31Ma
Strain gradient			tightening of D2 fold		-		-	
Exhumation to greenschist facies	D2		Main schistosity = S1/S2 composite foliation; isoclinal folds	late D2 top W-NW thrusting	Main schistosity = S1/S2 composite foliation; isoclinal folds	early D2 top W-NW thrusting	Main schistosity = S1/S2 composite foliation; isoclinal folds	43-35 Ma
Suduction & peak pressure	D1		S1schistosity; isoclinal folds	-	S1schistosity; isoclinal folds	relics	S1schistosity; isoclinal folds	50-43 Ma

available for the Monte Rosa area (Ring 1995) and supported by the modeling of Merle & Guillier (1989).

The new findings described in this contribution ask for a modification of the ECORS-CROP profile published by Schmid & Kissling (2000). Figure 13 shows the modified version of this section, based on the data presented in the cross sections of Fig. 9. It exhibits three main features.

Firstly, this section clearly depicts the correlation of the Valsavaranche mega-fold described for our working area with the Valsavaranche backfold of Argand (1911). Note, that the trace of this mega-fold can be followed along the profile by some 30 km (Fig. 13). Hence it represents a major feature at the scale of the orogen.

Secondly, the profile shows that the original nappe stack was overturned over the same distance of about 30 km across strike, but only between the axial traces of the two mega-folds. Note that the area between these axial planes is characterized by foreland-dipping foliations and tectonic contacts. This nappe stack is bent back into a right-way-up position around the Valsavaranche mega-fold. This implies that no late stage thrusting (such as proposed by Butler & Freeman 1996 and Caby 1996) is needed to explain presence of a normal nappe stack in frontal and structurally highest parts of the internal Western Alps, such as preserved in form of the Grande Sassière klippe, or in form of the outcrops of the P-L oceanic unit found north of the Aosta valley (Fig. 2).

Thirdly, the modified cross section suggests that the Ruitor mega-fold may be continued subsurface to the SE for some considerable distance, before it reaches the earth's surface

again within the frontal parts of the Gran Paradiso massif. This is due to the changing dip of the axial plane, caused by the late doming of the Gran Paradiso massif. The axial plane of the Ruitor mega-fold runs into the Gran Paradiso unit across an earlier formed (D2?) synform, made up of the P-L oceanic sediments of the Grivola (Fig. 13). This deduction, together with the structural data of Vearncombe (1985), suggests the existence of a normal nappe stack on top of the Gran Paradiso unit, and it also confirms that the Gran Paradiso unit is part of the Briançonnais paleogeographic domain.

Large portions of overturned nappe stacks, linked to large-scale nappe refolding, are described along the entire Alpine arc. Similar large-scale nappe refolding and refolded tectonic contacts have been described for the southern Western Alps (Tricart 1984, Philippot 1990, Henry et al. 1993). The Mischabel and related late stage folds of the western Swiss Alps (Müller 1983, Keller & Schmid 2001, Kramer 2002) and the Niemet-Beverin fold of the Schams nappes in the central Swiss Alps (Schmid et al. 1990, Schreurs 1993) are other examples. Hence, this large-scale nappe refolding is an important and common late-stage tectonic feature of the post-collisional evolution of the Alps. Evidently, this feature goes along with vertical shortening, given the flat-lying axial planes of the late-stage mega-folds mentioned above. Note that the flat-lying axial planes of all these folds are in contrast with the steeply dipping axial planes of the classical backfolds, that are related to backthrusting along the Insubric line (Schmid et al. 1987), such as the Vanzone antiform, formed later in respect to the Mischabel backfold (Milnes et al. 1981). Furthermore, note

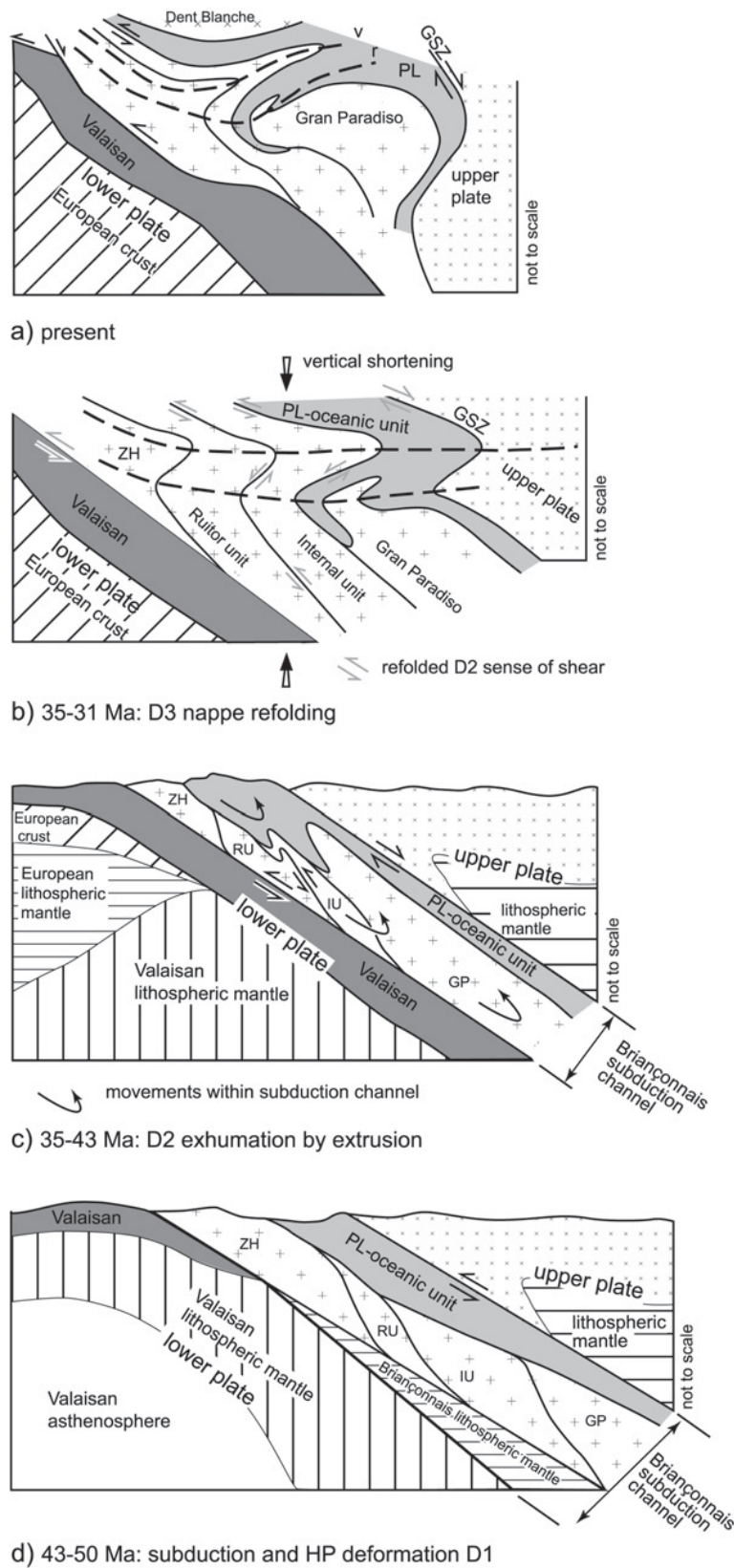


Fig. 14. Sketch of the tectonic evolution, modified after Bucher et al. (2003): a) Present situation; b) Evolution of D3 large-scale nappe refolding; note refolding of the nappe contacts without inversion of the sense of shear; similar structures are shown in the models of Pfiffner et al. (2000). c) Exhumation by extrusion within and parallel to the subduction channel (D2); note that exhumation takes place during the final stages of nappe stacking; also note that the sense of shear on top of the subduction channel is inverted in respect to the situation during the subduction; displacement vectors within the subduction channel derive from the models of Burov et al. (2001). d) Subduction and deformation under peak metamorphic conditions. Abbreviations are: r: Rutor mega-fold; v: Valsavaranche mega-fold; GP: Gran Paradiso massif; DB: Dent Blanche unit; PL: Piemont-Ligurian oceanic unit; ZH: Zone Houillère unit; RU: Rutor unit; IU: Internal unit; GSZ: Gressoney shear zone.

that no evidence for back-thrusting or normal faulting was found anywhere in the working area.

While the interpretation of the present geometry can largely be explained by D3 nappe refolding, differences in P-T conditions found amongst the different tectonic units of the working area (Bucher et al. 2003) are unrelated to this folding. These differences ask for a careful examination of the kinematics and the timing during the pre-D3 formation of the tectonic contacts between the different Briançonnais units. The tectonic contacts between Gran Paradiso unit, P-L oceanic unit, Internal unit and Ruitor unit are all clearly refolded by D2 folds. Hence they must have previously formed, namely at the end of D1, or alternatively, during early stages of D2 (Table 1). Note, however, that top-NW shearing was still active during D2 folding, particularly in the external part of the study area, e.g. at the tectonic contact between the Ruitor- and Zone Houillère unit, where top-NW shearing is still active during the final stages of nappe stacking (D2).

In contrast, the contact between Ruitor unit and Zone Houillère unit is not refolded by D2, and the axial planes of the D2 folds are cut by this tectonic contact. This indicates that this thrust of the Ruitor unit over the Zone Houillère unit formed late during D2 (Table 1). P-T estimates (Bucher et al. 2003) display a major gap in pressures (about 7 kbar) between these two units. This was interpreted in terms of late-D2 thrusting that emplaced higher metamorphic units (in terms of P and T) over less metamorphic units (Bucher et al. 2003). This inverse field metamorphic gradient, together with decompression documented during D2, suggests that the blueschist and eclogite facies units (Ruitor and more internal units) came to lie over the LP units (Zone Houillère and more external units) during exhumation, i.e. during the final stages of top-W to top-N nappe stacking (D2).

While D2 is related to exhumation within the entire working area, the differences in peak pressures and temperatures found within the individual tectonic units of the working area were established during D1. Peak pressures range from 10–14 kbar (at temperatures of about 450°C) in the Internal unit to 5 kbar (at around 400°C) in the Zone Houillère unit (Bucher et al. 2003).

Conclusions and summary of the tectonic evolution

The work presented here, together with the P-T estimates of Bucher et al. (2003) and new geochronological data (Agard et al. 2002, Bucher 2003) suggest the following tectonic evolution of the tectonic units of the Briançonnais domain (Figure 14, Table 1):

During D1 (50–43 Ma) all units reached peak pressure conditions resulting from southward subduction (Fig. 14d). Clear relationships between original paleogeographic position and depth are observable, more internal units having been subducted deeper than more external units. The external parts of the Zone Houillère unit remained within sub-greenschist facies conditions.

Exhumation and nappe stacking took place during D2 (43–35 Ma, Fig. 14c). We emphasize that, contrary to common belief (Ballèvre et al. 1990, Rolland et al. 2000), extension played no significant role during the exhumation from HP to greenschist facies conditions of the high-pressure units of the Western Alps. Instead, we propose ascent by extrusion within and parallel to a subduction channel, as discussed in Bucher et al. (2003). D2 nappe stacking started with the thrusting of the PL-oceanic units over the Briançonnais. Progressively, thrusting migrated across the Briançonnais domain. Ongoing deformation refolded these contacts during the late stages of D2 deformation, while top-NW to -NNW shearing was still going on (Fig. 14c). Finally, the Ruitor unit was thrust onto the Zone Houillère unit at a latest stage during D2.

Large-scale nappe refolding (D3; 35–31 Ma) post-dated early exhumation of the tectono-metamorphic units (Fig. 14b). The subhorizontal Ruitor and Valsavaranche axial planes indicate vertical shortening of a part of the former nappe pile in front of a very thick Gran Paradiso unit and below the Dent Blanche Austroalpine klippe (Fig. 13). D3 folding formed by a combination of inhomogeneous simple shearing (Merle & Guillier 1989, Bucher et al. 2003) and vertical shortening during the differential WNW-directed movement of the Gran Paradiso unit. Later, this geometry produced during D3 was only slightly modified by D4 doming (Ruitor area, Gran Paradiso area, Fig. 14a).

According to the data of Ceriani et al. (2001) and the age constraints of Fügenschuh & Schmid (2003), our D1 and D2 deformation phases, as well as most of the D3 deformation, predate top-W thrusting along the Roselend thrust, initiating at about 32 Ma ago. During this post-32 Ma deformation in the external Western Alps, following the closure of the Valais ocean, the internal units of the study area were only passively transported to the west. This passive top-W thrusting led to final exhumation of the study area by erosion at around 30 Ma, as indicated by fission track data (Hurford & Hunziker 1989, Fügenschuh & Schmid 2003).

Acknowledgements

We thank our colleagues from the informal “Groupe Briançonnais”, as well as Andrea Loprieno, Ghislain Trullenque and Lukas Keller for stimulating discussions. Michel Marthaler and Mario Sartori are thanked for their help in making the data of Saadi and Adatte et al. from the Benevolo area available to us. Pierre Tricart and François Guillot provided constructive and careful reviews. Substantial funding by the Swiss National Science Foundation (project 20-63391.00) and precursor projects since 1995 is gratefully acknowledged.

REFERENCES

- ADATTE, P., DUBAS, A., TACHE, E. & STRAUSS, F. 1992: Géologie et minéralogie du haut Val di Rhêmes (Vallée d’Aoste). Unpublished diploma thesis, Univ. Lausanne, 132 pp.
- AGARD, P., MONIÉ, P., JOLIVET, L. & GOFFÉ, B. 2002: Exhumation of the Schistes Lustrés complex: in situ laser probe $^{40}\text{Ar}/^{39}\text{Ar}$ constraints and implications for the Western Alps. *J. Metamorph. Geol.* 20, 599–618.

- AMSTUZ, A. 1955: Rocher du ravin de Lessert dans le Val d'Aoste. *Arch. Sc. Genève* 8, 6–9.
- 1962: Notice pour une carte géologique de la Vallée de Cogne et de quelques autres espaces au sud d'Aoste. *Arch. Sc. Genève* 15, 1–104.
- ANTOINE, P. 1971: La zone des brèches de Tarentaise entre Bourg-Saint-Maurice (Vallée de l'Isère) et la frontière Italo-Suisse. *Mem. Lab. Géol.* 9, 1–367.
- APRAHAMIAN, J. 1988: Cartographie du métamorphisme faible à très faible dans les Alpes françaises externes par l'utilisation de la cristallinité de l'illite. *Geodyn. Acta* 2, 25–32.
- ARGAND, E. 1911: Sur les plissements en retour et la structure en éventail dans les Alpes occidentales. *Bull. Soc. Vaud. Sc. Nat.* XLVII, 1–4.
- 1912: Les rythmes du proplissement penninique et le retour cyclique des encapuchonnements. *Bull. Soc. Vaud. Sc. Nat.* XLVIII, 1–4.
- 1916: Sur l'arc des Alpes Occidentales. *Eclogae Geol. Helv.* XIV, 145–191.
- BALLÈVRE, M., LAGABRIELLE, Y. & MERLE, O. 1990: Tertiary ductile normal faulting as a consequence of lithospheric stacking in the Western Alps. *Mém. Soc. Géol. Suisse* 1, 227–236.
- BALLÈVRE, M. & MERLE, O. 1993: The Combin Fault: compressional reactivation of a Late Cretaceous-Early Tertiary detachment fault in the Western Alps. *Schweiz. Mineral. Petrogr. Mitt.* 73, 205–227.
- BAUDIN, T. 1987: Étude géologique du Massif du Ruitor (Alpes franco-italiennes): évolution structurale d'un socle Briançonnais. Unpublished PhD thesis, Univ. Grenoble, 243 pp.
- BERTRAND, J. M. 1968: Étude structurale du versant occidental du massif du Grand Paradis (Alpes Graies). *Géol. Alpine* 44, 55–87.
- BERTRAND, J. M., AILLÈRES, L., GASQUET, D., MACAUDIÈRE, J. 1996: The Pennine Front zone in Savoie (Western Alps), a review and new interpretations from the Zone Houillère Briançonnaise. *Eclogae Geol. Helv.* 89, 297–320.
- BERTRAND, J. M., GUILLOT, F., LETERRIER, J., PERRUCHOT, M. P., AILLÈRES, L., MACAUDIÈRE, J., M. 1998: Granitoïdes de la zone Houillère Briançonnaise en Savoie et en Val d'Aoste (Alpes occidentales): géologie et géochronologie U-Pb sur zircon. *Schweiz. Mineral. Petrogr. Mitt.* 80, 225–248.
- BERTRAND, J. M., PIDGEON, R. T., LETERRIER, J., GUILLOT, F., GASQUET, D. & GATTIGLIO, M. 2000: SHRIMP and IDTIMS U-Pb zircon ages of the pre-Alpine basement in the Internal Western Alps (Savoie and Piemont). *Geodyn. Acta* 11, 33–49.
- BOCOQUET [DESMONS], J. 1974: Le socle Briançonnais de Vanoise (Savoie): arguments en faveur de son âge anté-alpin et de son polymétamorphisme. *C.R. Acad. Sc. Paris* 278, 2601–2604.
- BOCOQUET, J. 1974: Études minéralogiques et pétrographiques sur les métamorphismes d'âge alpin dans les Alpes françaises. Unpublished Thèse d'État, Univ. Grenoble, 490 pp.
- BORGHI, A., COMPAGNONI, R. & SARDONE, S. 1996: Composite P-T paths in the internal Penninic massifs of the Western Alps; Petrological constraints to their thermo-mechanical evolution. *Eclogae Geol. Helv.* 89, 345–367.
- BOUSQUET, R., GOFFÉ, B., VIDAL, O., OBERHÄNSLI, R., AND PATRIAT, M., 2002: The tectono-metamorphic history of the Valaisan domain from the Western to the Central Alps: New constraints on the evolution of the Alps. *Geol. Soc. Am. Bull.*, 114, 207–225.
- BROUWER, F. M., VISSERS R. L. M. & LAMB, W. M., 2002: Structure and metamorphism of the Gran Paradiso massif, western Alps, Italy. *Contr. Mineral. Petrol.* 143, 450–470.
- BUCHER, S. (2003): The Briançonnais units along the ECORS-CROP transect (Italian-French Alps): structures, metamorphism and geochronology. Unpublished PhD thesis, Univ. Basel, 201 pp.
- BUCHER, S., SCHMID, S. M., BOUSQUET, R. & FÜGENSCHUH, B. 2003: Late-stage deformation in a collisional orogen (Western Alps): nappe refolding, back-thrusting or normal faulting? *Terra Nova* 15, 109–117.
- BUROV, E., JOLIVET, L., LE POURHIE, L. & POLIAKOV, A., 2001. A thermo-mechanical model of exhumation of high pressure (HP) and ultra-high pressure (UHP) metamorphic rocks in Alpine-type collision belts. *Tectonophysics* 342, 113–136.
- BUTLER, R. W. H. & FREEMAN, S. 1996: Can crustal extension be distinguished from thrusting in the internal parts of mountain belts? A case history of the Entrelor shear zone, Western Alps. *J. Struct. Geol.* 18, 909–923.
- CABY, R. 1968: Contribution à l'étude structurale des Alpes occidentales: subdivisions stratigraphiques et structure de la Zone du Grand-Saint-Bernard dans la partie sud du Val d'Aoste (Italie). *Géol. Alpine* 44, 95–111.
- 1996: Low-angle extrusion of high-pressure rocks and the balance between outward and inward displacements of Middle Penninic units in the Western Alps. *Eclogae Geol. Helv.* 89, 229–267.
- CERIANI, S., FÜGENSCHUH, B. & SCHMID, S. M. 2001: Multi-stage thrusting at the "Penninic Front" in the Western Alps between Mont Blanc and Pelvoux massifs. *Int. J. Earth Sci.* 90, 685–702.
- CHOPIN, C. 1977: Une paragenèse à margarite en domaine métamorphique de haute pression-basse température (massif du Grand Paradis, Alpes françaises). *C.R. Acad. Sc. Paris* 285, 1383–1386.
- CIGOLINI, C. 1981: Garnet chemistry and zonation in the Italian sector of the Grand Saint Bernard Nappe. *Atti. Acc. Sc. Torino* 115, 331–344.
- 1995: Geology of the Internal Zone of the Grand Saint Bernard Nappe: a metamorphic Late Paleozoic volcano-sedimentary sequence in the South-Western Aosta Valley (Western Alps). In: *Studies on metamorphic rocks and minerals of the western Alps. A Volume in Memory of Ugo Pognante* (Ed. by B. LOMBARDO). *Bollettino del Museo Regionale di Scienze Naturali* (suppl.) 13, n°2, Torino, 293–328.
- COMPAGNONI, G. & LOMBARDO, B. 1974: The Alpine age of the Gran Paradiso eclogites. *Rendic. Soc. It. Min. Pet.*, 30, 227–237.
- DAL PIAZ, G. V. 1965: Il lambo di ricoprimento della Becca di Toss: struttura retroflessa della zona del Gran San Bernardo. *Mem. Acad. Patavina* 77, 107–136.
- DAL PIAZ, G. V. 1999: The Austroalpine-Piedmont nappe stack and the puzzle of Alpine Tethys. *Mem. Sci. Geol. Padova* 51, 155–176.
- DAL PIAZ, G. V. & GOVI, M. 1965: Osservazioni geologiche sulla "Zona del Gran San Bernardo" nell'alta valle d'Aosta. *Bull. Soc. It.* 84, 105–119.
- DAL PIAZ, G. V. & LOMBARDO, B. 1986: Early Alpine eclogite metamorphism in the Pennine Monte Rosa – Grand Paradiso basement nappes of the northwestern Alps. *Geol. Soc. Am. Mem.* 164, 249–265.
- DEBELMAS, J., CABY, R. & DESMONS, J. 1991a: Notice explicative, Carte géologique de la France à 1/50000, Feuille Ste-Foy-Tarentaise. *Bur. Rech. Géol. Min. Orléans* 728, 43 pp.
- DEBELMAS, J., CABY, R., ANTOINE, P., ELTER, G., ELTER, P., GOVI, M., FABRE, J., BAUDIN, MARION, R., JAILLARD, É., MERCIER, D. & GUILLOT, F. 1991b. Carte Géologique de la France à 1/50000 Feuille Ste-Foy-Tarentaise. *Bur. Rech. Géol. Min. Orléans*, 728.
- DESMONS, J., COMPAGNONI, R., CORTESOGNO, L., FREY, M. & GAGGERO, L. 1999: Pre-Alpine metamorphism of the Internal zones of the Western Alps. *Schweiz. Mineral. Petrogr. Mitt.* 79, 23–39.
- DESMONS, J. & MERCIER, D. 1993: Passing through the Briançon Zone. In: *Pre-Mesozoic Geology in the Alps* (Ed. by J. F. VON RAUMER & F. NEUBAUER). Springer-Verlag, Heidelberg, 279–295.
- DROOP, G. T. R., LOMBARDO, B. & POGNANTE, U. 1990: Formation and distribution of eclogite facies rocks in the Alps. In: *Eclogite facies rocks* (Ed. by D. A. CARSWELL). Blackie, Glasgow and London, 225–259.
- DEWEY, J. F. 1988: Extensional collapse of orogens. *Tectonics* 7, 1123–1139.
- ELLENBERGER, F. 1958: Étude géologique du pays de Vanoise. *Mém. Serv. Expic. Carte géol. dét. Fr.* 561 pp.
- ELTER, G. 1960: La zona penninica dell'alta e media Val d'Aosta e le unità limitrofe. *Mem. Ist. Geol. Univ. Padova* 22, 113 pp.
- 1972: Contribution à la connaissance du Briançonnais interne et de la bordure piémontaise dans les Alpes Graies nord-orientales et considérations sur les rapports entre les zones du Briançonnais et des Schistes Lustrés. *Mem. Ist. Geol. Univ. Padova* 28, 19.
- ELTER, G. & ELTER, P. 1965: Carta geologica della regione del Piccolo San Bernardo (versante italiano). Note illustrative. *Mem. Ist. Geol. Univ. Padova* 25, 1–51.
- ESCHER, A. AND BEAUMONT, C. 1997: Formation, burial and exhumation of basement nappes at crustal scale: a geometric model based on the Western Swiss-Italian Alps. *J. Struct. Geol.* 19, 955–974.
- ESCHER, A., MASSON, H. & STECK, A. 1993: Nappe geometry in the Western Swiss Alps. *J. Struct. Geol.* 15, 501–509.
- FABRE, J. 1961: Contribution à l'étude de la Zone Houillère Briançonnaise en Maurienne et en Tarentaise (Alpes de Savoie). *Mém. Bur. Rech. Géol. Min.* 2, 315 pp.
- FEYS, R. 1963: Étude géologique du Carbonifère Briançonnais (Hautes-Alpes). *Mém. Bur. Rech. Géol. Min.* 6, 387 pp.

- FREY, M., DESMONS, J. & NEUBAUER, F. 1999: Metamorphic Maps of the Alps. CNRS (Paris), Swiss N.S.F. (Berne), BMWFV and FWF (Vienna).
- FRISCH, W. 1979: Tectonic progradation and plate tectonics of the Alps. *Tectonophysics* 60, 121–139.
- FROITZHEIM, N., SCHMID, S. M. & FREY, M. 1996: Mesozoic paleogeography and timing of eclogite-facies metamorphism in the Alps: A working hypothesis. *Eclogae Geol. Helv.* 89, 81–110.
- FÜGENSCHUH, B., LOPRIENO, A., CERIANI, S. & SCHMID, S. 1999: Structural analysis of the Subbriançonnais and Valais units in the area of Moûtiers (Savoy, Western Alps): paleogeographic and tectonic consequences. *Int. J. Earth Sci.* 88, 201–218.
- FÜGENSCHUH, B. & SCHMID, S. M. 2003: Late stages of deformation and exhumation of an orogen constrained by fission-track data: a case study in the Western Alps. *Geol. Soc. Am. Bull.* 115, 1425–1440.
- GOFFÉ, B. & BOUSQUET, R. 1997: Ferrocapholite, chloritoïde et lawsonite dans les métapélites des unités du Versoyen et du Petit Saint Bernard (zone valaisanne, Alpes occidentales). *Schweiz. Mineral. Petrogr. Mitt.* 77, 137–147.
- GOUFFON, Y. 1993: Géologie de la “nappe” du Grand St-Bernard entre la Doire Baltée et la frontière suisse (Vallée d’Aoste-Italie). *Mémoires de Géologie (Lausanne)* 12, 147.
- GOUFFON, Y. & BURRI, M., 1997: Les nappes de Pontis, de Siviez-Mischabel et du Mont Fort dans les vallées de Bagnes, d’Entremont (Valais, Suisse) et d’Aoste (Italie). *Eclogae Geol. Helv.* 90, 29–41.
- GRÉBER, C. 1965: Flore et stratigraphie du Carbonifère des Alpes françaises. *Mém. Bur. Rech. Géol. Min.* 21, 380 pp.
- GUILLOT, F., SCHALTEGGER, U., BERTRAND, J. M., DELOULE, É. & BAUDIN, T., 2002: Zircon U-Pb geochronology of Ordovician magmatism in the polycyclic Ruitor Massif (Internal W Alps). *Int. J. Earth Sci.* 65, 814–828.
- HENRY, C., MICHARD, A. & CHOPIN, C. 1993: Geometry and structural evolution of ultra-high-pressure and high-pressure rocks from the Dora-Maira massif, Western Alps, Italy. *J. Struct. Geol.* 15, 965–981.
- HURFORD, A. J. & HUNZIKER, J. C. 1989: A revised thermal history for the Gran Paradiso massif. *Schweiz. Mineral. Petrogr. Mitt.* 69, 319–329.
- JAILLARD, É. 1989: La transition Briançonnais externe – Briançonnais interne en Savoie. L’Aiguille des Aimes, le Roc du Bourget et le massif d’Ambin. *Géol. Alpine* 65, 105–134.
- 1990: Lithostratigraphie et paléogéographie des séries briançonnaises internes de Haute-Tarentaise. *Géologie de la France* 1, Orléans, 33–44.
- KELLER, L.M. & SCHMID, S.M., 2001. On the kinematics of shearing near the top of the Monte Rosa nappe and the nature of the Furgg zone in Val Loranco (Antrona valley, N. Italy): Tectono-metamorphic and paleogeographical consequences. *Schweiz. Mineral. Petrogr. Mitt.*, 81, 347–367.
- KRAMER, J. 2002: Strukturelle Entwicklung der penninischen Einheiten im Monte Rosa Gebiet (Schweizer und italienische Alpen). Unpublished PhD thesis, Univ. Basel, 154 pp.
- LEMOINE, M. 1961: Le Briançonnais interne et la zone des Schistes Lustrés dans les vallées du Guil et de l’Ubaye (Hautes et Basses Alpes) (Schéma structural). *Trav. Lab. Géol. Fac. Sci. Grenoble* 47, 181–201.
- LOPRIENO, A. 2001: A combined structural and sedimentological approach to decipher the evolution of the Valaisan domain in Savoy (Western Alps). Unpublished PhD thesis, Univ. Basel, 285 pp.
- MARION, R. 1984: Contribution à l’étude géologique de la Vanoise, Alpes occidentales. Le massif de la Grande Sassièrre et la région de Tignes-Val d’Isère. Unpublished PhD thesis, Univ. de Savoie, 172 pp.
- MERCIER, D. & BEAUDOIN, B. 1987: Révision du Carbonifère Briançonnais: Stratigraphie et évolution du bassin. *Géol. Alpine* 63, 25–31.
- MERLE, O. & GUILLIER, B. 1989: The building of the Central Swiss Alps: an experimental approach. *Tectonophysics* 165, 41–56.
- MILNES, A. G. 1974: Structure of the Pennine Zone (Central Alps): New Working Hypothesis. *Geol. Soc. Am. Bull.* 85, 1727–1732.
- MILNES, A. G., GRELLER, M. & MÜLLER, R. 1981: Sequence and style of major post-nappe structures, Simplon-Pennine Alps. *J. Struct. Geol.* 3, 411–420.
- MÜLLER, R. 1983: Die Struktur der Mischabelfalte (Penninische Alpen). *Eclogae Geol. Helv.* 76, 391–416.
- NICOLAS, A., HIRN, A., NICOLICH, R., POLINO, R. AND ECORS-CROP Working Group. 1990: Lithospheric wedging in the Western Alps inferred from the ECORS-CROP traverse. *Geology* 18, 587–590.
- PIFFNER, O. A., ELLIS, S. & BEAUMONT, C., 2000: Collision tectonics in the Swiss Alps: Insight from geodynamic modeling. *Tectonics* 19, 1065–1094.
- PHILIPPOT, P. 1990: Opposite vergence of nappes and crustal extension in the French-Italian Western Alps. *Tectonics* 9, 1143–1164.
- PLATT, J. P., LISTER, G. S., CUNNINGHAM, P., WESTON, P., PEEL, F., BAUDIN, T. & DONDEY, H. 1989: Thrusting and back-thrusting in the Briançonnais domain from the western Alps. In: *Alpine Tectonics* (Ed. by M. COWARD et al.). *Geol. Soc. Spec. Publ. London* 45, 135–152.
- RAMSAY, J. G. & HUBER, M. I. 1987: *The Techniques of Modern Structural Geology, Volume 2: Folds and Fractures*. Academic Press, London, 391pp.
- RING, U., 1995: Horizontal contraction or horizontal extension? Heterogeneous Late Eocene and Early Oligocene general shearing during blueschist and greenschist facies metamorphism at the Pennine-Austroalpine zone in the Western Alps. *Geol. Rundsch.* 84, 843–859.
- ROLLAND, Y., LARDEAUX, J. M., GUILLOT, S. & NICOLLET, C. 2000: Extension syn-convergence, poinçonnement vertical et unités métamorphiques contrastées en bordure ouest du Gran Paradis (Alpes Franco-Italiennes). *Geodyn. Acta* 13, 133–148.
- ROURE, F., BERGERAT, B., DAMOTTE, J.-L., MUGNIER & POLINO R. 1996: The ECORS-CROP Alpine seismic traverse. *Mém. Soc. Géol. France* 170, 113 pp.
- SAADI, M. 1992: Géologie du haut Val di Rhêmes (Vallée d’Aoste). Unpublished diploma thesis, Univ. Genève, 120 pp.
- SCHMID, S. M. & KISSLING, E. 2000: The arc of the Western Alps in the light of new data on deep crustal structure. *Tectonics* 19, 62–85.
- SCHMID, S. M., ZINGG A. & HANDY, M. 1987: Kinematics of movements along the Insubric Line and the emplacement of the Ivrea Zone. *Tectonophysics* 135, 47–66.
- SCHMID, S. M., RÜCK, PH. & SCHREURS, G. 1990: The significance of the Schams nappes for the reconstruction of the paleotectonic and orogenic evolution of the Pennine zone along the NFP 20 East traverse (Grisons, eastern Switzerland). *Mém. Soc. géol. France*, 156; *Mém. Soc. Géol. Suisse* 1; *Vol. spec. Soc. Geol. It.* 1, 263–287.
- SCHMID, S. M., PFIFFNER, O. A., FROITZHEIM, N., SCHÖNBORN, G. & KISSLING, E. 1996: Geophysical-geological transect and tectonic evolution of the Swiss-Italian Alps. *Tectonics* 15, 1036–1064.
- SCHMID, S.M., FÜGENSCHUH, B., KISSLING, E. & SCHUSTER, R. 2004: Tectonic map and overall architecture of the Alpine orogen. *Eclogae Geol. Helv.* 97: 93–117.
- SCHREURS, G. 1993: Structural analysis of the Schams nappes and adjacent tectonic units: implications for the orogenic evolution of the Pennine zone in eastern Switzerland. *Bull. Soc. géol. France* 164, 415–435.
- SIMPSON, C. & SCHMID, S. M. 1983: An evolution of criteria to deduce the sense of movement in sheared rocks. *Geol. Soc. Am. Bull.* 94, 1281–1288.
- STAMPFLI, G. M. 1993: Le Briançonnais, terrain exotique dans les Alpes? *Eclogae Geol. Helv.* 86, 1–45.
- THÉLIN, P., SARTORI, M., BURRI, M., GOUFFON, Y., CHESSEX, R. 1993: The pre-Alpine Basement of the Briançonnais (Wallis, Switzerland). In: *Pre-Mesozoic Geology in the Alps* (Ed. by J. F. VON RAUMER & F. NEUBAUER). Springer-Verlag, Heidelberg, 297–315.
- TRICART, P. 1984: From passive margin to continental collision: A tectonic scenario for the Western Alps. *Am. J. Sci.* 284, 97–120.
- TRÜMPY, R. 1955: Remarques sur la corrélation des unités penniques externes entre Savoie et Valais et sur l’origine des nappes préalpines. *Bull. Soc. géol. de France* 6ème série, 217–231.
- 1966: Considérations générales sur le «Verrucano» des Alpes Suisses. In: *Atti del symposium sul Verrucano, Pisa 1966*. *Soc. Toscana Sci. Nat.*, 212–232.
- ULARDIC, C. 2001: Strukturgeologische und petrographische Untersuchungen im Valgrisenche (Briançonnais der italienischen Alpen). Unpublished diploma work, Univ. Freiburg, Germany, 100 pp.
- VEARNCOMBE, J. R. 1985: The structure of the Gran Paradiso basement massif and its envelope, Western Alps. *Eclogae Geol. Helv.* 78, 49–72.

Manuscript received: September 30, 2003

Revision accepted: December 2, 2004

Chapter 2
**Metamorphic evolution of the Briançonnais units along
the ECORS-CROP profile (Western Alps): New data on
metasedimentary rocks**

By Stefan Bucher & Romain Bousquet,
Paper in review in "Schweizerische Mineralogische und Petrographische Mitteilungen"

Metamorphic evolution of the Briançonnais units along the ECORS-CROP profile (Western Alps): New data on metasedimentary rocks

Stefan Bucher^{1,‡}, Romain Bousquet^{1,*}

¹ Department of Earth Sciences, Universität Basel, Bernoullistrasse 32 CH-4056 Basel, Switzerland

Corresponding author: R. Bousquet
e-mail: romain@geo.uni-potsdam.de
Fax: 0049 331 977 5060

[‡] Present address: Muséum d'histoire naturelle de Neuchâtel 14, rue des Terreaux CH-2000 Neuchâtel, Switzerland

* Present address: Geowissenschaften Institut, Universität Potsdam, Karl Liebknecht Str. 24 D-14476 Potsdam, Germany

Short title: Metamorphic evolution of the Briançonnais units (Western Alps)

Abstract

The Briançonnais units are squeezed between two Mesozoic eclogitic belts (the Piemont-Ligurian ocean and the Valaisan ocean) along the ECORS-CROP seismic line in the Italian-French Western Alps (France, Italy). The metamorphic evolution of this area plays a key role for understanding of the evolution of the Western Alps and is discussed on the basis of detailed petrographic investigations carried out on post-Hercynian sediments. In the Zone Houillère as well in the Permo-Triassic cover of the Briançonnais basement, the index metamorphic mineral assemblage is mainly composed of white micas differing in chemistry, chloritoid, garnet. This same mineralogical assemblage occurs within different lithologies (metaarkoses, metapelites, metasandstones). Consequently, equilibrium phase diagrams were computed for the different whole rock chemistries, using DOMINO software. The results of the P-T investigations clearly show that each unit underwent a different metamorphic history. An increase in metamorphic grade from greenschist facies conditions in the Northwest (Zone Houillère) to the transition between blueschist and eclogite facies conditions in the Southeast (Internal unit) is observed. A major discontinuity in metamorphic grade is located at the contact between Zone Houillère and Rutor unit, documented by a pressure gap of ~ 7 kbar related to thrusting during exhumation. In general the observed metamorphic field pattern is an inverse one, and is interpreted to represent different depths of burial during subduction, which correlates with the paleogeographic position of the different units.

Keywords: metasediments, Western Alps, HP metamorphism, chloritoid

Introduction

At first sight one is tempted to think that the knowledge of the overall structure of the Alps has not progressed much since the well-known synthesis of Argand (1916). However, new data presented in subsequent studies have forced researchers to revise some key points concerning the structure and evolution of the Alpine chain. In particular, seismic investigations along transects over the Alps (NFP 20, Pfiffner et al. 1997; ECORS-CROP, Roure et al. 1996) allow for a better understanding of the deep structure of the alpine belt (see for example Polino et al., 1990; Schmid et al. 1996; Schmid and Kissling 2000). In addition, significant progress has been made concerning the understanding of the tectono-metamorphic history of the Alps (see review in Oberhänsli et al., 2004, Schmidt et al., 2004). Surprisingly, combined metamorphic and structural data are still lacking in some key areas, even though they are crucial for the understanding of the evolution of the Alps. Many of these areas are composed of basement rocks that underwent several metamorphic events. In such rocks it is not always easy to distinguish between metamorphic events of different orogenies. One of these areas is the Briançonnais domain of the northwestern Alps. While for the southern part of the Western Alps, composed mainly of sediments, substantial evidence for alpine high-pressure overprint has been evidenced (Goffé, 1977; Goffé & Velde, 1984), the alpine metamorphic evolution of the northern part, composed mainly of basement rocks, is still subject to debate.

In this paper, based on a careful study of the petrology in the post-Hercynian metasediments occurring scarcely in the Briançonnais units along the ECORS-CROP seismic line, a new metamorphic evolution for the whole area is proposed. New PT-estimations provide new constraints for the geodynamic evolution of an area that plays a key role for the understanding of the evolution of the Western Alps.

Alpine HP metamorphism in the Briançonnais area along the ECORS-CROP profile?

In the area along the ECORS-CROP seismic line in the Italian-French Western Alps the Briançonnais units appear squeezed between two Mesozoic oceanic units that both underwent high-pressure (HP) metamorphic overprint. Eclogitic rocks are known from the Piemonte-Ligurian domain (“Grivola”, Dal Piaz 1928; Droop et al., 1990) in the southeast as well as from the Valaisan in the northwest (Schürch 1987; Oberhänsli, 1994; Goffé & Bousquet 1997). The most internal part of the Briançonnais domain, the Gran Paradiso massif, which underlies the Schistes Lustrés, also furnishes evidences for a HP history (Compagnoni and Lombardo, 1974; Dal Piaz & Lombardo 1986; Ballèvre, 1990). The Briançonnais domain s.str. is located in between these eclogitic units, but its metamorphic evolution is not well constrained in the northwestern part of the Alps, while in the south a significant pressure increase is evidenced from the external to the internal Briançonnais zones (Goffé & Chopin, 1986; Goffé et al., 2004). Although some petrological studies have been carried out in these units (Baudin 1987; Cigolini 1981; Boquet 1974, 1999; Caby & Kienast 1989), its metamorphic history during the alpine orogeny is still a matter of debate (see Monié, 1990).

For example, whereas in the Ruitor unit all authors agree on the presence of Barrovian type metamorphism of pre-Alpine age (e.g. Boquet 1974, Baudin 1987, Caby 1968, 1996, Gouffon 1993), the grade of the Alpine metamorphic imprint is still under discussion. Baudin (1987) ascribed epidote-blueschist facies conditions to a first alpine metamorphic stage and postulated pressures around 5-7 kbar at temperatures between 350 °C and 400 °C. Boquet (1974) extensively studied mineral compositions and described large amounts of pre-Alpine garnet, and a minor amount of Alpine garnet besides. This author also inferred Alpine epidote blueschist conditions for the Ruitor unit. Caby & Kienast (1989) and Caby (1996), however, interpreted eclogite facies conditions to have prevailed during the peak of the Alpine evolution in the Ruitor unit. Due to the fact that all these

studies only investigated pre-alpine basement rocks the debate centers largely around the distinction between minerals of Alpine and pre-Alpine age. In the Internal unit Cigolini (1995) evidenced pre-Alpine relics in basement rocks, but he also evidence a HP metamorphic event in the post-Variscan rocks of the most internal part: Na-amphibole overgrowing relic magmatic hornblende in the Cogne-Savarenche pluton and pseudomorphs after jadeite in Permian metasediments. In this study only samples from the momo-metamorphic sedimentary cover of the different units, which allow for a clear attribution of the metamorphic grade to the Alpine metamorphic cycle, are presented in order to contribute to this discussion.

Geological setting

The investigated area extends along the ECORS-CROP seismic line from the Pt. St. Bernard pass in the NW to the border of the Gran Paradiso massif in the SE (Fig.1) and it covers most of the Briançonnais units of the northern Western Alps. In the NW the Zone Houillère unit represents the most external part of the Briançonnais paleogeographic domain, which is separated from the Valaisan units by the Houiller Front (Nicolas et al., 1990; Fügenschuh et al. 1999). Towards the SE follows the more internal Ruitor unit, which is is classically divided into an external (“Ruitor externe”) and an internal part (“Ruitor interne”), respectively (Caby 1996). The Internal unit, still further to the SE, is separated from the underlying Piemonte-Liguria (P-L) oceanic unit by a refolded former thrust, referred to as the “Enigmatic tectonic contact” (ETC) by Bucher et al. (2003). In this area, the Briançonnais unit is composed of three different zones:

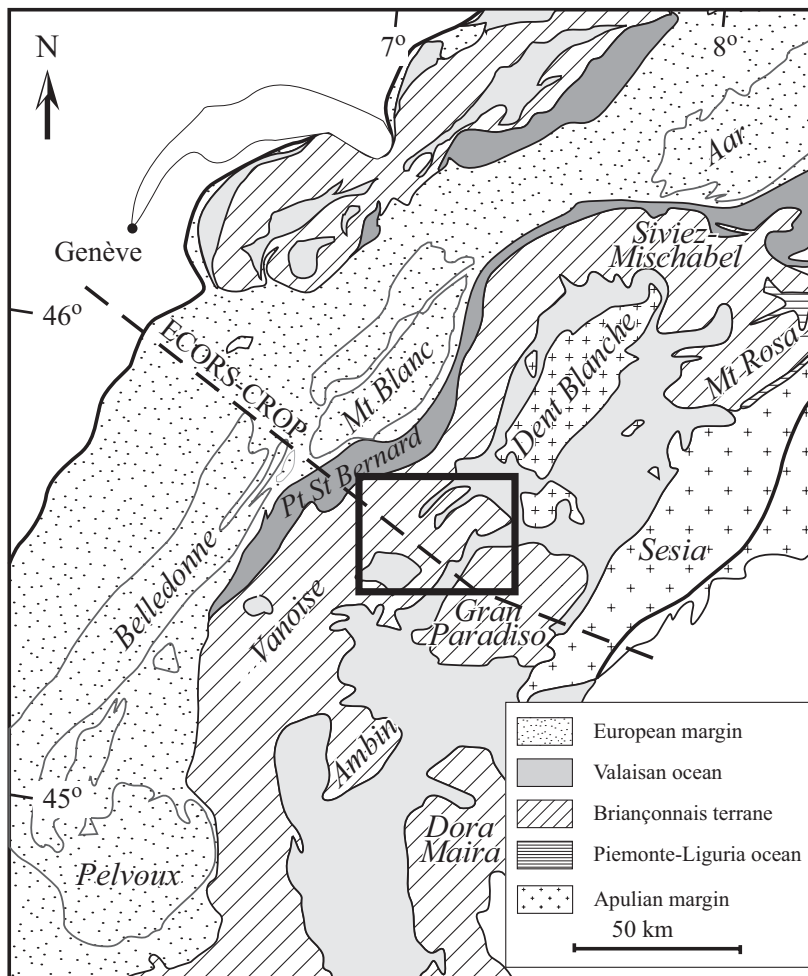


Figure 1: Paleogeographic domains of the Western Alps. The rectangle indicates the studied area.

Zone Houillère unit

This unit is characterised by a Paleozoic sequence of continental deposits (Fabre 1961). The lower part of this sequence consists of black schists with anthracitic lenses and arkoses (Namurien to Stefanien in age; Feys 1963, Gerber 1965). The upper part is dominated by arkoses and conglomerates, probably of Stefano-Autunien age (Fabre 1961). The clasts mainly consist of polycrystalline quartz, micaschists and paragneisses. The latter display a poly-phase metamorphic imprint (Desmons & Mercier 1993). A Permo-Triassic sequence discordantly overlies this Carboniferous sequence (Ellenberger 1958, Elter 1960). During the Alpine deformation the Zone Houillère was decoupled from its former basement, whose present-day position remains unknown, since it does not outcrop at the earth's surface (Desmons & Mercier 1993, Bucher et al., 2004).

Ruitor unit

The Ruitor unit dominantly consists of pre-Permian garnet micaschists and paragneisses with abundant intercalated metabasites (Baudin, 1987). There is definitely an Alpine metamorphic overprint (Caby, 1996), but some relicts of pre-alpine metamorphism survived the alpine cycle (Boquet, 1974). Its sedimentary cover is made up by a thin Permo-Triassic sequence (Debelmas et al., 1991b), consisting of “Verrucano”-type conglomerates (Trümpy, 1966) at the base, followed by lower Triassic meta-arkoses, which are stratigraphically overlain by quartz-phyllites and ankerite-bearing micaschists (Baudin, 1987; Gouffon, 1993; Ulardic, 2001). This sequence crops out throughout the entire Valgrisenche (Fig. 2).

The existence of a separation of the Ruitor unit into an external and an internal part is debated, since there is no unequivocal tectonic contact. Desmons & Mercier (1993) question this separation. Some authors have made a separation based on the dominant mineral assemblages (alpine vs. pre-alpine, Debelmas et al. 1991a), while others have used intensity of alpine deformation as a criterion (i.e. Gouffon 1993) for defining a boundary between two parts of the Ruitor unit. However, Bucher et al. (2004) showed that the criteria are questionable and interpreted based structural and stratigraphical data, only one unit.

Internal unit

The Internal unit (“Zona Interna” or the “Briançonnais interne”) corresponds to the Vanoise-Mont Pourri unit found further south (Elter 1972). Northwards the Internal unit was correlated with the Mont Fort unit (Gouffon 1993). It's made up of a lower part, formed by paragneisses and micaschists with a polymetamorphic history (Boquet 1974, Cigolini 1995), and of a mono-metamorphic upper part that consists of lower Permian to Mesozoic formations. According to Amstuz (1955, 1962), the lower part is mainly of volcano-clastic origin. This succession is intruded by Paleozoic granitic and granodioritic bodies (i.e. the Cogne-Valsavaranche granodiorite, Bertrand et al. 2000).

Leucocratic gneisses define the basis of the mono-metamorphic upper part. These are followed by a typical Permo-Triassic sequence, consisting of conglomerates (“Verrucano”), quartzitic meta-sandstones, impure quartzites and ankerite-bearing micaschists. The younger Mesozoic cover is only preserved in the southern part of the study area (Adatte et al. 1992, Saadi 1992).

Mineral and whole rock chemistry

Methods of investigation

The mineral compositions were determined with a JEOL JXA-8600 electron microprobe at the University of Basel (15 kV, 10 nA, PROZA correction procedure) using wollastonite (Si,Ca), albite (Na, Al), graffonite (Mn, Fe), rutile (Ti), albite (Na), orthoclase (K), Olivine (Mg) as standards. The structural formulae were calculated for chlorite on 14 oxygens, for phengite on 11 oxygens, for chloritoid on 12 oxygens following Chopin et al. (1992), for Na-amphibole on 13 cations and on 23 oxygens, for garnet on 12 oxygens, and Fe^{3+} is calculated from the deficit in Al into octahedral site.

Bulk rock compositions were determined on melted pellets by XRF using a Bruker AXS SRS-3400 at the Geochemical Laboratory in Basel. No major layering was observed in thin sections and therefore bulk rock chemistries were taken from adjoining parts of the rock sample without a further volume reduction, except for sample Vga0139.

Sample selection and whole rock chemistry

In the whole area, from the Zone Houillère to in the Permo-Triassic cover, the index metamorphic mineral assemblage is composed of chloritoid, garnet and white micas (\pm chlorite) (Fig. 2). Only few samples contain Na-amphiboles.

Four samples, one of the Zone Houillère unit, one of the Rutor unit and two of the Internal unit showing well preserved microstructures and early metamorphic stage mineral assemblage were selected for detailed P-T investigations. In the meantime a microstructural study is carried out in order to constrain the tectonic evolution proposed by Bucher et al. (2004). A detailed study of five different samples coming from metasedimentary cover of each zone will be presented in the following. The bulk rock data of the studied samples are summarized in Table 1, and representative microprobe analyses are given in Table 2.

A first sample Rui9906, collected in the internal Zone Houillère unit near the tectonic contact to the Rutor unit, is a highly deformed metaarkose from the Stefano-Autunien, i.e. the upper sequence of the Carboniferous sediments. This Al-rich (20-25% Al_2O_3) metaarkose contains 5 to 10 % of ferro-magnesian ($\text{FeO}+\text{MgO}+\text{MnO}$) and alkaline ($\text{K}_2\text{O}+\text{Na}_2\text{O}$), indicating bulk rock chemistry intermediate between pure sandstone and pelite (Fig. 3). Sample Cere0035 is from the Permo-Triassic cover pinched in the Rutor unit, which is cropping out between Planaval and the Tour de Tignet (Fig. 2; Bucher et al. 2003, 2004 for a detailed discussion). Its bulk rock chemistry is typical for metapelites (i.e. poorer in SiO_2 compared to sample Rui9906, Fig. 3). The third sample Vga0139 derives from the Permo-Triassic cover sequence of the Internal unit in the area of the uppermost Valgrisenche. The fourth one (Cret006 & SB 1.38-2) comes from upper Permian quartzite cropping out in the Val di Rhêmes (Fig. 2).

Note that although samples Cere0035, Vga0139, Cret006 & SB 1.38-2 all derive from the Permo-Triassic sequence, they show different whole rock compositions (Fig. 3) due to their different stratigraphic age. Whereas sample Cere0035 is a lower Triassic quartz phyllite with a metapelitic whole rock composition, sample Vga0139 belongs to the upper Permian "Verrucano" facies and is of an intermediate whole rock composition between metapelite and metasandstone (Fig 3). Sample Cret006 has a typical quartzite composition (Fig. 3).

Sample description and microstructures

Sample Rui9906

Petrology. Sample Rui9901 is a highly deformed metaconglomerate from the Zone Houillère unit (Fig. 2). Minerals are phengite, chlorite, garnet, chloritoid and quartz, the main foliation being mainly defined by quartz, phengite and chlorite (Fig. 4a). Relics of Mn-rich garnet, phengite, chlorite and

chloritoid occur in the main foliation (Fig. 4b). Garnet shows no zoning and the Mn-rich composition ($X_{\text{Sps}} \sim 0.4$, $X_{\text{Alm}} \sim 0.45$, $X_{\text{Prp}} < 0.1$, $X_{\text{Grs}} \sim 0.15$; Fig. 5a) is typical for low-grade metamorphic conditions (i.e. Spear 1993). In these small garnets ($\sim 150 \mu\text{m}$) inclusions of chloritoid are observable ($X_{\text{Mg}} \sim 0.12$; $X_{\text{Mn}} > 0.16$, Tab. 2). Chloritoid has a high Mn-content, indicating a strong interaction with the host mineral garnet. Two mineralogical assemblages can be distinguished in this sample: the first one {1} is composed of garnet, chloritoid, phengite, chlorite and quartz while a second one {2} is only composed of a second generation of phengite, chlorite and quartz. Additionally, albite overgrows the main foliation during a late stage. Such late albite growth is a common observation in the northern western Alps (Desmons et al. 1999c).

Microstructures. Figure 4a shows the intense main foliation S2 defined by mainly quartz and chlorite. Garnet appears as porphyroclasts within the S2 foliation. The metastability of garnet in the S2 foliation is indicated by the overgrowth of chlorite and phengite (Fig. 4b). Furthermore, the irregular grain boundary of garnet indicates that this mineral predates the main deformation event D2. Chloritoid is only observed as inclusions in garnet and is therefore also attributed to assemblage {1}. In summary, these clear relationships allow for attributing mineral assemblage {1}, composed of phengite, chloritoid, garnet chlorite and phengite to the first deformation phase D1 (Tab. 3). In contrast, assemblage {2}, only consisting of phengite and chlorite, defines the main foliation S2 and is therefore ascribed to D2 (Tab. 3).

Table 1: Bulk rock compositions of the investigated samples.

	Rui9906	Cere0035	Vga0139	SB 1.38-2	Cret006
SiO ₂	69.67	57.81	76.96	91.51	92.8
TiO ₂	0.57	0.86	0.47	0.16	0.18
Al ₂ O ₃	14.94	20.67	8.53	3.95	3.59
FeO	5.06	7.98	4.41	1.17	0.77
MnO	0.08	0.07	0.03	0.02	0.01
MgO	1.01	1.70	2.48	0.23	0.21
CaO	0.33	0.26	0.74	0.14	0.1
Na ₂ O	1.65	0.45	2.71	0.15	0.2
K ₂ O	4.4	5.05	0.61	1.23	0.98
P ₂ O ₅	0.17	0.20	0.11	0.04	0.03
Total	97.88	95.05	97.05	98.60	98.87

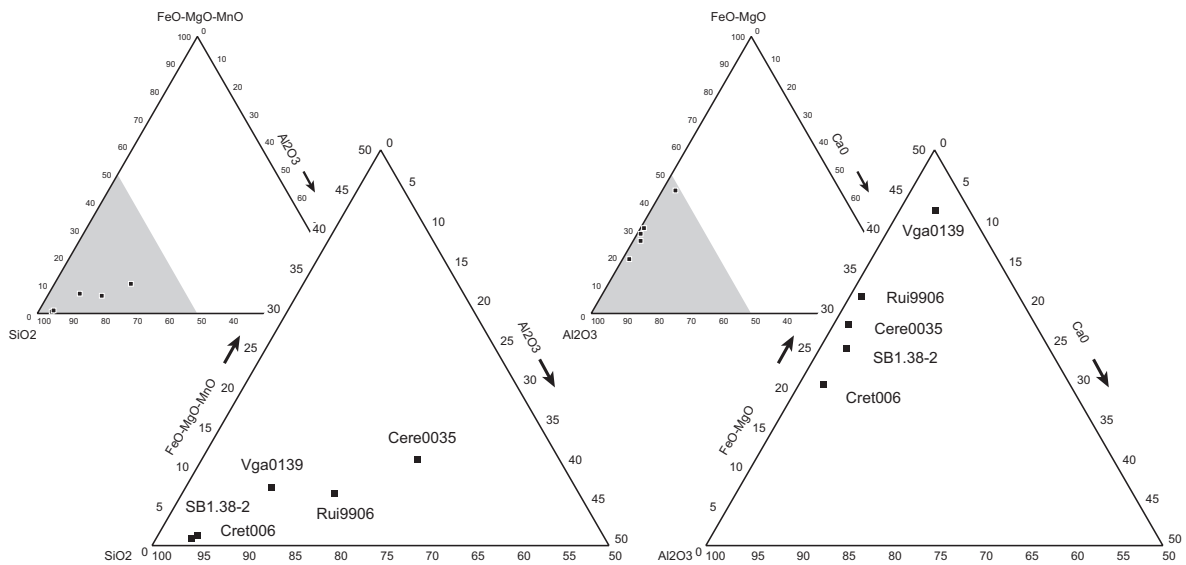


Figure 3: Ternary diagrams (SFA and ACF) for the bulk rock compositions of studied samples. See details in the text.

Sample Cere0035

Petrology. This sample was collected in an intermediate structural position of the Ruitor unit from the Permo-Triassic cover of the Ruitor unit (Fig. 2). The occurring minerals are chloritoid, garnet, phengite, paragonite, chlorite, clinozoisite, quartz b and accessory opaque minerals. Chloritoid is overprinted by the main foliation defined by phengite, chlorite and clinozoisite and forms relic fold hinges (Fig. 4c). Furthermore, overgrowth of chloritoid by clinozoisite indicates that the main foliation postdates chloritoid growth (Fig. 4d). Two phengite populations are micro-structurally and chemically distinguishable. A detailed combined EMP and microstructural analysis of the different phengite populations from this sample is carried out in a. The first population (D1), preserved as microlithons, is characterized by high Si-contents (> 3.3 p.f.u.) while the Si-content of the second population formed during D2 ranges from 3.2 to 3.3 p.f.u. Although not always easy to detect, a third population of phengite can be interpreted as detrital grains which survived the alpine metamorphic cycle (Bucher, 2003).

Chloritoid and garnet show rather constant compositions with a high Fe-content. In the chloritoid, X_{Mg} varies between 0.09 and 0.13, while garnet is almandine-rich ($\geq 70\%$) with around 10% of grossular, spessartine and pyrope component (Fig. 5a). From these observations, two metamorphic stages can be distinguished in thin section: the first one {1} characterised by the association of Grt + Phe (1) + Pg + Ctd, and the second one {2} with Phe (2) + Chl + Czo.

Microstructures. As shown in Figure 3c chloritoid is aligned within a first foliation (S1), preserved in relic fold hinges formed during D2, i.e. when the main foliation (S2) formed. The main foliation S2 is defined by phengite, chlorite and clinozoisite. Figure 3f shows a top-to-the-W shear band associated with synkinematical growth of chlorite. Note that the shear plane dissects chloritoid. These observations allow attributing the assemblage {1} to the first deformation phase D1 and assemblage {2} to the D2 event (Tab. 3).

Table 2: Representatives microprobe analysis

Sample Mineral	Rui9906				Cere0035				Vga0139			Cret006		
	Phe	Grt core	Grt rim	Ctd	Phe	Grt	Chl	Ctd	Phe	Grt	Gln	Phe	Grt	Ctd
SiO ₂	47.14	36.62	36.91	27.66	50.12	36.52	25.65	24.11	49.81	36.56	58.31	44.55	37.97	23.55
TiO ₂	0.39	0.26	0.00	0.15	0.26	0.00	0.01	0.04	0.35	0.11	0.08	0.14	0.05	0.05
Al ₂ O ₃	30.96	20.28	19.83	30.44	26.57	19.54	19.53	37.71	25.66	19.50	10.43	34.03	18.23	36.74
FeO	4.90	21.03	22.01	21.93	3.50	35.17	31.85	26.46	3.70	30.53	13.45	2.25	28.30	26.57
MnO	0.18	18.22	16.63	9.44	0.06	3.08	0.22	0.58	0.05	4.68	0.04	0.00	5.52	0.71
MgO	1.33	0.64	0.70	1.66	2.38	2.05	10.98	1.95	3.13	0.88	8.85	0.31	0.55	1.44
CaO	0.01	3.15	3.99	1.54	0.00	4.78	0.01	0.05	0.00	7.46	0.17	0.00	7.95	0.02
Na ₂ O	0.24	0.04	0.00	0.03	0.40	0.02	0.04	0.12	0.38	0.02	6.90	0.85	0.02	0.00
K ₂ O	8.20	0.04	0.04	0.04	10.59	0.00	0.00	0.00	11.15	0.00	0.02	10.44	0.06	0.00
Total	93.35	100.28	100.11	92.89	93.88	101.16	88.15	91.02	94.23	99.74	98.25	92.57	98.65	89.16
Si	3.21	2.99	3.02	2.31	3.42	2.97	2.78	2.04	3.41	2.99	7.97	3.08	3.12	2.04
Ti	0.02	0.02	0.00	0.01	0.01	0.00	0.00	0.00	0.02	0.01	0.01	0.01	0.00	0.00
Al	2.49	1.95	1.91	3.00	2.14	1.87	2.49	3.76	2.07	1.88	1.68	2.77	1.77	3.76
*Fe ³⁺	-	0.06	0.09	0.61	-	0.17	-	0.19	-	0.13	0.49	-	0.23	0.19
Fe ²⁺	0.28	1.38	1.42	0.93	0.20	2.22	2.85	1.69	0.21	1.96	1.05	0.13	1.71	1.74
Mn	0.01	1.26	1.15	0.67	0.00	0.21	0.01	0.04	0.00	0.32	0.00	0.00	0.38	0.05
Mg	0.14	0.08	0.09	0.21	0.24	0.25	1.83	0.25	0.32	0.11	1.80	0.03	0.07	0.19
Ca	0.00	0.28	0.35	0.14	0.00	0.42	0.00	0.00	0.00	0.65	0.02	0.00	0.70	0.00
Na	0.03	0.01	0.00	0.00	0.05	0.00	0.00	0.02	0.05	0.00	1.83	0.11	0.00	0.00
K	0.71	0.01	0.00	0.00	0.92	0.00	0.00	0.00	0.97	0.00	0.00	0.92	0.01	0.00

Sample Vga0139

Petrology. Sample Vga0139 derives from the cover of an external part of the Internal unit (Fig. 1). The occurring minerals are glaucophane, phengite, paragonite, garnet, chlorite, quartz and minor amounts of opaque phases. Glaucophane, garnet, paragonite are associated with a first generation of phengite and represent peak pressure conditions. Abundant chlorite overgrows glaucophane, which has a rather constant X_{Fe} of 0.3-0.4 (Fig. 5b). Garnets show no zoning in their chemical composition ($X_{Alm} \sim 0.65$; $X_{Grs} \sim 0.20$; $X_{Prp} \sim 0.05$ and $X_{Sps} \sim 0.10$, see Fig. 5a) but are strongly retrogressed into chlorites that define the main foliation S2 in association with a second generation of phengite. Despite the presence of chlorite, the HP-mineral assemblage is dominating in this sample. The same mineral assemblage, but without garnet occurs also south of the Grand Sassièrè klippe within white quartzites (Fig. 2).


Microstructures. Figure 4g shows that chlorite grows in expense of glaucophane, suggesting that chlorite is the stable mineral in the main foliation S2. In many cases, due to the intense transposition during D2 glaucophane also appears to be aligned in the main foliation although it formed earlier: Backscatter images (Figs. 4h,f) clearly show that chlorite is the stable mineral in the main foliation, growing in expense of glaucophane (Fig. 4i) and garnet (Fig. 4h). Hence, only chlorite is stable in the main foliation S2. In conclusion, mineral assemblage garnet, glaucophane, phengite (1), and paragonite predates the main foliation and is therefore attributed to D1 (Tab.3). During the second deformation phase D2 only chlorite and phengite appear to be stable.

Samples Cret006 and SB 1.38-2

Petrology. These two samples derive from the same outcrop. Stratigraphically they belong to a late Permian to Early Miocene (?), reddish quartzite cropping out in Val di Rhêmes (Cigolini, 1992, 1995). In this quartzite two different mineralogical assemblages occur. In the sample Cret006 the mineral assemblage only consists white mica, garnet, quartz and \pm chlorite, while in the second

Table 3: Relationship between petrology and deformation in metasediments of the Briançonnais domain,

Mineral	detrital relicts	D1	D2	D3
garnet		Mn rich		
phengite				minor < 100 um
paragonite				
chloritoid				
glaucophane				
epidote				
quartz				
chlorite				
albite				



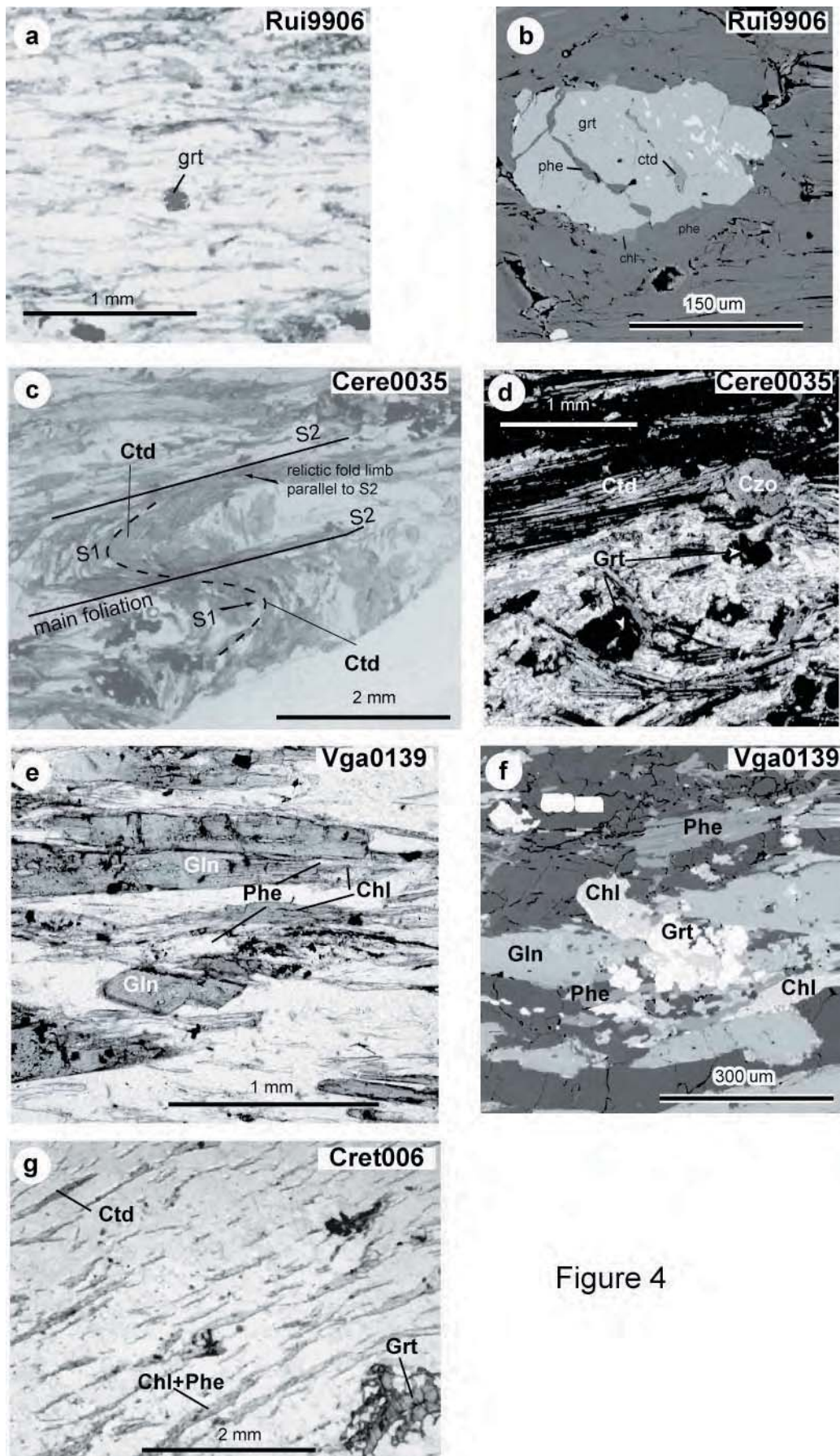


Figure 4

Figure 4: Sketch after photomicrographs (a, c, d, e, g) or REM images (b, f) of representative mineralogy observed in studied samples. a) & b) Sample Rui990 shows inclusions of chloritoid within small Mn-rich garnets. c) Earlier schistosity (S1) underlined by Ctd needles preserved in S2 fold hinges in sample Cere0035.

sample SB 1.38-2 only chloritoid, white mica, quartz and \pm chlorite is found.

In both samples the MgO content in the bulk rock is low (Table 1), and therefore garnet and chloritoid have Mg-poor compositions. Hence garnets have a mean composition of $X_{\text{Alm}} \sim 0.60$; $X_{\text{Gro}} \sim 0.30$; $X_{\text{Prp}} \sim 0.02$ and $X_{\text{Sps}} \sim 0.18$ (Fig. 5a) and X_{Mg} in chloritoid never exceeds 0.10.

Microstructures. The assemblages garnet-white mica, and chloritoid-white mica, respectively, occur as thin layers in the quartzitic matrix. However, chloritoid and garnet were never observed together in the same thin section although they occur in the same microstructural context. Both, chloritoid and garnet seem to predate the main foliation S2, underlined by chlorite and white micas. Often chloritoid is crosscut by S2, while dismembered garnet is often replaced by chlorite.

P-T estimates

Methods used

Equilibrium phase diagrams of natural samples, as well as model compositions, were calculated with the computer program DOMINO (De Capitani, 1994) for the NaCaKFMASH system. These diagrams visualise stable assemblages, including mode and composition of solution phases, for specific bulk rock compositions. The independent variables may be any combination of temperature, pressure, activity of a particular phase or compositional vectors. In order to include highly non-ideal solution models for minerals with potential miscibility gaps, stable mineral assemblages are computed using a Gibbs free energy minimization (De Capitani & Brown, 1987).

The main advantage of such equilibrium phase diagrams is that all phases are considered for each point, and that the diagrams are very easy to interpret if attention focuses on assemblages. Each field represents the predicted stability-field of a particular assemblage. However, the interpretation of the diagrams is limited by the accuracy of the thermodynamic data, and additionally, by the degree of equilibrium reached in that portion of a rock used for determining the bulk composition. The database of Berman (1988) was used for all calculations. However the latter was completed by the following recent thermodynamic data: the Mg-chloritoid data of B. Patrick (listed in Goffé and Bousquet, 1997), the Fe-chloritoid data of Vidal et al. (1994), the chlorite data of Vidal et al. (2001), the glaucophane data of Holland and Powell (1998), and the aluminos-celadonite data from Massonne and Szpurka (1997) to this database. The solution models for phengite are those from Keller et al. (2004), for chlorite those from Vidal et al. (2001), and for glaucophane those

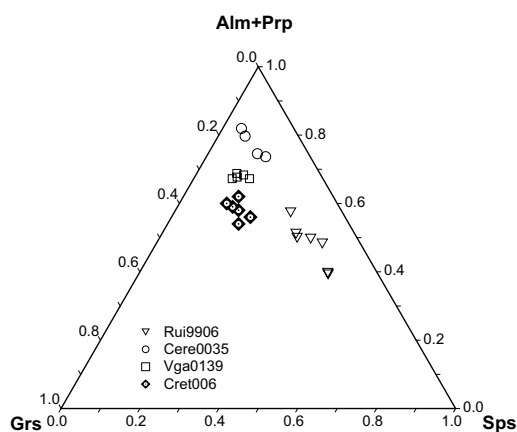


Fig. 5: Mineral chemistry: **a)** Ternary plot of garnet compositions for sample Cere0035 (open circle), Rui9906 (triangle), Vga0139 (filled circle); Cret006 (diamond) **b)** Na-amphibole compositions of sample Vga0139 (cf. Leake 1978)

from Holland and Powell (1998).

Figure 4 continued: d) In the same sample, Czo-Phe2-Chl mineral assemblage grows over the former one formed by Ctd-Grt-Phe1 e) & f) Gln-Grt assemblages occurring in Na-rich metasediments (Sample Vga0139). g) Relics of Ctd and Grt preserved in quartzite from the Internal unit (sample Cret006).

Because of the high Mn-content found in the metamorphic minerals (garnet, chloritoid, see Table 1) of sample Rui9906, whose whole rock chemistry does not indicate any Mn-enrichment (Table 1), the P-T estimates for this sample from the Zone Houillère unit were calculated by using the TWQ software package of Berman (1991). The calculations were done with the same database presented above, except for the white micas. Atom site repartition for white micas is calculated after Bousquet et al. (2002), and thermodynamic data are from Vidal and Parra (2000). Water activity was kept constant at value one, and no other fluid components were added.

Sample Rui9906 (Zone Houillère unit)

P-T estimates using the phase diagram equilibrium was not possible due to the lack of thermodynamic data for many Mn-rich phases. A multi-equilibrium (TWQ) approach taking into account the activity of minerals and the Mn-content of each mineral was applied to this sample in order to compute P-T estimates. Calculated equilibrium are done in the KFMASH system with the following phases: chlorite, garnet, phengite chloritoid and quartz. P-T estimates evidence greenschist metamorphic conditions around 5 kbar and 375 °C (Fig. 6). These estimates are consistent with evidences for incipient metamorphism in Mn-poor rocks, in which Mn-rich minerals such as spessartine-rich garnets often grow first (see for example Spear 1993).

Sample Cere0035 (Ruitor unit)

Figure 7a shows the resulting equilibrium diagram, calculated for the system $K_2O-Na_2O-CaO-FeO-MgO-Al_2O_3-SiO_2-H_2O$, and a water activity of one for the measured bulk rock composition of sample Cere0035. The stability field of the first mineralogical assemblage {1} composed of Grt, Pg, Phe, Chl and Ctd ranges from 440 to 480°C for pressures between 8.5 kbar and 15kbar (Fig. 7a). The temperature interval is constrained by the appearance of Lws towards lower temperatures, and by the disappearance of Pg towards higher temperatures. The appearance of Gln towards higher and the appearance of Czo towards lower pressures delimits the stability field. Calculation of the isopleths for X_{Mg} in chloritoid, which vary between 0.9 and 0.12 in this sample, allow for a further restriction of the pressure between 11 and 13.5 kbar for temperatures ranging form 450 to 480°C (Fig. 7a).

The retrograde path is constrained by the assemblage Czo, Chl, Phe that forms the main foliation and is stable for pressure conditions below 7 kbar and temperature below 450°C.

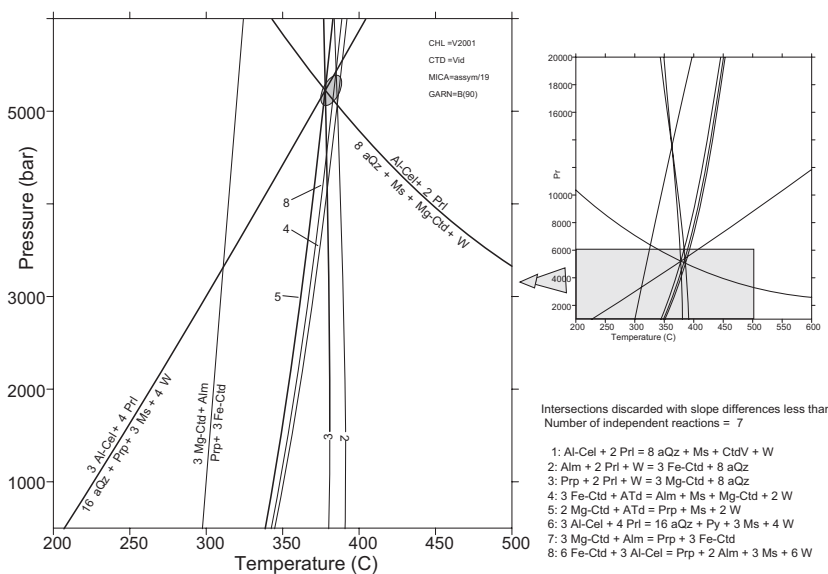


Figure 6: Multi-equilibria calculations for the sample Rui9906. The observed mineral assemblage Ctd-Grt-Phe is stable for P-T conditions around 5.2 kbar and 375°C

Sample Vga0139 (external part of the Internal unit)

Figure 7b shows the equilibrium phase diagram calculated in the K_2O - Na_2O - CaO - FeO - MgO - Al_2O_3 - SiO_2 - H_2O system for the bulk rock composition of sample Vga0139, which is an intermediate between metapelite and sandstone. The dominant mineral assemblage stable at HP stage is formed by Gln-Grt-Phe-Pg. The overgrowth of garnet and glaucophane by chlorite clearly documents metastability of these minerals during the exhumation. The equilibrium diagram predicts that the HP mineral assemblage is stable from 10 kbar to 17 kbar and from 440° C to 540° C. Temperature is as was the case in the previously discussed sample confined by the absence of lawsonite and the disappearance of paragonite towards lower and higher temperatures, respectively. The pressure limits are given by the appearance of jadeite towards higher pressures, and by the growth of clinozoisite and feldspar towards lower pressures. Absence of jadeite in this sample indicates that pressures did not exceed 17 kbar in this part of the Internal unit. In contrast, the absence of Czo and Fsp, expected to form at lower pressures, is seen as an indication that this sample escaped intense retrogression. Although chlorite is clearly a retrograde product, its presence alone is not sufficient for further constraining retrograde P-T conditions. Analogous to sample Cere0035, further restrictions on pressures and temperatures within the stability field by the composition of phengite are not possible, due to the small variations (only ~4 %) predicted by the phengite isopleths (Fig. 7b).

Sample Cret006 (Internal unit)

Figure 7c shows the equilibrium phase diagram calculated in the K_2O - Na_2O - CaO - FeO - MgO - Al_2O_3 - SiO_2 - H_2O system for sample Cret006. In this sample the HP mineral assemblage is composed of Ctd, Grt, Phe, Qz. This assemblage is only stable in a small field between 16 and 17.5 kbar at $500 \pm 10^\circ$ C (Fig. 7c), which is limited by the same reactions as described for the previous sample. The occurrence of Lws delimits the stability field towards lower temperatures, while the breakdown of Ctd delimits it towards higher temperature. The maximum in pressure is constrained by the disappearance of Chl at higher pressure. Because no biotite occurs in this sample, and since Chl is the only retrograde mineral, rather cooling than isothermal decompression characterises the retrograde path of this sample (Fig. 7c).

Interpretation***Peak metamorphic conditions***

P-T estimates from the Zone Houillère unit indicate pressures of ~5 kbar at temperatures of ~375° C (Fig. 8) for the internal parts of the Zone Houillère unit situated near the contact with the Ruitor unit. Slightly lower metamorphic conditions of 2.5 to 4 kbar at 300° C are proposed by Ceriani et al. (2003) for the external part of the Zone Houillère unit further to the south and confirmed by fission track analysis (Fügenschuh & Schmid, 2003; Malusà et al., 2005). Taking into account the uncertainty of the measurements and the different used methods these small differences within the Zone Houillère unit could be considered as an increasing metamorphic grade towards the internal parts of the Zone Houillère unit. The disappearance of the coal measures and fossil plants, and the appearance of Mn-rich garnet, towards the SE (internal) are excellent arguments supporting an increase metamorphic grade towards the SE, where spessartine-rich garnet occurs (Desmons et al., 1999a).

In the Ruitor unit the P-T estimates evidence peak pressures ranging between about 11-13.5 kbar at temperatures between 450-480° C (Fig. 8). These data clarify the Alpine metamorphic history of the Ruitor unit, and indicate a HP imprint for this unit. So far, two different interpretations for the

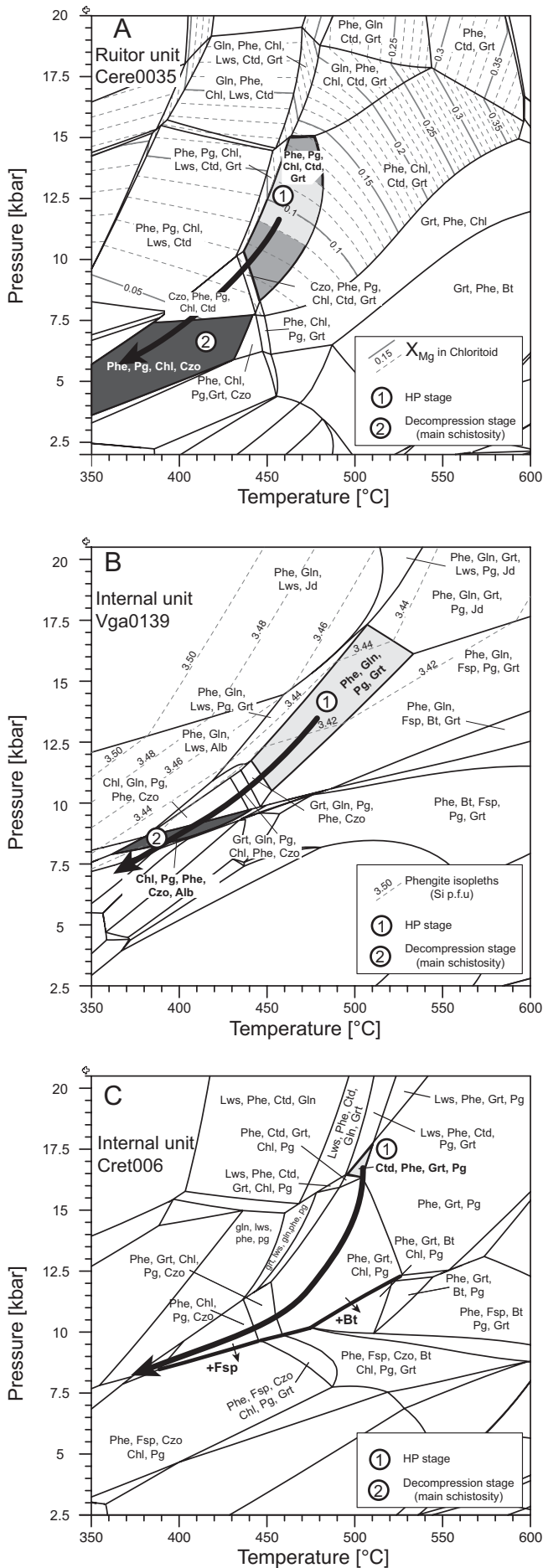


Figure 7: Equilibrium phases diagrams and P-T paths computed with DOMINO for different kind of metasediments of the Briançonnais terrane. All these rocks [a) Cere0035, b) Vga0136, c) Cret006] display an HP metamorphic imprint and a cold retrograde path. a) For the sample Cere0035, peak pressure (~13 kbar, 460°C) is constrained by Grt-Phe-Pg-Ctd-Chl assemblage stability field and by the Ctd composition and retrograde path (at ~6kbar, 400°C) by Phe-Chl-Czo assemblage. b) Phengite isopleths and occurrence of Gln together with Grt-Phe-Pg (sample Vga0139) define an HP stability field (~13 kbar, 480°C), and appearance of Czo at ~9kbar, 430°C documents a cold retrogression. c) In quartzite (sample Cret006) in which metamorphic minerals are scarce stability field of Ctd-Grt-Phe1-Pg is well constrain at 16 kbar, 500°C.

P-T evolution exist in the literature for the Ruitor unit. While several authors only inferred elevated greenschist facies conditions (~ 7 kbar/ 400°C ; e.g. Baudin 1987, Desmons et al. 1999c), others (mainly Caby 1996), have postulated eclogite facies conditions (12-14 kbar, 450°C). The debate regarding the P-T conditions has been mainly about the attribution of specific minerals to either Alpine or pre-Alpine assemblages in the basement.

Within the third investigated unit, the Internal unit, P-T estimates indicate still higher metamorphic conditions when compared to other units. P-T conditions range from 10 to 17 kbar and 440 to 540°C in the external part of this unit near the contact to the Ruitor unit (Fig. 8, Vga0139), and from 16 to 17.5 kbar and 490 to 510°C in a structural position one kilometre further to the SE (Fig. 8, Cret006, Fig. 9). The pressure range from 10 kbar to 17 kbar at temperatures of 440°C to 540°C , inferred from the external part of the internal unit (Vga0139), is very large. This large uncertainty is given by the stability of glaucophane. Unfortunately, with the observed mineralogical assemblages, it is not possible to better constrain peak metamorphic conditions. Because sample Vag0139 and sample Cere006 are collected within a distance of only about one kilometre when projected along strike (Fig. 9), it is assumed that they underwent identical peak P-T conditions. Therefore the overlap of the stability fields of the samples with different rock chemistries (Vga0139, Cret006) represents the best estimate for the (external) part of the Internal unit, giving P-T estimates around 16 kbar and 500°C (Fig. 9). At the contact with the Schistes Lustrés, Cigolini (1995) estimated pressures higher than 12 kbar at temperatures around 500°C , based on the observation of pseudomorphs after jadeite in Permian quartzites of the Internal unit. All these data shows that there are clear evidences for HP metamorphism in the Ruitor unit and the Internal unit.

Correlation between petrology and deformation

In summary, the P-T investigations on the post-Hercynian sediments of the Briançonnais terrane along the ECORS-CROP profile clearly show that each tectonic unit recorded a different metamorphic history (Fig. 9). We observe an increase in peak pressure metamorphic conditions from greenschist facies conditions in the Northwest (Zone Houillère) to the transition between blueschist and eclogite facies conditions (in reference to the facies grid of Bousquet et al., 1997) in the Southeast (Internal unit). Regionally, three main deformation phases (D1-D3) have been observed in

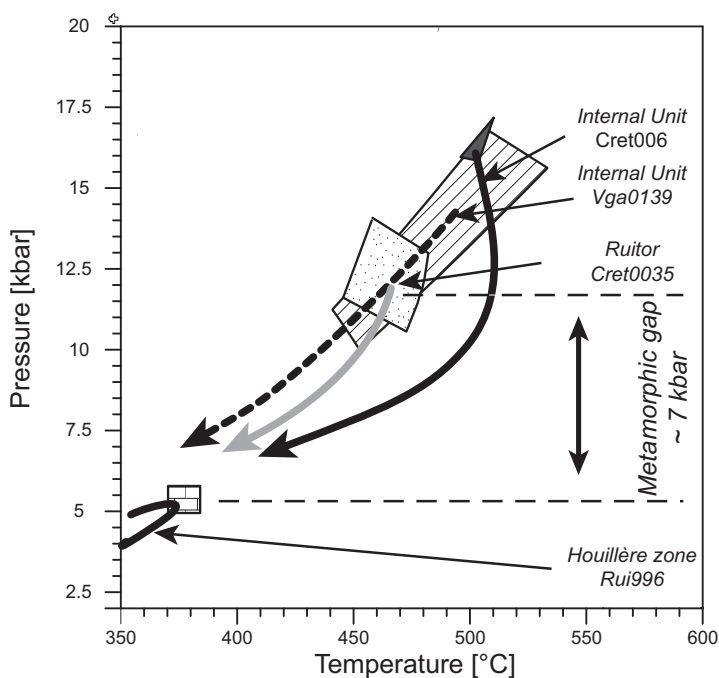


Figure 8: Summary of P-T estimates for all studied samples. We note two kinds of metamorphic histories: a deep evolution for the Ruitor massif and the Internal unit and a shallow one for the Houillère zone with a pressure gap of about 7 kbar.

the studied area and have been described in a previously by Bucher et al. (2004). The main foliation, underlined by the mineral assemblages Phe-Chl-Czo or by late growth of chlorite, is connected with the development of a second deformation phase D₂ (Caby 1968; Cigolini 1995; Bucher et al. 2004). HP mineral assemblages, preserved as microlithons or inclusions in the investigated samples, indicate that higher metamorphic conditions predate the main foliation in all units. Hence, as shown by microstructural analysis, the metamorphic peak can be attributed to a first deformation phase D₁.

In the P-T diagram peak pressure conditions for the different tectonic units define a linear trend indicating a continuous metamorphic gradient during D1. The estimated geotherm of 8° C/ km is typical for subduction. Furthermore, the assumption that the presently stacked tectonic units once represented a lateral continuity is also confirmed by the occurring gradient. However, stacking of more internal units over more external units during exhumation (D2) following peak pressure conditions (D1) generated metamorphic discontinuities at the different tectonic contacts. For example the Ruitor unit was thrust over the Zone Houillère unit during a late stage of D2 (Bucher et al. 2004). Between these two units, a difference in peak pressures of about 7 kbar results. This large difference of 7 kbar can hardly be explained by a metamorphic gradient corresponding to about 25 km difference depth. Presently, the localities of sample Rui9906 (Zone Houillère unit) and Cere0035 (Ruitor unit) are at a distance of only 2.5 km (Fig. 9). Of course, due to D3 refolding, the present day distance does not exactly correspond to the original distance in the undeformed nappe stack. However a reduction of the thickness by a factor ten seems unlikely. Hence, we exclude a metamorphic gradient internally of the Ruitor unit to cause the observed pressure difference of ~7 kbar. Instead, we interpret the difference of ~7 kbar in peak pressure between the Ruitor unit and the Zone Houillère unit to represent a metamorphic discontinuity at the tectonic contact created during D2 nappe stacking.

P-T-d paths

While in the all studied samples HP mineral assemblages, preserved as microlithons or inclusions are contemporaneous to the first phase of deformation D1, the main foliation attributed to D2 is underlined by the mineral assemblages Phe-Chl-Czo in the Permo-Triassic cover of the Ruitor unit (Cere0035) and by growth of chlorite after garnet, glaucophane or chloritoid in the Internal unit (Vga0139, Cret006) (Table 3). P-T estimates for the D2 mineral assemblage indicate pressures lower than 7 kbar and temperatures lower than 450°C in the Ruitor unit (Fig. 9), resulting in a decompression of at least 4 kbar and a cooling of ~50° C during D2 exhumation. This contrasts with the interpretation of Bucher et al. (2003), which interpreted isothermal decompression, although estimates for D1 and D2 differ only slightly. This is due to the resulting stability fields in the calculated P-T diagrams, which excludes an isothermal decompression by the presence of Czo (Fig. 7a).

The retrograde path of the Internal unit is not well constrained, however, some observations at least allow for some restrictions. The absence of biotite in sample Cret006 excludes isothermal decompression below 11 kbar (at temperatures around 500° C, Fig. 9), and the tectonic contact between the Ruitor unit and the Internal unit is active at an early stage during D2, the latter being passively transported onto the Zone Houillère unit during a late stage of D2. Therefore, the Ruitor unit and Internal unit share a common P-T evolution from an early stage of D2 onwards. Consequently the P-T path of these two units must join in the stability field of D2 from the Ruitor unit (Fig. 9). Combining all these arguments leads to the conclusion that the Internal unit came in contact with the Ruitor unit at around 8 kbar for temperatures around 420° C, resulting in a cooling of ~100° C and a decompression of ~7 kbar. It seems that all units share a common late P-T history (Fig. 9) at least from temperature around 300°C, as has been shown by fission track studies (Fügenschuh & Schmid, 2003; Malusà et al., 2005).

Discussion

In the Western Alps, the paleogeographic significance and the metamorphic evolution of the Briançonnais microcontinent have always been subject to debate (Stampfli, 1993; Monié, 1990). In the southwestern Alps, a HP imprint is well documented by occurrences of Fe,Mg-carpholite (Goffé, 1977, 1984; Goffé et al., 1973, 2004; Goffé & Chopin, 1986), aragonite (Goffé & Velde, 1984) or relatively well organized graphite structure (Beysac et al., 2002) in metasediments and by occurrences of lawsonite and jadeite in metabasites (Lefèvre & Michard, 1976; Schwartz et al., 2000). Paradoxically, in the northwestern Alps, only the upper most unit of the Briançonnais domain (the Mont Fort nappe) displays the deepest evolution into high-pressure metamorphic evolution in epidote-blueschist facies conditions (Schaer, 1959, Bearth, 1963, Bousquet et al., 2004).

In contrast to the latter this study shows that in the central part of the Western Alps along the trace of the ECORS-CROP seismic line, petrology of post-Hercynian metasediments clearly indicate a deep evolution in blueschist-eclogite transition (BET, Oberhänsli et al., 2004) facies conditions for the internal (eastern) part. Peak pressure conditions have been correlated with the first deformation phase (D1), which predates the main stage of nappe stacking (Bucher et al. 2004). Exhumation of HP rocks took place during nappe stacking (D2) of more internal units overthrust northwestwards over external ones. The external (western) area displays a metamorphic evolution within greenschist conditions. Pressures of ~5 kbar found in the internal parts of Zone Houillère unit allow to conclude that this unit was never deeply subducted, and therefore only incorporated into the nappe stack at a very late stage and during the exhumation of the higher pressure Ruitor unit and Internal unit. Along the ECORS-CROP profile, the major metamorphic gap (~7 kbar) occurs at the contact between Ruitor

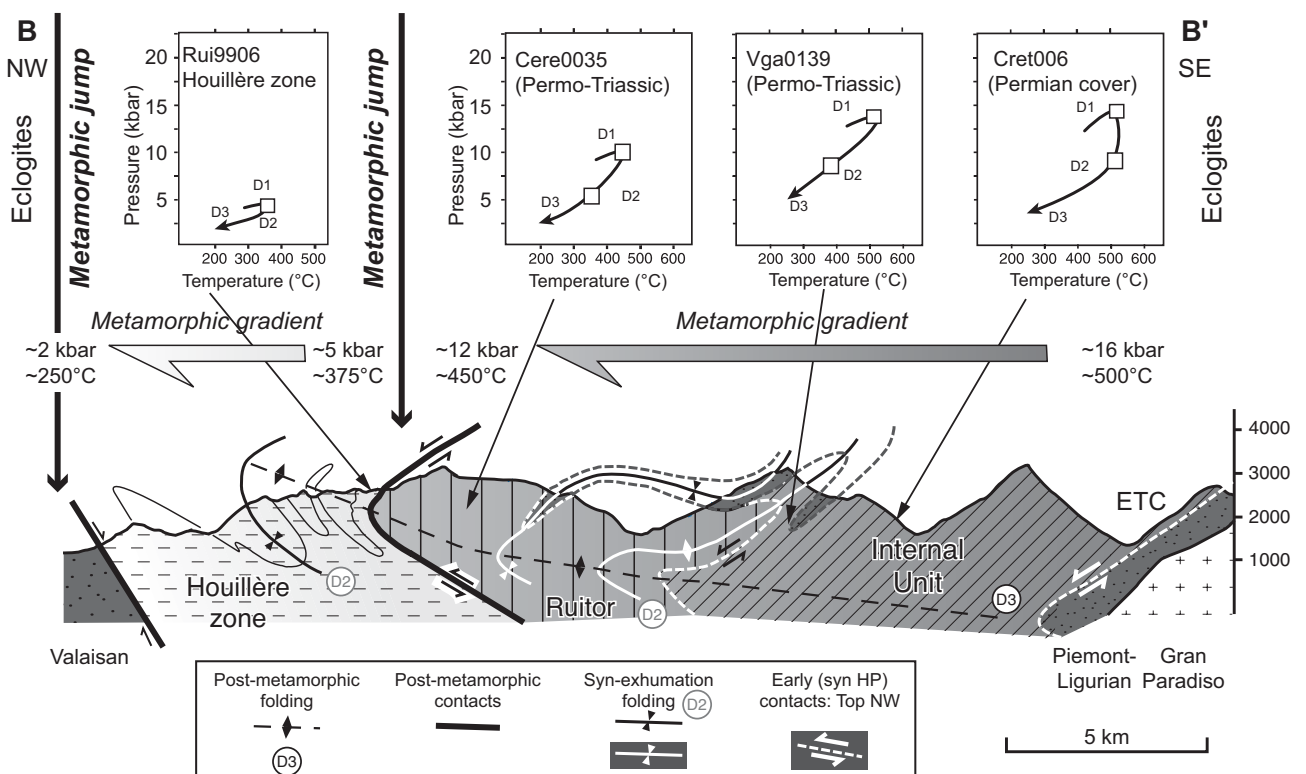


Figure 9: Schematic cross section (modified after Bucher et al., 2003) in which metamorphic evolution of each unit has been reported. Retrodeforming of the late deformation phase (D3) documents an apparent inverse metamorphic field gradient results from the stacking of the internal units (Internal & Ruitor) over the more external one (Houillère zone) during exhumation (D2).

unit (~12 kbar) and the Houillère zone (~4.5 kbar), as it was already predicted by Caby et al. (1978). The occurring difference in peak pressures is interpreted in this study as the result of the late D_2 activity of the tectonic contact between both units by overthrusting the higher metamorphic Ruitor unit over the low metamorphic Zone Houillère unit during the exhumation of the HP units.

Conclusion

In the present study, we have showed that petrologic investigation of metasediments is not only of mineralogical interest but also provides us with fine tools for dissecting the geodynamic evolution of mountain belts. We documented that a detailed metamorphic history and an HP imprint could be evidenced in many kind of sediments (quartzites, pelites, coal). Hence, according to the bulk rock chemistry, the same mineralogical assemblage as Grt-Ctd_Phe could result from different metamorphic evolutions. In coal-rich metasediments of the Houillère zone in the West the assemblage composed of Grt (Mn-rich)-Ctd-Phe indicates pressures of ~5kbar at ~375° C, while the same assemblage in quartzite documents HP conditions (~16 kbar, 500°C) in the East.

These results argue for groups, according to the metamorphic evolution, within continental rocks of Briançonnais terrane during the alpine orogeny. PT-estimations suggest deep burial for rocks located in the East (Ruitor and Internal units) at the contact with the Piemont-Ligurian ocean and only shallow burial for rocks at the contact with the Valaisan ocean in the West .A major tectonic contact, with top-to-the-northwest kinematics is active during exhumation of HP rocks and separates these two groups. The resulting apparent inverse metamorphic field gradient can be interpreted as representing different depths of subduction due to the paleogeographic position of the different units.

Acknowledgements

Substantial funding by the Swiss National Science Foundation (projects 20-55559.98 and 2000-63391.00) is gratefully acknowledged. This work has benefited from comments, help and support by C. de Capitani, L. Keller and K. Waite. S. Schmid is thanked for fruitful discussions and constructive criticism an earlier version of the manuscript. W. Stern, H. Hürlimann and R. Milke from the Geochemical laboratory of the Basel University are thanked for performing the chemical analyses. Katy Waite helped with the microprobe analyses.

References

- Adatte, P., Dubas, A., Tache, E. and Strauss, F. (1992): Géologie et minéralogie du haut Val di Rhêmes (Vallée d'Aoste). Unpubl. diploma thesis Univ. Lausanne, 134 pp.
- Amstuz, A. (1955): Rocher du ravin de Lessert dans la Val D'Aoste. *Arch. Sc. Genève* **8**, 6-9.
- Amstuz, A. (1962): Notice pour une carte géologique de la Vallée de Cogne et de quelques autres espaces au Sud d'Aoste. *Arch. Sc. Genève* **15**, 1-104.
- Baudin, T. (1987): Étude géologique du Massif du Ruitor (Alpes franco-italiennes): évolution structurale d'un socle briançonnais. Unpubl. Thèse du 3ième cycle, Grenoble, 243 pp.
- Bearth, P. (1963): Contribution à la subdivision tectonique et stratigraphique du cristallin de la nappe du Grand Saint-Bernard dans le Valais (Suisse). In: Durand Delga, M. (ed.): Livre à la mémoire du Professeur Fallot 2. Mémoire de la Société géologique de France, Paris, 407-418
- Berman, R.G. (1988): Internally-Consistent Thermodynamic Data for Minerals in the system $\text{Na}_2\text{O}-\text{K}_2\text{O}-\text{Ca}-\text{MgO}-\text{FeO}-\text{Fe}_2\text{O}_3-\text{Al}_2\text{O}_3-\text{SiO}_2-\text{TiO}_2-\text{H}_2\text{O}-\text{CO}_2$. *J. Petrology* **29/2**, 445-522.
- Berman, R.G. (1991): Thermobarometry using multiequilibrium calculations: a new technique, with petrological applications. *Can. Mineral.* **29**, 833-855.
- Bertrand, J.M., Pidgeon, R.T., Leterrier, J., Guillot, F., Gasquet, D. and Gattiglio, M. (2000): SHRIMP and IDTIMS U-Pb zircon ages of the pre-Alpine basement in the Internal Western Alps (Savoy and Piemont). *Schweiz. Mineral. Petrogr. Mitteil.* **80**, 225-248.
- Beyssac, O., Goffé, B., Chopin, C. and Rouzaud, J.-N. (2002): Raman spectra of carbonaceous material in metasediments: a new geothermometer. *J. Metamorph. Geol.* **20/9**, 859-872.
- Bocquet [Desmons], J. (1974): Le socle briançonnais de Vanoise (Savoie): arguments en faveur de son âge anté-alpin et de son polymétamorphisme. *C.R. Acad. Sc. Paris* **278**, 2601-2604.
- Bocquet, J. (1974): Études minéralogiques et pétrographiques sur les métamorphismes d'âge alpine dans les Alpes françaises. Unpubl. Thèse d'État, Grenoble, 490 pp.
- Bousquet, R., Goffé, B., Henry, P., Le Pichon, X. and Chopin, C. (1997): Kinematic, Thermal and Petrological model of the Central Alps: Lepontine Metamorphism in the Upper Crust and Eclogitisation of the Lower Crust. *Tectonophysics* **273**, 105-127.
- Bousquet, R., Goffé, B., Vidal, O., R., O. and Patriat, M. (2002): The tectono-metamorphic history of the Valaisan domain from the Western to the Central Alps: New constraints on the evolution of the Alps. *Geol. Soc. Am. Bull.* **114/2**, 207-225.
- Bousquet, R., Engi, M., Gosso, G., Oberhänsli, R., Berger, A., Spalla, M.I., Zucali, M. and Goffé, B. (2004): Transition from the Western to the Central Alps. In: Oberhänsli, R. (ed.): Explanatory note to the map "Metamorphic structure of the Alps" 149. Mitteilungen Österreichische Mineralogische Gesellschaft, Wien, 145-156
- Bucher, S., Schmid, S.M., Bousquet, R. and Fügenschuh, B. (2003): Late-stage deformation in a collisional orogen (Western Alps): nappe refolding, back-thrusting or normal faulting? *Terra Nova* **15/2**, 109-117.
- Bucher, S., Ulardic, C., Bousquet, R., Ceriani, S., Fügenschuh, B., Gouffon, Y. and Schmid, S.M. (2004): Tectonic evolution of the Briançonnais units along a transect (ECORS-CROP) trough the Western Alps. *Eclog. Geol. Helv.* **97/3**, 321-346.

- Caby, R., Kienast, J.-R. and Saliot, P. (1978): Structure, métamorphisme et modèle d'évolution tectonique des Alpes Occidentales. *Revue de Géographie physique et de Géologie dynamique* **XX/4**, 307-322.
- Caby, R. and Kienast, J.-R. (1989): Meso-Alpine high-pressure assemblages and excavation of the Ruitor Briançonnais basement (Savoie, Val d'Aoste, Graie Alps). *Terra Abstr.* **1/266**
- Caby, R. (1996): Low-angle extrusion of high-pressure rocks and the balance between outward and inward displacements of Middle Penninic units in the western Alps. *Eclogae Geol. Helv.* **89/1**, 229-267.
- Chopin, C., Seidel, E., Theye, T., Ferraris, G., Ivaldi, G. and Catti, M. (1992): Magnesiochloritoid and the Fe-Mg series in the chloritoid group. *Eur. J. of Mineral.* **4**, 67-76.
- Cigolini, C. (1981): Garnet chemistry and zonation in the Italian sector of the Grand Saint Bernard nappe. *Att. Accad. Scienz. Torino* **115**, 331-344.
- Cigolini, C. (1992): Note Illustrative alla Carta Geologica del Ricoprimento del Gran San Bernardo tra la Valsavarenche e la Val di Rhêmes (Valle d'Aosta). Regione Autonoma della Valle d'Aosta. 1:20.000.
- Cigolini, C. (1995): Geology of the Internal Zone of the Grand Saint Bernard Nappe: a metamorphic Late Paleozoic volcano-sedimentary sequence in South-Western Aosta Valley (Western Alps). In: Lombardo, B. (ed.): Studies on metamorphic rocks and minerals of the western Alps. A Volume in Memory of Ugo Pognante. 13, n°2. Bollettino del Museo Regionale di Scienze Naturali (suppl.), Torino, 293-328
- Dal Piaz, G.V. and Lombardo, B. (1986): Early Alpine eclogite metamorphism in the Pennine Monte Rosa - Grand Paradiso basement nappes of the northwestern Alps. *Geol. Soc. Am. Mem.* **164**, 249-265.
- De Capitani, C. and Brown, T.H. (1987): The computation of chemical equilibrium in complex systems containing non-ideal solutions. *Geochimica et Cosmochimica Acta* **51**, 2639-2652.
- Debelmas, J., Elter, G., Antonie, P., Elter, M., Baudin, T., Caby, R., J., F., Mercier, D., Marion, R., M., G. & Jaillard, E (1991): Carte Géologique de la France à 1/50000 Feuille Ste-Foy-Tarentaise. Bur. Rech. Géol. Min. 1:50000.
- Debelmas, J., Caby, R. and Desmons, J. (1991): Notice explicative, Carte géologique de la France à 1/50000, Feuille Ste-Foy-Tarentaise. *Bur. Rech. Géol. Min., eds. Orléans* **728**, 43pp.
- Desmons, J. and Mercier, D. (1993): Passing through the Briançon Zone. In: Neubauer, J.F.V.R.F. (ed.): Pre-Mesozoic Geology in the Alps. Springer-Verlag, Heidelberg, 279-295
- Desmons, J., Aprahamian, J., Compagnoni, R., Cortesogno, L. and Frey, M. (1999): Alpine Metamorphism of the Western Alps: I. Middle to high T/P metamorphism. *Schweiz. Mineral. Petrogr. Mitteil.* **79**, 89-110.
- Desmons, J., Aprahamian, J., Compagnoni, R., Cortesogno, L., Frey, M. and Gaggero, L. (1999): Pre-Alpine metamorphism of the Internal zones of the Western Alps. *Schweiz. Mineral. Petrogr. Mitteil.* **79**, 23-39.
- Desmons, J., Aprahamian, J., Compagnoni, R., Cortesogno, L., Frey, M., Gaggero, L., Dallagiovanna, G., Seno, S. and Radelli, L. (1999): Alpine metamorphism of the Western Alps: II. High-P/T and related pre-greenschist metamorphism. *Schweiz. Mineral. Petrogr. Mitteil.* **79**, 111-134.
- Ellenberger, F. (1958): Étude géologique du pays de Vanoise. *Mém. Serv. Explic. Carte géol. dét. Fr.* 561 pp.
- Elter, G. (1960): La zona pennidica dell'alta e media Val d'Aosta e le unità limitrofe. *Mem. Ist. Geol. Univ. Padova* **22**, 113pp.

- Elter, G. (1972): Contribution à la connaissance du Briançonnais interne et de la bordure piémontaise dans les Alpes Graies nord-orientales et considérations sur les rapports entre les zones du Briançonnais et des Schistes lustrés. *Mem. Ist. Geol. Univ. Padova* **26**, 1-19.
- Fabre, J. (1961): Contribution à l'étude de la Zone Houillère Briançonnaise en Maurienne et en Tarantaise (Alpes de Savoie). *Bur. Rech. Géol. Min.* **2**, 315pp.
- Feys, R. (1963): Etude géologique du Carbonifère brinaçonnais (Hautes-Alpes). *Bur. Rech. Géol. Min.* **6**, 387 pp.
- Fügenschuh, B., Loprieno, A., Ceriani, S. and Schmid, S. (1999): Structural analysis of the Subbriançonnais and Valais units in the area of Moûtiers (Savoy, Western Alps): paleogeographic and tectonic consequences. *Int. Journ. Earth Sciences* **88**, 201-218.
- Fügenschuh, B. and Schmid, S.M. (2003): Late stages of deformation and exhumation of an orogen constrained by fission-track: A case study in the Western Alps. *Geol. Soc. Am. Bull.* **115/11**, 1425-1440.
- Gerber, C. (1965): Flore et stratigraphie du Carbonifère des Alpes françaises Bull. B.R.G.M 21, 380 pp.
- Goffé, B., Goffé-Urbano, G. and Saliot, P. (1973): Sur la présence d'une variété magnésienne de la ferrocapholite en Vanoise (Alpes françaises): sa signification probable dans le métamorphisme alpin. *C. R. Acad. Sci. Paris* **277**, 1965-1968.
- Goffé, B. (1977): Succession de subfacies métamorphiques en Vanoise méridionale (Savoie). *Contrib. Mineral. Petrol.* **62**, 23-41.
- Goffé, B. (1984): Le facies à carpholite-chloritoïde dans la couverture briançonnaise des Alpes Ligures: un témoin de l'histoire tectono-métamorphique régionale. *Mem. Soc. Geol. It.* **28**, 461-479.
- Goffé, B. and Velde, B. (1984): Contrasted metamorphic evolution in thrust cover units of the Briançonnais zone (french Alps): a model for the conservation of HP-BT metamorphic mineral assemblages. *Earth and Planetary Science Letters* **68**, 351-360.
- Goffé, B. and Chopin, C. (1986): High-pressure metamorphism in the Western Alps: zoneography of metapelites, chronology and consequences. *Schweiz. Mineral. Petrogr. Mitteil.* **66**, 41-52.
- Goffé, B. and Bousquet, R. (1997): Ferrocapholite, chloritoïde et lawsonite dans les métapelites des unités du Versoyen et du Petit St. Bernard (zone valaisanne, Alpes occidentales). *Schweiz. Mineral. Petrogr. Mitteil.* **77**, 137-147.
- Goffé, B., Schwartz, S., Lardeaux, J.-M. and Bousquet, R. (2004): Metamorphic structure of the Western and Ligurian Alps. In: Oberhänsli, R. (ed.): Explanatory note to the map "Metamorphic structure of the Alps" 149. Mitteilungen Österreichische Mineralogischen Gesellschaft, Wien, 125-144
- Gouffon, Y. (1993): Géologie de la «nappe» du Grand St-Bernard entre la Doire Baltée et la frontière Suisse (Vallée d'Aoste- Italie. *Mémoires de Géologie (Lausanne)* **12**, 147.
- Holland, T.J.B. and Powell, R. (1998): An internally consistent thermodynamic data set for phases of petrological interest. *J. Metamorph. Geol.* **16/3**, 309-343.
- Keller, L.M., Abart, R., Schmid, S.M. and De Capitani, C. (2005): Phase Relations and Chemical Composition of Phengite and Paragonite in Pelitic Schists During Decompression: a Case Study from the Monte Rosa Nappe and Camughera-Moncucco Unit, Western Alps. *J. Petrology* **in press**, doi:10.1093/petrology/egi051.

- Lefèvre, R. and Michard, A. (1976): Les nappes briançonnaises internes et ultra-briançonnaises de la bande d'Acceglio (Alpes franco-italiennes). Une étude structurale et pétrographique dans le faciès des schistes bleus à jadéite. *Sci. Géol., Bulletin* **29/3**, 183-222.
- Loprieno, A. (2001): A combined structural and sedimentological approach to decipher the evolution of the Valaisan domain in Savoy (Western Alps) Unpublished PhD thesis, Univ. Basel. Unpubl. Basel, 285 pp.
- Malusà, M.G., Polino, R., Zattin, M., Bigazzi, G., Martin, S. and Piana, F. (2005): Miocene to Present differential exhumation in the Western Alps: Insights from fission track thermochronology. *Tectonics* **24**, TC3004.
- Massonne, H.-J. and Szpurka, Z. (1997): Thermodynamic properties of white micas on the basis of high-pressure experiments in the systems K_2O - MgO - Al_2O_3 - SiO_2 - H_2O and K_2O - FeO - Al_2O_3 - SiO_2 - H_2O . *Lithos* **41**, 229-250.
- Monié, P. (1990): Preservation of Hercynian Ar-40/Ar-39 Ages Through High-Pressure Low-Temperature Alpine Metamorphism In The Western Alps. *Eur. J. of Mineral.* **2/3**, 343-361.
- Nagel, T., De Capitani, C. and Frey, M. (2002): Isograds and PT evolution in the eastern Lepontine Alps, Switzerland. *J. Metamorph. Geol.* **20/3**, 309-324.
- Nicolas, A., Polino, R., Hirn, A., Nicolich, R. and Group, E.-C.W. (1990): ECORS-CROP traverse and deep structure of the Western Alps: a synthesis. In: Roure, F., Heitzmann, P. and Polino, R. (eds): Deep structure of the Alps. Mémoire de la Société géologique de France 156, Paris, 15-28
- Oberhänsli, R. & coll. (2004): Metamorphic structure of the Alps. Commission for the Geological Map of the World. Paris. 1:1'000'000.
- Pfiffner, O.A., Lehner, P., Heitzmann, P. and Mueller, S. (1997): Deep Structures of the Alps: Results from NRP 20. In: Pfiffner, O.A.. (ed.). Birkhäuser, Basel, 73-114
- Polino, R. and Dal Piaz, G.V. (1978): Geologia dell'Alta Val d'Isère e del Bacino del lago Serrù. *Memorie degli Istituti di Geologia e Mineralogia dell'Università di Padova* **22**, 1-20.
- Polino, R., Dal Piaz, G.V. and Gosso, G. (1990): The alpine cretaceous orogeny: an accretionary wedge model based on integrated stratigraphic, petrologic and radiometric data. In: Roure, F., Heitzmann, P. and Polino, R. (eds): Deep structure of the Alps. Mémoire de la Société géologique de France 156, Paris, 345-367
- Roure, F., Heitzmann, P. and Polino, R. (1990): Deep structure of the Alps. Mémoires de la société géologique de France 156, Paris, 367 pp.
- Saadi, M. (1992): Géologie du haut Val di Rhêmes (Vallée d'Aoste). Unpubl diploma thesis. Univ. Genève, 120 pp.
- Schaer, J.-P. (1959): Géologie de la partie septentrionale de l'éventail de Bagnes (entre le Val d'Hérémence et le Vaal de Bagnes, Valais, Suisse). *Archives des Sciences (Genève)* **12**, 473-620.
- Schmid, S.M., Pfiffner, O.A., Froitzheim, N., Schönborn, G. and Kissling, E. (1996): Geophysical-geological transect and tectonic evolution of the Swiss-Italian Alps. *Tectonics* **15/5**, 1036-1064.
- Schmid, S.M. and Kissling, E. (2000): The arc of the Western Alps in the light of new data on deep crustal structure. *Tectonics* **19/1**, 62-85.
- Schmid, S.M., Fugenschuh, B., Kissling, E. and Schuster, R. (2004): Tectonic map and overall architecture of the Alpine orogen. *Ecolgae Geol. Helv.* **97/1**, 93-117.

- Schwartz, S., Lardeaux, J.-M. and Tricart, P. (2000): La zone d'Acceglio (Alpes cottiennes): un nouvel exemple de croûte continentale éclogitisée dans les Alpes occidentales. *C. R. Acad. Sci. Paris* **320**, 859-866.
- Schürch, M.L. (1987): Les ophiolites de la zone du Versoyen: témoin d'un bassin à évolution métamorphique complexe. Unpubl. PhD, Genève, 157 pp.
- Spear, F.S. (1993): *Metamorphic Phase Equilibria and Pressure-Temperature-Time Paths*. Mineralogical Society of America, Washington, D. C, 799 pp.
- Trümpy, R. (1966): Considérations générales sur le «Verrucano» des Alpes Suisses. In: Atti del simposio sul Verrucano. Pisa 1966. *Atti. Soc. Toscana Sci. Nat.*, 212-232.
- Ulardic, C. (2001): *Strukturgeologische und petrographische Untersuchungen im Valgrisenche (Briançonnais der italienischen Alpen)*. Unpubl. Univ. Freiburg, Germany.
- Vidal, O., Theye, T. and Chopin, C. (1994): Experimental study of chloritoid stability at high pressure and various fO_2 conditions. *Contrib. Mineral. Petrol.* **118**, 256-270.
- Vidal, O. and Parra, T. (2000): Exhumation of high pressure metapelites obtained from local equilibria for chlorite phengite assemblage. *Geological Magazine* **35**, 139-161.
- Vidal, O., Parra, T. and Trotet, F. (2001): A thermodynamic model for Fe-Mg aluminous chlorite using data from phase equilibrium experiments and natural pelitic assemblages in the 100-600°C, 1-25 kbar range. *Am. J. Sci.* **301**, 557-592.

Chapter 3

Late stage deformation in a collisional orogen (Western Alps): Nappe refolding, back-thrusting or normal faulting?

By Stefan Bucher, Stefan M. Schmid, Romain Bousquet and Bernhard Fügenschuh
Paper published in "Terra Nova", 2003, Volume 15, pages 109-117.

Late-stage deformation in a collisional orogen (Western Alps): nappe refolding, back-thrusting or normal faulting?

Stefan Bucher, Stefan M. Schmid, Romain Bousquet and Bernhard Fügenschuh

Department of Earth Sciences, Basel University, Bernoullistr. 32, CH-4056 Basel, Switzerland

ABSTRACT

Nappe refolding, back-thrusting and normal faulting frequently cause severe late-stage overprinting of the architecture of an orogen. A combined investigation of nappe stack polarity, kinematics of shearing and metamorphic gradients in the Western Alps develops criteria for distinguishing between these three modes of late-stage deformation. This distinction is a prerequisite for any retro-deformation necessary for understanding the main tectonic and metamorphic evolution of

collisional orogens. In the case of the Western Alps overprint was by mega-scale nappe refolding in the Oligocene. This implies exhumation of the HP-rocks prior to postnappe folding, i.e. during nappe stacking and by foreland-directed ascent within a subduction channel.

Terra Nova, 15, 109–117, 2003

Introduction

Retro-deformation of the latest stages of deformation is a prerequisite for unraveling the main stages of the tectonic and metamorphic evolution of an orogen (Dewey, 1988; Platt *et al.*, 1989; Escher *et al.*, 1993; Alsop *et al.*, 2001). Such late-stage deformation may severely modify pre-existing large-scale structural and metamorphic patterns, preferentially within the more internal and metamorphic parts of the pre-existing nappe stack (Müller, 1983). Similar structures related to late-stage deformation are also observed and may also be discussed in a similar way outside the Western Alps: the Brooks Range in Alaska (Vogl, 2002), the Hercynian orogen in SW England and Spain (Coward and McClay, 1983 and Macaya *et al.*, 1991) or the Canadian Cordillera (Brown *et al.*, 1986) are several examples.

The Alps result from the collision of the European plate, with the Apulian plate, in Tertiary times (Argand, 1916; Schmid *et al.*, 1996). For large parts of the Western Alps (Fig. 1), and along the so-called ECORS-CROP seismic traverse (Roure *et al.*, 1996), all major nappe contacts and foliations are hinterland- (i.e. SE-) dipping (Fig. 2a). Yet, from the Gran Paradiso massif to some 30 km further to the north-west, foliations and major

tectonic contacts are foreland- (i.e. NW-) dipping. Three mechanisms, illustrated in Fig. 2(b)–(d), have so far been proposed to produce this corridor of foreland-dipping foliations. These are: (i) hinterland-verging thrusting or ‘back-thrusting’ (Butler and Freeman, 1996); (ii) normal faulting, ‘collapse’ or hinterland-directed ‘extrusion’ structures (Caby, 1996); and (iii) large-scale refolding of previously stacked nappes, referred to as ‘nappe refolding’ (Milnes *et al.*, 1981).

Criteria to distinguish between back-thrusting, normal faulting and nappe refolding

Nappe stack polarity and palaeogeography

During foreland- (in the case of the Alps NW-) directed nappe stacking, palaeogeographically more internal units are emplaced over palaeogeographically more external units. Such ‘in-sequence’ thrusting is well preserved at the north-west front of the Alpine orogen. There the Dauphinois unit is overthrust by the Valaisan unit (Frisch, 1979; Froitzheim *et al.*, 1996), the latter being overridden by the Briançonnais units (Fig. 2a). More internally, however, a foreland-dipping tectonic contact of uncertain origin (enigmatic tectonic contact ‘ETC’ in Fig. 2a) separates the Briançonnais units from the still more internal Piemont–Liguria unit. The latter, finally, overlies the Gran Paradiso massif, attributed to the most internal parts of the Briançonnais

microcontinent by most workers (e.g. Stampfli, 1993).

Later modifications by back-thrusting or normal faulting (Fig. 2b–c) create new fault zones, which postdate nappe stacking. These fault zones separate two blocks with normal nappe stack polarity, except for very local overturning above the ETC in case of back-thrusting. In contrast, nappe refolding leads to an overturned nappe stack within the overturned limbs of mega-folds, and older fault zones related to nappe stacking are preserved (Fig. 2d).

Back-thrusting and nappe refolding (Fig. 2b–d) are compatible with the palaeogeographical zonation and NW-directed nappe stacking of the Alps outlined above. However, the more internal position of the Briançonnais with respect to the Piemont–Liguria ocean invokes either normal faulting (assuming earlier NW-directed nappe stacking) or ‘SE-directed’ nappe stacking (assuming the palaeogeographical zonation given above) (Fig. 2c), associated with NW-directed subduction.

Sense of shearing

In the case of back-thrusting, the sense of shear observed along and in the vicinity of the back-thrust will be hinterland-directed (Fig. 2b). Nappe refolding around an axis perpendicular to the direction of early nappe transport will preserve the foreland-directed sense of shearing related to former nappe stacking (Fig. 2d). Interestingly, this sense of shearing,

Correspondence: Stefan Bucher, Department of Earth Sciences, Basel University, Bernoullistr. 32, CH-4056 Basel, Switzerland. E-mail: stefan.bucher@unibas.ch

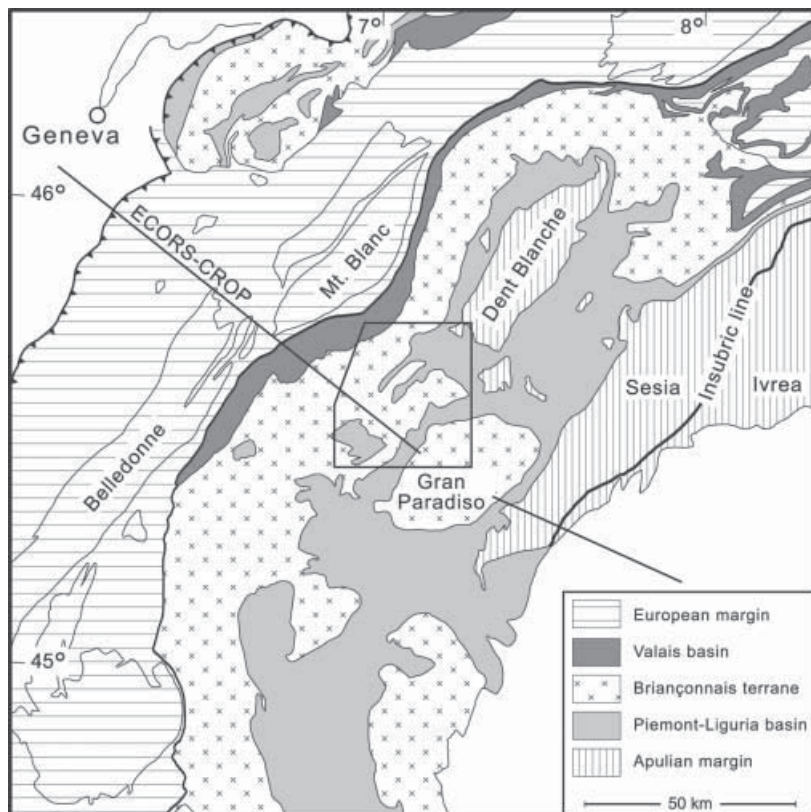


Fig. 1 Palaeogeographical map of the Western Alps after Ceriani *et al.* (2001, and references therein). The rectangle indicates the study area.

associated with an overturned nappe contact, is identical with that which would be produced by late-stage normal faulting (Fig. 2c). Hence, in the absence of additional criteria, sense-of-shear criteria alone are not decisive (Wheeler and Butler, 1994). Back-thrusting may be considered to have evolved from nappe refolding, with increasing-to-hinterland shearing in the reverse limb of a backfold. Also in this case, if the back-thrusting component is of importance, the proposed criteria are applicable and they would allow a relative chronology between nappe refolding and back-thrusting to be established.

Changes of metamorphic grade

Late-stage back-thrusting is expected to cause an offset of a pre-existing metamorphic zonation across a younger fault contact (Fig. 2b). Observations on metamorphic grade commonly indicate that back-thrusts displace earlier formed mineral zones, for example bringing 'hot' over 'cold'

(Schmid *et al.*, 1989). The inverse applies to normal faulting which brings 'cold' over 'hot' (Mancktelow, 1992). By contrast, nappe refolding preserves the pre-existing metamorphic zonation, but reorients it together with the nappe contacts (Fig. 2d).

Regional setting of the study area

The studied area (Fig. 3a) is situated in a region where the main schistosity changes from a SE-dip to a dominant NW-dip (Caby, 1996). Four major tectonic units can be distinguished in this area, i.e. the Zone Houillère unit (ZH), the Rutor unit (RU) and the Internal unit (IU), all parts of the Briançonnais microcontinent and the Piemont-Liguria oceanic unit (PL) (Fabre, 1961; Elter, 1972; Mercier and Beaudoin, 1987; Cigolini, 1995).

The change in dip – referred to as 'fan structure of the Briançonnais' (Fabre, 1961; Caby, 1968) – is explained by back-thrusting that followed outward-directed displacements (nappe stacking). Butler and Freeman

(1996) supported this view by invoking SE shearing along a back-thrust (called the 'Entrelor shear zone', which corresponds to the 'ETC'; Fig. 2a) situated between the Briançonnais and Piemont-Liguria units. However, their interpretation of top-to-the-SE shearing (Fig. 2b) contrasts with the observations of Caby (1996), who documented top-to-the-NW displacements along this same tectonic contact, in agreement with the present authors' observations discussed later. This led Caby (1996) to interpret the ETC as a normal fault (Fig. 2c). Consequently he postulated W-directed subduction, predating extension and E-directed 'extrusion'. This scenario appears rather unlikely in the light of the seismic results obtained along the ECORS-CROP profile (Nicolas *et al.*, 1990).

New Structural and petrological data

The new set of structural data presented here (Figs 3–6) is grouped into three deformation phases, compatible with the work of previous authors (Caby, 1968, 1996; Baudin, 1987; Cigolini, 1995), who worked in the study area.

Evidently **D1** structures have been largely overprinted by subsequent deformation. Macroscopically a first foliation S1 is preserved only in F2 fold hinges. In thin section, this relict S1 is defined either by chloritoid preserved within D2 microlithons, or as an internal foliation within garnet (Fig. 6b). The D1 mineral assemblage (garnet, phengite, chloritoid) is associated with peak pressure conditions (Fig. 4). Peak pressures range from 10 to 14 kbar (at temperatures around 450 °C) in the IU to 5 kbar (at around 400 °C) in the ZH.

D2 represents the dominant deformation event, characterized by isoclinal folds on all scales. Owing to the intense transposition, the main foliation is a composite of D1 and D2. F2 folds show a wide spread in plunge azimuth from ESE to WNW between the Houiller Front and the Valgrisenche, and they plunge to the WNW over the rest of the study area. L2 stretching lineations are orientated parallel to the F2 folds (Figs 3b and 5a). The transport direction, including that observed along the

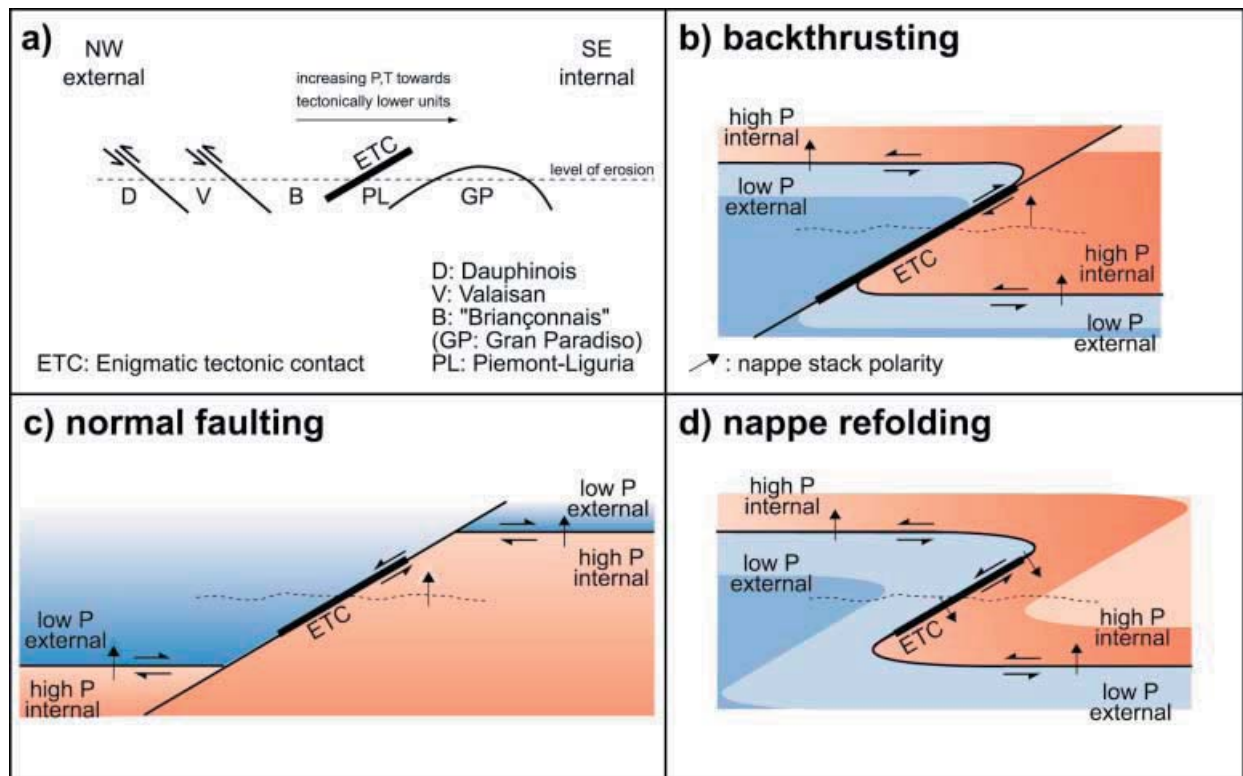


Fig. 2 (a) Schematic cross-section through the central part of the Western Alps (see Figs 4a and 5 for more realistic profiles); (b)–(d) sketches illustrating the three possible mechanisms of late-stage modifications of an original nappe stack discussed in this paper for late-stage modification.

ETC, is consistently top-to-the-WNW (Fig. 6a–e), as indicated by shear bands and asymmetric porphyroclasts. Parallelism between fold axes (F2) and stretching lineation (L2; Fig. 5a) indicates pervasive top-to-the-WNW shearing during D2. S2 in the IU is defined by the mineral assemblage garnet, phengite, epidote, chlorite and plagioclase replaces the peak-pressure mineral assemblage (Fig. 6c). P–T estimates indicate that D2 is contemporaneous with decompression from 14 to 5 kbar for temperatures around 500 °C (Fig. 4).

D3 is characterized by open meso-scale parasitic folds, refolding the composite S1/S2 main foliation (Fig. 5b) and causing a wide range of orientations of L2 stretching lineations (and F2 fold axes). D3 fold axes are moderately NE or SW plunging (Figs 3c and 5a) with gently, generally SE-dipping axial planes. An axial plane cleavage (pressure solution cleavage) is only locally observed (Fig. 5b). F3 folds become tighter towards structurally higher positions.

Based on mapping of the vergency of mesoscopic D3 folds, the axial traces of two D3 mega-folds could be identified in map (Fig. 3a) and profile (Fig. 4) view. A first and W-closing mega-fold (Rutor mega-fold) affects all previous structures, including former nappe contacts (Fig. 4). Hence, the gradual change of the D1/D2 main schistosity (apparent 'fan-structure') from a SE-dip over a subvertical orientation into a NW-dip is a consequence of this mega-fold (Fig. 4).

A second and tectonically higher D3 mega-fold closes towards the east. It returns the whole nappe stack back into an upright position, as observed, for example, in the area of the Grande Sassièrè, a Piemont–Liguria klippe tectonically overlying the IU (Fig. 3a). This hitherto undetected D3 mega-fold can be correlated with the well-known Valsavaranche 'backfold' of Argand (1911) (Fig. 3a). However, because the Valsavaranche fold is not apparently linked kinematically to back-thrusting, the term Valsavaranche mega-fold is proposed.

Interpretation

D3 nappe refolding affected D1/D2 nappe contacts such as the ETC. The observed top-to-the-WNW sense of shear (Fig. 6a–d) excludes back-thrusting along the ETC. However, no significant metamorphic jump could be observed across the ETC (nor across any of the other nappe contacts; Fig. 4). This also excludes postmetamorphic normal faulting. Instead, it provides additional and independent evidence for the interpretation of the ETC and other foreland-dipping tectonic boundaries in terms of re-orientated former nappe contacts (Fig. 4).

The interpretation in terms of nappe refolding calls for a new interpretation on the kinematics of movement during the main stages of the tectonic and metamorphic evolution (see Fig. 7). In spite of uncertainties related to an accurate retro-deformation of the L2 stretching lineations (Ramsay and Huber, 1987), the senses of shear associated with L2 could not

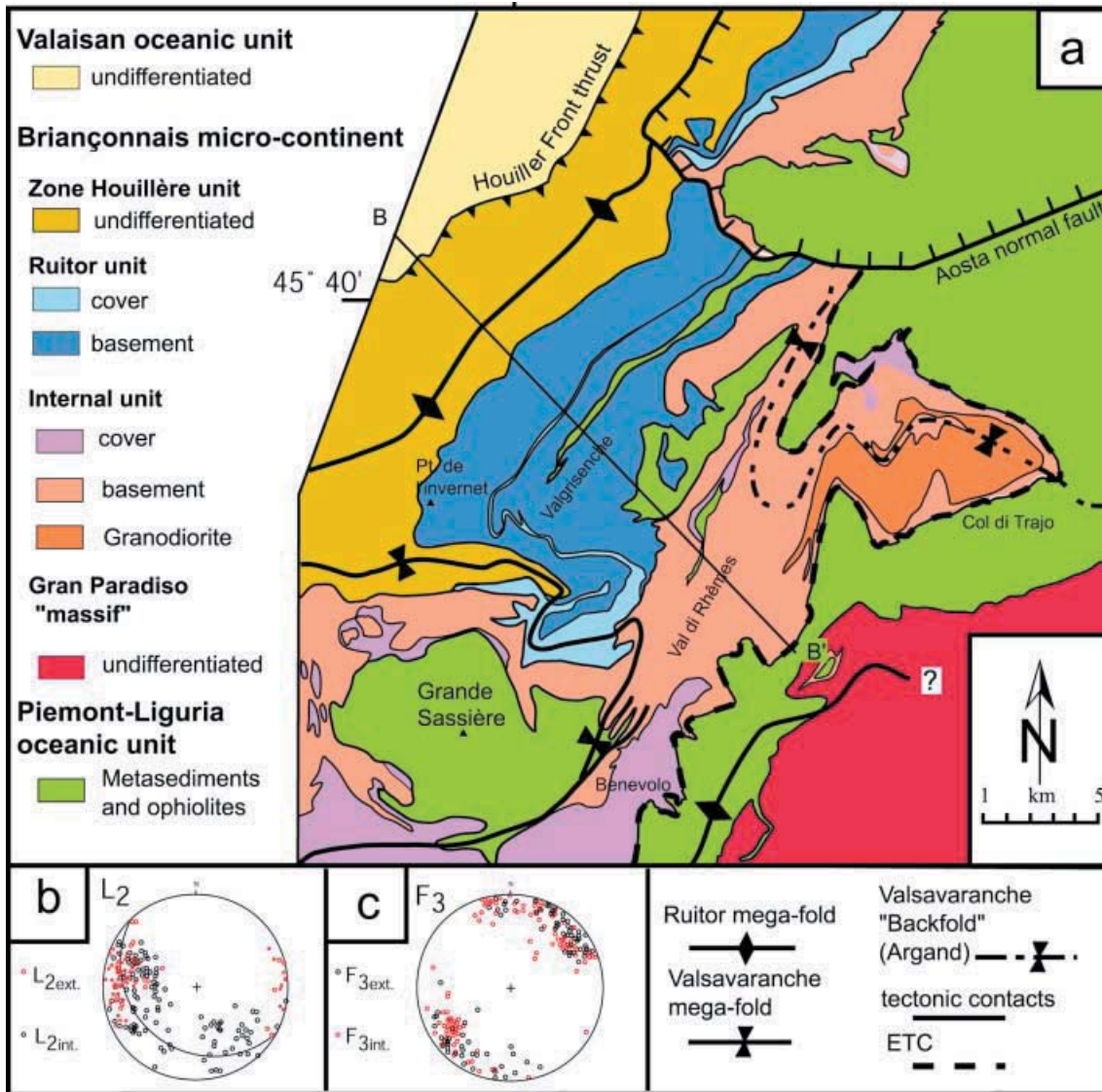


Fig. 3 (a) Geological map of the study area. B–B' indicates the trace of the cross-section of Fig. 4(a). (b) L2 stretching lineations (L2_{int.}, area from the Front Houiller to the Valgrisenche; L2_{ext.}, area SE of the Valgrisenche) and (c) F3 fold axes (F3_{ext.} and F3_{int.}, same separation as L2).

have been inverted because L2 is orientated perpendicular to the D3 fold axes. Hence, qualitative retro-deformation around D3 suggests that these folded tectonic contacts represent original top-to-the-W–N thrusts formed during the final stages of nappe stacking (D2). These thrusts emplaced higher grade metamorphic units (P and T) over lower grade metamorphic units. This inverse metamorphic field gradient, together with decompression documented during D2 (Fig. 4), suggests that the HP units came to lie over the LP units during exhumation, during the final

stages of top-to-the-W–N nappe stacking (D2). D2 (Fig. 7c) immediately followed subduction and deformation under peak metamorphic conditions (Fig. 7d). Hence, exhumation of HP units is unrelated to late-stage normal faulting and/or back-thrusting. Instead, it is suggested that ascent and extrusion of HP units did occur within and parallel to a subduction channel, by active 'extrusion' (Burov *et al.*, 2001) and/or buoyant ascent (fig. 13 of Wheeler, 1991). Given top-to-the-W–N senses of shear during exhumation, the present study area must have been

located near the lower (i.e. European) interface of the extruding HP units (Fig. 7c).

At the scale of the orogen (Fig. 7b), the subhorizontal Ruitor and Valsavaranche axial planes suggest vertical shortening of a part of the nappe pile. Commonly, vertical shortening is associated with crustal thinning. However, this classical interpretation would demand that the thrust contacts were steeply dipping originally, implying in turn a steeply dipping subduction channel. Because thrust contacts are flat in other parts of the orogen (i.e. below the Dent Blanche

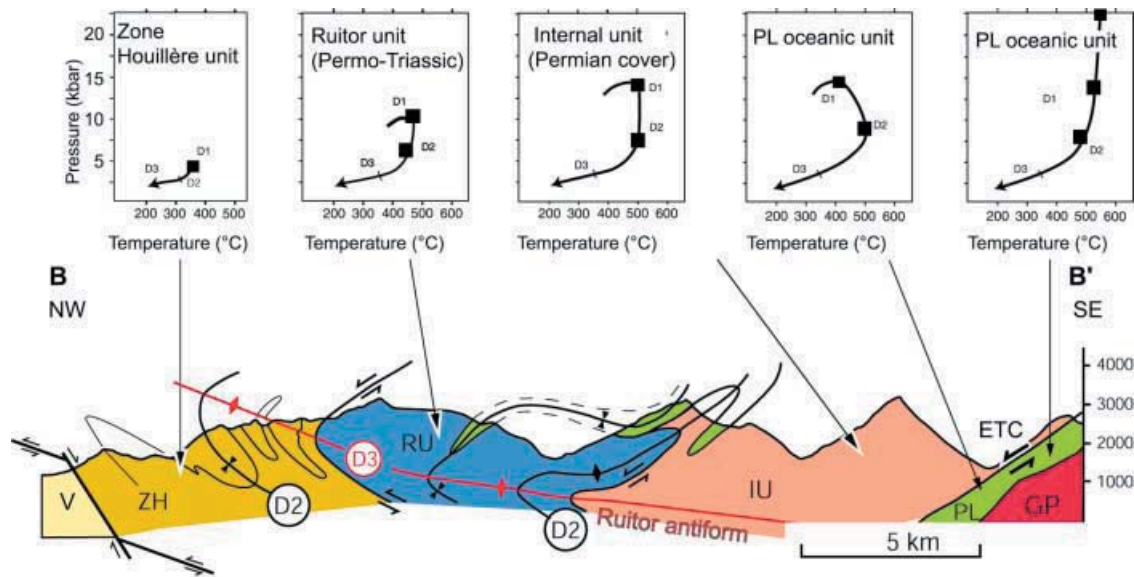


Fig. 4 Schematic cross-section B–B' (for location see Fig. 3) and P–T path of different tectonic units in the study area. P–T conditions were calculated using GEO-CALC software (Brown *et al.*, 1988) on the updated JAN92.RGB thermodynamic database (Berman, 1988), and Mg-chloritoid data from B. Patrick (listed in Goffè and Bousquet, 1997). The chlorite and mica solid-solution models and their thermodynamic properties are from Vidal *et al.* (2001) and Vidal and Parra (2000). Atom-site repartition for the micas from Bousquet *et al.* (2002). V, Valaisan oceanic unit; ZH, Zone Houillère unit; RU, Ruitor unit; IU, Internal unit; GP, Gran Paradiso 'massif'; PL, Piemont–Ligurian oceanic unit; ETC, Enigmatic tectonic contact.

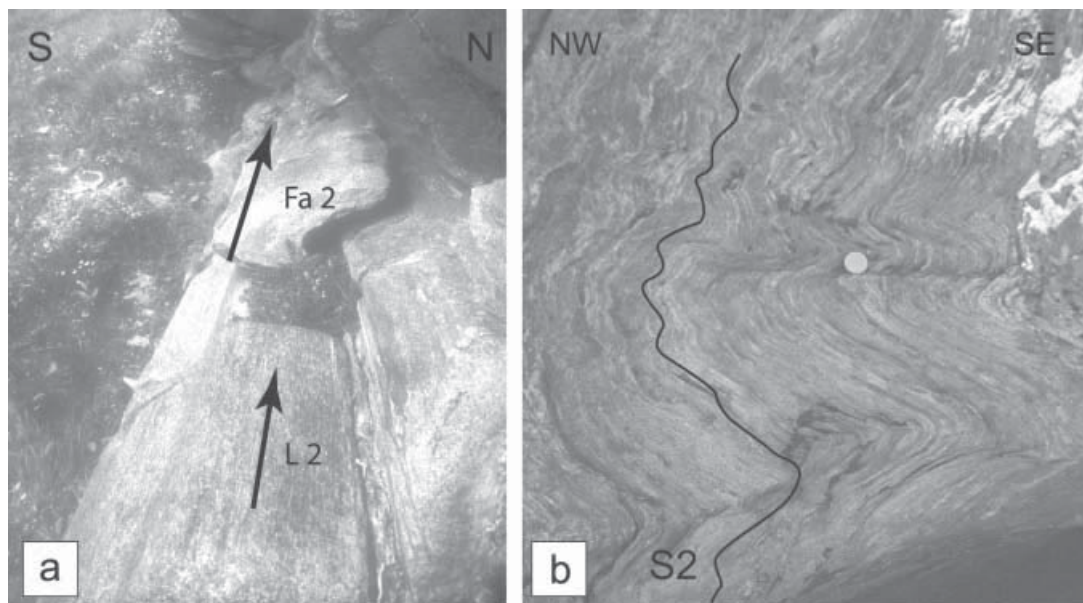


Fig. 5 (a) E–W-orientated L2 stretching lineation, parallel to the F2 fold axes on the eastern flank in the uppermost Val di Rhêmes. (b) M-shaped open D3 folds from the hinge area of the Ruitor mega-fold in the external part of the study area.

nappe; Fig. 7a) and steep subduction is unlikely in a collisional scenario, it is proposed that, at the scale of the orogen, vertical shortening associated with D3 mega-folding is of local significance only. As discussed else-

where (Fügenschuh *et al.*, 1999; Schmid and Kissling, 2000; Ceriani *et al.*, 2001), late-stage out of sequence top-to-the-WNW thrusting along the Penninic front is related to postcollisional lithosphere-scale thrusting of

the Briançonnais microcontinent over the European margin in the Oligocene. During this stage, the Gran Paradiso unit moved differentially to the WNW with respect both to the Valaisan suture and the overlying

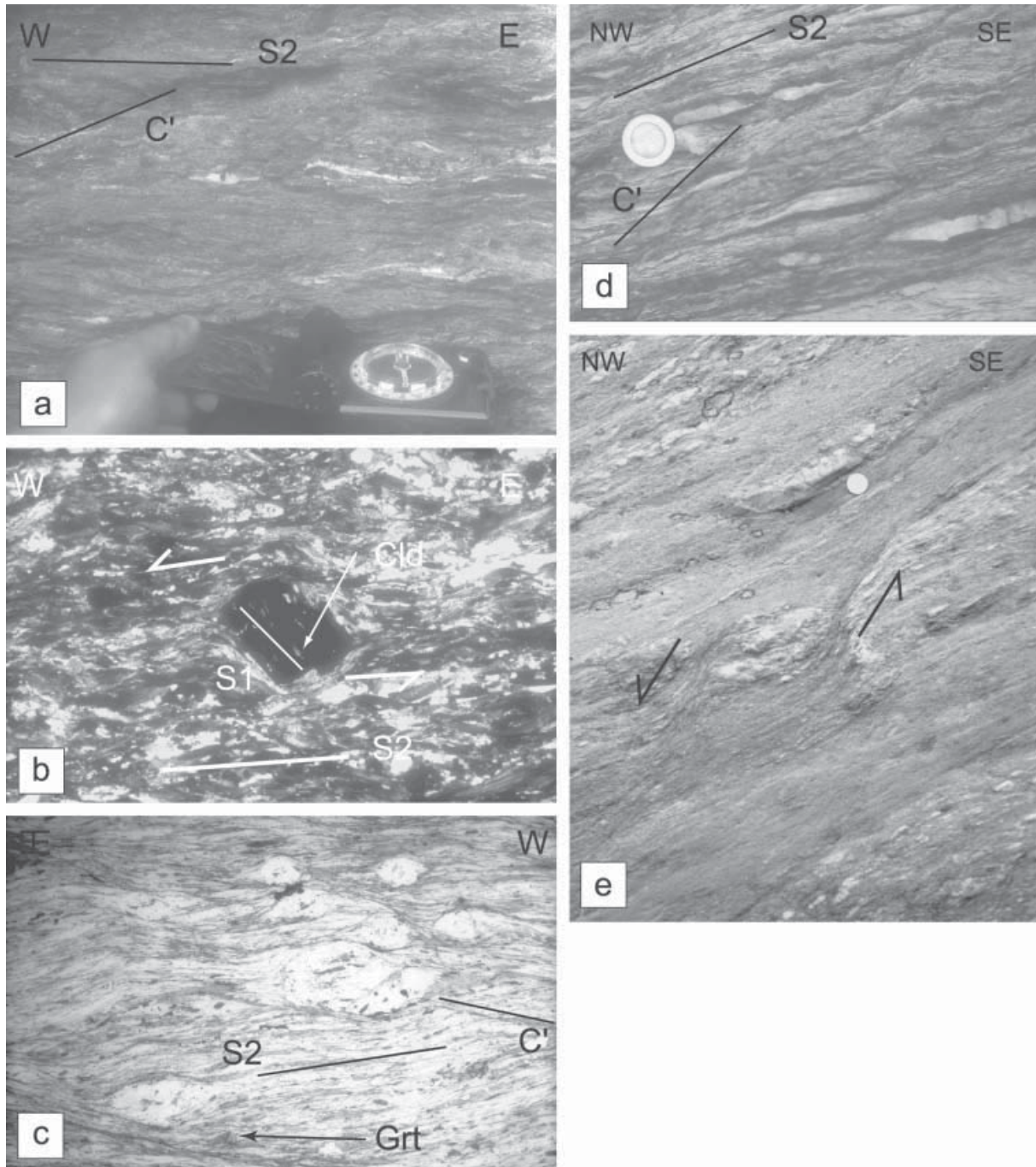


Fig. 6 (a) Macroscopic top-to-the-W sense of shear immediately below the ETC in the SL near the Col di Trajo. (b) Top-to-the-W sense of shear at the ETC in the Conge area (micrograph with crossed polarizers). (c) Top-to-the-W sense of shear at the ETC on the eastern flank in the uppermost Val di Rhêmes (micrograph without polarizers). (d) Macroscopic top-to-the-W sense of shear in the Permo-Triassic cover near the Rifugio Benevolo. (e) Macroscopic top-to-the-W sense of shear at the tectonic contact between RU and the ZH. (east of the Pointe de l'Invernet)

Austroalpine units (Dent Blanche nappe). It is proposed that this mega-folding occurred in front of and above the relatively rigid Gran Paradiso unit by a combination of

inhomogeneous simple shearing and vertical shortening during the differential WNW-directed movement of the Gran Paradiso unit (Merle and Guillier, 1989).

Subduction and foreland-directed extrusion of the HP units occurred during D1/D2 nappe stacking (Fig. 7c–d) in the Eocene (Schmid and Kissling, 2000) and was top-

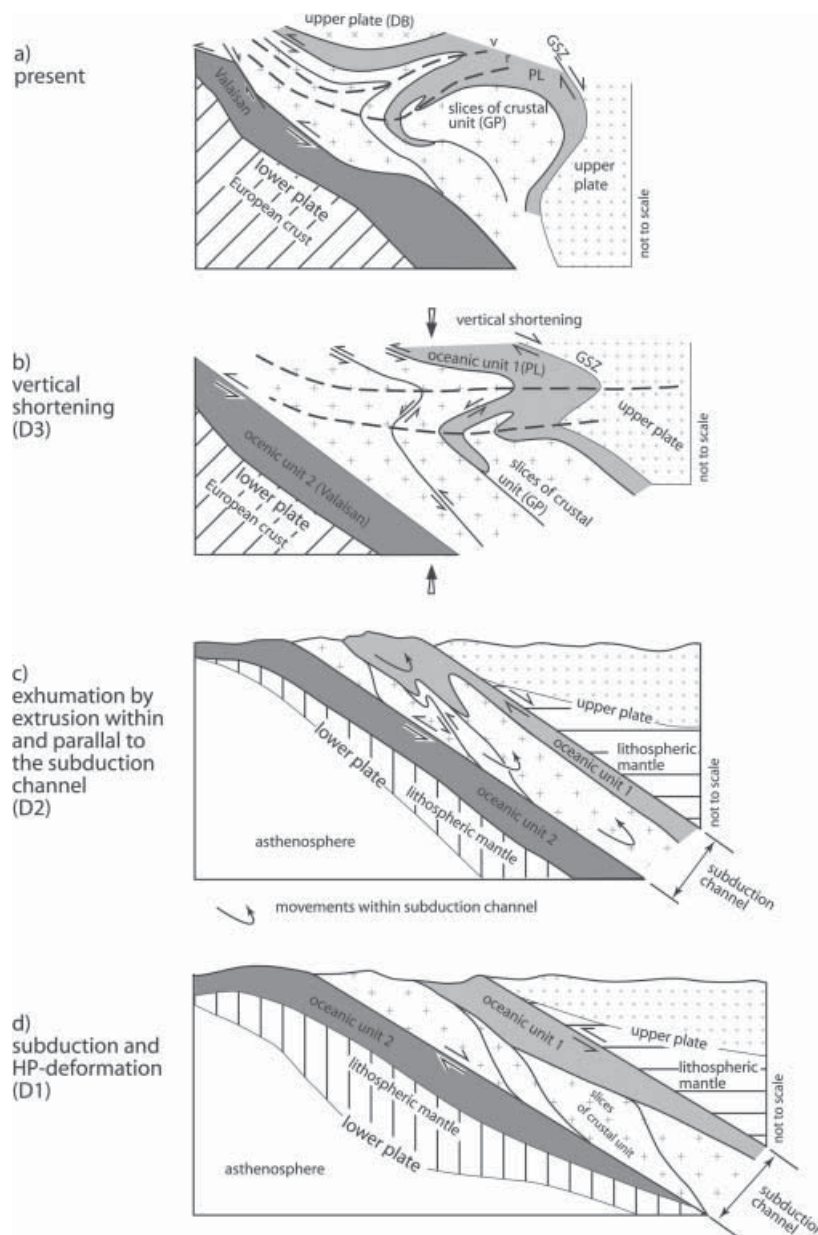


Fig. 7 Sketch of the tectonic evolution of the Western Alps. (a) Present situation. (b) Evolution of the large-scale nappe refolding (D3). Note refolding of the nappe contacts without inversion of the sense of shear. Similar structures are shown in the models of Pfiffner *et al.* (2000). (c) Exhumation by extrusion within and parallel to the subduction channel (D2). Note that in such a situation exhumation takes place during the final steps of nappe stacking and that the sense of shear is inverted with respect to the situation during the subduction on top of the subduction channel. Movements within the subduction channel derive from the models of Burov *et al.* (2001). (d) Subduction and deformation at peak metamorphic conditions. r, Ruitor mega-fold; v, Valsavaranche mega-fold; GP, Gran Paradiso 'massif'; DB, Dent Blanche unit; PL, Piemont–Ligurian oceanic unit; GSZ, Gressonney shear zone.

to-the-NNW–N according to Ceriani *et al.* (2001). The working area examined herein exposes the lower parts of the HP internal Penninic units extruded during D2. Extrusion of the upper

parts of these HP units towards the foreland must be associated with hinterland-directed, i.e. 'normal fault mode' shearing. They are evident near the base of the Dent Blanche nappe

('Combin fault' of Ballèvre and Merle, 1993), and at the NW margin of the Sesia zone ('Gressonney Shear Zone' of Reddy *et al.*, 1999), GSZ in Fig. 7(a)–(b).

Discussion

Overtaken nappe stacks linked directly to large-scale nappe refolding are known along the entire Alpine arc. In the external southern Western Alps similar large-scale nappe refolding and refolded tectonic contacts with a top-to-the-W sense of shear are described by Tricart (1984). Philippot (1990), Henry *et al.* (1993) and Agard *et al.* (2001) show evidence for ductile top-to-the-W shearing in the internal parts (Queyras, Mont Viso and Dora Maira). Similar structures are described by Müller (1983) and Schreurs (1990) in the western and central Swiss Alps. Hence the understanding of these structures is essential for reconstructing the evolution of the entire Western and Central Alps. Moreover similar structures are also observed in other orogens, as mentioned in the introduction.

Conclusions

Nappe refolding, back-thrusting and normal faulting cause severe late-stage modifications of the architecture of an orogen. The combined investigation of nappe stack polarity, kinematics of shearing and metamorphic gradients in the Western Alps presented herein presents criteria for distinguishing between these three modes of late-stage deformation.

Nappe refolding, rather than normal faulting or back-thrusting, severely overprinted the internal parts of the ECORS-CROP seismic profile during the Oligocene. Retro-deformation of this mega-folding implies exhumation of the HP rocks prior to nappe refolding, during nappe stacking in the Eocene. This exhumation was by ascent and extrusion of HP units within and parallel to a subduction channel.

Acknowledgments

We thank our colleagues from the 'Groupe Briançonnais' and of Basel S. Ceriani, A. Loprieno, G. Trullenque, and Ch. Ullard (Freiburg) for stimulative discussions.

N. Mancktelow, J. Wheeler, J. Malavieille and C. Sue provided constructive reviews. Substantial funding by the Swiss National Science Foundation (project 20-63391.00 and precursor projects) over many years is gratefully acknowledged.

References

- Agard, P., Jolivet, L. and Goffé, B., 2001. Tectonometamorphic evolution of the Schistes Lustrés complex: implications for the exhumation of the UHP rocks in the western Alps. *Bull. Soc. Géol. Fr.*, **172**, 617–636.
- Alsop, G.I., Bryson, R. and Hutton, D.H.W., 2001. Tectonic and kinematic evolution within mid-crustal orogenic root zones: a case study from the caledonides of northwestern Ireland. *Geol. Mag.*, **138**, 193–211.
- Argand, E., 1911. Sur les plissements en retour et la structure en éventail dans les Alpes occidentales. *Bull. Soc. Vaud. Sc. Nat.*, **XLVII**.
- Argand, E., 1916. Sur l'arc des Alpes Occidentales. *Ecol. Geol. Helv.*, **XIV**, 146–151.
- Ballèvre, M. and Merle, O., 1993. The Combin Fault: compressional reactivation of a Late Cretaceous-Early Tertiary detachment fault in the Western Alps. *Schweiz. Mineral. Petrogr. Mitt.*, **73**, 205–227.
- Baudin, T., 1987. *Étude géologique du Massif du Rutor (Alpes franco-italiennes): Evolution structurale d'un socle Briançonnais*. Unpubl. doctoral dissertation, University of Grenoble, 259 pp.
- Berman, R.G., 1988. Internally-consistent thermodynamic data for minerals in the system Na₂O-K₂O-Ca-MgO-FeO-Fe₂O₃-Al₂O₃-SiO₂-TiO₂-H₂O-CO₂. *J. Petrol.*, **29**, 445–522.
- Bousquet, R., Goffé, B., Vidal, O.R., and Patriat, M., 2002. The tectono-metamorphic history of the Valaisan domain from the Western to the Central Alps: New constraints on the evolution of the Alps. *Bull. Geol. Soc. Am.*, **114**, 207–225.
- Brown, T.H., Berman, R.G. and Perkins, E.H., 1988. GeO-CALC: software package for calculation and display of pressure-temperature-composition phase diagrams using an IBM or compatible personal computer. *Comput. Geosc.*, **14**, 279–289.
- Brown, R.L., Journeay, J.M., Lane, L.S., Murphy, D.C. and Rees, C.J., 1986. Obduction, backfolding and piggyback thrusting in the metamorphic hinterland of the southeastern Canadian Cordillera. *J. Struct. Geol.*, **8**, 255–268.
- Burov, E., Jolivet, L., Le Pourhiet, L. and Poliakov, A., 2001. A thermomechanical model of exhumation of high pressure (HP) and ultra-high pressure (UHP) metamorphic rocks in Alpine-type collision belts. *Tectonophysics*, **342**, 113–136.
- Butler, R.W.H. and Freeman, S., 1996. Can crustal extension be distinguished from thrusting in the internal parts of mountain belts? A case history of the Entrelor shear zone, Western Alps. *J. Struct. Geol.*, **18**, 909–923.
- Caby, R., 1968. Contribution à l'étude structurale des Alpes occidentales: subdivisions stratigraphiques et structure de la zone du Grand Saint-Bernard dans la partie sud du val d'Aoste (Italie). *Geol. Alpine*, **44**, 95–111.
- Caby, R., 1996. Low-angle extrusion of high-pressure rocks and the balance between outward and inward displacements of Middle Penninic units in the western Alps. *Ecol. Geol. Helv.*, **89**, 229–267.
- Ceriani, S., Fügenschuh, B. and Schmid, S.M., 2001. Multi-stage thrusting at the 'Penninic Front' in the Western Alps between Mont Blanc and Pelvoux massif. *Int. J. Earth Sci.*, **90**, 685–702.
- Cigolini, C., 1995. Geology of the Internal Zone of the Grand Saint Bernard Nappe: a metamorphic Late Paleozoic volcano-sedimentary sequence in South-Western Aosta Valley (Western Alps). In: *Studies on Metamorphic Rocks and Minerals of the Western Alps. A Volume in Memory of Ugo Pognante* (B. Lombardo, ed.). *Boll. Mus. Reg. Sci. Nat., Torino*, **13**, 293–328.
- Coward, M.P. and McClay, K.R., 1983. Thrust tectonics of S Devon. *J. Geol. Soc. London*, **140**, 215–228.
- Dewey, J.F., 1988. Extensional collapse of orogens. *Tectonics*, **7**, 1123–1139.
- Elter, G., 1972. Contribution à la connaissance du Briançonnais interne et de la bordure piémontaise dans les Alpes Graies nord-orientales et considérations sur les rapports entre les zones du Briançonnais et des Schistes lustrés. *Mem. Ist. Geol. Univ. Padova*, **28**, 1–18.
- Escher, A., Masson, H. and Steck, A., 1993. Nappe geometry in the Western Swiss Alps. *J. Struct. Geol.*, **7**, 955–974.
- Fabre, J., 1961. Contribution à l'étude de la Zone Houillère en Maurienne et en Tarentaise (Alpes de Savoie). *Mém. Bur. Rech. Géol. Min.*, **2**, 308 pp.
- Frisch, W., 1979. Tectonic progradation and plate tectonics of the Alps. *Tectonophysics*, **60**, 121–139.
- Froitzheim, N., Schmid, S.M. and Frey, M., 1996. Mesozoic paleogeography and timing of eclogite-facies metamorphism in the Alps: a working hypothesis. *Ecol. Geol. Helv.*, **89**, 81–110.
- Fügenschuh, B., Loprieno, A., Ceriani, S. and Schmid, S., 1999. Structural analysis of the Subbriançonnais and Valais units in the area of Moûtiers (Savoy, Western Alps): paleogeographic and tectonic consequences. *Int. J. Earth Sci.*, **88**, 201–218.
- Goffé, B. and Bousquet, R., 1997. Ferrocapholite, chloritoïde et lawsonite dans les métapelites des unités du Versoyen et du Petit St Bernard (zone valaisanne, Alpes occidentales). *Schweiz. Mineral. Petrogr. Mitt.*, **77**, 137–147.
- Henry, C., Michard, A. and Chopin, C., 1993. Geometry and structural evolution of ultra-high-pressure and high-pressure rocks from the Dora-Maira massif, Western Alps, Italy. *J. Struct. Geol.*, **18**, 965–981.
- Macaya, J., González-Lodeiro, F., Martínez-Catalán, J.R. and Alvarez, F., 1991. Continuous deformation, ductile thrusting and backfolding of cover and basement in the Sierra de Guadamarrama, Hercynian orogen of central Spain. *Tectonophysics*, **191**, 291–309.
- Mancktelow, N., 1992. Neogene lateral extension during convergence in the Central Alps: Evidence from interrelated faulting and backfolding around the Simplonpass (Switzerland). *Tectonophysics*, **215**, 295–317.
- Mercier, D. and Beaudoin, B., 1987. Révision du Carbonifère Briançonnais: Stratigraphie et évolution du bassin. *Geol. Alpine*, **13**, 25–31.
- Merle, O. and Guillier, B., 1989. The building of the Central Swiss Alps: an experimental approach. *Tectonophysics*, **165**, 41–56.
- Milnes, A.G., Gfeller, M. and Müller, R., 1981. Sequence and style of major post-nappe structures, Simplon-Pennine Alps. *J. Struct. Geol.*, **3**, 411–420.
- Müller, R., 1983. Die Struktur der Mischhelfalte (Penninische Alpen). *Ecol. Geol. Helv.*, **76**, 391–416.
- Nicolas, A., Hirn, A., Polino, R., Nicolich, R. and ECORS-CROP Working Group, 1990. Lithospheric wedging in the western Alps inferred from the ECORS-CROP traverse. *Geology*, **18**, 587–590.
- Pfiffner, O.A., Ellis, S. and Beaumont, C., 2000. Collision tectonics in the Swiss Alps: Insight from geodynamic modeling. *Tectonics*, **19**, 1065–1094.
- Philippot, P., 1990. Opposite vergence of nappes and crustal extension in the French-Italian Western Alps. *Tectonics*, **9**, 1143–1164.
- Platt, J.P., Lister, G., Cunningham, P. *et al.*, 1989. Thrusting and backthrusting in the Briançonnais domain from the Western Alps. In: *Alpine Tectonics* (M. Coward *et al.*, eds). *Spec. Publ. Geol. Soc. London*, **45**, 135–152.
- Ramsay, J.G. and Huber, M.I., 1987. *The Techniques of Modern Structural Geology, Vol. 2: Folds and Fractures*. Academic Press, San Diego.
- Reddy, S.M., Wheeler, J. and Cliff, R.A., 1999. The geometry and timing of orogenic extension: an example from the

- Western Italian Alps. *J. Metamorph. Geol.*, **17**, 573–589.
- Roure, F., Bergerat, F., Damotte, B., Mugnier, J.-L. and Polino, R., 1996. The ECORS-CROP Alpine seismic traverse. *Mém. Soc. Géol. Fr.*, **170**, 113 pp.
- Schmid, S.M. and Kissling, E., 2000. The arc of the Western Alps in the light of new data on deep crustal structure. *Tectonics*, **19**, 62–85.
- Schmid, S.M., Aebli, H.R., Heller, F. and Zingg, A., 1989. The role of the Peri-adriatic Line in the tectonic evolution of the Alps. In: *Alpine Tectonics* (M. Coward *et al.*, eds). *Spec. Publ. Geol. Soc. London*, **45**, 153–157.
- Schmid, S.M., Pfiffner, O.A., Froitzheim, N., Schönborn, G. and Kissling, E., 1996. Geophysical-geological transect and tectonic evolution of the Swiss-Italian Alps. *Tectonics*, **15**, 1036–1064.
- Schreurs, G., 1990. Structural analysis of the Schams nappes and adjacent tectonic units: implications for the orogenic evolution of the Penninic zone in the eastern Switzerland. In: *Deep Structure of the Alps* (F. Roure *et al.*, eds). *Mém. Soc. Géol. Fr.*, **156**, 415–435.
- Stampfli, G.M., 1993. Le Briançonnais, terrain exotique dans les Alpes? *Eclog. Geol. Helv.*, **86**, 1–45.
- Tricart, P., 1984. From passive margin to continental collision: a tectonic scenario for the Western Alps. *Am. J. Sci.*, **284**, 97–120.
- Vidal, O. and Parra, T., 2000. Exhumation of high pressure metapelites obtained from local equilibria for chlorite phengite assemblage. *Geol. Mag.*, **35**, 139–161.
- Vidal, O., Parra, T. and Trotet, F., 2001. A thermodynamic model for Fe-Mg aluminous chlorite using data from phase equilibrium experiments and natural pelitic assemblages in the 100–600 °C, 1–25 kbar range. *Am. J. Sci.*, **301**, 557–592.
- Vogl, J.J., 2002. Late orogenic backfolding and extension in the Brooks Range collisional orogen, northern Alaska. *J. Struct. Geol.*, **24**, 1753–1776.
- Wheeler, J., 1991. Structural evolution of a subducted continental sliver: the northern Dora Maira massif, Italian Alps. *J. Geol. Soc.*, **148**, 1101–1113.
- Wheeler, J. and Butler, R.W.H., 1994. Criteria to identify crustal extension. *J. Struct. Geol.*, **16**, 1023–1027.

Received 11 July 2002; revised version accepted 23 December 2002

Chapter 4

From HP to late stage deformation: Dating the tectono-metamorphic evolution along a transect (ECORS-CROP) through the Italian-French Western Alps

Stefan Bucher¹, Igor M. Villa², Ilka C. Kleinhanns², Lukas M. Keller¹, Romain Bousquet¹, Stefan M. Schmid¹

¹Department of Earth Sciences, University of Basel, Bernoullistr. 32, Ch-4056 Basel Switzerland
(Stefan.Bucher@unibas.ch)

²Isotopengeologie, Institut für Geologie, Erlachstr. 9a, University of Berne, Ch-3012 Bern, Switzerland

Abstract

Along the NW-SE running ECORS-CROP profile domain in the Western Alps white micas from 15 samples covering a section from the Zone Houillère to the Piemont-Liguria oceanic unit have been analysed by ³⁹Ar/⁴⁰Ar stepwise heating. Ages decrease from ca. 300 Ma in the westernmost samples (Zone Houillère, which reached ca. 350 °C) to < 48 Ma in the internal units to the East, whose peak metamorphic temperatures were ca. 500 °C. In conventional “thermochronology”, this is a classic, but paradox and unlikely case of Cretaceous Eo-Alpine high-pressure metamorphism giving younger “cooling ages” in the higher-temperature samples. In this theoretical framework, Eocene Lu-Hf and Sm-Nd ages cannot but be interpreted as post-metamorphic cooling ages.

However, if one focuses on petrology, it is seen that from West to East there is a mineralogical difference. Samples from the Zone Houillère mostly contain detrital micas; progressing eastward, high-pressure micas with Si > 3.3 become more abundant. Across the whole traverse, D1 micas correlate with HP conditions and D2 micas with exhumation and nappe stacking under greenschist facies conditions. Thus, the petrology records a variable freezing of an evolution from a detritus-dominated sedimentation zone to HP-LT subduction and exhumation via greenschist facies hydrous retrogression. HP phengitic micas from the D1 foliation are very often corroded and overgrown/intergrown by Si-poorer D2 micas. It is important to point out that D2 recrystallization is not only limited to the S2 schistosity *sensu stricto* but pervades pseudomorphs and crystals that microscopically would be mistaken for the D1 generation. A useful discriminant is the Cl concentration in white mica, as the D2 retrogression was associated to a hyposaline fluid.

Once the petrological stage is set, geochronology is straightforward. All samples consist of mixtures of detrital, D1 and D2 micas, but in greatly varying proportions according to the local PTX conditions. The age-Cl/K correlation clearly identifies 47 ± 1 Ma as the age of D1 micas along the whole traverse, and 39-43 Ma (possibly locally variable) as the age of the greenschist-facies low-Si mica generation. The coexistence of D1 and D2 ages, and the constancy of the former along the ECORS-CROP profile, are strong evidence that all white micas record formation ages. It is only under these assumptions that the prograde Eocene Lu-Hf garnet can be viewed as formation ages. Regarding the literature data, it is quite easy to harmonize them in the present petrological and geochronological framework.

Keywords

Western Alps, ECORS-CROP profile, High-pressure deformation ages, disequilibrium textures, dating retrograde reactions, Lu-Hf-K-Ar comparison

Introduction

Quantifying rates of processes during the evolution of orogens requires dating. One challenging task is dating deformation phases in large basement-cover assemblies that underwent polyphase metamorphism. Many literature studies only addressed, for example, the deformation history, or single points along a PT-path within a single tectonic unit, but often did not fully identify the structural and/or chronological perspective for the lack of a sufficiently broad context. As a consequence, there arose large inconsistencies, as well as discussions about the evolution of orogens in general or the meaning of geochronological data. New techniques, such as laser ablation in situ dating, are sometimes regarded more reliable than classic methods. However the very recent literature documents that also these methods have their limitations, especially in young metamorphic terrains such as the Alps. The precision suffers from low concentrations of radiogenic isotopes and the size of the metamorphic minerals is often smaller than the effective spatial resolution of the laser ablation volume (Agard et al. 2002; Challandes et al. 2003). On the other hand laser ablation studies clearly show that different population are often present, even on the scale of a thin section.

In this light the $^{39}\text{Ar}/^{40}\text{Ar}$ stepheating technique, together with the possibility of the chemical control, is a strong tool for detecting the “true” formation age of the different populations (Villa et al. 1997, 2000; Villa 2001). Different studies showed that incremental heating and single spot fusion are complementary methods producing consistent results (Philippot et al. 2001; Müller et al. 2002; Challandes et al. 2003). A recent summary (Müller 2003) discusses the general principles of isotopic dating. Regarding the retentivity of white mica, modern empirical data of very high quality have been reviewed by Di Vincenzo et al. (2004, 2003, and references therein). Hence, investigations on rocks with known metamorphic and structural histories, performed from the microscopic to the regional scale, provide the possibility to strengthen our understanding about the processes controlling the behavior of isotopic systems. As the dating of tectono-metamorphic conditions requires a combined tectonic, petrologic and isotopic study, it will be necessary to ensure that the reconstructed evolution is not internally inconsistent or inconsistent with certain initial assumptions.

In this study we collected samples from a continuous section throughout the entire Briançonnais domain, from which new combined structural and petrological data are now available (Bucher et al. 2003a, b). Thereby the behavior of the K-Ar system can be studied under different P-T conditions and in full control of the deformation. The presented study not only offers the opportunity to verify and quantify the geodynamic evolution proposed by Bucher et al (2003, 2004) but also represents a case study for empirically assessing the importance of the different processes that control K-Ar.

Several authors proposed time constraints on the tectono-metamorphic evolution in the Italian-French Western Alps. Dal Piaz et al. (2001) analysed metabasic eclogites in the very internal part of the Piemonte-Liguria oceanic unit with the $^{39}\text{Ar}/^{40}\text{Ar}$ stepheating technique and proposed an age of 43 Ma (average of individual samples scattering between 41 and 46 Ma) for the HP conditions of this unit. These authors interpreted the $^{39}\text{Ar}/^{40}\text{Ar}$ ages as formation ages, because Rb-Sr dating yields the same age. This latter interpretation has some interesting implications. Firstly, if one adopts the “closure temperature (T_c)” approach, Dal Piaz et al’s statement amounts to assigning a T_c to the K-Ar system which is not very different from that of the Rb-Sr system, and moreover, substantially above 500 °C. Secondly, if the early formed HP minerals are already interpreted as formation ages, the possibility of obtaining mixed ages produced by the subsequent retrograde tectono-metamorphic evolution is very likely (albeit not mentioned by Dal Piaz et al. 2001). Earlier, Butler et al. (1997) had proposed an interpretation of the greenschist facies evolution in the same tectonic unit on the basis of Rb-Sr microsampling ages on white micas. They used their obtained average mineral age of 36 Ma for dating back-thrusting. However, the stretching lineation used by these authors as structural control is related to normal faulting or refolded thrusting by other authors (Caby 1996; Bucher et al.

2003a, 2004a). In the Zone Houillère unit, adjacent to the Houiller Front and the Valaisan domain (Fügenschuh et al. 1999), Freeman et al. (1998) dated white mica with Rb-Sr. All these ages are clearly pre-Alpine and scatter between 324 Ma and 187 Ma for the most internal dated sample. The authors interpret them to be of igneous origin.

The above-mentioned data are the only geochronological time constraints available regarding the alpine evolution. Further data are available only within the Piemonte-Liguria oceanic unit, where structural control provided by literature studies is poor. This work will attempt to synthesize more detailed data from a broader area in order to draw new conclusions regarding the tectonic and metamorphic evolution of the (Italian-French) Western Alps.

Geological setting

In the studied area, situated along the ECORS-CROP seismic line (Roure et al. 1996), four major tectonic units are distinguished (Figs. 1&2; Schmid and Kissling 2000). These are, going from external (NW) to internal (SE): Zone Houillère unit, Rutor unit, Internal unit and Piemonte-Liguria (PL) oceanic unit, the first three being derived from the Briançonnais paleogeographic domain (Fig. 1; Fabre 1961, Elter 1972, Mercier and Beaudoin 1987, Cigolini 1995).

The Zone Houillère is characterised by a Lower Carboniferous sedimentary sequence (Fabre, 1961). The lower part of this sequence consists of black schists with antracitic lenses and arkoses (Namurien to Stefanien in age; Feys 1963, Gréber 1965), while the upper part is dominated by arkoses and conglomerates probably of Stefano-Autunien age (Fabre 1961). A Permo-Triassic sequence discordantly overlies this Carboniferous sequence (Ellenberger 1958, Elter 1960).

The Rutor unit dominantly consists of pre-Permian garnet micaschists and paragneisses with abundant intercalated metabasites (Baudin 1987). There is definitely an Alpine metamorphic overprint (Caby 1996), but some relics of pre-Alpine metamorphism survived the Alpine cycle (Boquet

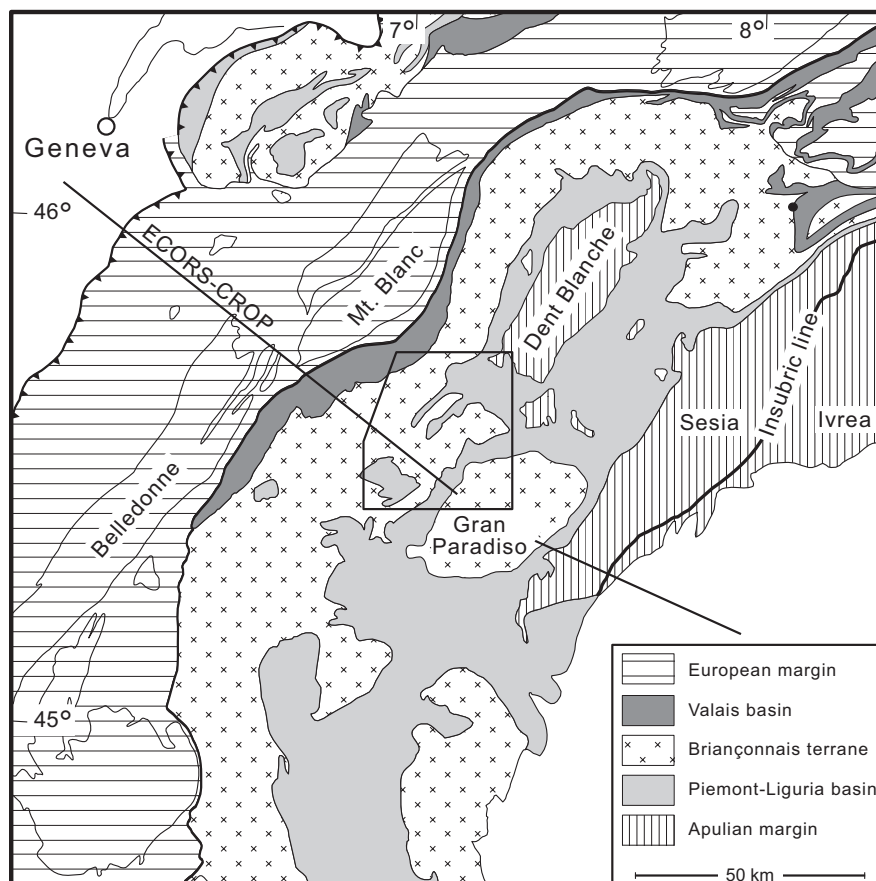


Fig. 1: Paleogeographic domains of the Western Alps, after Bucher et al. (2003). The rectangle indicates the study area. The black dot indicates location of the the additional samples from Monte Rosa.

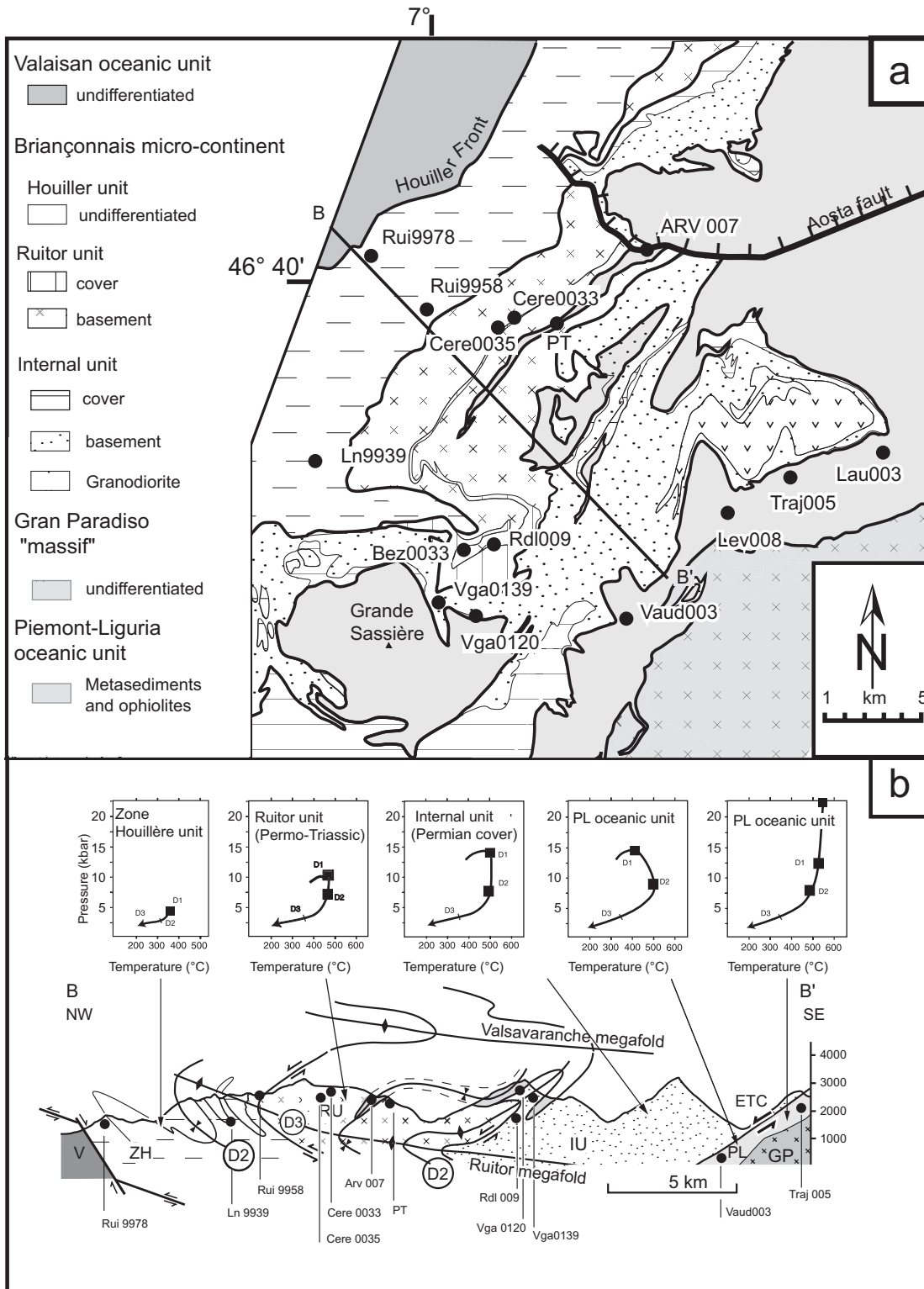


Fig. 2: a) Geological map of the study area after Bucher et al. (2003) showing the locations of the samples. B–B' indicates the trace of the cross-section of b; b) Schematic cross-section B–B' modified after Bucher et al. (2003) and P–T path of different tectonic units in the study area. P–T conditions were calculated using geo-calc software (for details see Bucher et al. 2003). Furthermore all the samples were projected onto this cross section to show their structural position. V, Valaisan oceanic unit; ZH, Zone Houillère unit; RU, Rutor unit; IU, Internal unit; GP, Gran Paradiso massif; PL, Piemont–Ligurian oceanic unit; ETC, Enigmatic tectonic contact.

(Desmons) 1974). Its sedimentary cover is made up by a thin Permo-Triassic sequence, consisting of “Verrucano”-type conglomerates (Trümpy 1966) at the base, followed by lower Triassic meta-arkoses, which are stratigraphically overlain by quartz-phyllites and ankerite-bearing micaschists (Ulardic 2001). This sequence crops out throughout the entire Valgrisenche (Fig. 2).

The Internal unit (“Zona Interna”) of the Italian authors (Cigolini 1995) corresponds to the Vanoise-Mont Pourri unit as defined by French authors (i.e. Caby, 1996). Northwards this Internal unit was correlated with the Mont Fort unit (Gouffon 1993). The Internal unit is made up of a lower part, formed by paragneisses and micaschists with a polymetamorphic history (Boquet 1974, Cigolini 1995), and of a mono-metamorphic upper part, consisting of lower Permian to Mesozoic formations. According to Amstutz (1955, 1962), the lower part is mainly of volcano-clastic origin. This succession is intruded by Paleozoic granitic and granodioritic bodies of different size (i.e. the Cogne-granodiorite, Bertrand et al. 2000). Leucocratic gneisses define the base of the mono-metamorphic upper part. These are followed by a typical Permo-Triassic sequence consisting of conglomerates (“Verrucano”), quartzitic meta-sandstones, impure quartzites and ankerite-bearing micaschists. The younger Mesozoic cover is only preserved in the southern part of the study area.

The PL-oceanic unit predominantly consists of calcschists. These are interlayered with different amounts of metabasites (Elter 1972, Cigolini, 1995). Two different types of metabasites do occur: eclogites that are retrogressed in most places and prasinities. While some authors proposed a subdivision of the Piedmont-Liguria oceanic unit within our working area into an eclogitic (“Zermatt-Saas Fee”) and a non-eclogitic (“Combin”) part (Droop et al. 1990; Ballèvre & Merle 1993; Dal Piaz 1999), our observations indicate that both subunits represent a mélange consisting of eclogitic and blueschist mafic boudins, embedded in a matrix of HP metasediments (Bucher et al. 2003a, b).

Tectono-metamorphic evolution

A reinterpretation of the tectono-metamorphic evolution of the Western Alps was recently presented by Bucher et al. (2003a, 2004a), based on new structural and petrological data. Three phases of Alpine deformation (D1-D3) were found to be associated with different P-T conditions prevailing in the individual units (Bucher et al. 2003a and references therein).

The D1 structures have largely been overprinted by the subsequent deformation, but relics of D1 are preserved on the macroscopic and microscopic scale. For example eclogitic boudins from the PL-oceanic unit within a matrix of mainly greenschist facies calcschists preserved the S1 foliation including the D1 mineral assemblage. The D1 mineral assemblage is associated with peak pressure conditions (Fig. 2 B). The PL-oceanic unit reaches eclogite facies (>500°C) conditions during this first phase of deformation (Fig. 2b). Petrological observations suggest a separation of D1 in an early and late stage. This because white mica in mafic rocks is not stable under eclogite facies conditions and must therefore postdate the HP mineral assemblage consisting of garnet, omphacite and glaucophane. The latter is attributed to the early stages of D1, while mica growth, clearly predating D2 is interpreted to take place during a late stage of D1. In the Internal unit and the Ruitor unit pressures range from 10-14 kbar (at temperatures around 400-450°C; Bucher et al. 2003a; Fig. 2b).

While in the internal part of the Zone Houillère unit P-T estimations suggest 5 kbar and 350°C +/- 25° close to the tectonic contact with the Ruitor unit (Bucher et al. 2003a, b), the external part never exceeded 300°C +/- 25°, as is indicated by vitrinite reflectance of coal (Bucher et al 2004b).

D2 represents the dominant deformation event, characterized by isoclinal folds on all scales. Owing to intense transformation the main foliation is a composite of D1 and D2. Intensity of D2 deformation is increasing from west to east. Due to this strain-gradient the amount of the pre-Alpine relics decrease eastwards (see also Bucher et al. 2004a): in the external part of the Ruitor unit pre-Alpine relics are common (Baudin 1987), and they gradually get scarcer in the internal part of the

Ruitor unit and in the Internal unit (Cigolini 1995). This strain gradient turns out to be important for the interpretation of Ar-Ar dating as will be discussed in a later section. North-northwestward nappe-stacking during D2 led to decompression to greenschist facies conditions.

The last ductile deformation phase D3 produced large scale post-nappe folding. (Bucher et al. 2003a; Bucher et al. 2004a). All the major tectonic contacts are clearly refolded by D3 and hence ascribed to D2. Therefore dating of these mylonites allows to assign the age to D2. No substantial mineral growth is evidenced during D3. Continuous cooling follows D3 and at about 30 Ma temperatures < 300-350 °C were reached, as is indicated by FT-zircon ages (Hurford and Hunziker, 1989; Fügenschuh and Schmid, 2003).

Analytical techniques

Out of about 150 tectonically and petrologically well-characterized samples, 15 were selected for dating by $^{40}\text{Ar}/^{39}\text{Ar}$ incremental heating. From each tectonic unit, several samples pertaining to the same P-T conditions and the same dominating deformation phase were dated, so as to have a redundant data set that allows verifying or falsifying the working hypothesis.

They were crushed and sieved in different sizes between 125 and 500 μm for each sample. White micas are enriched by standard magnetic and gravimetric techniques then further purified by hand picking for different grain size fractions between 125-500 μm . The detailed procedure of $^{39}\text{Ar}/^{40}\text{Ar}$ analyses is described by Belluso et al. (2000). The $^{39}\text{Ar}/^{40}\text{Ar}$ technique provides the possibility to monitor the chemical signature of each step, because ^{37}Ar , ^{38}Ar , ^{39}Ar isotopes are produced by reactions with the isotopes of calcium, chlorine and potassium. These three Ar isotopes allow distinguishing between different phases or generations of a dated sample by analyzing its chemical information (Villa et al. 2000). However contamination of the dated samples by minerals other than mica disturbs the age spectra. Normally such impurities can be detected by Cl/K ratios different than those of the bulk separate and Ca/K ratios different from zero. Furthermore, different mica populations with distinct compositions can also be detected by varying Cl/K and Ca/K ratios. Therefore the influence of the purity of the sample on the age spectra is essential for the detection of possible mixed ages.

In a recent review of rare gas systematics, Villa (2001) points out that binary or ternary mineral mixtures can be detected on the basis of correlations of common-denominator three isotope plots; this suggests that internally discordant age spectra can be interpreted as mineral mixtures, provided these can be documented petrographically. This has been demonstrated for a magmatic-hydrothermal phengite mixture by Villa et al. (1997). By supplementing the chemical information provided by Ar-isotope systematics with the microchemical analyses provided by AEM (analytical electron microscopy) or EMP (electron microprobe), ages can be modeled by extrapolating to end-member minerals. This approach is essential to carefully distinguish between two mechanisms potentially causing younger ages in micas: Ar loss from a homogeneous population of mica grains belonging to one single generation, or coexistence of multiple, diachronic and heterochemical mica generations in isotopic disequilibrium. The former predicts that there must be no correlation between chemical composition and age, as the mineral is homogeneous and only Ar is lost. The latter predicts that ages and chemical composition correlate. The data of the measurements are shown in the Appendix III.

Microstructural observations and Microchemistry of multiple mica generations

The Zone Houillère unit exhibits a clear gradient from a dominance of detritic mica in the most external parts of the study area where metamorphic conditions never exceeded subgreenschist facies conditions, towards mixed detritic and newly grown mica in the East. In the immediately adjacent Ruitor unit, inherited grains are still present in all samples. This is evidenced by both microstructural observations and by electron microprobe X-ray mapping, showing clear evidence for relics of white mica zonations in these samples. This confirms that mixed populations are common in metamorphic portions of orogens and that detrital mica and HP relics can survive during subsequent deformation and metamorphism (see also e.g. Agard et al. 2002).

The composition of white mica was analyzed in order to identify microchemical variations related to the different microstructural populations present in the samples. Several recent studies evidenced that petrologically distinct populations are also recognizable in the $^{39}\text{Ar}/^{40}\text{Ar}$ isotopic system (e.g. Di Vincenzo et al. 2001, 2004; Agard et al. 2002, Challandes et al. 2003). Three mica populations could be microstructurally evidenced and verified by electron microprobe X-ray mapping: detrital grains and grains formed during D1 and D2, respectively. The celadonite content, monitored by Si and Al element distribution, varies significantly in these different populations. The trend from a dominance of detritic micas in the external part to the dominance of metamorphic micas in the internal part will be illustrated by selecting six samples (see Fig. 2a for location).

In a first sample (Rui9978) from the very external part of the Zone Houillère unit close to the Houiller Front (Figs. 2a, b), the presence of detrital micas is obvious in thin section. The very weak Alpine foliation is defined by very fine-grained mica (Fig. 3a). In contrast the detrital micas are much larger, show no preferred orientation and are randomly distributed in the matrix (Fig. 3a). A wide range in the Si-content is evidenced by electron microprobe analyses (Fig. 3b). While metamorphic micas have Si-contents varying between 6.8 and 6.3, easily identifiable detrital micas have Si-contents lower than 6.3.

A second sample (Ln9939) derives from the intermediate Zone Houillère unit, where the intensity of the Alpine deformation is relatively higher than in the very external part. Neocrystallized white mica is still subordinate, but the individual grains are larger than in the previously described sample. Figure 3c shows a 3-D view of thin sections parallel and perpendicular to the stretching lineation. While in the section parallel to the stretching lineation nearly all micas are aligned in the foliation, only a weak foliation is observable in the section perpendicular to the stretching where most of the micas can be clearly identified as undeformed and of detritic origin. This shows that a 3D microstructural analysis is indispensable for careful dating and interpretation of the results, respectively.

The following two samples, Cere0035 and Cere0033, are representative for the Ruitor unit (Figs. 2a, b). In all the samples of the Ruitor unit microstructural observations and electron microprobe X-ray analysis evidence of three mica populations (Figs. 3d-f). Beside the micas grown during D2 defining the main foliation S2, relictic D1 mica and even detrital grains are visible. In Figure 3d and 3e the horizontally aligned micas define the S2 foliation and are interpreted as recrystallized syn-kinematically to D2. Interlayered are two other types of micas: microlithons oriented perpendicular to the S2 foliation and interpreted as D1 micas (Figs. 3d, e) and much larger grains compared to the D1 microlithons and the D2 micas, interpreted as relictic, detrital grains (Fig. 3d). Furthermore, D1 micas are also preserved in fold hinges (Fig. 3e). Homogeneity of the newly formed (Alpine) micas suggests that diffusional loss was negligible during the Alpine metamorphic events around 450 ± 25 °C. This is in agreement with the results of Hames and Cheney (1997), who state that diffusional loss is ineffective at temperatures lower than 450°C. Therefore a pre-Alpine zoning seems more reasonable, further supported by the findings of pre-Alpine relics in the Ruitor basement (Baudin 1987, Gigoris 1999).

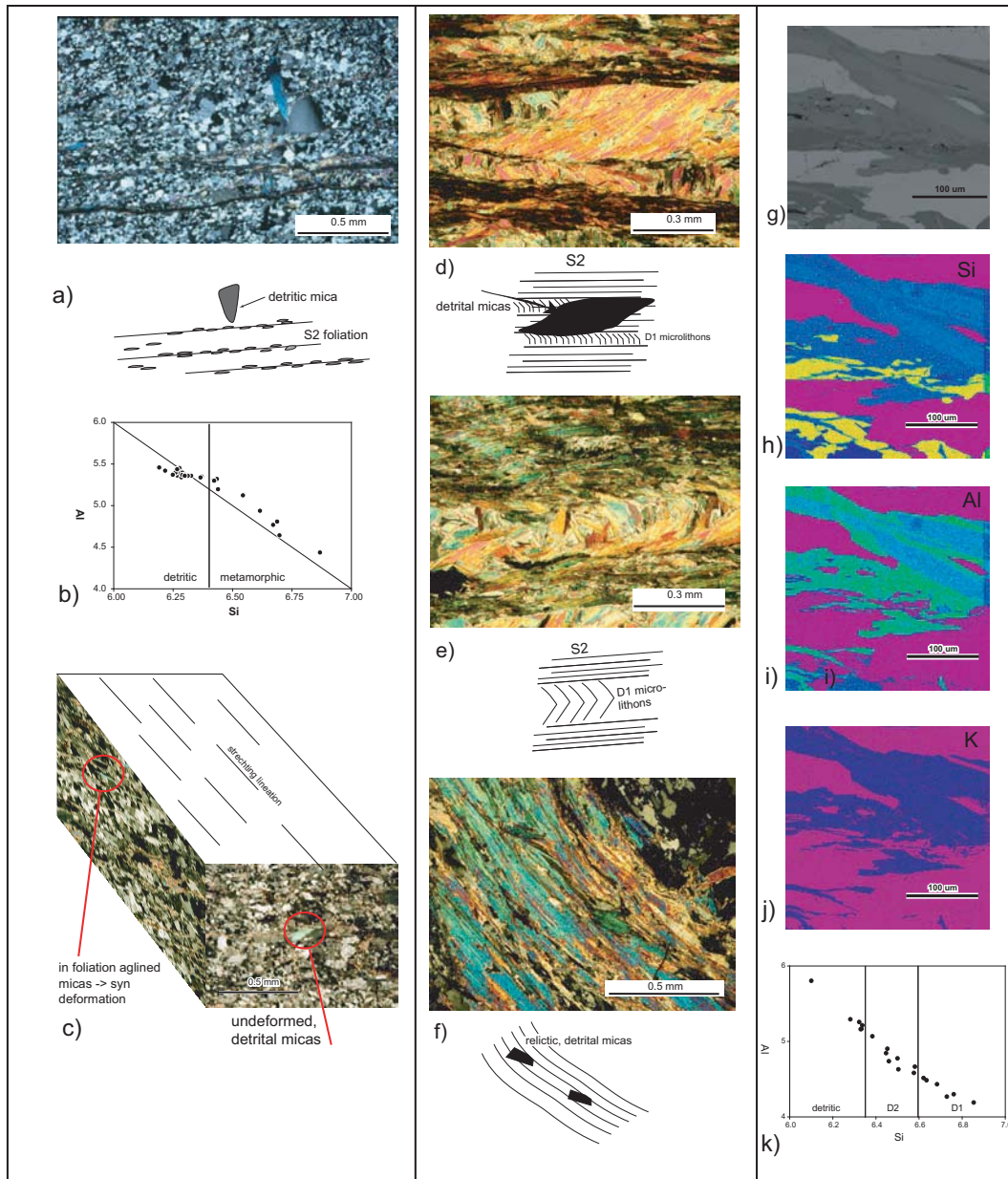


Fig. 3: **a)** Thin section of sample Rui9978 from the external Zone Houillère unit evidencing the difference between the detrital and the metamorphic phengitic white micas. **b)** Composition of the micas from sample Rui9978 measured by EMP. The limit between the metamorphic high-Si and the detrital low-Si population is based on detailed EMP-analysis of this study. **c)** 3D-distribution of the metamorphic and detrital white mica grains in sample Ln9939 from the intermediate Zone Houillère unit. **d)** detrital white mica in sample Cere0033; **e)** D1 microlithons in sample Cere0033; **f)** relictive, detrital white mica in sample Cere0035; **g)** backscatter image of detrital white mica in sample Cere0035; **h)** Si-element distribution image showing a clear zonation in the detrital micas; **i)** Al-element distribution image verifying the zonation; **j)** K-element distribution image evidencing no zonation in the potassium content; **k)** Mica compositions of the three populations in sample Cere0035 evidenced EMP analysis.

In sample Cere0035 small detrital grains are observable beside large detrital micas (Fig. 3f). X-ray mapping by electron microprobe documents a zoning in these detrital micas (Figs. 3g-j). Some important indications are linked to this observation: only inherited detrital micas are zoned while Alpine newly formed grains are homogenous. In addition, the D1 and D2 micas have significantly different compositions.

The three microstructurally identified mica populations (detrital, D1 and D2) are responsible for the large range in mica composition evidenced by electron microprobe analysis (Fig. 3g): Si

contents of D1 micas are higher than 6.7 and those of D2 micas vary between 6.5 and 6.7. The substantial amounts of inherited, detrital micas are responsible for the large number of measurements showing Si-contents below 6.5 (Fig. 3g).

Two samples with strongly contrasting microstructures from the PL-oceanic unit were analyzed. Sample Vaud003 is from an eclogitic boudin, whereas Traj005 is a calcschist forming the matrix of these eclogitic boudins. Sample Vaud003 was chosen since it only contains D1 (HP) micas, as is indicated by (i) structural and (ii) petrological observations. (i) The eclogitic boudin shows an internal foliation, which is discordant to the main foliation of the second phase of deformation (S2). Hence the internal foliation of the boudin must be older and is classified as S1. The attribution to D1 is independently confirmed by the mineral assemblage Grt-Px-Qz implying pressures > 15 kbar.

From these observations dating of micas in Vaud003.1-Vaud003.3 allows to determine the age of the first phase of deformation (D1). However, as already mentioned, micas are not stable in eclogite facies conditions and grow therefore only during the latest stages of D1. Consequently these white micas determine the age of the latest stages during D1.

Sample Traj005 is a calcschist and strongly overprinted by the S2 main foliation (Fig. 4). At first glance one could get the impression that all the micas are syn-kinematic to this second foliation (S2), but at a closer it becomes obvious that relics of the first phase of deformation are also preserved (Fig 4). Albeit omnipresent microlithons, relictic D1 fold hinges (Fig. 4a&b) and (large) relictic single grains of D1 showing internal foliation discordant to the main foliation S2 (Fig. 4c), are clear evidences for the preservation of D1 relics.

Microprobe analyses of sample Traj005 show different compositions for different populations and support the microstructural observations (Fig 5). Figure 5 shows two exemplary details of Figure 4: In Figure 5a a relictic D1 fold hinge is shown, which does not indicate heterogeneities or a zonation that would point to recrystallization during D2. Si-contents scatter between 6.8 and 6.45 across the fold hinge (Fig. 4a bottom). That this scatter is part of the variation of the D1 composition is confirmed on the one hand by the Al-distribution image, which does not display any zonation and on the other hand by the composition of the large relictic D1 mica shown in Figure 5b. The textural difference to the micas of the S2 foliation is visible in Figure 4. The element distribution images of Si and Al (Fig. 5b) confirm this observation. The exemplary measurements allow a quantification and point to Si-contents > 6.45 for D1. D2 micas have Si-contents ranging from 6.15 to 6.4 (Fig. 5a & b). Micas with Si contents below 6.15 can be attributed to micas postdating the D2 micas (Fig. 5b), but their occurrence is occasional. Note that Si content depends also on metamorphic grade and that in low-grade units such as the Zone Houillère unit a pyrophyllite component can contribute to high Si contents. Therefore the Si-content can only serve as a supporting argument in addition to detailed microstructural analyses and EMP analyses. Nevertheless Si-contents in the individual samples clearly indicate consistent, distinct variation of the compositions for the different populations.

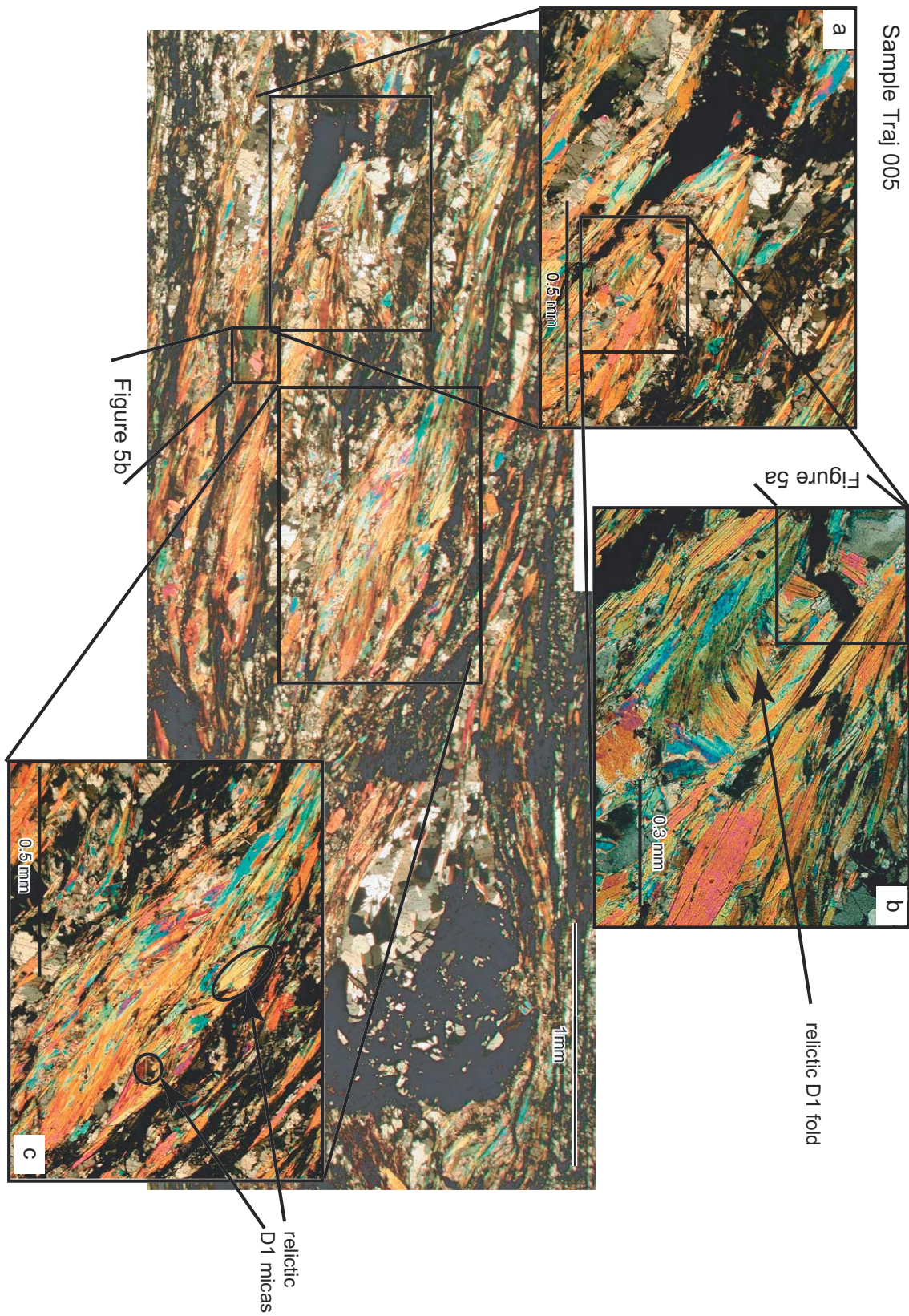


Fig. 4: Thin section of sample Traj005 evidencing different mica generations (crossed polarizers); a) Enlargement of a relictic D1 fold hinge; b) close up of figure 4a; the inset shows the area chosen for the detailed EMP analysis shown in Fig 5a; c) Enlargement showing relictic, detritic micas; d) localization of Figure 5b.

Element distribution of details from Figure 4

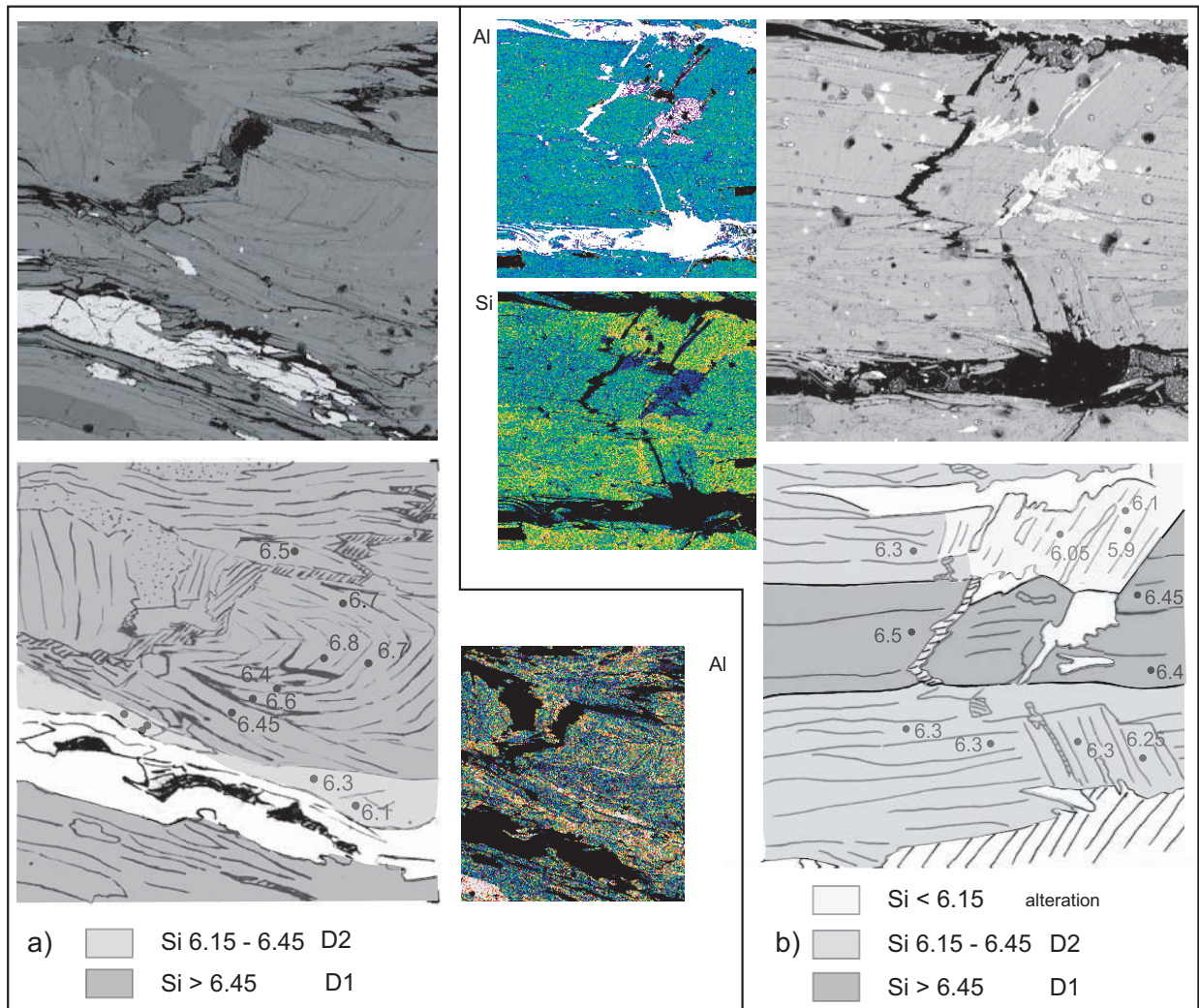


Fig. 5: a) top: BSE image of the area shown in figure 4b; bottom left: contour map of the Si content and single analysis; bottom right: Al element distribution image; b) top: backscatter image of the area shown in figure 4d; bottom left: contour map of the Si content and single analysis. Note that although D1 micas and D2 micas show similar orientation they are texturally different, as visible in figure 4d; bottom right: difference in composition evidenced by Al- and Si-element distribution images.

Introductory sample and theoretical foundations

The classical approach

Before all samples will be discussed in detail it will be shown why in this study the classical approach of the “closure temperature” (T_c) is regarded with reservation. All $^{39}\text{Ar}/^{40}\text{Ar}$ ages of this study are plotted against the estimated temperature of the greenschist facies alpine metamorphism (Fig. 6). In the classical approach, only units falling below the white mica T_c of 350°C (Prudy & Jäger 1976), allow an estimation of the HP-age. The application of this classical approach of the “closure temperature” suggests that the HP must be older than the $^{39}\text{Ar}/^{40}\text{Ar}$ ages occurring in the units that exceeded 350°C during the Alpine metamorphic cycle. The data throughout the profile from this study are shown in Fig. 6. In contrast to the internal units (Internal unit and PL-oceanic unit), where $^{39}\text{Ar}/^{40}\text{Ar}$ ages around 50 Ma are observed, the Ruitor unit shows a continuous increase from 50 Ma to 100 Ma towards the Zone Houillère unit. The same trend seems to continue in the

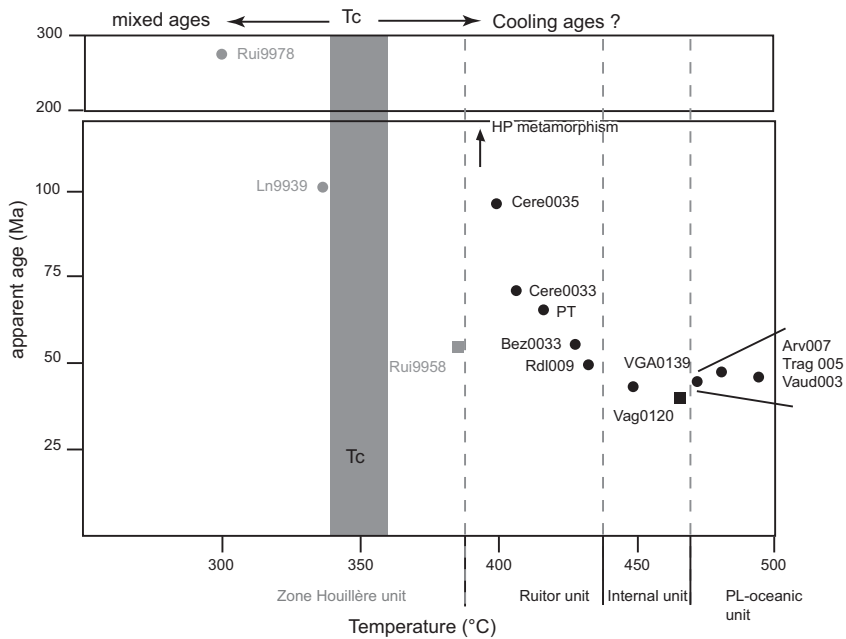


Fig. 6: Dependence ^{39}Ar - ^{40}Ar ages on metamorphic peak Temperature. Following the “closing temperature” concept the HP-metamorphism in the Western Alps must be older than 95 Ma, because all units to the east of the Zone Houillère unit reached temperatures higher than 350°C . The young ages of the internal parts would represent the commonplace interpretation that the internal parts of orogens are cooled late. Circles represent samples overprinted by multiple deformation phases and rectangles are mylonitic samples.

Zone Houillère unit where an age of about 300 Ma is observable close to the Houiller Front (Fig. 6); in the external parts of the Zone Houillère unit temperatures never exceeded 350°C . Hence, the classic “closure temperature” approach would predict an age for the HP metamorphism, of ca. 100 Ma. Consequently a Mid-Cretaceous Eo-Alpine age for the HP metamorphism would have to be postulated. This however contrasts with the Lu/Hf data on garnets (Bucher 2003), which show a clear evidence of an Eocene metamorphic peak. The easiest solution would be to argue for a Tc around 450°C instead of 350°C , because then all the ages older than 60 Ma would not represent cooling ages anymore. However, while at a first cursory glance it might appear feasible to modify one “closure temperature” for one sample, what is often overlooked is that the theory behind Purdy & Jäger’s (1973) calibration of “closure temperatures” is a strongly interlinked edifice, in which modifying one value requires modifying all others.

The argument by Reddy et al (2003) does not take into account the necessity of self-consistency (as already pointed out by Villa (1998): a simple chain of very rigorous and correctly applied logical implications predicts that the “closure temperature” of monazite must be about 450°C (Hunziker & Steck, 1993, their fig. 12) if that of muscovite is 500°C for Rb-Sr and even lower for K-Ar. This prediction is not based on a single sample but on the bulk of hundreds of “thermochronological” data obtained up to 1993. This insistence on the Central Alps is crucial, as it was here that all the canonical calibrations were based. There is no single field-based datum in the literature in support of Purdy & Jäger’s (1976) calibration that is not explicitly or implicitly based on the calibration it is meant to check. As laboratory determinations of diffusivity for hydrous minerals are usually unreliable (for a documentation of the various artefacts known to have occurred, see Villa & Puxeddu 1994, and Villa et al. 1996; see also Reddy & Potts 1999), the whole temperature range between 350°C (the fission track retention temperature of titanite: Coyle & Wagner 1998) and 750°C (the retention temperature of titanite for Pb: Scott & St Onge 1996) is uncharted and can only be constrained by putting all data in their proper context.

Any modification of Purdy & Jäger’s (1976) calibration ends up denying its very base. Consider, for instance, the triplet $Tc1 < Tc2 < Tc3$, where Tc1 is that of muscovite K-Ar, Tc2 that of monazite U-Pb and Tc3 that of muscovite Rb-Sr (the inequalities are based on the hundreds of data compiled by Steck & Hunziker 1993). Increasing Tc1 to 450°C would mean increasing Tc2 to above 500°C . Monazites U-Pb ages being younger than Rb-Sr ages of muscovites across the entire Central Alps (Steck & Hunziker 1993), the latter cannot but have “closure temperatures” in excess of 500°C .

°C. However, the isograds drawn by Hunziker & Steck (1993), which are slightly but significantly lower in temperature than those by Todd & Engi (1997), require all micas to record cooling ages < 38 Ma, the canonical age of the Lepontine event in the Alps. If one denies this concept, some of the micas between Biasca and Splügen (Steck & Hunziker 1993, their Fig. 12) unit are seen to contain inherited ⁸⁷Sr; therefore the age of the Lepontine event cannot be 38 Ma but must be younger than ca. 25 Ma. In turn, this implies that K-Ar ages > 25 Ma also contain inherited Ar, i.e. do not record “cooling ages”. The ubiquitous presence of inherited Ar and its implications will be discussed several times in this paper. Thus, the original Purdy & Jäger white mica data-set does not represent what it was asserted to do, namely date “cooling below T_c”, and the existence of genuine, inheritance-free “cooling ages” in the Central Alps appears to be a very restricted and quite exceptional occurrence.

In principle, the “closure temperature” wouldn’t a priori be an absurd working hypothesis, at least up to the point when an accurate calibration becomes available. In practice, however, it is precisely the accurate calibrations that deny the practical applicability of T_c to most geological situations. In order for temperature to be the only parameter controlling isotope exchange, the “closure temperature” of a mineral must be lower than the stability field of that mineral. If this is not the case, heterochronic generations can coexist as overgrowths without isotope resetting. Isotopic inheritance then would parallel the petrologists’ findings of increasing numbers of polygenic disequilibrium assemblages. One could then classify mineral geochronometers in two classes: “class I” minerals allow no heterochronic generations as T_c < stability field; examples are fission track chronometers and U-He chronometers; “class II” minerals are all those for which T_c is sufficiently high that polygenic mixtures retain their isotopic disequilibrium, and this includes all other mineral chronometers. Thus, while temperature does play a role in enhancing reaction kinetics and the more or less thorough recrystallization of a mineral, it is not the sole parameter controlling isotopic closure. An isotopic age of a Class II mineral can thus not be used to solve the inverse problem (“given a fractional loss, what was the temperature that caused it”), as thermally activated diffusion is always slower than competing processes such as fluid-induced recrystallization and deformation-induced recrystallization and thus not a decisive factor influencing isotope transport.

The mismatch between Purdy & Jäger’s (1976) calibration and independent checks is made clear by the progress reports by petrologists regarding the improved temperature estimates of stilpnomelane and staurolite isograds (see Villa & Puxeddu 1994, and Holdaway et al. 1997, respectively) which are never incorporated by the supporters of Purdy & Jäger’s (1976) preliminary working hypothesis.

The role of diffusion

The classical “closure temperature” (T_c) approach (Dodson 1973) assumes that, for minerals grown above the T_c, diffusion is fast enough to reset the isotopic clock constantly so that old inherited minerals and newly grown ones have the same isotopic ratios at any time. If the temperature falls below T_c, diffusion is interpreted to drastically slow down and the isotopic system is frozen. Unfortunately, as discussed above, diffusion coefficients are not well known so that T_c is only empirically constrained by comparison with other isotopic systems (Purdy & Jäger 1976). In one case study on a muscovite megacryst, Hames and Cheney (1997) showed that diffusion is very slow and the diffusion coefficient D is of the order of 1e-22 at ca. 450 °C. This is in agreement with the estimation of Graham (1981) based on an experimental study on the diffusion coefficient of hydrogen. The latter author argued that D for Ar must be orders of magnitudes smaller than the estimated D (10e-19) for hydrogen. Hames and Cheney (1997) concluded that diffusion is negligible in white micas at temperatures below 450°C and that the scatter in the observed ages is due to deformation and recrystallization. Similar conclusions, amongst others, were already drawn by Foland (1979), Chopin and Maluski (1980), Chopin and Monié (1984) and Monié (1985). However,

Kelley (2002) proposed to explain all data that deviate from the assumption of very high diffusivities and very low T_c by excess argon, effectively clouding the profound difference between inheritance and introduction from outside by a circular argument: excess argon is a tool to explain problematic ages (in the absence of multichronometric controls), but the choice of what ages are defined as “problematic” only depends on the calibration chosen for T_c . Because „mixed ages” are the normal observation below T_c , a shift of the T_c to higher temperatures changes “problematic” ages attributed to excess Ar into “normal” mixed ages with inherited Ar but without excess Ar.

A clarification is provided by a combination of petrological and isotope studies. These show that mixtures formed by low-temperature deformation are detectable by EMP or TEM and that the different isotopic reservoirs are distinguishable by microchemical analysis (Wijbrans and McDougall 1986, Villa et al. 1997, Di Vincenzo 2001, 2002, 2003, Challandes 2002). The presence of a mixture can be tested in a Cl/K vs. age correlation diagram, which allows the identification of the chemical identity of different argon reservoirs (populations) as it is demonstrated by several authors (e.g. Villa 2001, Müller 2002).

This allows dating of the individual populations of mixtures. Therefore we base our study on microchemical and microstructural observations.

Deformation induced resetting: an example from the Monte Rosa

Two samples from the Monte Rosa unit will show the importance of the microstructural control. The temperatures during the early stages of Alpine metamorphism are $> 550^\circ\text{C}$ (Engi et al. 2001) in the investigated part of the Monte Rosa nappe. With the classical approach of the closure temperature the $^{39}\text{Ar}/^{40}\text{Ar}$ system should therefore date the time of cooling during exhumation, when these samples cooled below 350°C .

The samples Mrlk 1 and Mrlk 3 (Sample 1 and sample 3 respectively of Keller et al. in press) originate from an outcrop where a pre-Alpine foliation is gradually deflected into parallelism with a shear zone during early stages of Alpine deformation (D1) and mylonitisation (Keller & Schmid, 2001). Sample 1 was taken from the pre-Alpine wall rock of the shear zone, whereas sample 3 was taken from the shear zone, inferred to represent the Alpine metamorphic and deformed equivalent of sample 1 (see Keller et al. 2004. their Fig. 2). Note that the two samples were taken in a distance of about one meter from each other. Together with the deformation there is a gradual change in mineralogy from the pre-Alpine garnet-biotite-plagioclase-muscovite-kyanite schist in the wall rock to garnet-phengite-paragonite schist in the shear zone; P-T conditions of about 650°C at 12.5 kbar are obtained for this early metamorphic transition (Keller et al., 2004). In the wall rock only small progress of the same mineralogical change was attained during the Alpine metamorphic overprint and the pre-Alpine mineral assemblage is largely preserved; the microstructural observation evidencing the presence of a small amount of neofomed alpine mica in this sample (Keller et al. 2004). Note that the preservation of pre-Alpine micas is primarily indicated by petrological and microprobe investigations (for details see Keller et al. 2004). Sample 1 (wall rock) shows an upwards-convex shaped age spectrum, with the oldest steps (6 and 7) around 75 Ma (Fig. 7). From step 7 on the step ages are decreasing continuously to 47 Ma. The shape of this spectrum suggests a mixture and is compatible with. The deformed sample 3 of the same host rock shows a flat age spectrum at 47 Ma (Fig. 7) and confirms the petrological observation of the dominance of the alpine mica in this sample, but strongly contrast the upwards-convex age spectrum of the undeformed sample. Wijbrans & McDougall (1986) demonstrated that the oldest steps of the age spectrum of a synthetic mixture define the minimum age for the older phengite population and the youngest steps define the maximum age for the muscovite population Applying these systematics for mixed ages to the undeformed sample, we predict that the older population must be older than 75 Ma and the younger population

has a maximum age of 47 Ma. The coincidence of the plateau age of the deformed sample (Mrk 3) with the maximum age for the younger population of the undeformed sample (Mrk 1) suggests that the microstructural observations correctly predict the behaviour of the $^{39}\text{Ar}/^{40}\text{Ar}$ isotopic system. We consider the 47 Ma age for D1 as reliable.

It should be noted that our interpretation of the $^{39}\text{Ar}/^{40}\text{Ar}$ date on these samples reflects the microstructural observations. A further important observation is that the pre-Alpine mica relics, which were petrologically evidenced and confirmed by microchemical analyses, also retained, at least partly, their original isotopic signature although the temperatures reached 650°C (according to Keller et al. 2004). This confirms and extends the results obtained by Di Vincenzo et al. 2004.

In summary this means that the undeformed sample clearly represents a mixed age although it reached temperatures above 600°C. $^{39}\text{Ar}/^{40}\text{Ar}$ data record that the pre-Alpine micas have not been totally reset. On the contrary the age spectrum of the sample totally recrystallized by mylonitization proves to be a plateau age and suggests an age for D1 (HP metamorphism) of 47 ± 1 Ma.

Precisely because thermally activated diffusion was minor in these two samples, the petrological and structural control of the dated sample becomes important in determining if a mica will retain inherited Ar or lose it during recrystallization.

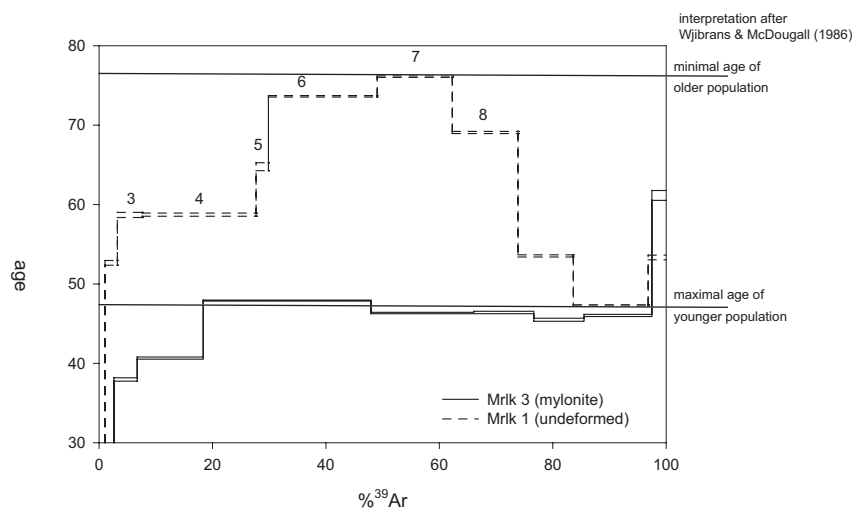


Fig. 7: Age spectra of the samples from the Monte Rosa unit. Mrk1 1 and Mrk1 3 belong to the same host rock. Sample Mrk 3 is a mylonite, while Sample Mrk1 1 is little deformed during the Alpine orogeny of the same host rock as the . In the latter the pre-alpine relics are evidenced by the detailed petrological study of Keller et al. (2004).

Influence of the purity of samples for $^{39}\text{Ar}/^{40}\text{Ar}$

In order to quantify of the influence of the purity, for three samples we analyzed a carefully handpicked and the unpicked fraction. The samples represent typical petrogenetic varieties encountered in our work: (i) sample Ln9939 from the Zone Houillère unit, where detrital micas are predominant; (ii) a D2 mylonite (Vga0120) from the Internal unit, where only one mica population is present; and (iii) sample Traj005 showing evidence for a mixture between a D1 and D2 population without the presence of detrital micas.

Sample Ln9939

Staircase shaped age spectra for both fractions (picked & unpicked, Fig. 8a) are evidenced for the mixture between newly grown/recrystallized and detrital micas, as already documented by the microstructural observations. Two major differences between the picked and the unpicked fraction are evident. Firstly, we observe substantially (ca. 60Ma) older ages in the first two steps of the unpicked fraction (Fig. 8a), best explained by contaminant such as e.g. chlorite.

The second difference is surprising; all other steps of the picked fraction, except the first two, consistently yield step ages older by 10-15 Ma (Fig. 8a). The only explanation for this observation is

that hand-picking selectively enriched the detrital micas. During hand-picking the operator keeps the “pure” looking grains and removes those visibly intergrown by other minerals (e.g. chlorite). Alpine micas, however, formed synkinematically together with chlorite are therefore preferentially removed by hand-picking leading to enrichment of detrital micas. This observation implies that these two ages do not contain any contamination by other minerals pointing to an alpine population with an age of 45 ± 3 Ma (for detailed discussion see below).

Sample Vga0120 and Sample Traj005

The other two investigated samples are derived from the internal part of the study area and experienced higher metamorphic conditions during the Alpine metamorphic cycle (Fig 2).

Age spectra of the picked and unpicked fraction of sample Vga0120 were obtained using the same heating-routine. No major differences occur in the age spectra (Fig. 8b) except in the first two steps. Practically all other steps are within ~ 0.5 Ma the same for both fractions (Fig. 8b) Just as for Ln9939, this difference is best explained by a contamination of Cl-rich minerals other than mica in the unpicked fraction.

Traj005 derives from the PL-oceanic unit (Fig. 2). This sample displays only minor differences between the picked and unpicked separates (Fig. 8c). Although this sample clearly contains two populations, only insignificant differences between the picked and the unpicked sample can be observed. The details about the interpretation of these upward-convex age spectra will be discussed in the next paragraph.

From these observations it is concluded that hand-picking generally leads to better results, but can provoke selective enrichment if two populations are present. Especially if the age difference between the two populations is large (i.e. detrital pre-Alpine and Alpine) hand-picking can lead to unrepresentative results. However in samples where no selective enrichment is occurring (Vga0120, Traj005) it is clearly shown that minor contaminants were successfully removed by hand-picking.

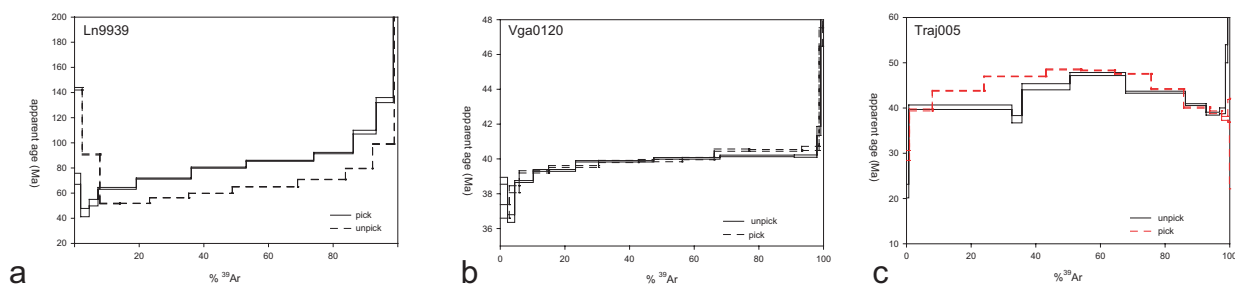


Fig. 8: a) Age spectra of the picked and unpicked fraction of sample a) Ln9939. Grain size for both fraction 125-160 μm ; b) Vga0120 (125-160 μm); c) Traj005 (125-160 μm).

Influence of grain size on ages

As discussed earlier diffusional loss is interpreted to be an important factor causing problematic ages. In order to test the role of diffusion from two samples different grain sizes have been dated, because different ages for the different grain sizes are expected if diffusional loss plays an important role. A first sample (PT) is from the Permo-Triassic cover of the avise synform near the contact between the Ruitor unit and the PL- oceanic unit (Fig. 2b)

PT

From this sample two very different grain sizes were analyzed: 160-500 μm (PT1), 125-160 μm (PT2). Both display, except for first two steps, similar age spectra (Fig. 9a). The age spectra of these two size-fractions are again characterized by an increase in the first steps and an apparent plateau between 62-63 Ma for both grain size fractions (Fig. 9a).

Vaud003

Three different grain sizes (125-160 μm , Vaud003.2; 160-250 μm , Vaud003.1 and 250-500 μm , Vaud003.3, respectively) were analyzed for this sample. The age spectra are nearly identical (Fig. 9b). Although the average grain radii vary between 70 μm and 190 μm no differences concerning their age spectra are observed, except for the first and last steps. All three age spectra are flat over 80% of the released gas.

Note that the observation of identical age spectra for all three grain sizes excludes both inherited and “excess” argon to play an important role, because both would be predicted by diffusion theory to affect varying grain sizes to a different degree. Already these results give a strong indication that diffusion can not play an important role.

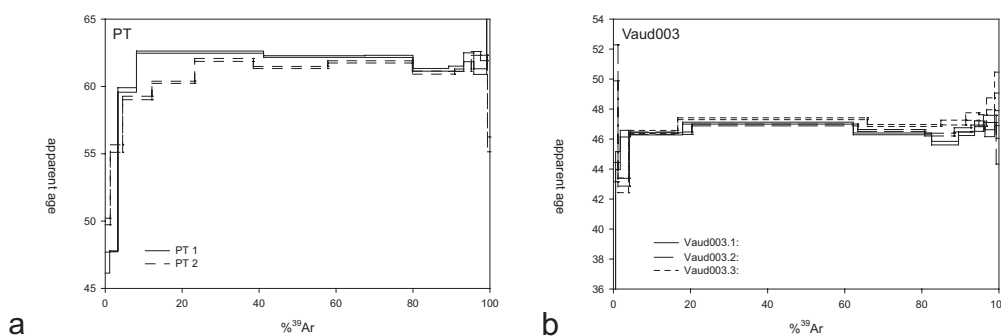


Fig. 9: a) Age spectra of the sample PT1 and PT2; the grain sizes are 160-500 μm and 125-160 μm respectively, the flat portion of the age spectra (80% release) are the same within 1 Ma; b) Age spectra of the sample Vaud003.1, Vaud003.2 and Vaud003.3; the grain sizes are 160-250 μm and 125-160 μm and 250-500 μm respectively. Note that the age spectra are identical within one Ma, what clearly exclude diffusion to play an important role.

Results

The samples will be discussed in respect to their structural position from external to internal (Fig. 2b). The measurements and calculated integrated ages for each sample are presented in the appendix III.

Zone Houillère unit

Rui9978

Sample Rui9978 was collected close to the Houiller Front (Fig. 2) where detrital mica grains are predominant. The age spectrum shows a staircase (Fig. 10a). The youngest step has an age of 120 Ma and over the next five steps the age is increasing continuously to an age of 260 Ma, before an apparent plateau at 270 Ma is reached, characterized by three steps. For the last steps the age increases up to 300 Ma (Fig. 10a). In the literature such staircase-shaped age spectra are sometimes described as due to diffusive loss (e.g. Markley et al. 1998). In this interpretation the disturbance is dated at ≤ 120 Ma by the first step. However as was mentioned above they are best interpreted as mixed ages instead.

The Cl/K vs. age diagram (Figure 9b) clearly evidences a linear relationship between the Cl/K content and the apparent ages of the different steps. This verifies the occurrence of a binary mixture in agreement with the petrological constraints. Alpine mica is subordinate and very small in grains size ($<100 \mu\text{m}$). None of the step ages reflects only Alpine micas; all steps yield mixed ages very far removed from an Alpine age.

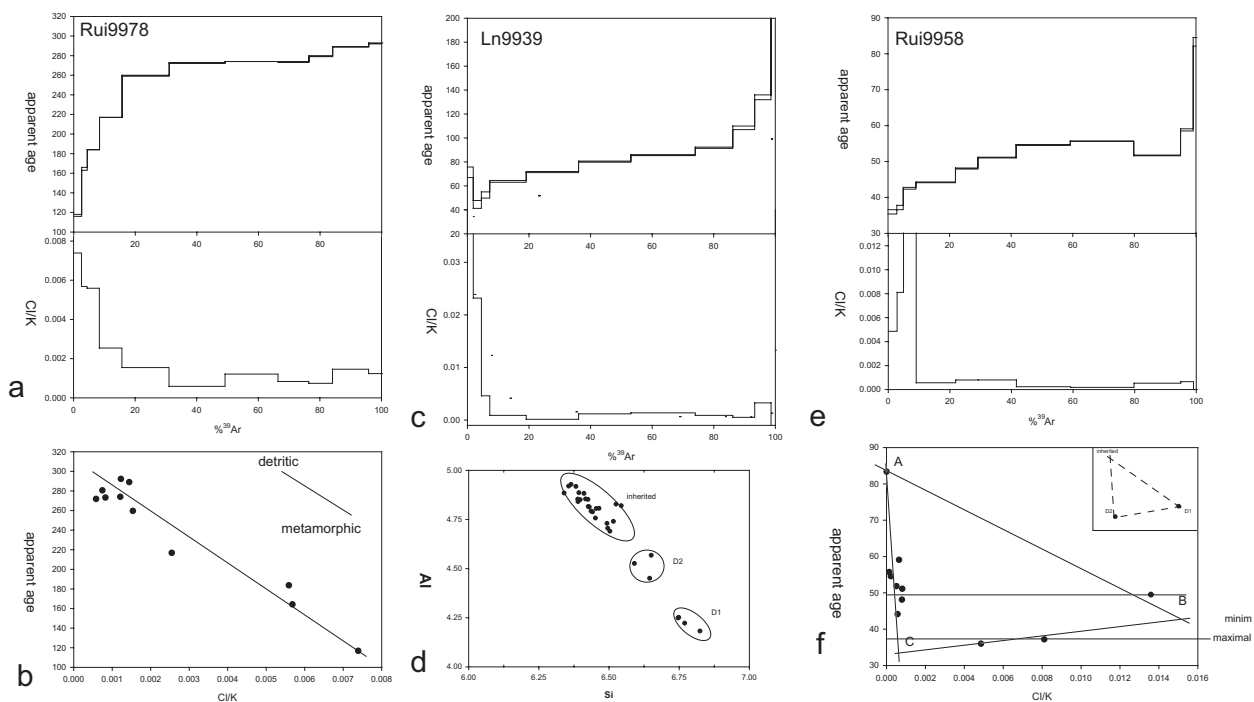


Fig. 10: **a)** ^{39}Ar - ^{40}Ar age spectrum and Cl/K ratio of sample Rui9978 showing a staircase shape. The integrated age of all steps is 260 ± 0.4 Ma; **b)** linear trend of the Cl/K ratio with the step age, evidencing a mixture. **c)** ^{39}Ar - ^{40}Ar age spectrum and Cl/K ratio of sample Ln9939 showing a staircase shape. (integrated ages: 74.9 ± 0.4 Ma, 90.2 ± 2.5 Ma unpicked and picked fraction respectively; the difference between the fractions was already discussed); **d)** Mica composition of sample Rui9958 for the different populations evidenced by EMP analysis. **e)** ^{39}Ar - ^{40}Ar age spectrum and Cl/K ratio of sample Rui9958 showing a staircase shape. The integrated age of all steps is $51,7 \pm 0.3$ Ma. Note that, in contrast to the other samples of this unit, this mylonite contains a substantial amount of metamorphic micas, as evidenced by very high Cl/K ratios; **f)** Cl/K vs. age correlation diagram evidencing a population B (D1) with a minimal age of 43 Ma and an maximal age for population C (D2) of 35 Ma.

Rui9978 is from an intermediate position with respect to the samples analysed by Freeman et al. (1998) and agrees well with their results, which show an age trend from >300 Ma close to the Houiller Front to 187 Ma towards more internal positions. The fact that Sample Rui9978 follows this trend supports the abundant evidence for a mixture between a metamorphic and a detrital population, because all these samples are well below the Tc for the Rb-Sr and Ar-Ar isotopic system. On the other hand this trend is also compatible with the observation of a decreasing intensity of the deformation towards the NW. The fact that Rb-Sr and $^{39}\text{Ar}/^{40}\text{Ar}$ data yield the same age indicates that deformation rather than diffusion is responsible for this age trend as conventionally no Sr diffusion is expected in white mica at such low temperatures.

Ln9939

This sample from the intermediate Zone Houillère also contains relictic, detrital micas (Fig. 3z). It has been stated that clear evidence from the microstructural observations on one hand and an inverse relationship between Cl/K ratio and step ages on the other hand (Fig. 10c bottom) point to a binary mixing age between a detrital and a metamorphic component for this sample. It was shown that comparing the picked and unpicked fractions a contamination in the first steps can be excluded. Therefore the second step of the picked sample represents the step with the smallest contamination by detrital micas, which allows for an estimate on the maximum age of 45 ± 3 Ma for an alpine metamorphic population.

Rui9958

Sample Rui9958 is a mylonitic Carboniferous meta-conglomerate and derives from the D2 tectonic contact between the Zone Houillère unit and the Rutor unit (Fig. 2). The intensity of the deformation in this mylonitic sample is higher compared to the under and overlying units (Zone Houillère unit and Rutor unit, respectively). Microstructural observations in thin section evidence a dominance of alpine metamorphic micas. Some isolated detrital micas are still present, but clearly subordinate. Moreover, micas formed during the first phase of deformation (D1) survived the subsequent mylonitisation during D2. The variation in mica composition and the correlation with the different deformation phases are shown in figure 9d.

The resulting age spectrum shows a staircase with increasing step ages from 35 Ma up to 85 Ma (Fig. 10e). This points once more to a mixed age and confirms the microstructural observation. Following Villa (2001), the stepwise-heating data are plotted on a Cl/K vs. age diagram (Fig. 10f). Data points all fall in a triangle, whose vertices are A, B and C, which define the “end-members” of the different populations. A precise determination of the “endmembers” is not possible because most of the steps define the trend from vertex A (inherited component) towards vertex C (D2) and therefore the vertex B (D1) is not well defined (Fig. 10f). Nevertheless the correlation diagram points towards an inherited component at least as old as 80 Ma (A in Fig. 10f), a minimum age for D1 of 43 Ma (B in Fig. 10f) and a maximum age of 38 Ma (C in Fig. 10f) for the second phase of deformation.

Rutor Unit

In order to have control on the processes taking place during the alpine metamorphic cycle and exclude pre-Alpine relics, only Permo-Mesozoic sediments were dated in this unit. Note that detrital micas are still expected to have been present in the sediment, but less than in polymetamorphic basement. Five Permo-Triassic samples were dated (Fig. 2). The previously mentioned gradient in the intensity of the deformation is responsible for a mineralogical difference from west (external) to east (internal), expressed by a decreasing amount of detrital micas and an increasing amount of metamorphic micas.

Cere0033 & Cere0035

Samples Cere0033 and Cere0035 are taken from the Permo-Triassic cover, which forms decametric thick band cropping out throughout the entire Valgrisenche (Caby 1996, Bucher et al. 2004a). Sample Cere0035 was taken in a slightly more external position, by ca. 500m (Fig. 2).

Cere0035 shows a mixture discordant age spectrum. The single step ages vary between 65 and 230 Ma (Fig. 11a). The mixture between Alpine metamorphic micas and detrital grains evidenced by petrological and microstructural observation is confirmed by the variations of the Cl/K (Fig. 11b).

Sample Cere0033 displays an apparent plateau age at 69 Ma, which includes all steps, except the first and last three steps (Fig 11a). An age increase in the last steps is explained by contamination of other minerals having high Cl/K ratios.

Although a clear relationship between the Cl/K ratio and the percentage of the released ^{39}Ar exists for both samples (Fig. 11 b) the resolution in the Cl/K vs. age diagram is not sufficient enough for any interpretation on the age of different “endmembers”. Even if no age determination can be done on these samples the upward-convex age spectrum of the sample Cere0035, the inverse correlation between the Cl/K ratio and step ages clearly indicates a mixture. This is in agreement the microstructural observation suggesting also the presence of a detrital population in these samples, as was shown above. Therefore, integrated ages of 93 Ma and of 69 Ma for sample Cere0035 and Cere0033, respectively, point towards a non-Alpine component/population, as also supported by microstructural and electron microprobe analyses shown previously. Moreover, reported presence of pre-Alpine micas in the basement rocks of the Ruitor unit (Baudin, 1987; Giorgis et al., 1999) further supports this suggestion and indicates also that the K-Ar isotopic system was not (completely) reset in the Ruitor unit during the Alpine metamorphic events.

PT

Sample PT has a more internal position than Cere0033 and Cere0035, near the contact between the Ruitor unit and the PL- oceanic unit of the Avise synform (Caby 1996, Fig. 2).

The age spectrum is characterized by an increase in the first steps and an apparent plateau between 62-63 Ma. (Fig. 11c) The Cl/K-age correlation diagram leaves some uncertainties, but still show indications for a second mica population with a minimum age of 49.5 Ma and a trend to a third population younger than 46 Ma (Fig. 11d). The observation of microlithons and relictic, detritic white mica in the main foliation supports the interpretation of a mixture between Alpine and inherited detrital grains. The interpretation will be discussed later together with the following samples.

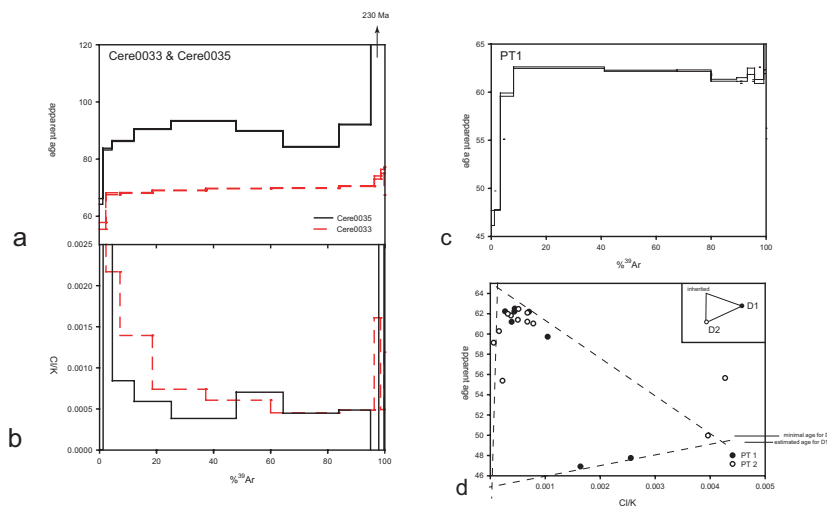


Fig. 11: a) ^{39}Ar - ^{40}Ar age spectrum and b) Cl/K ratio of sample Cere0033 and Cere0035; c) ^{39}Ar - ^{40}Ar age spectrum of sample PT and d) Cl/K vs. age correlation diagram evidencing a mixture between alpine metamorphic micas and an inherited component. Note that the plateau in the age spectrum is geologically meaningless.

Bez0033

Bez0033 was collected in a more internal position in relation to the previous samples (Fig. 2). The age spectrum (Fig. 12a) displays a continuous increase over the first four steps (~20% of the gas) and changes into a flat portion with an apparent age of 55 Ma (step 5-7; ~70% of the gas). In the last three steps (~10% gas) a further increase of the age up to over 90 Ma is observable. The calculated integrated age for all steps is 54 ± 0.4 Ma. Three vertices are defined in the Cl/K vs. age plot (Fig. 12b). Vertices B and C indicate, similar to the samples PT and Rui9958, we interpret vertices B and C as the representatives of two alpine populations. While A represents inherited pre-Alpine relics B and C are very dependent on three steps (2, 3, 9) and hence not well constrained. Nevertheless, all the other steps fall into the triangle defined by A, B and C, which supports a mixture between the “endmembers” defined by the vertices (Fig. 12b). Note that step 1 was excluded as probable alteration phases and and step 8 was excluded due to inconsistencies during the measurement. As a consequence of this observation, the “plateau” visible in the age spectrum is only apparent and has no geological meaning. It is formed by a mixture of Alpine metamorphic and inherited (detrital) micas, which degas over very similar temperature intervals. Furthermore it should be noted that the shape of the age spectrum is mainly a function of the mass balance between the two populations; in case of a mixture affecting in all steps, a precise quantification of the “endmembers” is difficult, as is the case for this sample.

Rdl009

Sample Rdl009 was collected in the internal part of the Ruitor unit (uppermost Valgrisenche, Fig. 2) and belongs to the younger Triassic sequence. This sample is representative for the most intensely deformed, internal part of this unit.

The age spectrum displays a staircase shape. The ages of the different steps vary between 35 Ma and 160 Ma (Fig. 12a). The first five steps show a continuous increase to 51 Ma. Over the next five steps, each containing between 10-15 % gas, a continuous decrease to 47.5 Ma is observable and cumulatively 75% of the gas is released during these steps. In the Cl/K vs. age correlation diagram two trends are observed defining a vertex close to the cluster of the steps 5 to 9 (Fig. 12b). The two other vertices are not constrained precisely, however they allow an interpretation. The trends defined

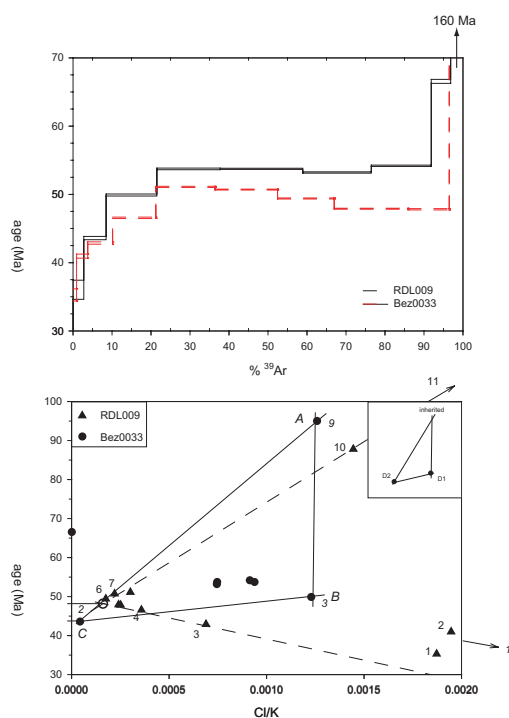


Fig. 12: a) ^{39}Ar - ^{40}Ar stepwise heating spectrum of sample Bez0033 and Rdl009; b) Cl/k-age diagram indicating one inherited (A) and two alpine (B & C) and components for sample Bez0033; the Cl/K-age diagram of Rdl009 shows a vertex pointing to an age of 47 ± 0.5 Ma for the alpine D1 population.

by steps 6,7,10,11 and by the steps 1,3,4 respectively indicate a second alpine population and a minor portion of inherited minerals respectively (Fig. 12b). The dominant population represented by the vertex B shown in the correlation diagram (Fig. 12b) has an age of 47.5 Ma and is interpreted as D1 since microstructural observations attest that this is the predominant generation..

In summary, the similarity of the age spectra on one hand and the progressive evolution of the ages in the Ruitor unit are shown in Figure 13. Integrated ages for individual samples show a continuous decrease from 93 Ma to 55, in relation to their structural position, Ma (Fig 13a). All samples show indications for mixed ages. The resolution of the correlation diagram is not always sufficient to determine all possible reservoirs precisely. However their similarities suggest a common process to be responsible for these observations. Therefore all samples from the Ruitor unit are plotted in one correlation diagram (Cl/K vs. apparent age, Fig. 13b). They define a well-constrained polygon with vertices defined by the measurements of multiple samples. The resulting ages of the three vertices, interpreted to represent the three microstructurally evidenced populations are shown in Fig. 13a. One vertex defines an age of about 47 Ma, which is compatible with the observation from sample Rdl009, and is interpreted to represent D1. The second vertex points to a population with an age of 40 Ma, compatible with the observations for D2 (i.e. Vga0120, see below). The last vertex defined by the extrapolation of the measurements suggests an age of about 135 Ma. On the basis of microstructural and electron microprobe analyses, the Cretaceous age is believed to be derived from inherited (detrital) micas that were partly (re)opened. This is supported by observation of zoned micas.

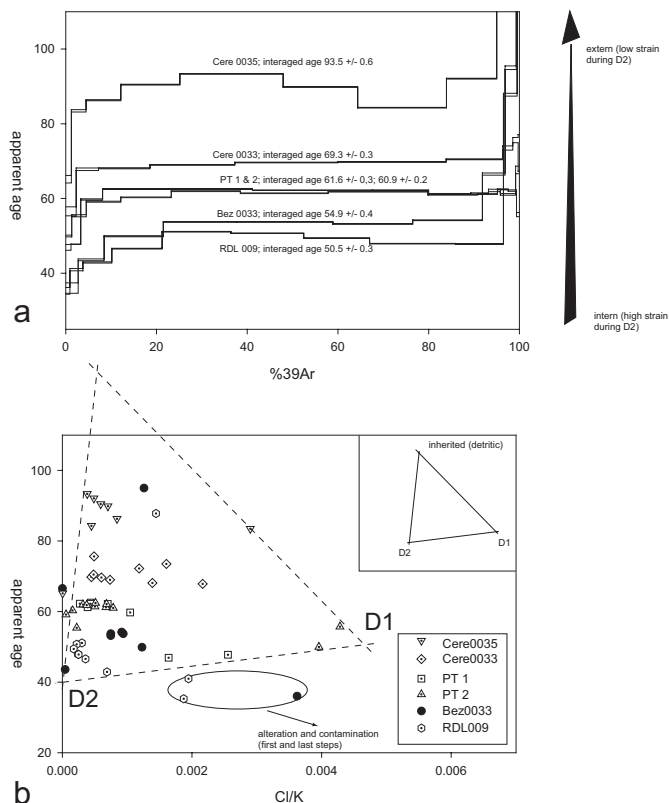


Fig. 13: a) Age spectra of all samples from the Ruitor unit. Note the relationship between the structural position and the integrated age. **b)** Compilation of all samples from the Ruito unit in a Cl/K vs. age correlation diagram. The three vertices pointing to an age of 47 ± 1 Ma for D1; 40 ± 1 Ma for D2; and in inherited component of about 135 Ma. The inherited micas are probably partly reopened as evidence by a zoning.

Internal unit

Vga0120

VGA0120 is a mylonitic Triassic quartzite collected at the tectonic contact between the Internal unit and the PL-oceanic unit (Fig 2). These mylonites associated with the tectonic contact are attributed to the second phase of deformation (D2; Bucher et al. 2003a). From a microstructural and a microchemical point of view, neither a second population, nor substantial retrogression are present in this sample. Therefore the age of this sample can be interpreted to represent the age of the second phase of deformation (D2). The age spectrum shows a flat but slightly increasing age spectra (Fig. 14a). In literature, such almost flat age spectra (step 3 to 8) are sometimes interpreted as plateau ages (e.g. Dal Piaz et al. 2001), despite small but significant differences of the step ages. However application of Cl/K vs. age correlation diagram (Fig. 14b) reveals a trend, i.e. that these are heterochemical mixtures (compare examples in Villa et al. 1997). This requires to only consider the step with the last diluted chemical signature as that representing the true age of one specific reservoir (steps 8 and 10 in Vga0120 unpick and pick, respectively) and not the average of the five to six heterochemical steps. The clear attribution of this quartzitic mylonite to the second phase of deformation allows therefore placing the age for D2 at 40.3 ± 0.5 Ma.

Vga0139

Sample Vga0139, a Permo-Triassic metasediment, is dominated by D2-micas. In weakly deformed portions the D1 mineral assemblage grt-phg-cld is still preserved (see Fig.3c in Bucher et al. 2003a) and hence, a mixed age is expected for this sample.

The age spectrum represents is indeed discordant (Fig. 14a). Over the first four steps, the step ages continuously increase from 34 Ma to 45 Ma. Then they decrease to 42 Ma (3 steps, 30% gas), before rising again to 46 Ma (Fig. 14a).

The distinction of the different populations by the Cl/K correlation diagram is shown in Figure 14b. The “minimum triangle” defined by all steps points towards an age between 47 and 48 Ma for the older (D1) population. The age of the D2 population is not well constrained (Fig. 14b) as it is masked by the alteration trend with $Cl/K > 0.006$ and $t < 33$ Ma.

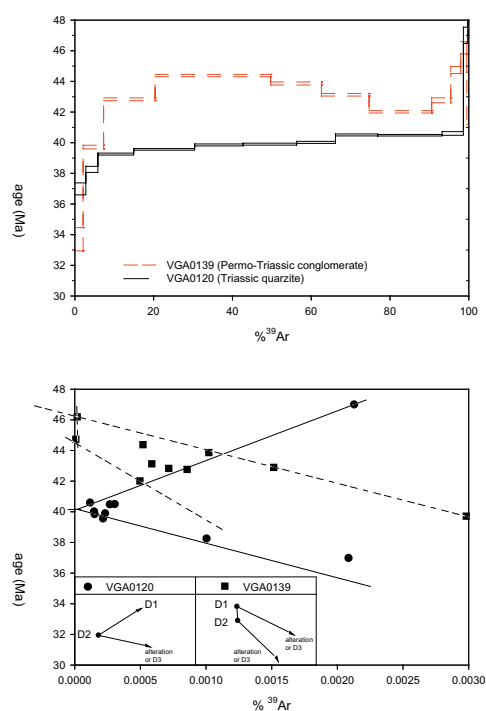


Fig. 14: Samples of the Internal unit a) ^{39}Ar - ^{40}Ar age spectra of the D2 mylonite sample Vga0120 and sample Vga0139 b) Cl/K vs. age correlation diagrams pointing to a vertex at 40.2 Ma for D2 mylonitization (sample Vga0120) and a vertex at 47-48 Ma for D1 in sample Vag0139.

In summary, the $^{39}\text{Ar}/^{40}\text{Ar}$ data confirm the microstructural observations of a mixture between a D1 population and a younger population in this sample. The inferred age for D1 is ca. 47-48 Ma, confirming the other samples (i.e. Rdl009).

Piemont-Ligurian unit (Schistes lustrés)

In the PL-oceanic unit three samples (Arv007, Vaud003 and Traj005) were dated. Two of them are calcschists (Arv007, Traj005) and one is an eclogitic boudin (Vaud003.1-3), from which three different grain sizes were individually dated. Sample Arv007 derives from a very external position of the Avise synform (Caby 1996; Fig. 2), a D2 synform, pinched in the Ruitor unit (Bucher et al., 2003a). The two other samples were collected in more internal positions (Valsavaranche, Fig. 2).

Arv 007

Arv007 is an impure limestone derived from the Avise synform (Caby 1996), the most external occurrence of the Piemont-Liguria oceanic unit in the study area. Deformation in this sample, especially the second foliation S2, is weak, because it is pinched between less competent calcschists.

This sample yields a staircase shaped age spectrum with step ages continuously increasing from 33 Ma to 45.5 Ma at step seven (Fig. 15a), followed by slight decrease to 43 Ma in the last steps. The Cl/K correlation diagram is well constrained and suggests an age of 39.5 Ma for the younger and of 46.5 Ma for the older population (Fig. 15b).

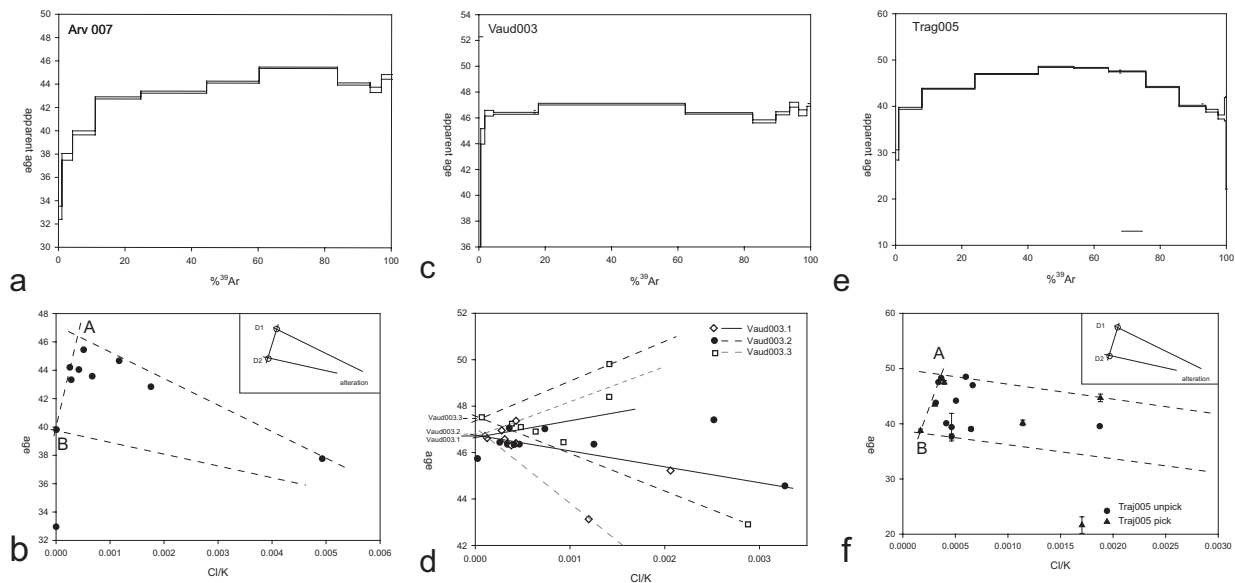


Fig. 15: **a)** ^{39}Ar - ^{40}Ar age spectra and **b)** Cl/K-age diagram of sample Arv007. Vertex A represents the D1 population and B the D2 population with and an of ca. 46.5 Ma and ca. 40 Ma respectively; **c)** ^{39}Ar - ^{40}Ar age spectra and **b)** Cl/K-age diagram of sample Vaud003. Note that the relative difference present in the stepwise heating spectra is equally represented in the Cl/K-age diagram. The size fractions of Vaud003.1, Vaud003.2 and Vaud003.3 are 160-250 μm , 125-160 μm and 250-300 μm respectively. **e)** ^{39}Ar - ^{40}Ar age spectra of sample Traj005. Maximal and minimal age for the two populations after the systematic of Wijbrans and McDougal are 47 Ma and 40 Ma respectively **f)** Cl/K-age diagram of sample Traj005 indicating and D1 (A) population of 48 ± 1 Ma and a D2 (B) population of 39 ± 1 Ma.

Vaud003

The difference in the age spectra of the three dated grain sizes are, as discussed in a former section, The age spectrum is flat over 80% of the released gas and all steps of these samples, except the first two and the last step, plot in a narrow field in the Cl/K vs. age correlation diagram ($Cl/K < 0.0005$; Fig. 15d). The dominating population is interpreted as micas grown during D1 and its vertex plot close to step 7 as shown Figure 14d, (step7 & 8 in Vaud003.2 and Vaud003.3 respectively; Fig. 15d). In sample Vaud003.1 the vertex itself is not represented by a particular step; nevertheless the interpolation between the different points suggests a vertex close to that of sample Vaud003.2. The resulting vertices of the Cl/K vs. age diagram are equal, within the error (Vaud003-1: 46.6 +/- 0.23 Ma; Vaud003.2: 46.6 +/- 0.21; Vaud003.3: 47,0 +/- 0.32). Sample Vaud003 shows (i) that structural and petrological observations suggesting the presence of only one mica population in this sample are verified by the uniform chemical signature (Cl/K) for the three fractions; (ii) that therefore the ages determined by the Cl/K vs. age correlation diagram and the integrated ages of the step heating spectra are identical.

Traj005

As mentioned above the picked and unpicked fraction of sample Traj005 give almost identical age spectra and Cl/K vs. age correlation diagrams. Both age spectra increase from < 30 Ma to 48 Ma in the intermediate temperature steps and decrease again to 39 Ma in the last steps (Fig 14e). This upwards-convex age spectrum represents the typical shape for a phengite-muscovite mixture (Wijbrans and Mc Dougall, 1986).

These authors demonstrated that the oldest steps of the age spectrum of a synthetic mixture define the minimum age for the older phengite population and the youngest steps define the maximum age for the muscovite population. Applying these systematics to Traj005 suggests that the older population has an age of 47.5 and 48.5 Ma for the unpicked and the picked fraction respectively (Fig. 15e). The younger population is $40 \pm 0,5$ Ma for both fractions (Fig. 15e). Application of the chemical criteria results in very similar conclusions. The polygon resulting from the Cl/K vs. age correlation diagram is the same for the picked and unpicked fraction and suggests an age for the younger population (D2) of 39-40 Ma and an age between 47.5 and 48.5 Ma for the older (D1) population (Fig. 15f). Note that the visual estimation following Wijbrans and Mc Dougall (1986) and the “reservoir” determination of the Cl/K vs. age diagram give identical ages.

In summary the following observations characterize the PL oceanic unit: (i) only Alpine (deformation)-ages are observed; no indications for “excess” argon or inherited ages do occur. (ii) While in samples characterized by flat age spectra microstructural and petrological observations indicate the dominance of only one phase of deformation, in samples with discordant age spectra the presence of multiple mica populations can be documented. The different populations can be chemically distinguished and the “endmembers” have the same ages as the plateau ages provided by samples with a single population only (Vaud003, Vga0120).

Summary and Interpretation

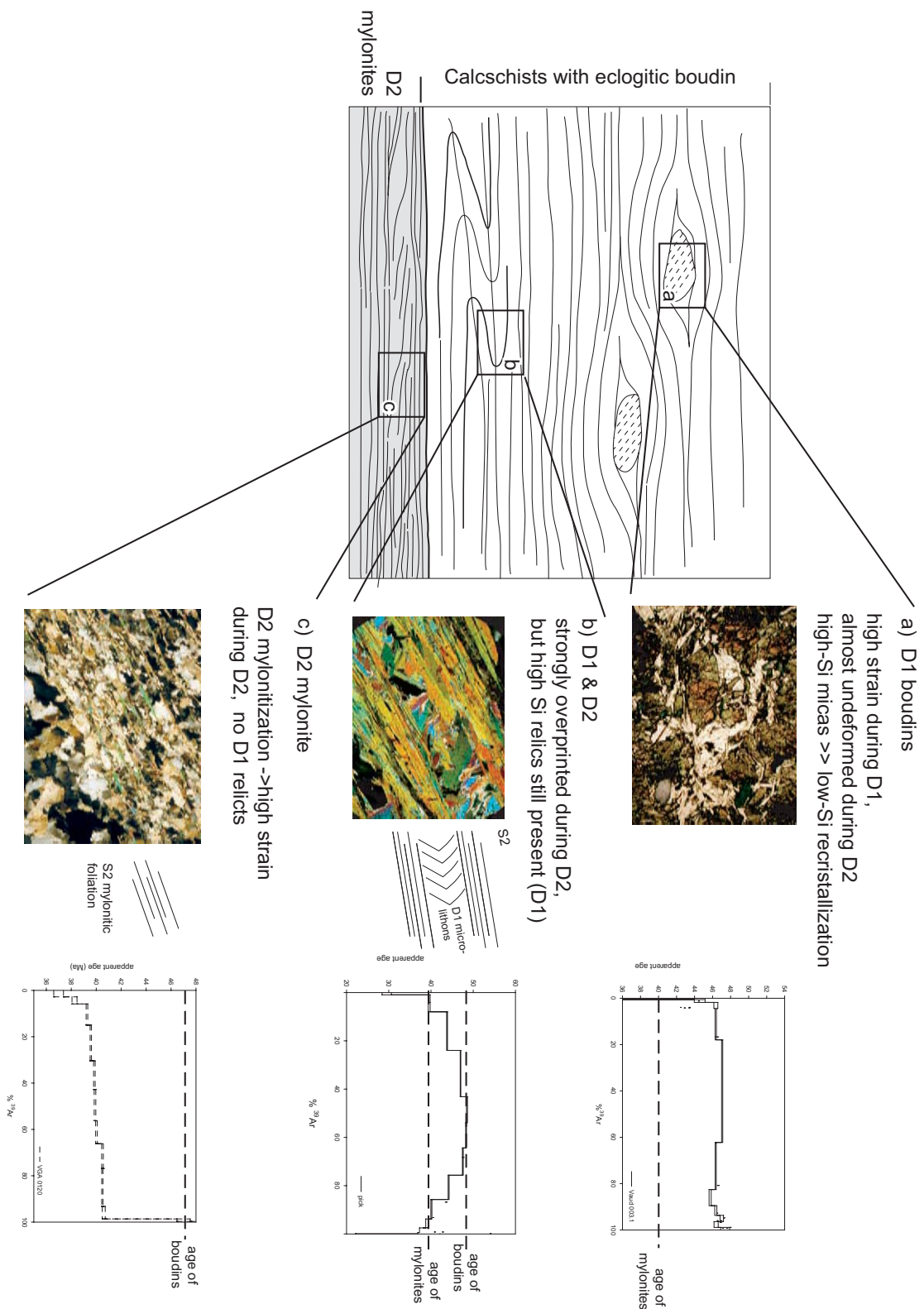
The entire sample selection from the Zone Houillère unit to the Piemont-Liguria oceanic unit is characterised by mixed generations of white mica, and consequently $^{39}Ar/^{40}Ar$ mixed ages. In the external part (Zone Houillère unit) temperatures never exceeded 350° C and observed mixed ages are dominated by the detrital component. All samples from the Zone Houillère unit and the Ruitor unit show the common feature: moderately staircase-shaped age spectra with more or less flat portions ranging between 55 Ma and 280 Ma. These “plateau ages are geologically meaningless.

The observed age spectra and Cl/K-age correlations are typical for a mixture between different mica generations leading to mixed ages. The microstructural and electron microprobe results confirm the Ar isotopic evidence for multiple populations in these samples. Samples from the Ruitor unit display a continuous decrease of the (meaningless) “plateaus” from 90 Ma in the external part to 55 Ma for the most internal samples. Lithologically, all samples represent Permo-Triassic quartz-phyllites and grain size of all dated fractions is 125-160 μm . Therefore the difference in age between the samples can neither be due to a difference in the bulk rock composition, nor due to a grain size dependence of Ar retention. Instead, based on detailed thin section analyses and electron microprobe x-ray mapping, a variable mixture of Alpine D1- and D2-micas together with relictic, detrital micas could be demonstrated.

Furthermore, the observed decrease in total fusion age (i.e. the bulk K-Ar age) is in agreement with the observed increase in Alpine deformation (Bucher et al. 2003a, 2004a) leading to an increase in neofomed white mica. The limiting factor for rejuvenation of bulk K-Ar ages appears thus to be the extent of deformation-induced neofomation of white mica. “Endmembers”, dedectable by microchemical analysis, point to an age of 47 ± 1 Ma for D1, $35\text{-}42 \pm 1$ Ma for D2 and a detritic component with ages between 80 Ma and 280 Ma. The typical upwards-convex age spectra for mixtures are observable in the Ruitor unit, in the Internal and PL-oceanic units. There is a clear relationship between the observed age pattern and the microstructural evidence for single-generation micas. In sample Vaud003, an almost pure D1 mica, both Cl/K ratios (< 0.0006) and step ages (47 ± 1 Ma, Fig. 16a) are constant; similarly, sample Vga0120 consiting almost purely of D2 mica, has constant Cl/K ratios (< 0.0004) and step ages (40 ± 1 Ma, Fig. 16c). In mixed D1-D2 micas, upward-convex age spectra with the oldest step ages at 47 Ma and the youngest of 40 Ma are typified by Figure 16b. These observations rule out “excess” argon or any other kind of diffusional loss to be responsible for the occurrence of the discordant age spectra as already shown by Wijbrans and McDugall (1986). Our observations require Ar retention at temperatures higher than 500°C along the ECORS-CROP profile and even higher than 600°C with respect to the Monte Rosa samples. Ar retention above 550°C has also been suggested by other recent studies (Hammerschmidt and Frank 1991, Di Vincenzo et al. 2001, Philippot et al. 2001).

Dal Piaz et al. (2001) analyzed white micas from the very internal part of the PL-oceanic unit by the $^{39}\text{Ar}/^{40}\text{Ar}$ incremental heating technique. These authors, not discussing Cl/K systematics, interpreted their ages in the range between 41 Ma to 46 Ma to represent HP formation ages. However interpretation in terms of formation ages instead of “cooling ages” implies that neofomed micas during the post HP exhumation/retrogression must be recorded as well. This would have the implication that their ages are mixed ages between HP phengites and subsequent secondary muscovites. Therefore, the pure HP age must be older, compatible to the 47 Ma for the HP (late D1) evidenced in this study. Note that Dal Piaz et al. (2001) also analysed mafic rocks and therefore, in analogy to sample Vaud003, only date the late stages during D1. In another recent study, carried out by Agard et al. (2002), white micas from the PL-oceanic unit further to the south have been dated and presented ages for the different metamorphic events similar to the result of this study. A more detailed discussion about these ages will be given in the next section.

From this study we can conclude that mixed populations are common in metamorphic portions of orogens and even HP relicts can survive subsequent deformation and metamorphism, consistent with observations in more recent literature (e.g. Agard et al. 2002). Furthermore the presence of relictic detrital, partially reopened micas is evidenced. The samples from the Monte Rosa unit show that in undeformed basement rocks pre-Alpine relicts are not reset even at 600°C , on the other hand neofomed micas from a D1 mylonite of the same host rock display great uniformity of the Cl/K ratio coupled to uniform step ages of 47 ± 1 Ma for the alpine HP-age. The combination of the different independent observations provide a straightforward explanation for the 60-130 Ma ages recorded



in most of the HP portions of the Alps (e.g. Sesia, Monte Rosa, Gran Paradiso, etc., for overview see Fig. 3 of Agard et al. 2002) to be due to inherited pre-Alpine or detrital micas, which were incompletely degassed due to a combination of $T < 600^\circ\text{C}$ and incomplete neocrystallization (due to low water activity and low deformation rate).

In the Siviez-Mischabel nappe, which forms the continuation of the investigated units towards the north (and corresponds to the Ruitor unit of this study, according to Gouffon, 1993), white mica $^{39}\text{Ar}/^{40}\text{Ar}$ ages between 25 Ma and 300 Ma were reported by Markeley et al. (1998). Although these authors mainly interpret a relationship between grain size and apparent age for the central Siviez-Mischabel nappe their data do not show a difference in age for different grain sizes. Furthermore these authors describe Hercynian micas rimmed by 60 Ma old micas and stated this as a problem but concluded that these micas overestimate the timing of deformation by 20 Ma. On the other hand Giorgis et al. (1999) stated the presence of pre-Alpine ages and even proposed a Variscan P-T path from the $^{39}\text{Ar}/^{40}\text{Ar}$ data. Cretaceous $^{39}\text{Ar}/^{40}\text{Ar}$ ages are well known from further south (e.g. Chopin & Maluski 1980, Monié 1990). In their geochronological compilation Agard et al. (2002, Fig. 3) point out that apparent mica ages between 120 Ma and 40 Ma were observed along the entire Western Alps.

It seems likely that the observations from this study are not only limited to the proper study area, but hold as well true for corresponding units further north and south of the study area.

Interestingly Reddy et al. (2003) conclude that bulk Rb-Sr data for recrystallized white mica indicate a activity of the Gressoney shear zone (GSZ) associated with top-to-the SE kinematics between 45 Ma and 36 Ma (Reddy et al. 1999). Despite all differences in the interpretation of the $^{39}\text{Ar}/^{40}\text{Ar}$ data the proposed age for the GSZ perfectly fits the geodynamic model of Bucher et al. (2003a, 2004a). These authors interpret the GSZ, associated with top-to-the SE shearing, as the upper boundary of the extrusion channel during the D2 exhumation to be contemporaneous with top-to-the NW kinematics of the different tectono-metamorphic units at the lower levels of the extrusion channel. D2 is interpreted in this study to be active between 43 and 35 Ma, in perfect agreement with the study of Reddy et al. (2003). Finally it is concluded that the $^{39}\text{Ar}/^{40}\text{Ar}$ isotopic system records normally formation and/or deformation ages, in agreement with Agard et al. (2002). We note that our incremental heating and their laser ablation show consistent results. These ages brackets identical to those of this study, strongly confirm that the different “endmembers” of mixed populations are datable by $^{39}\text{Ar}/^{40}\text{Ar}$ incremental heating leading the same results as laser ablation data.

Our complete $^{39}\text{Ar}/^{40}\text{Ar}$ time constraints complete the geodynamic model proposed by Bucher et al. (2003a, 2004a). The $^{39}\text{Ar}/^{40}\text{Ar}$ data of Agard et al. (2002) from the south and the Rb-Sr data for the GSZ of Reddy et al. (1999) can easily be integrated into this geodynamic model. Agreements of the P-T evolution, the kinematics and the geochronological data with the afore mentioned studies verify the validity of the geodynamic model of Bucher et al. (2003a) for the entire Western Alps.

Changing intensity of the deformation in combination with different P-T conditions is interpreted to be responsible for the large variety of white micas recrystallization ages in the samples throughout the Briançonnais domain. Such petrological diversity is mirrored by the variety in $^{39}\text{Ar}/^{40}\text{Ar}$ age spectra. Generally samples from the same tectonic unit show the similar characteristics. The most internal unit, the PL-oceanic domain, shows no indications for pre-Alpine inheritance, but mixed ages between D1 and D2 are common. In the Internal Unit, the next unit further to the NW, weakly Alpine deformed samples show first indications for pre-Alpine inheritance, but intensely deformed samples still show Alpine ages. In the Ruitor unit all samples contain inherited detrital grains and age spectra alone would point towards a Cretaceous age, but microstructural observations and electron microprobe X-ray mapping evidence zoned micas, a clear indication for a relictic, detritic, component in these samples. The confirmation for this interpretation is given by the data from the Zone Houillère unit. Here deformation was weak throughout its Alpine structural evolution and the metamorphic conditions never exceeded subgreenschist facies conditions. As expected, a clear gradient from mixed ages between detritic micas and Alpine metamorphic grains is observable,

resulting in total fusion ages between 300 Ma in samples dominated by detritic micas and 60 Ma in samples with only small amounts of pre-Alpine mica.

Two kinds of samples show no mixed ages: firstly, intensely deformed samples of D2 mylonites; secondly, D1 eclogitic boudins undeformed during D2. D1 eclogitic boudins have uniform Cl/K ratios and constant step ages of 47 ± 1 Ma. D2 mylonites have a similar chemically homogeneous signature and an age of 40 ± 1 Ma. Furthermore, the sample Rui9958 from the tectonic contact between the Zone Houillère unit and the Ruitor Unit only preserved minor amounts of inherited, detritic micas and predominantly contains D2 micas, whose age of ca. 35 Ma thus dates the late-D2 tectonic contact. The uniformity of chemical signature and young step ages confirms the key role of sample-specific deformation-induced recrystallization for the retention of Ar, or lack thereof.

Tectonic Implications

The new geochronological data from this study allow to constrain the timing of the tectono-metamorphic evolution of the Italian-French Western Alps along the ECORS-CROP transect and to test the geodynamic model proposed by Bucher et al. (2003a). By including data from Agard et al. (2002) this geodynamic model can be extrapolated to the entire Western Alps.

The Lu-Hf data from this study (Bucher 2003b) show that prograde garnet growth on the way to eclogite facies conditions is reached in the Eocene. Generally Lu-Hf data are interpreted to date garnet growth and therefore the pre- to synkinematic peak pressure conditions of the eclogite facies. This would correspond to the early stages of D1 of the evolution after Bucher et al. (2004a), whereas micas grown syn-kinematically to the late stages of D1 are dated at 47 ± 1 Ma. Greenschist facies conditions during the exhumation (D2), are reached between 43 Ma and 35 Ma, whereby an east-to-west migration of the deformation (Bucher et al. 2004a) is responsible for this diachronism. The 35 Ma are observed at the tectonic contact between the Ruitor unit and the Zone Houillère unit, which is active in the late stage of D2 (Bucher et al. 2004a). This P-T-t evolution is consistent for the Briançonnais domain and the PL-oceanic unit along the ECORS-CROP and respects both structural and petrological constraints.

The compatibility of the data presented by Agard et al. (2002) and the data from this study, together with the consistency of data throughout all tectonic units along the ECORS-CROP and correspondence between microstructures and $^{39}\text{Ar}/^{40}\text{Ar}$ ages obtained for each individual sample strongly suggest that the deformation-induced recrystallization is the dominant parameter responsible for the recorded ages. There is always danger of excess Ar being invoked to disqualify the existence of inherited Ar. As already pointed out by Agard et al. (2002), the consistency between the absolute chronology and the relative tectono-metamorphic evolution would require a homogenous composition of excess argon at the scale of the whole orogen, across several oceanic units, which is very unlikely. While the study of Agard et al. (2002) is limited to the PL-oceanic unit, this study evidences the same consistency for most of the Briançonnais paleogeographic domain and PL-oceanic unit along the ECORS-CROP transect. Our own Lu-Hf data further reduce the likelihood of excess Ar (Bucher 2003b). Therefore we believe that excess Ar plays a minor role in respect to the deformation, and we disagree with the internally inconsistent criteria used by Reddy et al. (2003) to reject some samples. The evidence of Ar retention vastly above 500 °C in connection with the Lu-Hf garnet ages supports the interpretation that inherited Ar is abundant and excess Ar is negligible. Therefore, monogenetically recrystallized, neo-formed micas record D1 and D2 deformation ages.

Conclusion

The prograde phase of HP metamorphism in the Piemonte-Liguria oceanic unit occurred in the Eocene, as indicated by Lu-Hf ages on garnets (early D1 stage, Bucher 2003b).

At 47 ± 1 Ma, in all the tectono-metamorphic units white micas grew at pressures between 10-15 kbar during the final stage of D1. Exhumation during D2 took place between 43 and 35 Ma. Nappe refolding (D3), not associated with neofomed minerals, took place between 35 Ma and 31 Ma. This lower limit is given by the FT zircon data from the literature (Hurford and Hunziker 1989, Fügenschuh and Schmid 2003).

The proposed P-T-t evolution is compatible with data from the PL-oceanic unit in the south (Agard et al. 2002) and suggests that the geodynamic model of Bucher et al. (20003a, 2004a) is valid for the entire Western Alps. The comparison between the $^{39}\text{Ar}/^{40}\text{Ar}$ laser ablation data of Agard et al. (2003) and the data of this study confirms that mixed populations are correctly unravelled with the chemical information provided by the $^{39}\text{Ar}/^{40}\text{Ar}$ incremental heating technique (cfr. also Müller et al. 2002).

The consistency of the samples within the tectonic units and also along the ECORS-CROP transect rule out diffusional loss of $^{40}\text{Ar}^*$ respectively excess argon to play a significant role. Ar inheritance and the preservation of petrographic pre-Alpine relics plays a dominant role in all samples < 500 °C and 600 °C along the ECORS-CROP and in the ;Monte Rosa unit respectively. Chemically and petrologically homogeneous $^{39}\text{Ar}/^{40}\text{Ar}$ data are observed in highly deformed samples where micas of only one generation (D1 and D2, respectively) are present. On the contrary in samples where microchemical and microstructural observations indicate incomplete recrystallization and the preservation of multiple populations, staircase-shaped and/or upwards-convex age spectra are observed. This is best explained by the intensity of deformation playing a key role in promoting white mica recrystallization, which controls the isotopic ages. In weakly deformed and poorly recrystallized samples the mass fraction of inherited grains is very high. Whenever mixtures seem to be the most common case, they are detectable by the microchemical information given by the Ar isotope measurements. The correlation diagrams allow the identification of the heterochemical reservoirs together with their ages.

Acknowledgements

We thank our colleagues from the “Groupe Briançonnais”, Rainer Abart, Annett Büttner, Stefano Ceriani, Christian de Capitani and Jan Kramers for stimulating discussions. Funding by the Swiss National Science Foundation (project 20-63391.00) and precursor projects since 1995 is gratefully acknowledged

References

- Agard, P., Monié, P., Jolivet, L. & Goffé, B. 2002: Exhumation of the Schistes Lustrés complex: in situ laser probe $^{40}\text{Ar}/^{39}\text{Ar}$ constraints and implications for the Western Alps. *J. Metamorph. Geol.* 20, 599-618.
- Amstuz, A. 1955: Rocher du ravin de Lessert dans la Val D'Aoste. *Arch. Sc. Genève* 8, 6-9.
- Amstuz, A. 1962: Notice pour une carte géologique de la Vallée de Cogne et de quelques autres espaces au Sud d'Aoste. *Arch. Sc. Genève* 15, 1-104.
- Ballèvre, M. & Merle, O. 1993: The Combin Fault: compressional reactivation of a Late Cretaceous-Early Tertiary detachment fault in the Western Alps. *Schweiz. Mineral. Petrogr. Mitt.* 73, 205-227.
- Baudin, T. 1987: Étude Géologique du Massif du Ruitor (Alpes franco-italiennes): Evolution structurale d'un socle Briançonnais. Unpublished PhD thesis, Grenoble, 243 pp.
- Belluso, E., Ruffini, R., Schaller, M. & Villa, I. M. 2000: Electron-microscope and Ar characterization of chemically heterogeneous amphiboles from the Palala Shear Zone, Limpopo Belt, South Africa. *Eur. J. Mineral.* 12, 45-62.
- Bertrand, J. M., Pidgeon, R. T., Leterrier, J., Gouillot, F., Gasquet, D. & Gattiglio, M. 2000: SHRIMP and IDTIMS U-Pb zircon ages of the pre-Alpine basement in the Internal Western Alps (Savoy and Piemonte). *Schweiz. Mineral. Petrogr. Mitt.* 80, 225-248.
- Bocquet (Desmons), J. 1974: Le socle Briançonnais de Vanoise (Savoie): arguments en faveur de son âge anté-alpin et de son polymétamorphisme. *C.R. Acad. Sc. Paris* 278, 2601-2604.
- Bocquet, J. 1974: Études minéralogiques et pétrographiques sur les métamorphismes d'âge alpin dans les Alpes françaises. Unpublished Thèse d'État, Grenoble, 490 pp.
- Bucher, S., Schmid, S. M., Bousquet, R. & Fügenschuh, B. 2003a: Late-stage deformation in a collisional orogen (Western Alps): nappe refolding, back-thrusting or normal faulting? *Terra Nova* 15, 109-117.
- Bucher, S., Schmid, S. M., Bousquet, R. & Fügenschuh, B. 2003b: The Briançonnais units along the ECORS-CROP transect (Italian-French Alps): structures, metamorphism and geochronology. Unpublished PhD thesis, University Basel, 175pp.
- Bucher, S., Ullardic, C., Bousquet, R., Ceriani, S., Fügenschuh, B., Gouffon, Y. & Schmid, S. M. 2004a: Tectonic evolution of the Briançonnais units along a transect (ECORS-CROP) through the Western Alps. *Eclog. Geol. Helv.* 97, 321-346
- Bucher, S., Fügenschuh, B., Bousquet, R., Villa, I., Ferreiro-Mählmann, R., Schmid, S.M.: 2004b Geodynamic evolution of the French-Italian Alps along the ECORS-CROP seismic line. 2nd Swiss Geoscience meeting, 19-20. 11. 2004, Lausanne. p. 100.
- Butler, R. W. H. & Freeman, S. 1996: Can crustal extension be distinguished from thrusting in the internal parts of mountain belts? A case history of the Entrelor shear zone, Western Alps. *J. Struct. Geol.* 18, 909-923.
- Caby, R. 1996: Low-angle extrusion of high-pressure rocks and the balance between outward and inward displacements of Middle Penninic units in the Western Alps. *Eclog. Geol. Helv.* 89, 229-267.
- Challandes, N., Marquer, M. & Villa, I. M. 2003: Dating the evolution of C-S microstructures: a combined $^{40}\text{Ar}/^{39}\text{Ar}$ and UV laserprobe analysis of the Alpine Roffna shear zone. *Chem. Geol.* 197, 3-19.
- Chopin, C. & Maluski, H. 1980: ^{40}Ar - ^{39}Ar Dating of High Pressure Metamorphic Micas From the Gran Paradiso Area (Western Alps): Evidence Against the Blocking Temperature. *Contrib. Mineral. Petrol.* 74, 109-122.
- Chopin, C. & Monié, P. 1984: A unique Magnesiochloritoid-bearing, high-pressure assemblage from the Monte Rosa, Western Alps: petrologic and ^{40}Ar - ^{39}Ar radiometric study. *Contrib. Mineral. Petrol.* 87, 388-398.
- Cigolini, C. 1995: Geology of the Internal Zone of the Grand Saint Bernard Nappe: a metamorphic Late Paleozoic volcano-sedimentary sequence in South-Western Aosta Valley (Western Alps). In: *Studies on metamorphic rocks and minerals of the western Alps. A Volume in Memory of Ugo Pognante.* (edited by B. Lombardo). *Bollettino del Museo Regionale di Scienze Naturali (suppl.)*, Torino, 13, 293-328.
- Coyle, D. A. & Wagner, G. A. 1998: Positioning the titanite fission-track partial annealing zone. *Chem. Geol.* 149, 117-125.

- Crank, J. 1975. Mathematics of diffusion. Second edition, Clarendon Press, Oxford, 488pp.
- Dal Piaz, G. V. 1998: Evoluzione litosferica e magmatismo nel dominio Austroalpino dall'orogenesi varisica al rifting mesozoico. Mem. Soc. Geol. It. 53, 43-62.
- Dal Piaz 1999: The Austroalpine-Piedmont nappe stack and the puzzle of alpine Tethys. Mem. Sci. Geol 51, 155-176.
- Dal Piaz, G. V., Cortiana, G., Del Moro, A., Martin, S., Pennacchioni, G. & Tartarotti, P. 2001: Tertiary age and paleostructural inferences of the eclogitic imprint in the Austroalpine outliers and Zermatt-Saas ophiolite, western Alps. Int. J. Earth Sci. 90, 668-684.
- De Sigoyer, J., Chavagnac, V., Blichert-Toft, J., Villa, I. M., Luais, B., Guillot, S., Cosca, M. A. & Mascle, G. 2000: Dating the Indian continental subduction and collisional thickening in the northwest Himalaya: Multichronology of the Tso Moriri eclogites. Geology 28, 487-490.
- Di Vincenzo, G., Ghiribelli, B., Giorgetti, G. & Palmeri, R. 2001: Evidence of a close link between petrology and isotope records; constraints from SEM, EMP, TEM and *in situ* ^{40}Ar - ^{39}Ar laser analyses on multiple generations of white micas (Lanternman Range, Antarctica). Earth and Planetary Science Letters 192, 389-405.
- Di Vincenzo, G., Carosi, R. & Palmeri, R. 2004: The relationship between Tectono-metamorphic Evolution and Argon Isotope Records in White Mica: Constraints from *in situ* ^{40}Ar - ^{39}Ar Laser Analysis of the Variscan Basement. J. Petrol. 45, 1013-1043.
- Dodson, M. H. 1973: Closure temperature in cooling geochronological and petrological systems. Contrib. Mineral. Petrol. 259-274.
- Droop, G. T. R., Lombardo, B. & Pognante, U. 1990: Formation and distribution of eclogite facies rocks in the Alps. In: Eclogite facies rocks (edited by D. A. Carswell). Blackie, Glasgow and London, 225-259.
- Dunlap, W. J. 1997: Neocrystallization or cooling? $^{40}\text{Ar}/^{39}\text{Ar}$ ages of white micas from low grade mylonites. Chem. Geol. 143, 181-203.
- Ellenberger, F. 1958: Étude géologique du pays de Vanoise. Mém. Serv. Carte géol. Fr. 561 pp.
- Elter, G. 1960: La zona penninica dell'alta e media Val d'Aosta e le unità limitrofe. Mem. Ist. Geol. Univ. Padova 22, 113.
- Elter, G. 1972: Contribution à la connaissance du Briançonnais interne et de la bordure piémontaise dans les Alpes Graies nord-orientales et considérations sur les rapports entre les zones du Briançonnais et des Schistes Lustrés. Mem. Ist. Geol. Univ. Padova 28, 19pp.
- Engi, M., Scherrer, N. & Burri, T. 2001: Metamorphic evolution of pelitic rocks of the Monte Rosa Nappe; constraints from petrology and single grain monazite age data. Schweiz. Mineral. Petrogr. Mitt. 81, 305-328.
- Fabre, J. 1961: Contribution à l'étude de la Zone Houillère Briançonnais en Maurienne et en Tarentaise (Alpes Savoie). Mém. Bur. Rech. Géol. Min., 2, 315 pp.
- Feys, R. 1963. Étude géologique du Carbonifère briançonnais (Hautes-Alpes), Mém. Bur. Rech. Géol. Min., 6, 387 pp.
- Foland, K. A. 1979: Limited mobility of argon in metamorphic terrains. Geochim. Cosmochim. Acta 43, 793-801.
- Freeman, S. R., Butler, R. W. H., Cliff, R. A., Inger, S. & Barnicoat, A. C. 1998: Deformation migration in an orogen-scale shear zone array: an example from the Basal Briançonnais Thrust, internal Franco-Italian Alps. Geol. Mag. 135, 349-367.
- Fügenschuh, B., Loprieno, A., Ceriani, S. & Schmid, S. 1999: Structural analysis of the Subbriançonnais and Valais units in the area of Moûtiers (Savoy, Western Alps): paleogeographic and tectonic consequences. Int. J. Earth Sci., 88, 201-218.
- Fügenschuh, B. & Schmid, S. M. 2003: Late stages of deformation and exhumation of an orogen constrained by fission-track data: a case study in the Western Alps. Geol. Soc. Am. Bull. 115, 1425-1440.
- Gerber, C. 1965: Flore et stratigraphie du Carbonifère des Alpes françaises. Mém. BRGM 21, 380pp.
- Giorgis, D., Thélin, P., Stampfli, G. M. & Bussy, F. 1999: The Mont-Mort metapelites: Variscan metamorphism and geodynamic context (Briançonnais basement, Western Alps, Switzerland). Schweiz. Mineral. Petrogr. Mitt. 79, 381-398.
- Gouffon, Y. 1993: Géologie de la «nappe» du Grand St-Bernard entre la Doire Baltée et la frontière suisse (

- Vallée d'Aoste- Italie). *Mémoires de Géologie (Lausanne)* 12, 147.
- Graham, C. M. 1981: Experimental Hydrogen Isotope Studies III: Diffusion of Hydrogen in Hydrous Minerals, and Stable Isotope Exchange in Metamorphic Rocks. *Contrib. Mineral. Petrol.* 76, 216-228.
- Hames, W. E. & Cheney, J. T. 1997: On the loss of $^{40}\text{Ar}^*$ from muscovite during polymetamorphism. *Geochim. Cosmochim. Acta* 61, 3863-3872.
- Hammerschmidt, K. & Frank, E. 1991: Relics of high pressure metamorphism in the Lepontine Alps (Switzerland) - $^{40}\text{Ar}/^{39}\text{Ar}$ and microprobe analyses on white K-micas. *Schweiz. Mineral. Petrogr. Mitt.* 71, 261-274.
- Holdaway, M. J., Mukhopadhyay, B., Dyar, M. D., Guidotti, C. V. & Dutrow, B. L. 1997: Garnet-biotite geothermometry revised; new Margules parameters and a natural specimen data set from Maine. *Am. Mineral.* 82, 582-595.
- Hurford, A. J. & Hunziker, J. C. 1989: A revised thermal history for the Gran Paradiso massif. *Schweiz. Mineral. Petrogr. Mitt.* 69, 319-329.
- Jäger, E. 1967: Die Bedeutung der Biotit Alterswerte. In: *Altersbestimmungen an Glimmern in den Zentralalpen* (edited by E. Jäger, E. Niggli and E. Wenk) 134. *Beitr. Geol. Karte, NF*, 11-21.
- Keller, L. M., Abart, R., Stünitz, H. & De Capitani, C. 2004: Deformation, mass transfer and reactions in an eclogite facies shear zone in a polymetamorphic metapelite, (Monte Rosa, Western Alps). *J. metam. Geol.* 22/2, 97-118
- Kelley, S. P. 2002: Excess argon in K-Ar and Ar-Ar geochronology. *Chem. Geol.* 188, 1-22.
- Markley, M. J., Teyssier, C., Cosca, M. A., Caby, R., Hunziker, J. C. & Sartori, M. 1998: Alpine deformation and $^{40}\text{Ar}/^{39}\text{Ar}$ geochronology of synkinematic white mica in the Siviez-Mischabel Nappe, western Pennine Alps, Switzerland. *Tectonics* 17, 407-425.
- Mercier, D. & Beaudoin, B. 1987: Révision du Carbonifère Briançonnais: Stratigraphie et évolution du bassin. *Geol. Alpine* 13, 25-31.
- Monié, P. 1985: La méthode ^{39}Ar - ^{40}Ar appliquée au métamorphisme alpin dans le massif du Mon-Rose (Alpes Occidentales). *Chronologie détaillée depuis 110 Ma. Eclog. Geol. Helv.* 78, 487-516.
- Monié, P. 1990: Preservation of Hercynian $^{40}\text{Ar}/^{39}\text{Ar}$ ages through high-pressure low-temperature Alpine metamorphism in the Western Alps. *Eur. J. Mineral.* 2, 343-361.
- Müller, W. 2003: Strengthening the link between geochronology, textures and petrology. *Earth and Planetary Science Letters* 206, 237-251.
- Müller, W., Kelly, S. P. & Villa I. M.. 2002: Dating fault-generated pseudotachylytes: comparison of $^{39}\text{Ar}/^{39}\text{Ar}$ stepwise-heating, laser ablation and Rb-Sr microsampling analyses. *Contrib. Mineral. Petrol.* 144, 57-77.
- Philippot, P., Blichert-Toft, J., Perchuk, A., Costa, S. & Gerasimov, V. 2001: Lu-Hf and Ar-Ar chronometry supports extreme rate of subduction zone metamorphism deduced from geospeedometry. *Tectonophysics* 342, 22-38.
- Reddy, S. M. & Potts, J. P. 1999: Constraining absolute deformation ages: the relationship between deformation mechanisms and isotopic systematics. *J. Struct. Geol.* 21, 1255-1265.
- Reddy, S. M., Wheeler, J., Butler, R. W. H., Cliff, R. A., Freeman, S., Inger, S., Pickles, C. & Kelley, S. P. 2003: Kinematic reworking and exhumation within the convergent Alpine Orogen. *Tectonophysics* 365, 77-102.
- Roure, F., Bergerat, F., Damotte, B., Mugnier, J.-L. & Polino, R. 1996: The ECORS-CROP Alpine seismic traverse. *Mém. Soc. Geol. France*, 170, 113pp.
- Scaillet, S., Feraud, G., Ballèvre, M., Amouric, M. 1992: *Mg/Fe and [(Mg,Fe)Si-Al₂] compositional control on argon behaviour in high-pressure white micas: A $^{40}\text{Ar}/^{39}\text{Ar}$ continuous laser-probe study from the Dora_Maira nappe of the internal western Alps, Italy.* *Geochim. Cosmochim. Acta* 56, 2851-2872.
- Scherer, E. E., Cameron, K. L. & Blichert-Toft, J. 2000: Lu-Hf garnet geochronology: Closure temperature relative to the Sm-Nd system and the effects of trace element inclusions. *Geochim. Cosmochim. Acta* 64, 3413-3432.
- Schmid, S. M. & Kissling, E. 2000: The arc of the Western Alps in the light of new data on deep crustal structure. *Tectonics* 19, 62-85.

- Scott, D. J. & St Onge, M. R. 1995: Constraints on Pb closure temperature in titanite based on rocks from the Ungava Orogen, Canada; implications for U-Pb geochronology and P-T-t path determinations. *Geology* 23, 1123-1126.
- Sherlock, S. C. & Arnaud, N. O. 1999: Flat plateau and impossible isochrons: Apparent ^{40}Ar - ^{39}Ar geochronology in high-pressure terrain. *Geochim. Cosmochim. Acta* 63, 2835-2838.
- Todd, C. S. & Engi, M. 1997: Metamorphic field gradients in the Central Alps. *J. Metamorph. Geol.* 15, 513-530.
- Trümpy, R. 1966: Considérations générales sur le «Verrucano» des Alpes Suisses. Atti del simposium sul Verrucano Pisa. 1966. Atti. Soc. Toscana Sci. Nat., 212-232.
- Ullrich, C. 2001: Strukturgeologische und petrographische Untersuchungen im Valgrisenche (Briançonnais der italienischen Alpen). Unpubl. diploma thesis, Univ. Freiburg, Germany, 100 pp.
- Villa, I. M. 1998: Isotopic closure. *Terra Nova* 10, 42-47.
- 2001: Radiogenic isotopes in fluid inclusions. *Lithos* 55, 115-124.
- Villa, I. M., Grobéty, B., Kelly, S. P., Trigila, R. & Wieler, R. 1996: Assessing Ar transport paths and mechanisms for Mc Clure Mountains Hornblende. *Contrib. Mineral. Petrol.* 126, 67-80.
- Villa, I. M., Hermann, J. & Müntener, O. 2000: ^{39}Ar - ^{40}Ar dating of multiply zoned amphibole generations (Malenco, Italian Alps). *Contrib. Mineral. Petrol.* 140, 363-381.
- Villa, I. M. & Puxeddu, M. 1994: Geochronology of the Larderello geothermal field; new data and the "closure temperature" issue. *Contrib. Mineral. Petrol.* 115, 415-426.
- Villa, I. M., Ruggieri, G. & Puxeddu, M. 1997: Petrological and geochronological discrimination of two white-mica generations in a granite cored from the Larderello-Travale geothermal field (Italy). *Eur. J. Mineral.* 9, 563-568.
- Wijbrans, J. R. & McDougall, I. 1986: $^{39}\text{Ar}/^{39}\text{Ar}$ dating of white micas from an Alpine high-pressure metamorphic belt on Naxos: the resetting of the argon isotopic system. *Contrib. Mineral. Petrol.* 93, 187-194.

Chapter 5

by Stefan Bucher, Romain Bousquet and Ilka Kleinhanns

Lu-Hf and Sm-Nd systematics in HP metamorphic rocks: preliminary results of a case study from the Piemonte-Ligurina oceanic unit (Italian-French Western Alps)

Introduction

The age of syn-D1 HP-metamorphism along the ECORS-CROP transect was addressed by dating of micas with the Ar incremental heating technique. High-Si micas interpreted by Bucher et al., (see chapter 4) to have grown during D1 show plateau ages of 47 ± 1 Ma. Micas, however, are not stable under peak eclogite facies conditions in mafic and ultra-mafic rocks. Consequently, although the D1 micas clearly predate the phase of most intensive deformation (D2), dated at ~ 40 Ma (Bucher et al., see Chapter 4), the resulting ages are expected to be slightly younger than the age of peak eclogitic conditions. Dating pre- to syn kinematically formed garnets with the Lu/Hf and Sm/Nd systematics therefore is expected to give more precise information on the timing of peak pressure conditions.

During the last years the discussion about the age of alpine HP-metamorphism was reanimated through the application of different new methods, such as U-Pb SHRIMP analysis or dating with the Lu-Hf isotopic system. Not only has the commonly accepted tertiary age of the HP-metamorphism in the Alps been newly discussed, but also new geodynamic models arguing for extremely fast exhumation (up to several cm/yr) were postulated. These also led to speculations about the generally accepted paleogeographic arrangement of the Alps (e.g. Froitzheim 2001), speculations but are at least partly based on age data (Gebauer, 1999).

A new method for dating garnets with the Lu-Hf isotope system was established during the last years (e.g. Duchêne et al. 1997). Several contributions showed the advantage of this method, over the classical older method based on the Sm-Nd isotope system. This method shows especially for HP-LT conditions indications for isotopic disequilibrium (Thöni & Jagoutz 1992, Naegler et al. 1995, Luais et al. 2001). The Sm-Nd isotope system has relentlessly been plagued by the complication that the inventories of the radiogenic isotopes measured in the garnet separates may be located in inclusions in garnet rather than in the garnet lattice itself (e.g. De Wolf et al., 1996; Scherer et al. 2000). By carrying out a dual garnet dating approach by combining both the Lu-Hf and the Sm-Nd isotope systems on the same samples it is possible to evaluate the advantage and/or limitations of both methods. The comparison with ^{39}Ar - ^{40}Ar data allows a further evaluation of the age interpretations. By means of Lu-Hf and Sm-Nd dating of HP mineral assemblages the following questions were addressed:

- (i) Dating of the age with eclogite facies in metabasic rocks that occur as boudins within matrix of the metasediments.
- (ii) Dating of the age of high pressure garnet in the metasediments that build up the matrix of the metabasic rock, and comparison with the age obtained in the metabasic rocks.
- (iii) Evaluation of the influence of later tectonic overprinting, and of the associated retrogression

In order to answer these questions three samples from the PL-oceanic unit were selected for combined Lu/Hf and Sm/Nd analysis. All three dated samples (Vaud003, Lan003 and Lev008) derive from the PL-oceanic unit of the Italian-French Western Alps. They were all collected along the ECORS-CORP transect (Roure et al. 1990, Schmid and Kissling 2000) and between the Val di Cogne and the Val di Rhêmes (Fig. 1). The PL oceanic unit predominantly comprises calcschists, which are interlayered with different amounts of metabasites (Elter 1972, Cigolini, 1995). For further details about geological framework and tectono-metamorphic evolution we refer to Bucher et al. (2003; chapter 3 of this thesis).

Sample (Vaud003) is from a mafic boudin and the obtained age data should indicate the age of peak pressure conditions during eclogite metamorphism. The other two samples investigated are metapelites (Lan003 and Lev008) from the boudin matrix and their metamorphic age is not expected to be the same one, either due to retrogression or alternatively due to mélange formation. Bucher et al. (chapter 4) attributed the eclogitic metamorphism preserved in the boudins correlated to the first deformation phase (D1), based ^{39}Ar - ^{40}Ar data of the mafic boudin sample Vaud003.

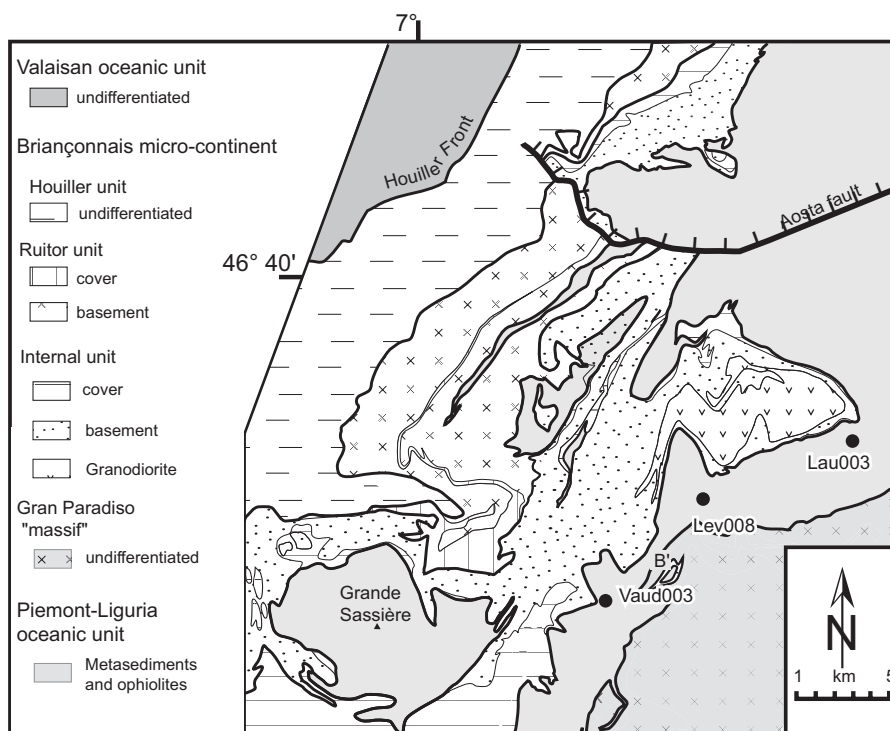


Fig. 1: Geological map of the study area after Bucher et al. (2003) showing the locations of the samples

Petrology and sample description

Metasediment sample Lan 003

This sample is from the internal part of the PL-oceanic unit and was collected in the Cogne area (Fig. 1). This Schistes-Lustrées type metasediment (metapelite-metasandstone) shows only minor indications for retrogression. The dominant minerals are garnet, chloritoid, phengite and paragonite representing HP conditions established during the first deformation phase (D1, Bucher et al. 2003). Although garnet and phengite are also stable during the retrograde part of the P-T path as well, there are no indications for a second population of garnet and phengite, nor for other, retrograde, minerals except for minor amounts of chlorite. Theoretically, this sample is therefore suitable for verifying the age of HP-metamorphism in the metasediments, provided that age of metamorphism is contemporaneous in boudins and matrix.

Metabasite sample Vaud 003

This sample was collected in a very external position of the PL-oceanic unit, i.e. close to the tectonic contact with the Internal unit (Fig. 1). It comprises the following minerals: glaucophane, garnet, omphacite, titanite, phengite, epidote-clinozoisite and green hornblende. Peak-metamorphic conditions of D1 are recorded by the assemblage glaucophane, garnet, omphacite. The retrograde path is evidenced by the overgrowth of glaucophane by green hornblende (Fig. 2). Furthermore, epidote and clinozoisite grow during the retrograde D2 stage, and it seems that titanite is also stable under the retrograde, upper greenschist/lower amphibolite facies conditions. Therefore, we chose garnet in combination with pyroxene (i.e. omphacite) for dating peak pressure conditions, because green hornblende, titanite and epidote/zoisite being formed by reactions that followed peak conditions.

Metasediment sample Lev008

This sample also derives from the metasediments (Schistes Lustrées) of the PL-oceanic unit and was collected in an intermediate structural position (Fig. 1). In contrast to the other metasedimentary sample Lan003, it suffered substantial retrogression along the retrograde path. This is evidenced by the occurrence of epidote-clinozoisite and a second population of phengite (phengite2), and possibly also garnet. Garnets of the second population occur, however, only occasionally and are on average much smaller (< 200 μm). Nevertheless, the HP-mineral assemblage garnet- glaucophane-phengite1 still dominates the mineral composition of the sample. The dating of this substantially retrogressed sample potentially allows to study the influence of retrogression and to test internal consistency of the results of the two other samples chosen for dating.



Fig. 2: Photo-Micrograph from sample Vaud003 showing the overgrowth of glaucophane (HP) by green hornblende during the retrogression.

Analytical Methods

Lu-Hf and Sm-Nd fractions were separated from one single sample digest following the procedure described by Kleinhanns et al. (2002). Measured values for Hf inhouse solution (isotopically indistinguishable from JMC 475 (Kleinhanns et al. 2002)) were 0.282148 ± 15 , 1.46728 ± 6 and 1.8869 ± 1 for $^{176}\text{Hf}/^{177}\text{Hf}$, $^{178}\text{Hf}/^{177}\text{Hf}$ and $^{180}\text{Hf}/^{177}\text{Hf}$, respectively. A Nd inhouse solution gave values of 0.511052 ± 18 , 0.348407 ± 10 and 0.23642 ± 5 for $^{143}\text{Nd}/^{144}\text{Nd}$, $^{145}\text{Nd}/^{144}\text{Nd}$ and $^{150}\text{Nd}/^{144}\text{Nd}$, respectively. The $^{143}\text{Nd}/^{144}\text{Nd}$ ratio of the inhouse solution corresponds to a La Jolla value of 0.511842 for this ratio (Kleinhanns et al., 2002)

Results

It is commonly accepted that mineral phases produced during one specific geologic event should lie on a linear array in an isochron plot. In the case of magma crystallisation this implies that even the whole rock (WR) data should lie on this regression as all mineral phases are thought to be in equilibrium. In the case of a metamorphic event, however, mineral relationships have to be taken into account. To allow precise dating of one specific metamorphic event only phases (re)opened or created at that event are to be used. In addition, the influence of retrogression in the presence of fluids and/or of inherited minerals as for example zircon, monazite and apatite is not yet well understood (e.g. Jagoutz et al 1993, Nagler et al. 1995, Scherer et al. 2000). To avoid this problem different mineral phases of the HP-mineral assemblage that were carefully observed in thin sections in order to estimate the amount of inheritance and/or crystal damages were analysed for dating.

In the following the results of the three dated samples will be discussed individually. The Lu-Hf and Sm-Nd data for whole rock and mineral separates are presented in Tables 2 and 3 respectively. Resulting isochrons for the individual samples are shown in Figure 3 and 4.

Lu-Hf and Sm-Nd isotope geochemistry

Introductory remark on the ^{176}Lu decay constant

The value of the decay constant of ^{176}Lu to be used for the Lu-Hf isotope system is presently highly debated in the literature (e.g. Scherer et al., 2001, Blichert-Toft et al., 2002; Bizzarro et al., 2003). The value of $1.94 \cdot 10^{-11} \text{a}^{-1}$ is derived by calibration using eucritic meteorites and age comparison with the Sm-Nd system (Blichert-Toft et al. 2002); the second value of $1.865 \cdot 10^{-11} \text{a}^{-1}$ for $\lambda^{176}\text{Lu}$ commonly used is derived by calibrations using a comparison between U-Pb and Lu-Hf age information of terrestrial samples that cooled and crystallised rapidly (Scherer et al. 2001). In this study the decay constant of Scherer et al. (2001) will be used for the calculations, as this constant is terrestrially defined and calibrated.

Metasediment sample Lan 003

From sample Lan003 two different size fractions of garnet (160-250 μm and 250-400 μm) and glaucophane were analysed in addition to WR. Glaucophane and garnet clearly represent peak pressure conditions in this sample.

Lu contents range from 0.078 ppm in the glaucophane to 1.92 ppm in the smaller garnet fraction, respectively whereas Hf concentrations vary from 0.26 in the larger garnet fraction to 1.68 ppm in the WR, respectively. $^{176}\text{Lu}/^{177}\text{Hf}$ ratios vary between 0.008 in glaucophane to 0.963 in the

larger garnet fraction and $^{176}\text{Hf}/^{177}\text{Hf}$ ratios range from 0.282664 (WR) to 0.284101 (Grt250). The analysed separates do not define a straight line, which indicates isotope disequilibrium. (Fig. 3a). This is supported by a comparison of glaucophane and WR having significantly different $^{176}\text{Hf}/^{177}\text{Hf}$ ratios for similar $^{176}\text{Lu}/^{177}\text{Hf}$ ratios. This implies inheritance of D1-unequilibrated material in the WR. The observation that WR is not in equilibrium with the HP-assemblage is reported by several authors (e.g. Thöni and Jagoutz 1992). Moreover, Scherer et al. (2000), based on a study examining the influence of inclusions, conclude that WR should be excluded and only minerals being part of the HP-assemblage should be used for age determinations of HP-metamorphism. Similar conclusions are reached by Thöni & Jagoutz (1992) regarding the Sm-Nd isotopic system. Following these suggestions WR was excluded, which results in a Lu-Hf garnet – glaucophane age of 55 ± 3 Ma (for Gln-Grt160) and of 59.5 ± 3.9 Ma (Gln-Grt250) (Fig. 3a). Age differences between two different garnet size fractions are reported by other authors as well and commonly explained by the presence of inclusions. Although the measured fractions were purified by handpicking in order to exclude inclusions, a spread in isotopic ratios is observable (Fig. 3a, Tab. 2), suggesting the presence of very small, optically not detectable inclusions. Generally fractions with the higher $^{176}\text{Lu}/^{177}\text{Hf}$ ratios are interpreted as the purer fractions. Therefore the Grt250-Gln isochron displaying an age of 59.5 ± 3.9 Ma is interpreted to be more reliable than the Grt160-Gln160 isochron. However the confidence limits of the glaucophane-garnet ages for both overlap.

Ages obtained when calculating Grt-WR isochrons are clearly older, giving an age of 83 ± 3.8 Ma and of 85.5 ± 2.6 (Grt250 and Grt160 respectively). This further supports our assumption on the inheritance of older, possibly detrital material. Inheritance of older, detrital material has already been observed in the case of 39Ar-40Ar ages from samples from the same area (Bucher et al., chapter 4 of this thesis).

Sm contents range from 2.4 ppm in glaucophane to 5.3 ppm in the larger garnet fraction (Grt250), respectively (Table 3). Nd concentrations vary from 3.4 ppm in the larger garnet fraction (grt250) to 21-22 ppm in the smaller garnet fraction (Grt160) and WR. Resulting $^{147}\text{Sm}/^{144}\text{Nd}$ ratios show a large variation from 0.1208 in the whole rock to 0.9361 in Grt250, whereas $^{143}\text{Nd}/^{144}\text{Nd}$ ratios range from 0.512134 in Grt250 to 0.513019 in the smaller garnet fraction (Grt160).

Obtained Sm-Nd isotope results do not define a linear array, but scatter strongly (Fig. 3b). Excluding WR, following the previous discussion, a poorly constrained negative slope results. Hence, no age information can be drawn from the Sm-Nd isotope systematics in the case of this sample.

Metabasite sample Vaud 003

In this sample WR, two garnet size fractions, pyroxene (omphacite), and green hornblende were analysed. Garnet glaucophane and pyroxene represent the HP-mineral assemblage. The overgrowth of glaucophane by green hornblende during retrogression could influence the isotopic composition of the former. Therefore glaucophane was not analysed.

Lu and Hf contents (Tab. 2) are in the same range as in sample Lan003. The same can be observed for the $^{176}\text{Lu}/^{177}\text{Hf}$ (0.034-1.190) and $^{176}\text{Hf}/^{177}\text{Hf}$ (0.283144-0.283973) ratios (Tab. 2).

There are, however, two major differences compared to the above discussed sample Lan003 as the larger garnet fraction (Grt250) shows high Hf concentrations, leading to a very low $^{176}\text{Lu}/^{177}\text{Hf}$ ratio. Such low $^{176}\text{Lu}/^{177}\text{Hf}$ ratios in garnet point towards zircon inclusions as not Lu is low, but Hf is higher concentrated. In the case of zircon inclusions, however, the different garnet fractions and whole rock should not define a regression, as it is observable for sample Vaud003 (Fig. 3c and 4a). Therefore, the isotopic composition of Grt250 is suspicious and not used for determining the age of high-pressure overprint. The regression between Grt160 and pyroxene defines an age of 59.7 ± 3.7 Ma (Fig. 3c), which is in perfect agreement with the age inferred for sample Lan003. Hence, this age indicates that the age of eclogitization of both matrix and boudins is identical. Analogous to sample Lan003 the WR does not define an isochron with the high-pressure minerals garnet (Grt160)

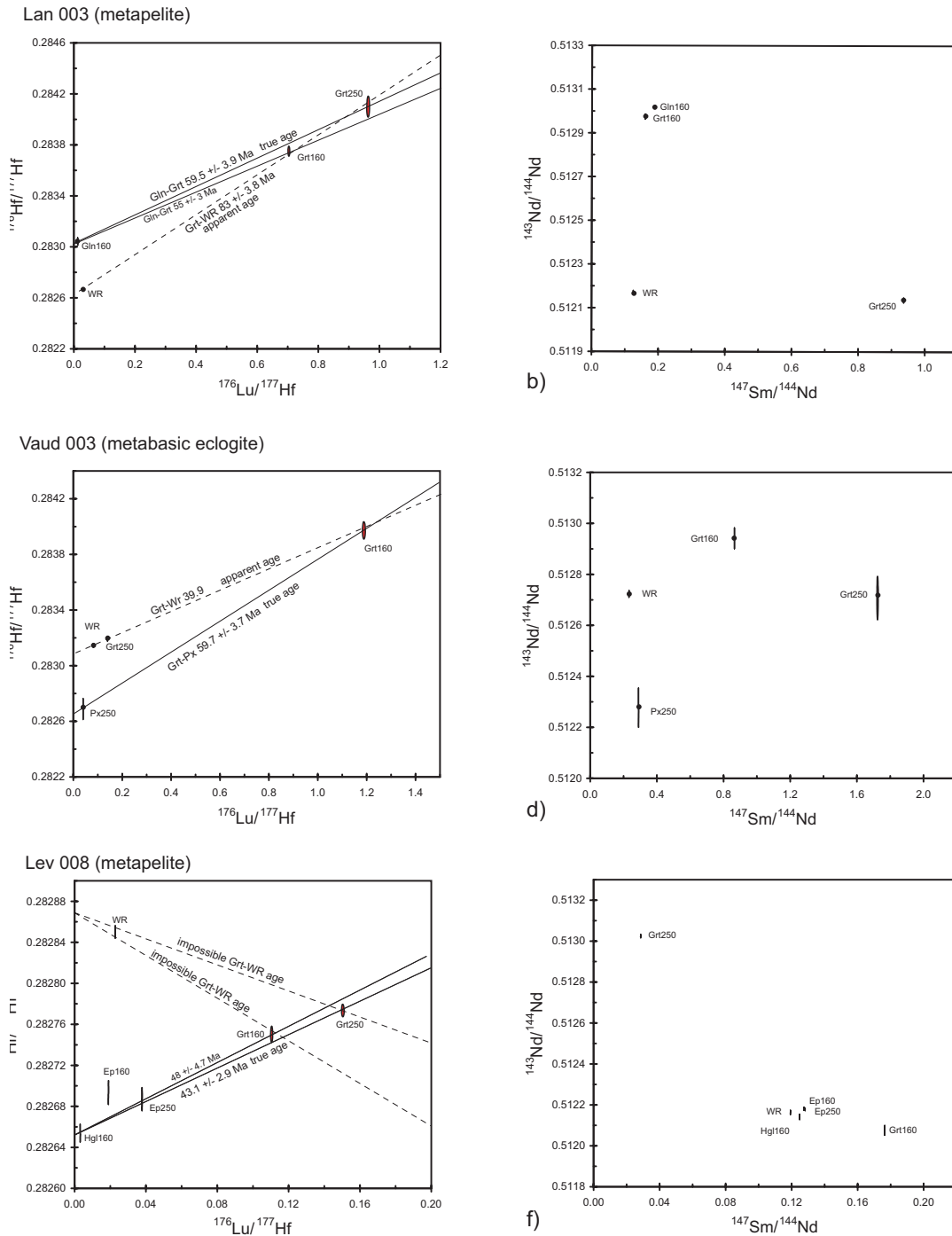


Fig. 3: Lu-Hf apparent and “true” age isochron for the analysed samples a) Lan003, c) Vaud003 and e) Lev008; and Sm-Nd errorchron for the analysed samples b) Lan003, d) Vaud003 and f) Lev008; and Lev008. All data calculated with $\lambda^{176}\text{Lu}$ of $1.865 \times 10^{-11} \text{ a}^{-1}$ (Scherer et al. 2001). Ages are calculated with Isoplot Version 2.49 (Ludwig 2001). WR=whole rock; Grt=garnet; Px = pyroxene; Gln = glaucophane, Hbl = green hornblende; Ep = epidote; Hgl = white mica; the numbers following the abbreviations indicate the size fractions. See Table 1 and Table 2 for data.

and pyroxene (Px250) and is therefore excluded (Fig. 3c) for the same reasons as given above.

However, in contrast to sample Lan003 the WR for this sample plots above the regression defined by the HP minerals (Grt160 and Px250; Fig. 3c). The possible influence of inherited minerals in the WR modelled for the example of zircon is shown in Figure 4a. Note that, in the case of zircon inclusions, it is not possible for the whole rock to plot above the “true age” regression line, as is observed in this sample.

Furthermore, it appears that the two garnet fractions (Grt250, Grt160) and the WR define an isochron (Fig. 3c). Obviously two mutually incompatible interpretations could be drawn here, either by ignoring pyroxene or the WR-Grt250 pair suggesting an age of either 39.9 ± 1.5 Ma or 59.7 ± 3.7 Ma for eclogite facies conditions, respectively (Fig. 3c). As mentioned above, the WR is not necessarily reliable (for details see discussion), and thus it is concluded that the Grt160-Px250 isochron represents the age of the HP-metamorphism. The younger age of 39.9 ± 3.7 Ma, however, corresponds to the age of the second deformation phase (D2) as inferred from ^{39}Ar - ^{40}Ar (Bucher et al., chapter 4). Therefore, it could be speculated that this sample suffered partial retrogression at that stage.

White micas from this sample dated by ^{39}Ar - ^{40}Ar incremental heating (Bucher et al., chapter 4 of this thesis) show a plateau age of 47 ± 1 Ma. Petrological and microstructural observations suggest that these white micas postdate garnet growth, but that they predate D2 (~ 40 Ma; ^{39}Ar - ^{40}Ar). Therefore the ^{39}Ar - ^{40}Ar geochronological data confirms the Lu/Hf ages and vice versa.

In contrast to sample Lan003 this sample generally has lower Sm and Nd contents ranging from 0.262 ppm in pyroxene to 2.06 ppm in titanite, and from 0.558 ppm in pyroxene to 4.97 in the whole rock, respectively (Tab. 3). The $^{147}\text{Sm}/^{144}\text{Nd}$ and $^{143}\text{Nd}/^{144}\text{Nd}$ ratios vary from 0.2181 to 0.8610, and 0.511657 to 0.512942, respectively (Tab. 3). Again a broad negative regression between the different minerals and the whole rock is observed (Fig. 3d). A regression of the HP mineral phases Grt160 and pyroxene giving a reasonable age in the Lu-Hf space, results in an unrealistically high age of 176 ± 19 Ma in the case of Sm-Nd. Thus, no reasonable age information can be obtained from the Sm-Nd data.

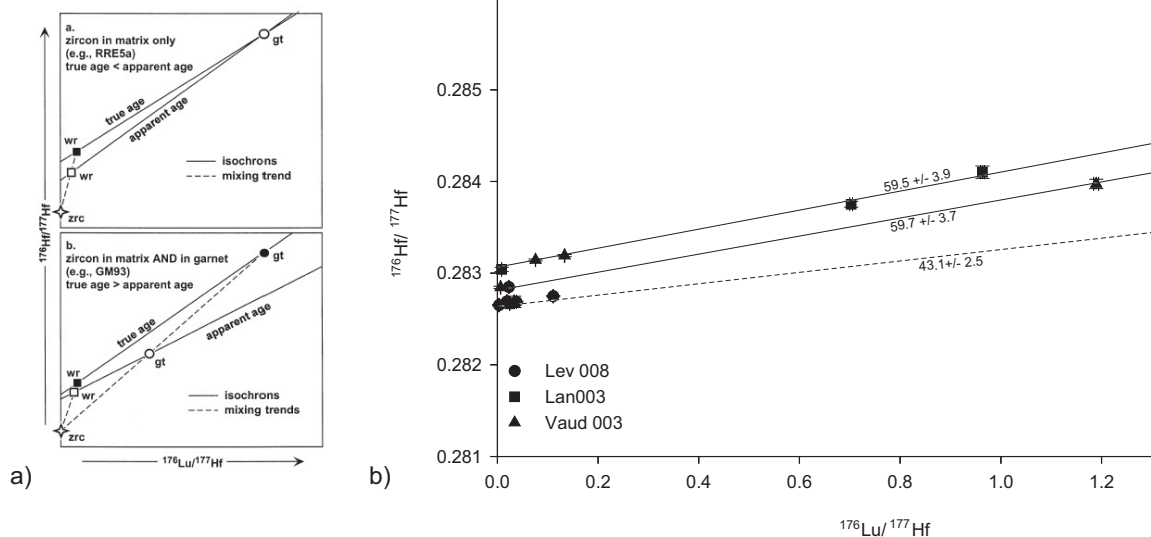


Fig. 4: a) Sketch from Scherer et al. (2002) showing the influence of inherited zircon present in the WR and/or garnet. b) Compilation of Lu-Hf isochrons for the analysed samples. All data calculated with $\lambda^{176}\text{Lu}$ of $1.865 \times 10^{-4} \text{ a}^{-1}$ (Scherer et al. 2001). Ages are calculated with Isoplot Version 2.49 (Ludwig 2001).

Metasediment sample Lev 008

This second sample with a pelitic whole rock composition was strongly overprinted during D2 retrogression. Two fractions of garnet (Grt160, Grt250) and epidote (Ep160, Ep250), white mica (Hgl160) and WR taken from this sample were analysed. The $^{176}\text{Lu}/^{177}\text{Hf}$ and $^{176}\text{Hf}/^{177}\text{Hf}$ ratios for measured minerals range from 0.003 (Hgl160) to 0.151 (Grt250), and from 0.282750 (Hgl160) to 0.282773 (Grt250), respectively. Some petrological constraints are provided by inspection of thin section in that garnet and mica can generally be attributed to the first phase of deformation (D1), but these minerals also remain stable during decompression. Individual second generation (D2) garnets (garnet2) and micas (mica2) are evidenced in thin section. This is in contrast to the mafic rocks where garnet does not remain stable during decompression and where micas are not stable in the eclogite facies. This sample shows an interesting scatter in Lu-Hf space. In contrast to both other investigated samples the WR provides negative slopes with any of the measured minerals (Fig. 3e) indicating additional highly radiogenic phases strongly supporting mineral disequilibria in this sample. Thus any further discussion about the significance of garnet-WR age for this sample is pointless, and this supports the exclusion of WR due to isotopic disequilibrium. All other investigated minerals define a clear trend (Fig. 3e). The age including all data points, except for WR, is of 41 ± 13 Ma. The age defined by the larger garnet and epidote fractions (Grt250 and Ep250), interpreted as the purer fractions, and mica is 48 ± 4.7 Ma (Fig. 3e). This age is significantly younger than the previously estimated age for eclogitization of ~ 60 Ma.

Considering the substantial retrogression, and the evidences for a second population of mainly phengite and possibly minor amounts of garnet, the age of 43 ± 2.9 Ma is in agreement with estimates for the eclogitization age provided by the previously discussed samples. The “contamination” by the second and younger populations must result in a slightly younger age, exactly as is observed. Furthermore, Ep250 clearly attributed to the syn-D2 retrogression is part of the Grt250-Hgl160 isochron and this also points to a “mixed age”-isochron (Fig. 3e). Despite possible impurities, Grt160 also defines an isochron when combined with Hgl160, Ep250. The resulting age of 43.1 ± 2.9 Ma is compatible with a mixed age and even allows to speculate that increasing amounts of garnet 2, rather than impurities, represent the isotopic composition of Grt160.

The Sm-Nd systematics of the investigated mineral separates and WR are based on the analyses of two garnet fractions, two epidote fractions and phengite. Grt250 shows the highest radiogenic $^{143}\text{Nd}/^{144}\text{Nd}$ ratio (0.513022) and Grt160 displays the lowest $^{143}\text{Nd}/^{144}\text{Nd}$ ratio (0.512071) (Tab. 3). All other investigated minerals and the WR have intermediate $^{143}\text{Nd}/^{144}\text{Nd}$ compositions (0.5122176–0.512137). The intermediate $^{147}\text{Sm}/^{144}\text{Nd}$ and $^{143}\text{Nd}/^{144}\text{Nd}$ ratios of WR in respect to epidote, phengite and both garnet fractions (Fig. 5c) result in a negative slope in the isochron plot. Again no age can be calculated.

Discussion and Interpretation

Two samples Vaud003 and Lan003 yield Lu-Hf ages that are consistent within uncertainty. These are 59.7 ± 3.7 Ma, 59.5 ± 3.9 Ma for the HP assemblages Grt160–Px and Grt250–Gln, respectively (Table 1, Fig. 4b). The observation of identical ages in metabasic eclogitic boudins (Vaud003) and metasediments (Lan 003) of the matrix clearly shows that eclogitisation of boudin and matrix took place at ~ 60 Ma in the Piemonte-Liguria oceanic unit. The fact that the same ages were recorded in the eclogitic boudins, which mainly escape deformation during the second phase of deformation (D2), and in the metasediments, strongly overprinted by D2 leads to the conclusion that the HP-minerals did not exchange Lu or Hf during subsequent retrogression. Moreover, apart from their different tectonic overprint, the different bulk rock compositions also petrologically/chemically behaved distinctly throughout the metamorphic cycle. Therefore, the identical ages recorded in samples Vaud003 and Lan003 allows concluding that the obtained ages for eclogitisation of ~ 60 Ma are robust. Furthermore, they are also compatible with the results of ^{39}Ar - ^{40}Ar study, presented by Bucher et al. (see chapter 4 of

this thesis) and geochronological data from the literature (i.e. Agard et al. 2002 and references therein)

Moreover, all measured minerals from sample Lev008, except WR, show a regression defining a Grt250-Ep250-Hgl160 isochron of 43 ± 2.9 Ma (Fig. 3e). Although significantly younger, this age agrees well with the obtained results from samples Vaud003 and Lan003, because a mixed age is expected due to the observed contamination of white mica and possibly garnet of younger D2 populations. The interpretation that the age of 43 ± 2.9 Ma obtained for sample Lev008 represents a mixed age is confirmed, because it lies as well below the HP garnet ages of sample Vaud003 and Lan003 and the 47 ± 1 Ma ^{39}Ar - ^{40}Ar age obtained on the late D1 white mica from the same sample Vaud003 (Bucher et al., see chapter 4). Therefore peak eclogite facies conditions must have been reached before, i.e. at around 60 Ma as indicated by the data from samples Vaud003 and Lan003.

While the ages obtained are consistent it should be pointed out that for all samples the WR never is in isotopic equilibrium with the HP minerals, neither for Lu-Hf nor for the Sm-Nd isotope system. Similar conclusions were drawn by Thöni & Jagoutz (1992) and Luais et al. (2001) regarding the Sm-Nd isotope system. Scherer et al. (2000) demonstrated the influence of inherited zircon present in the whole rock and /or garnet on the Lu-Hf isotope system and concluded that apparent WR - garnet isochrons are meaningless when inclusions are present (Fig. 4a). Only in sample Lan003 can the isotopic disequilibrium be explained by inherited zircon inclusions. In the case of the two other samples, the WR plots above the HP regression in the isochron plot, excluding inherited zircon inclusions as the origin for the isotopic disequilibrium. For sample Lev008, the WR even plots far above the regression defined by the HP minerals. This requires for additional phases for balancing this strong disequilibrium. Retrogression as another possibility for producing isotopic disequilibrium is indicated by petrological observations. Commonly HP-rocks are strongly dehydrated and it is generally accepted that retrogression in these rocks only becomes substantial by infiltration of fluids. The supply of fluids, however, allows for neof ormation of minerals. But these newly grown minerals have a different initial $^{176}\text{Hf}/^{177}\text{Hf}$ ratio than HP minerals, which cause a shift of the WR, away from the HP isochron. Newly formed minerals, however, also have high $^{176}\text{Lu}/^{177}\text{Hf}$, leading to a shift of the WR primarily to higher Lu/Hf ratios. Additionally, it is commonly believed that Hf is immobile in fluids, whereas Lu is seems very mobile. Unfortunately the combination of these arguments cannot explain the high $^{176}\text{Hf}/^{177}\text{Hf}$ ratios obtained for samples Vaud003 and Lev008. Nevertheless, advection of a fluid containing radiogenic Hf is the only way to explain such high $^{176}\text{Hf}/^{177}\text{Hf}$ ratios for WR as obtained for the samples from this study. In this case a shift of the WR towards higher $^{176}\text{Hf}/^{177}\text{Hf}$ results and is due to neof ormation of minerals during retrogression. Micas indicate retrogression in

Table 1: Compilatin of Lu-Hf and Sm-Nd analysis and the resulting age for the analysed samples.

Sample	Rock type	Lu-Hf ages		Sm-Nd age
		grt-HP*	grt-WR	grt-WR
Lan 003	metapelite	59.5 ± 3.9 55 ± 3	83.0 ± 3.8 85.5 ± 2.6	neg. slope (impossible)
Vaud 003	matabasite	59.7 ± 3.7	39.9 ± 1.2	22 ± 83
Lev 008	metapelite	43.1 ± 2.9	neg. slope	neg. slope (impossible)

the presence of fluids for the metabasic sample Vaud003. Because these minerals clearly postdate eclogite conditions they should cause a shift of WR towards higher $^{176}\text{Hf}/^{177}\text{Hf}$, exactly as is observed in the isochron plot of sample Vaud003. The value of this interpretation can be tested on the strongly retrogressed sample Lev008. The larger amounts of newly formed minerals (phengite₂, epidote₂) present in this sample, when compared to sample Vaud003, must result in a larger offset of WR. Indeed, the offset of WR in sample Lev008 is much larger than that of sample Vaud003 allowing for the conclusion that retrogression has a significant influence on the isotopic composition of WR.

Comparison of Lu-Hf age estimates from the Piemonte-Liguria oceanic unit shows that the ages obtained in this study are fairly compatible with other Lu-Hf data: Duchêne et al. (1997) found 51.2 ± 1.2 Ma (recalculated for the decay constant of Scherer) further to the south in the Monviso area. A recent study of Lapen et al. (2003) of the Lago di Cignana locality north of the study yielded an age of 48.8 ± 2.1 Ma, based on a regression between WR-garnet-clinopyroxene-blue amphibole. However, all these ages are slightly younger than those presented in this study. Interestingly the age of the most retrogressed sample Lev008 is next to the above mentioned ages taken from the literature. As shown above the influence of retrogression is obvious in this sample and it is this retrogression and mixture with D2 phases that leads to the younger age compared to the other samples of this study.

Different authors claim that the Lu-Hf isotope data probably reflect garnet growth. We would argue that this perfectly explains the age difference between non- or slightly retrogressed samples (Vaud003, Lan003) with ages between 55-60 Ma and the 43 Ma of the strongly retrogressed sample (Lev008). Lapen et al. (2003) also interpret their Lu-Hf age of 48.8 ± 2.1 Ma as the age of prograde garnet growth. Amato et al. (1999) obtained a Sm-Nd age of 40.6 ± 2.6 Ma (Amato et al. 1999). The difference between Lu-Hf and Sm-Nd of ~ 8 Ma, both interpreted to date peak pressures, is significant. Therefore Lapen et al. (2003) concluded that the Lu-Hf isotope system only dates initial prograde garnet growth, and that only Sm-Nd dates peak pressure conditions. Consequently the above mentioned authors interpreted ~ 40 Ma as the time for peak pressure conditions in the PL-oceanic unit. However, interpretation of Lapen et al. (2002) strongly contrasts the results of this study, and those of the ^{39}Ar - ^{40}Ar study presented by Bucher et al. (see chapter 4). Sample Vaud003 shows a Lu-Hf age of HP conditions of 59.7 ± 3.7 Ma and a ^{39}Ar - ^{40}Ar plateau age of 47 ± 1 Ma for white mica. White mica grows during retrogression and is not part of the peak pressure mineral assemblage. Consequently peak-pressure conditions must predate 47 ± 1 Ma, as given by white mica. It should be noted that additional ^{39}Ar - ^{40}Ar age data from Dal Piaz et al. (42-46 Ma; 2001) and Rb-Sr data from Reddy et al. (36-47 Ma, 1999) on white mica from areas close to the Lago di Cignana, not included in the discussion of Lapen et al. (2003), also suggest that peak pressure conditions predated 47 Ma in the Piemonte-Liguria oceanic unit. Similarly the 50.4 ± 4 Ma garnet Sm-Nd age of Mayer et al. (1999), which derives from an intermediate position between the Lago di Cignana and this study, demands peak pressure condition to at least 50 Ma or even older. Further to the south, in the Monviso area, Agard et al. (2002) obtained ^{39}Ar - ^{40}Ar laser ablation ages of around 55 Ma for HP phengite. Because these numerous geochronological data, derived for the same paleogeographic unit across the entire Western Alps, can easily be harmonized with the internally consistent results of study, it is concluded that peak pressures in the Piemonte-Liguria oceanic unit were reached at ~ 60 Ma.

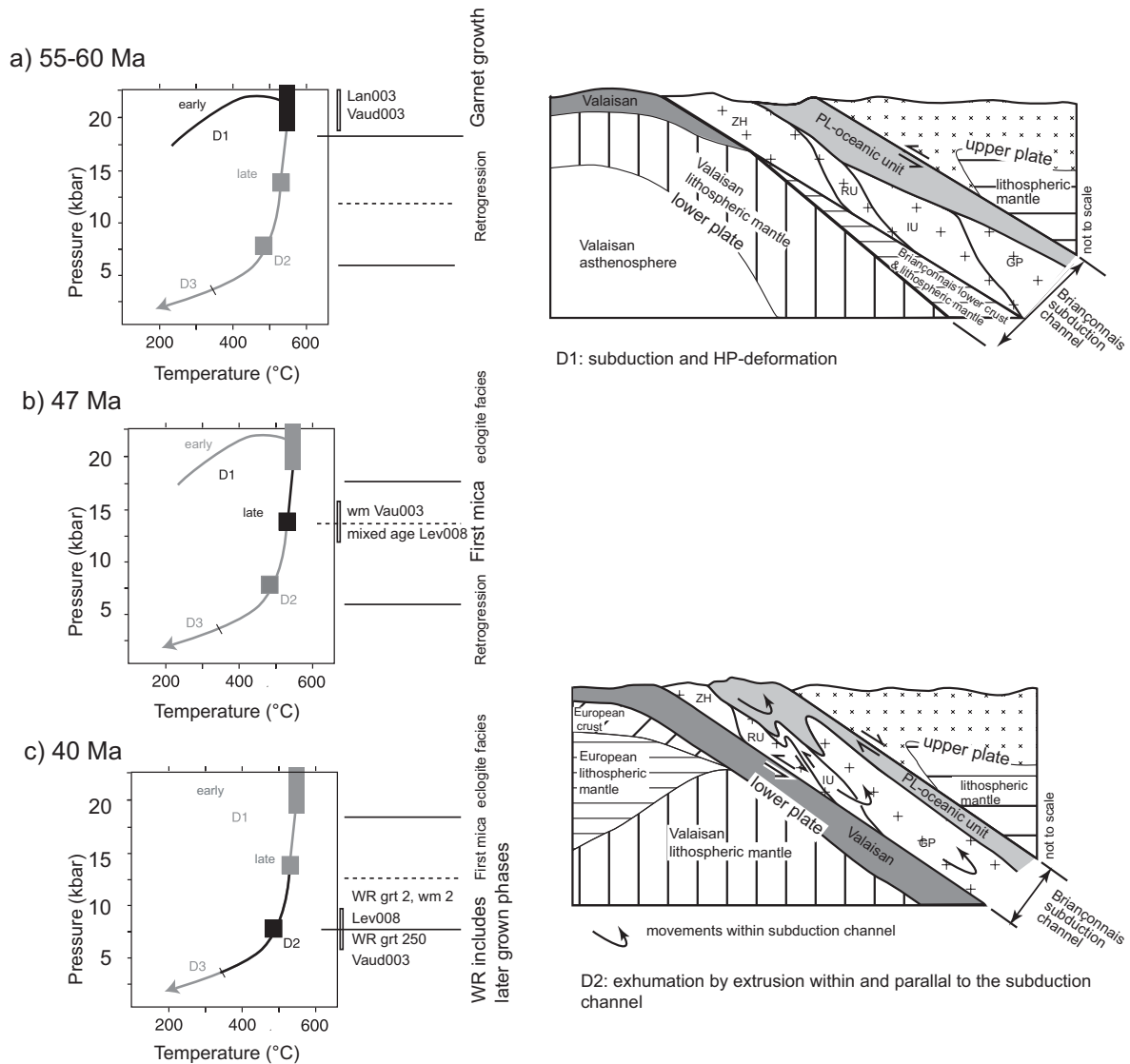


Fig 5: Integartion of the Lu-Hf geochronological data into the tectonic model from Bucher et al. (2003): **a)** early D1 stage represented by isochrons of sample Vaud003 and Lan003; **b)** initial stages of retrogression during late D1 around 47 Ma (^{39}Ar - ^{40}Ar data of sample Vaud003); **c)** D2 retrogression around 40 Ma responsible for partial equilibration of WR and Grt250 in samples Vaud003 and WR of Lev008 contemporaneously with growth of white mica (2) and garnet (2).

Summary and Conclusions

The results of this study are best summarized by the integrating into the geodynamic model proposed by Bucher et al. (2003). The Lu-Hf ages of 59.7 ± 3.7 Ma and 59.5 ± 3.9 Ma for samples Vaud003 and Lan003, respectively, represent HP conditions reached during the early stages of D1 and during subduction (Fig 5a). During a late stage of D1 retrogression starts and is reported in sample Vaud003 by the occurrence of white mica displaying a ^{39}Ar - ^{40}Ar plateau age of 47 ± 1 Ma (Fig 5b).

The main stage of retrogression is associated with exhumation by extrusion within and parallel to the subduction channel during D2 (Fig 5b). Contemporaneously neocrystallization of white mica (2) and possibly garnet (2) is initiated in the metapelitic sample Lev008. A garnet (possibly two phases)-white mica (two phases)-epidote (two phases) mixed age of 43 ± 2.9 Ma is observed (Fig

5c). Comparison between the ^{39}Ar - ^{40}Ar white mica plateau age of 47 ± 1 Ma from sample Vaud003 and the Lu-Hf eclogitisation ages (59.7 ± 3.7 Ma) from the same sample confirms the idea that the significantly younger Lu-Hf garnet age of 43 ± 2.9 Ma from sample Lev008 represents a mixed age due to the substantial retrogression and/or the presences of garnet and mica grown during D2.

Because minerals formed during retrogression are not in equilibrium with the HP minerals but included in the WR measurement, a large offset from the regression in the isochron plot is observed in sample Lev008 for WR. Sample Vaud003 and Lan003 largely escaped for most parts retrogression and HP minerals kept their original isotopic signature. In sample Vaud003 weak overprinting during retrogression leads to a partial equilibration of the WR, and some garnets (Grt250), as expressed by a second, somewhat speculative regression pointing to an age of 40 Ma. White mica ^{39}Ar - ^{40}Ar analyses of D2 mylonites also show an age of 40 Ma (Bucher et al., see chapter 4), supporting this speculation (Fig. 5c). In summary, Lu-Hf age information agrees well with other chronometers and with petrological observations. This is in strong contrast to information gained from of the Sm-Nd isotope system, from which no reasonable age information is obtained.

Acknowledgements

Substantial funding by the Swiss National Science Foundation (project 20-63391.00) and precursor projects since 1995 is gratefully acknowledged. Jan Kramers, Stefan Schmid, Igor Villa, Lukas Keller and Christian de Capitani are thanked for fruitful discussions and constructive criticism an earlier version of the manuscript.

Table 2: Lu-Hf isotope data for the investigated samples.

WR=whole rock; Grt=garnet; Px = pyroxene; Gln = glaucophane, Hbl = green hornblende; Ep = epidote; Hgl = white mica; the numbers following the abbreviations indicate the size fractions. 160 = fraction 160-250 μm ; 250 = fraction 250-500 μm .

Sample	mineral	deformation	Lu [ppm]	Hf [ppm]	$^{176}\text{Lu}/^{177}\text{Hf}$	$^{176}\text{Hf}/^{177}\text{Hf}$	2se abs.
Lan003		metapelite					
Gln160	glaucophane	D1	0.078	1.31	0.008	0.283040	± 0.000024
Grt160	garnet	D1	1.97	0.396	0.703	0.283751	± 0.000032
Grt250	garnet	D1	1.77	0.260	0.963	0.284101	± 0.000067
WR	whole rock		0.292	1.68	0.025	0.282664	± 0.000010
Vaud003		eclogite					
Grt150	garnet	D1	2.05	0.244	1.190	0.283973	± 0.000051
Grt250	garnet	D1 ?	1.12	1.18	0.134	0.283191	± 0.000013
Px250	omphacite	D1	0.086	0.362	0.034	0.282687	± 0.000062
WR	whole rock		0.585	1.09	0.076	0.283144	± 0.000010
Lev008		metapelite					
Grt250	garnet	D1	5.70	5.36	0.151	0.282773	± 0.000005
Grt160	garnet	D1 & D2?	5.47	7.00	0.111	0.282750	± 0.000007
Hgl160	white mica	D1 & D2	0.070	3.23	0.003	0.282653	± 0.000007
Ep250	epidote	D2	1.20	4.50	0.038	0.282686	± 0.000009
Ep160	epidote	D2	0.656	4.98	0.019	0.282693	± 0.000010
WR	whole rock		0.229	1.44	0.023	0.282850	± 0.000005

Table 3: Sm-Nd isotope data for the investigated samples.

WR=whole rock; Grt=garnet; Px = pyroxene; Gln = glaucophane, Hbl = green hornblende; Ep = epidote; Hgl = white mica; the numbers following the abbreviations indicate the size fractions. 160 = 160-250 μm ; 250 = 250-500 μm .

Sample	mineral	deformation	Sm (ppm)	Nd (ppm)	$^{147}\text{Sm}/^{144}\text{Nd}$	±2se abs
Lan 003		metapelite				
Gln160	glaucophane	D1	2.44	9.52	0.1551	± 0.000010
Grt160	garnet	D1	6.77	22.2	0.1845	± 0.000007
Grt250	garnet	D1	5.35	3.45	0.9361	± 0.000010
WR	whole rock		4.28	21.4	0.1208	± 0.000007
Vaud003		eclogite				
Grt150	garnet	D1	1.32	0.928	0.8610	± 0.000034
Grt250	garnet	D1 ?	1.03	0.360	1.7233	± 0.000070
Px250	omphacite	D1	0.262	0.558	0.2840	± 0.000064
WR	whole rock		1.83	4.97	0.2230	± 0.000011
Lev008		metapelite				
Grt250	garnet	D1	1.06	22.9	0.0281	± 0.000007
Grt160	garnet	D1 & D2?	0.697	2.39	0.1767	± 0.000020
Hgl160	white mica	D1 & D2	1.29	6.23	0.1247	± 0.000011
Ep250	epidote	D2	39.4	186	0.1283	± 0.000005
Ep160	epidote	D2	53.5	253	0.1277	± 0.000007
WR	whole rock		3.20	16.2	0.1192	± 0.000009

References

- Agard, P., Jolivet, L. & Goffé, B. 2001: Tectonometamorphic evolution of the Schistes Lustrés complex: implications for the exhumation of the UHP rocks in the western Alps. *Bull. Soc. géol. France*, 172, 617-636.
- Amato, J. M., Johnson, C. M., Baumgartner, L. P. & Bread, L. B. 1999: Rapid exhumation of the Termatt-Saas ophiolite deduced from high-precision Sm-Nd and Rb-Sr geochronology. *Earth and Planetary Science Letters* 171, 425-438.
- Ballèvre, M. & Merle, O. 1993: The Combin Fault: compressional reactivation of a Late Cretaceous-Early Tertiary detachment fault in the Western Alps. *Schweiz. Mineral. Petrogr. Mitt.* 73, 205-227.
- Bizzarro, M., Baker, J.-A., Haak, H., Ulfbeck, D. & Rosing, M. 2003: Early history of Earth's crust-mantle system inferred from hafnium isotopes in chondrites. *Nature* 421 931-932.
- Bucher, S., Schmid, S. M., Bousquet, R. & Fügenschuh, B. 2003: Late-stage deformation in a collisional orogen (Western Alps): nappe refolding, back-thrusting or normal faulting? *Terra Nova* 15, 109-117.
- Bucher, S., Ullardic, C., Bousquet, R., Ceriani, S., Fügenschuh, B., Gouffon, Y. & Schmid, S. M. submitted: Tectonic evolution of the Briançonnais units along a transect (ECORS-CROP) trough the Western Alps, submitted.
- Blichert-Toft, J., Boyet, M., Telouk, P. & Albarede, F. 2002: ^{147}Sm - ^{143}Nd and $^{176}\text{Lu}/^{177}\text{Hf}$ in eucrites and differentiation of HED parent body. *Earth and Planetary Science Letters* 204, 167-181.
- Cigolini, C. 1995: Geology of the Internal Zone of the Grand Saint Bernard Nappe: a metamorphic Late Paleozoic volcano-sedimentary sequence in South-Western Aosta Valley (Western Alps). In: *Studies on metamorphic rocks and minerals of the western Alps. A Volume in Memory of Ugo Pognante.* (edited by B. Lombardo) 13, n°2. *Bollettino del Museo Regionale di Scienze Naturali (suppl.)*, Torino, 293-328.
- Dal Piaz, G. V. 1999: The Austroalpine-Piedmont nappe stack and the puzzle of alpine Tethys. *Mem. Sci. Geol* 51, 155-176.
- Dal Piaz, G. V., Cortiana, G., Del Moro, A., Martin, S., Pennacchioni, G. & Tartarotti, P. 2001: Tertiary age and paleostructural inferences of the eclogitic imprint in the Austroalpine outliners and Zermatt-Saas ophiolite, western Alps. *Int. J. Earth Sci.* 90, 668-684.
- de Sigoyer, J., Chavagnac, V., Villa, I. M., Luais, B., Guillot, S., Cosca, M. A. & Mascle, A. 2000: Dating the Indian continental subduction and collisional thickening in the northwest Himalaya: Multichronology of the Tso Moriri eclogites. *Geology* 28, 487-490.
- De Wolf, C. P., Zeissler, C. J., Halliday, A. N., Mezger, K. & Essene, E. J. 1996: The role of inclusions in U-Pb and Sm-Nd garnet geochronology; stepwise dissolution experiments and trace uranium mapping by fission track analysis. *Geochim. cosmochim. Acta* 60, 121-134.
- Droop, G. T. R., Lombardo, B. & Pognante, U. 1990: Formation and distribution of eclogite facies rocks in the Alps. In: *Eclogite facies rocks* (edited by D. A. Carswell). Blackie, Glasgow and London, 225-259.
- Duchêne, S., Blichert-Toft, J., Luais, B., Télouk, P., Lardeaux, J. M. & Albarède, F. 1997: The Lu-Hf dating of garnets and the ages of Alpine high-pressure metamorphism. *Nature* 387, 586-589.
- Elter, G. 1972: Contribution à la connaissance du Briançonnais interne et de la bordure piémontaise dans les Alpes Graies nord-orientales et considérations sur les rapports entre les zones du Briançonnais et des Schistes Lustrés. *Ment. Ist. Geol. Univ. Padova* 28, 19.
- Froitzheim, N. 2001: Origin of the Monte Rosa Nappe in the Pennine Alps; a new working hypothesis. *Geol. Soc. Am. Bull.* 113, 604-614.
- Gebauer, D. 1999: Alpine geochronology of the Central and Western Alps: new constraints for a complex geodynamic evolution. *Schweiz. Mineral. Petrogr. Mitt.* 79 191-208.
- Jagoutz, E. 1993: Das radiometrische Datieren metamorpher Gesteine: Sein und Schein. Abstract Volume DMG 1993 München.
- Kleinhanns, I. C., Kreissig, K., Kamber, B. S., Meisel, T., Nägler, T. F. & Kramers, J. D. 2002: Combined Chemical Separation of Lu, Hf, Sm, Nd and REEs from a Single Rock Digest: Precise and Accurate Isotope Determinations of Lu-Hf and Sm-Nd Using Multicollector-ICPMS. *Anal. Chem.* 74.

- Lapen, T. H., Johnson, C. M., Baumgartner, L. P., Mahlen, J. N., Bread, L. B. & Amato, J. M. 2003: Burial rates during prograde metamorphism of an ultra-high-pressure terrane: an example from Lago di Cigana, western Alps, Italy. *Earth and Planetary Science Letters* 215, 52-72.
- Luais, B., Duchêne, S. & de Sigoyer, J. 2001: Sm-Nd disequilibrium in high-pressure, low-temperature Himalayan and Alpine rocks. *Tectonophysics* 342, 1-22.
- Ludwig, K. R. 2001: User's manual for Isoplot/Ex ver. 2.49, a geochronological toolkit for Microsoft Excel. Berkley Geochronological Center Spec. Publ. 1a 55 pp.
- Mayer, A., Abouchamin, W. & Dal Piaz, G. V. 1999: Eocene Sm-Nd age for the eclogitic metamorphism of the Zermatt-Saas ophiolite in Ayas Valley, Western Alps. *Eur. Union Geosci.* 10 10.
- Nägler, T. F., Holzer, L. & Frei, R. 1995: Nd and Pb in Monazite Inclusions within Polymetamorphic Garnets: Hell or Heaven? AGU fall meeting, supplements to EOS November 7.
- Reddy, S. M., Wheeler, J. & Cliff, R. A. 1999: The geometry and timing of orogenic extension: an example from the Western Italian Alps. *J. Metamorph. Geol.* 17, 573-589.
- Scherer, E. E., Cameron, K. L. & Bilchert-Toft, J. 2000: Lu-Hf garnet geochronology: Closure temperature relative to the Sm-Nd system and the effects of trace element inclusions. *Geochim. cosmochim. Acta* 64, 3413-3432.
- Scherer, E. E., Münker, C. & Mezger, K. 2001: Calibration of the lutetium-hafnium clock. *Science* 293, 683-686.
- Thöni, M. & Lagoutz, E. 1992: Some new aspects of dating eclogites in orogenic belts; Sm/Md, Rb/Sr and Pb-Pb isotopic results from the Austroalpine Saualpe and Koralpe type-locality (Canrinthia/Syria, southeastern Austria). *Geochim. cosmochim. Acta* 56, 347-368.

Synthesis

Here the various conclusions and discussions extracted from the individual chapters are synthesised. Thereby the structural, petrological and geochronological data obtained will be presented chronologically and integrated into the tectonic evolution, as derived from the structural analysis. Three ductile deformation phases (D1-D3) are indicated in the study area incorporating the NW-SE along the ECORS-CROP seismic transect from the Pt. St. Bernard pass to the Gran Paradiso massif.

HP-metamorphism (D1)

D1 structures were largely overprinted by subsequent deformation. On a macroscopical scale the first foliation is only preserved in F2 fold hinges. On thin section scale S1 is defined by chloritoid, refolded by D2, and as an internal foliation within garnet. In metapelites the mineral assemblage garnet-phengite-paragonite-chloritoid characterizes stable during D1. Mineral assemblages, however, also depend on bulk rock composition. Therefore the peak-pressure assemblage in samples with an intermediate composition between metapelite and metasandstone consisted of glaucophane-garnet-phengite-paragonite. No index mineral zonation is observed in the study area. Thus differences in pressure and temperature can only be estimated based on geobarometry or on equilibrium phase diagrams. Peak pressure conditions were estimated using the software packages DOMINO and TWQ. In the most external unit, the Zone Houillère unit, the mineral assemblage consisting of Mn-rich garnet-phengite-chlorite-chloritoid is interpreted to represent peak pressure conditions of ~5 kbar at temperatures of ~380° C. In the hitherto not petrologically investigated Permo-Triassic metapelitic cover rocks of the Ruitor unit, the intermediate tectono-metamorphic unit of the study area, the mineral assemblage garnet-chlorite-phengite-paragonite-chloritoid is the assemblage stable at peak pressure conditions and during the first deformation phase D1. P-T estimations yield 11-13.5 kbar at temperatures of 440-480 °C, in contrast to epidote-blueschist facies conditions interpreted so far (5-7 kbar/350-400° C, Baudin 1987). The so called Internal unit is the third unit investigated. In the Permo-Triassic metasediments the mineral assemblages glaucophane-garnet-phengite-paragonite and garnet-phengite-paragonite, respectively, represent peak metamorphic conditions. For the Internal unit phase equilibrium diagrams predict pressures of 14.5-16 kbar at temperatures around 525°C. Based on the P-T estimations, increasing peak pressures are observed from paleogeographic external to internal. They are interpreted to be related to deeper subduction of more internal units.

The timing of the first deformation phase (D1), correlated with peak pressure conditions, was addressed by a multichronological approach. ³⁹Ar-⁴⁰Ar incremental heating on phengite believed to have formed during D1 and Lu-Hf isotope analyses of garnet were combined in order to estimate the age of peak pressure within a self-controlling setting. Additional control on the isotope analyses was derived, however, from petrological and structural investigations of dated samples.

The eclogitic boudin analysed by ³⁹Ar-⁴⁰Ar and Lu-Hf shows an internal foliation discordant to the main foliation. The latter is ascribed to the second phase of deformation (D2). Consequently the internal foliation must be older and is therefore attributed to D1. These observations unambiguously allow correlate garnets and phengites occurring in the eclogitic boudin with the first phase of deformation. In metabasic rocks, however, micas are not stable in eclogite facies but occur as the first neofomed minerals during retrogression in the presence of fluids. Therefore garnets must be older

than micas. The geochronological results perfectly reflected these observations. While Lu-Hf analysis show a garnet-pyroxene age of 59.7 ± 3.7 Ma, phengites analysed by ^{39}Ar - ^{40}Ar incremental heating show a plateau age of 47 ± 1 Ma. Furthermore the peak pressure age is constrained by additional samples derived from the metasedimentary matrix of the eclogitic boudins. In a first sample, which escaped retrogression, an age of 59.9 ± 3.9 Ma was obtained, whereas a second strongly retrogressed sample is contaminated by neoformed phengite and garnet suggesting a mixed age of 48 ± 3.9 Ma.

Combining these results allows to conclude that during early stage of D1 at ~ 60 Ma during subduction, peak pressure conditions are reached. This was followed by the initial stage of retrogression during a late stage of D1, i.e. around 47 ± 1 Ma.

Exhumation and nappe stacking (D2)

D2 represents the dominant deformation event, characterized by final nappe stacking and isoclinal folding on all scales. Owing to intense transposition, the main foliation is a composite of S1 and S2. F2 folds show a wide spread in plunge and azimuth from ESE to WNW between the Houiller Front and the Valgrisenche, and they plunge to the WNW over the rest of the study area. The intensity of the deformation during D2 increases from east to west, as is indicated by the progressive tightening of F2 fold. L2 stretching lineations are oriented parallel to the F2 fold axes. Transport directions, including those observed at the ETC (Enigmatic tectonic contact; i.L. Entrelorre shearzone), are consistently top-to-the WNW, as indicated by shearbands and asymmetric porphyroclasts. Detailed structural analyses indicate that D2 deformation migrated from east to west. While the internal tectonic contacts between the PL-oceanic unit, the Internal unit and the Ruitor unit are refolded during ongoing top-to-the-W shearing, the tectonic contact between the Ruitor unit and the Zone Houillère unit cuts across D2 structures and is therefore not active before a late stage of D2. These structural interpretations are confirmed by ^{39}Ar - ^{40}Ar incremental heating data and P-T estimates. In all dated samples, except highly deformed samples, staircase or upward-convex shaped age spectra point to mixed ages. Samples taken from the Monte Rosa unit for comparison, metamorphosed at temperatures $>550^\circ\text{C}$, clearly indicate mixed ages due to inherited (pre-Alpine) white mica. This white mica (partly) kept its original isotopic composition over the entire HP metamorphic cycle. These examples, together with petrological and microstructural arguments, suggest that formation/deformation ages can be extracted from the ^{39}Ar - ^{40}Ar ages. Furthermore, the results from combined petrological and microchemical investigations clearly document multiple populations in all samples from various units. ^{39}Ar - ^{40}Ar total fusion ages at the Houiller Front are around 300 Ma and dominated by large amounts of detrital white mica. Towards the SE (internal) ages continuously decrease to 40 Ma such as found at the tectonic contact between the Internal unit and the PL-oceanic unit. Increasing amounts of metamorphic white mica, due to increasing intensity of deformation cause decreasing ^{39}Ar - ^{40}Ar total fusion ages. Cl/K – age correlation diagrams verify this hypothesis and allow for assigning an age between 43-35 Ma to D2 deformation. This large spread is due to the fact that D2 deformation becomes increasingly younger towards the west. The D2 mylonites from the tectonic contact between the Internal unit and the PL-oceanic unit give, for example, a plateau age of 40 ± 1 Ma, interpreted to date the activity along this contact. In contrast, at the tectonic contact between the Ruitor unit and the Zone Houillère unit an age of ~ 35 Ma is evidenced, confirming the structural interpretation that this tectonic contact is active during the latest stage of D2 deformation. The P-T estimates are in line with this interpretation. For the Zone Houillère unit maximum pressures of 5 kbar are estimated, suggesting that this unit has never been deeply subducted. Between the Ruitor unit and the Zone Houillère unit a metamorphic discontinuity of about 7 kbar is documented. Exhumation by erosion takes place contemporaneously with nappe stacking, hence the Zone Houillère unit is not incorporated until a late stage during D2. Exhumation taking place during D2 is evidenced by petrological observations, in combination with P-T estimates.

In the Ruitor unit the mineral assemblage Chl-cZo-Fsp-Phe, characterizing the D2 main foliation, clearly postdates the HP assemblage. P-T estimates predict a stability of this assemblage at pressures < 8 kbar, identical with the results from the Internal unit and the PL-oceanic unit. Therefore D2 is associated with decompression from peak pressures (D1) down to about 5 kbar. Hence most of the exhumation takes place during D2 and this mainly by erosion.

Large-scale nappe refolding (D3)

D3 is characterized by open mesoscale parasitic folds that refold the composite S1/S2 main foliation and, which cause the previously mentioned wide range in orientations of the L2 stretching lineations (and F2 fold axes). D3 fold axes are moderately NE and SW plunging and show a gently, generally SE-dipping axial planes. An axial plane cleavage is only locally observed. Based on mapping of the vergency of mesoscopic D3 folds, the axial plane traces of two D3 mega-folds were traced. In the external part of the study area there is a gradual change of the S1/S2 main foliation (apparent fan-structure; éventail Briançonnais), characterized by a SE-dip at the Houiller Front, through a subvertical orientation within the Zone Houillère unit into a predominant NW-dip observed in the rest of the study area. This change in orientation is caused by D3 folding rather than by back-thrusting. A first and W-closing mega-fold (Ruitor mega-fold) affects all previous structures, including former nappe contacts. Towards structurally higher levels (i.e. towards the SE) F3 folds become tighter indicating an increase of the strain during D3. A second and tectonically higher D3 mega-fold (Valsavaranche mega-fold) closes towards the east. This D3 megafold crops out in the uppermost Valgrisenche and Val di Rêhmes and it refolds the entire nappe stack back into an upright position. In the area of the Grande Sassièrè, for example, a Piemont–Liguria klippe lies above the Internal unit and the axial plane of the Valsavaranche mega-fold. This hitherto undetected D3 megafold can be correlated with the well-known Valsavaranche-backfold found and described by Argand (1911). The direct link between D3 mega-folding and overturning of the entire nappe stack, including the tectonic contacts calls for a new look at the geodynamic evolution of the Western Alps, briefly summarized below.

Implications on the scale of the Western Alps

Three mechanisms have been proposed for the previously mentioned apparent fan structure: (i) “back-thrusting” or hinterland-verging thrusting (Butler and Freeman, 1996); (ii) normal faulting, collapse or hinterland directed “extrusion” (Caby 1996) and (iii) large scale refolding of previously stacked nappes referred to as “nappe refolding” (Argand 1916, Milnes 1981). Based on combined investigations of nappe stack polarity, kinematics of shearing, metamorphic field gradients and dating, this study reveals nappe refolding (D3) rather than normal faulting or back-thrusting to be responsible for the present day geometry of the nappe stack in the internal part of the ECORS-CROP seismic profile. Retrodeformation of the late stage nappe refolding (D3) allows for unravelling the main stages of the metamorphic evolution on the scale of the entire ECORS-CROP transect. Integration of data from the Gressoney shear zone (Reddy et al. 1999) and the Combin fault (Ballèvre and Merle 1993), which both delimit the top of HP Penninic units and display a hinterland-directed (top-to-the SE) shearing, allows to constrain the dominant process for exhumation. The described top-to-the SE shearing at the top of the HP Penninic units active contemporaneously with top-to-the NW thrusting at the base of HP Penninic units, as described in the study area, evidence exhumation by extrusion within and parallel to the subduction channel.

References

- Adatte, S., Dubas, M., Tache, L. & Strauss, M. 1992: Géologie et minéralogie du haut Val di Rhêmes (Vallée d'Aoste). Unpublished diploma thesis, Université Lausanne, 132 pp.
- Agard, P., Jolivet, L. & Goffé, B. 2001: Tectonometamorphic evolution of the Schistes Lustrés complex: implications for the exhumation of the UHP rocks in the western Alps. *Bull. Soc. géol. France*, 172, 617-636.
- Agard, P., Monié, P., Jolivet, L. & Goffé, B. 2002: Exhumation of the Schistes Lustrés complex: in situ laser probe $^{40}\text{Ar}/^{39}\text{Ar}$ constraints and implications for the Western Alps. *J. Metamorph. Geol.*, 20, 599-618.
- Alsop, G. I., Bryson, R. & Hutton, D. H. W. 2001: Tectonic and kinematic evolution within mid-crustal orogenic root zones: a case study from the caledonides of northwestern Ireland. *Geol. Mag.*, 138, 193-211.
- Amato, J. M., Johnson, C. M., Baumgartner, L. P. & Bread, L. B. 1999: Rapid exhumation of the Zermatt-Saas ophiolite deduced from high-precision Sm-Nd and Rb-Sr geochronology. *Earth and Planetary Science Letters*, 171, 425-438.
- Amstuz, A. 1955: Rocher du ravin de Lessert dans la Val D'Aoste. *Arch. Sc. Genève*, 8, 6-9.
- 1962: Notice pour une carte géologique de la Vallée de Cogne et de quelques autres espaces au Sud d'Aoste. *Arch. Sc. Genève*, 15, 1-104.
- Aprahamian, J. 1988: Cartographie du métamorphisme faible à très faible dans les Alpes françaises externe par l'utilisation de la cristallinité de l'illite. *Geodyn. Acta*, 2, 25-32.
- Argand, E. 1911: Sur les plissements en retour et la structure en éventail dans les Alpes occidentales. *Bull. Soc. Vaud. Sc. Nat.*, XLVII.
- 1912: Les rythmes du proplissement penninique et le retour cyclique des encapuchements. *Bull. Soc. Vaud. Sc. Nat.*, XLVIII.
- 1916: Sur l'arc des Alpes Occidentales. *Eclog. geol. Helv.*, XIV, 1-19.
- Arnaud, N. O. & Kelly, S. P. 1995: Evidence for excess argon during high pressure metamorphism in the Dora Maira (western Alps, Italy), using an ultraviolet laser ablation microprobe ^{40}Ar - ^{39}Ar technique. *Contrib. Mineral. Petrol.*, 121, 1-11.
- Ballèvre, M., Langabrielle, Y. & Merle, O. 1990: Tertiary ductile normal faulting as a consequence of lithospheric stacking in the Western Alps. *Mém.Soc. géol. Suisse*, 1, 227-236.
- Ballèvre, M. & Merle, O. 1993: The Combin Fault: compressional reactivation of a Late Cretaceous-Early Tertiary detachment fault in the Western Alps. *Schweiz. Mineral. Petrogr. Mitt.*, 73, 205-227.
- Baudin, T. 1987: Étude Géologique du Massif du Ruitor (Alpes franco-italiennes): Evolution structurale d'un socle Briançonnais. Unpublished PhD thesis, University Grenoble, 243 pp.
- Bearth, P. 1957: Die Umbiegung von Vanzone (Valle Anzasca). *Eclog. geol. Helv.*, 50, 161-170.
- Belluso, E., Ruffini, R., Schaller, M. & Villa, I. M. 2000: Electron-microscope and Ar characterization of chemically heterogeneous amphiboles from the Palala Shear Zone, Limpopo Belt, South Africa. *Eur. J. Mineral.*, 12, 45-62.
- Berman, R. G. 1988: Internally-Consistent Thermodynamic Data for Minerals in the system Na_2O - K_2O - Ca - MgO - FeO - Fe_2O_3 - Al_2O_3 - SiO_2 - TiO_2 - H_2O - CO_2 . *J. Petrology*, 29, 445-522.
- 1991: Thermobarometry using multiequilibrium calculations: a new technique, with petrological

- applications. *Can. Mineral.*, 29, 833-855.
- Bertrand, J. M. 1968: Étude structurale du versant occidental du massif du Grand Paradis (Alpes Graies). *Géol. Alpine*, 55-87.
- 1998: Granitoides de la Zone Houillère Briançonnaise en Savoie et en Val d'Aoste (Alpes occidentales): géologie et géochronologie U-Pb sur zircon. *Geodyn. Acta*, 11, 33-49.
- Bertrand, J. M., Aillères, L., Gasquet, D. & J., M. 1996: The Pennine Front zone in Savoie (western Alps), a review and new interpretations from the Zone Houillère Briançonnaise. *Eclog. geol. Helv.*, 89, 297-320.
- Bertrand, J. M., Pidegon, R. T., Leterrier, J., Gouillot, F., Gasquet, D. & Gattiglio, M. 2000: SHRIMP and IDTIMS U-Pb zircon ages of the pre-Alpine basement in the Internal Western Alps (Savoy and Piemonte). *Schweiz. Mineral. Petrogr. Mitt.*, 80, 225-248.
- Biju-Duval, B., Dercuort, J. & Le Pichon, X. 1977: From the Tethys ocean the Mediterranean sea: a plate tectonic model of the evolution of the western Alpine system. In: Biju-Duval and L. Montadret (Editors), *Internal Symposium on the Structural History of the Mediterranean Basin*, 143-164.
- Bizzarro, M., Baker, J.-A., Haak, H., Ulfbeck, D. & Rosing, M. 2003: Early history of Earth's crust-mantle system inferred from hafnium isotopes in chondrites. *Nature*, 421, 931-932.
- Blichert-Toft, J., Boyet, M., Telouk, P. & Albarede, F. 2002: ^{147}Sm - ^{143}Nd and ^{176}Lu / ^{177}Hf in eucrites and differentiation of HED parent body. *Earth and Planetary Science Letters*, 204, 167-181.
- Boquet (Desmons), J. 1974: Le socle Briançonnais de Savoie (Savoie): arguments en faveur de son âge anté-alpin et de son polymétamorphose. *C.R. Acad. Sc. Paris*, 278, 2601-2604.
- Boquet, J. 1974a: Études minéralogiques et pétrographiques sur les métamorphismes d'âge alpin dans les Alpes françaises. Unpublished Thèse d'État, Grenoble, 490 pp.
- 1974b: K-Ar and Rb-Sr Dating of Blue Amphiboles, Micas and Associated Minerals from the Western Alps. *Contrib. Mineral. Petrol.*, 47, 7-26.
- Boriani, A. C. & Villa, I. M. 1997: Geochronology of regional metamorphism in the Ivrea-Verbano Zone and Serie dei Laghi, Italian Alps. *Schweiz. Mineral. Petrogr. Mitt.*, 77, 381-401.
- Bousquet, R., Goffé, B., Henry, P., Le Pichon, X. & Chopin, C. 1997: Kinematic, Thermal and Petrological model of the Central Alps: Lepontine Metamorphism in the Upper Crust and Eclogitisation of the Lower Crust. *Tectonophysics*, 273, 105-127.
- Bousquet, R., Goffé, B., Vidal, O., R., O. & Patriat, M. 2002: The tectono-metamorphic history of the Valaisan domain from the Western to the Central Alps: New constraints on the evolution of the Alps. *Geol. Soc. Am. Bull.*, 114, 207-225.
- Brouwer, F. M., Vissers, R. L. M. & Lamb, W. M. 2002: Structure and metamorphism of the Gran Paradiso massif, western Alps, Italy. *Contrib. Mineral. Petrol.*, 143, 450-470.
- Brown, R. L., Journeay, J. M., Lane, L. S., Murphy, D. C. & Rees, C. J. 1986: Obduction, backfolding and piggyback thrusting in the metamorphic hinterland of the southeastern Canadian Cordillera. *J. Struct. Geol.*, 8, 255-268.
- Brown, T. H., Berman, R. G. & Perkins, E. H. 1988: Ge0-CALC: software package for calculation and display of pressure-temperature-composition phase diagrams using an IBM or compatible personal computer. *Comput. Geosc.*, 14, 279-289.
- Bucher, S., Schmid, S. M., Bousquet, R. & Fügenschuh, B. 2003: Late-stage deformation in a collisional orogen (Western Alps): nappe refolding, back-thrusting or normal faulting? *Terra Nova*, 15, 109-117.
- Bucher, S., Ullardic, C., Bousquet, R., Ceriani, S., Fügenschuh, B., Gouffon, Y. & Schmid, S. M. submitted: Tectonic evolution of the Briançonnais units along a transect (ECORS-CROP) through the Western Alps.
- Burov, E., Jolivet, L., Le Pourhiet, L. & Poliakov, A. 2001: A thermomechanical model of exhumation of high pressure (HP) and ultra-high pressure (UHP) metamorphic rocks in Alpine-type collision belts. *Tectonophysics*, 342, 113-136.
- Butler, R. W. H. & Freeman, S. 1996: Can crustal extension be distinguished from thrusting in the internal parts of mountain belts? A case history of the Entrelor shear zone, Western Alps. *J. Struct. Geol.*, 18, 909-923.

- Caby, R. 1963: Etude géologique et métallogénique du bord interne de la Zone Houillère et de la bordure des schistes lustrés entre Modane et la Vallée Etroite (Haut Val Susa). Thèse 3ème cycle, Univ. Paris, 134 pp.
- 1968: Contribution à l'étude structurale des Alpes occidentales: subdivisions stratigraphiques et structure de la Zone du Grand-Saint-Bernard dans la partie sud du Val d'Aoste (Italie). *Geol. Alpine*, 44, 95-111.
 - 1974: Gneiss permocarbonifères d'origine granitique et volcanique dans la Zone Houillère et la Zone du Grand-Saint-Bernard en val d'Aoste (Italie). *Géol. Alpine*, 50, 39-44.
 - 1981: Le Mésozoïque de la Zone du Combin en Val d'Aoste (Alpes graies): Imbrications tectoniques entre séries issues des domaines pennique, austroalpin et océanique. *Géol. Alpine*, 57, 5-13.
 - 1996: Low-angle extrusion of high-pressure rocks and the balance between outward and inward displacements of Middle Penninic units in the Western Alps. *Eclog. geol. Helv.*, 89, 229-267.
- Caby, R. & Kienast, J.-R. 1989: Meso-Alpine high-pressure assemblages and excavation of the Ruitor Briançonnais basement (Savoie, Val d'Aoste, Graie Alps). *Terra Abstr.*, 1.
- Caby, R., Kienast, J.-R. & Saliot, P. 1978: Structure, métamorphisme et modèle d'évolution tectonique des Alpes Occidentales. *Revue de Géographie physique et de Géologie dynamique*, XX, 307-322.
- Cannic, S. 1996: L'évolution magmatique et tectono-métamorphique du Substratum du Domaine Valaisan (Complexe Versoyen, Alpes Occidental): implication dans l'histoire alpine), Unpublished PhD Thésis; Université Joseph Fourier-Grenoble 1 et Université de Lausanne, 215 pp.
- Cartwright, I. & Barnicoat, A. C. 2002: Petrology, geochronology, and tectonics of shear zones in the Zermatt-Saas and Combin zones of the Western Alps. *J. Metamorph. Geol.*, 20, 263-281.
- Ceriani, S., Fügenschuh, B., Potel, S. & Schmid, S. M. 2003: Tectono-metamorphic evolution of the Frontal Penninic units of the Western Alps: correlation between low-grade metamorphism and tectonic phases. *Schweiz. Mineral. Petrogr. Mitt.*, 83, X1-X21.
- Ceriani, S., Fügenschuh, B. & Schimid, S. M. 2001: Multi-stage thrusting at the "Penninic Front" in the Western Alps between Mont Blanc and Pelvoux massif. *Int. J. Earth Sci.*, 90, 685-702.
- Challandes, N., Marquer, M. & Villa, I. M. 2003: Dating the evolution of C-S microstructures: a combined $^{40}\text{Ar}/^{39}\text{Ar}$ and UV laserprobe analysis of the Alpine Roffna shear zone. *Chem. Geol.*, 197, 3-19.
- Chopin, C. 1977: Une paragenèse à margarite en domaine métamorphique de haute pression-basse température (massif du Grand Paradis, Alpes françaises. *C.R. Acad. Sc. Paris*, 285, 1383-1386.
- Chopin, C. & Maluski, H. 1980: ^{40}Ar - ^{39}Ar Dating of High Pressure Metamorphic Micas from the Gran Paradiso Area (Western Alps): Evidence Against the Blocking Temperature. *Contrib. Mineral. Petrol.*, 74, 109-122.
- Chopin, C. & Monié, P. 1984: A unique Magnesiochloritoid-bearing, high-pressure assemblage from the Monte Rosa, Western Alps: petrologic and ^{40}Ar - ^{39}Ar radiometric study. *Contrib. Mineral. Petrol.*, 87, 388-398.
- Chopin, C., Seidel, E., Theye, T., Ferraris, G., Ivaldi, G. & Catti, M. 1992: Magnesiochloritoid and the Fe-Mg series in the chloritoid group. *Eur. J. of Mineral.*, 4, 67-76.
- Choukourne, P., Ballèvre, M., Cobbold, P., Gautier, Y., Merle, O. & Vuichard, J. P. 1986: Deformation and Motion in the Western Alpine Arc. *Tectonics*, 5, 215-226.
- Cigolini, C. 1981: Garnet chemistry and zonation in the Italian sector of the Grand Saint Bernard nappe. *Atti Acc. Sc. Torino*, 115, 331-344.
- 1992a. Carta Geologica del Ricoprimento del Gran San Bernardo tra la Valsavarenche e la Val di Rhêmes (Valle d'Aosta). Regione Autonoma della Valle d'Aosta.
 - 1992b. Note Illustrative alla Carta Geologica del Ricoprimento del Gran San Bernardo tra la Valsavarenche e la Val di Rhêmes (Valle d'Aosta). Regione Autonoma della Valle d'Aosta, 25pp.
 - 1995: Geology of the Internal Zone of the Grand Saint Bernard Nappe: a metamorphic Late Paleozoic volcano-sedimentary sequence in South-Western Aosta Valley (Western Alps). In: *Studies on metamorphic rocks and minerals of the western Alps. A Volume in Memory of Ugo Pognante.* (edited by B. Lombardo) 13, n°2. Bollettino del Museo Regionale di Scienze Naturali (suppl.),

- Torino, 293-328.
- Compagnoni, R., Elter, G. & Lombardo, B. 1974: Eterogeneità stratigrafica del complesso degli "Gneiss Minuti" nel massiccio cristallino del Gran Paradiso. *Memorie della Società Geologica Italiana*, 13, 227-239.
- Coward, M. P. & McClay, K. R. 1983: Thrust tectonics of S Devon. *J. Geol. Soc.*, 140, 215-228.
- Coyle, D. A. & Wagner, G. A. 1998: Positioning the titanite fission-track partial annealing zone. *Chem. Geol.*, 149, 117-125.
- Crank, J. 1975. *Mathematics of diffusion*. Clarendon Press, 2nd ed.
- Dal Piaz, G. B. 1928: Geologia della catena Herbetet-Grivola-Gran Nomenon. *Mem. Ist. Geol. Univ. Padova*, 7, 1-83.
- Dal Piaz, G. V. 1965: Il lambo di ricoprimento della Becca di Toss: struttura retroflessa della zona del Gran San Bernardo. *Mem. Acad. Patavina*, 77, 107-136.
- 1998a: Ar-Ar and Rb-Sr dating of the Pillionet klippe and Sesia-Lanzo basal slice in the Ayas valley and evolution of the Austroalpine-Piedmont nappe stack. *Mem. Sci. Geol.*, 50, 177-194.
 - 1998b: Evoluzione litosferica e magmatismo nel domino Austroalpino dall'orogenesi Varisica al rifting mesozoico. *Mem. Soc. Geol. It.*, 53, 43-62.
 - 1999: The Austroalpine-Piedmont nappe stack and the puzzle of alpine Tethys. *Mem. Sci. Geol.*, 51, 155-176.
- Dal Piaz, G. V., Cortiana, G., Del Moro, A., Martin, S., Pennacchioni, G. & Tartarotti, P. 2001: Tertiary age and paleostructural inferences of the eclogitic imprint in the Austroalpine outliners and Zermatt-Saas ophiolite, western Alps. *Int. J. Earth Sci.*, 90, 668-684.
- Dal Piaz, G. V. & Govi, M. 1965: Osservazioni geologiche sulla "Zona del Garn San Bernardo" nella alta valle d'Aosta. *Bull. Soc. It.*, 84, 105-119.
- Dal Piaz, G. V. & Lombardo, B. 1986a: Early Alpine eclogite metamorphism in the Pennine Monte Rosa - Grand Paradiso basement nappes of the northwestern Alps. *Geol. Soc. Am. Mem.*, 164, 249-265.
- 1986b: Early Alpine eclogite metamorphism in the Pennine Monte Rosa-Gran Paradiso basement nappes of the northwestern Alps. In: *Blueschists and Eclogites* (edited by B. W. Evans and E. H. Brown). *Memoir 164. Geological Society of America, Boulder*, 249-265.
- De Capitani, C. 1994: Gleichgewichts-Phasendiagramme: Theorie und software. *Beihefte zum European Journal of Mineralogy*, 72. Jahrestagung der Deutschen Mineralogischen Gesellschaft, 6, 48.
- De Capitani, C. & Brown, T. H. 1987: The computation of chemical equilibrium in complex systems containing non-ideal solutions. *Geochim. cosmoch. Acta*, 51, 2639-2652.
- De Sigoyer, J., Chavagnac, V., Villa, I. M., Luais, B., Guillot, S., Cosca, M. A. & Mascle, A. 2000: Dating the Indian continental subduction and collisional thickening in the northwest Himalaya: Multichronology of the Tso Moriri eclogites. *Geology*, 28, 487-490.
- De Wolf, C. P., Zeissler, C. J., Halliday, A. N., Mezger, K. & Essene, E. J. 1996: The role of inclusions in U-Pb and Sm-Nd garnet geochronology; stepwise dissolution experiments and trace uranium mapping by fission track analysis. *Geochim. cosmoch. Acta*, 60, 121-134.
- Debelmas, J. 1980. *Carte géologique de France au 1/50000. Feuille Mont-Blanc*. Bureau de recherches géologiques et minières, Orléans,
- Debelmas, J., Caby, R. & Desmons, J. 1991a: Notice explicative, *Carte géologique de France (1/50000), feuille Sainte-Foy-Tarentaise*. *Bur Rech Géol Min, Orléans*, 43 pp.
- Debelmas, J., Elter, G., Antonie, P., Elter, M., Baudin, T., Caby, R., J., F., Mercier, D., Marion, R., M., G. & Jaillard, E. 1991b. *Carte Géologique de la France a 1/50000 Feuille 728 Ste-Foy-Tarentaise*. *Bur Rech Géol Min, Orléans*
- 1991c. Notice explicative de la feuille Moûtiers à 1/50 000, *Bur Rech Géol Min, Orléans*.
- Desmons, J. 1977: Mineralogical and petrological investigations of alpine metamorphism in the internal French Western Alps. *Am. J. Sci.*, 277, 1045-1066.
- 1992: The Briançonnais Basement (Pennine Western Alps): Mineral composition and polymetamorphic evolution. *Schweiz. Mineral. Petrogr. Mitt.*, 72, 37-55.

- Desmons, J. & Mercier, D. 1993: Passing through the Briançonnais. In: Pre-Mesozoic Geology in the Alps (edited by J. F. von Raumer and F. Neubauer). Springer-Verlag, Heidelberg, 279-295.
- Desmons, J., Laudron, D. & De Bethune, P. 1977: Grenats zones de la nappe du Grand-Saint-Bernard et de la nappe Piemontaise (Alpes occidentales). *Mém. Inst. géol. Univ. Louvain*, 29, 327-347.
- Desmons, J., Aprahamian, J., Compagnoni, R., Cortesogno, L. & Frey, M. 1999a: Alpine Metamorphism of the Western Alps: I. Middle to high T/P metamorphism. *Schweiz. Mineral. Petrogr. Mitt.*, 79, 89-110.
- Desmons, J., Compagnoni, R., Cortesogno, L., Frey, M. & Gaggero, L. 1999b: Pre-Alpine metamorphism of the Internal zones of the Western Alps. *Schweiz. Mineral. Petrogr. Mitt.*, 79, 23-39.
- Desmons, J., Compagnoni, R., Cortesogno, L., Frey, M., Gaggero, L., Dallagiovanna, G., Seno, S. & Radelli, L. 1999c: Alpine metamorphism of the Western Alps: II. High-P/T and related pre-greenschist metamorphism. *Schweiz. Mineral. Petrogr. Mitt.*, 79, 111-134.
- Dewey, J. F. 1988: Extensional collapse of orogens. *Tectonics*, 7, 1123-1139.
- Di Vincenzo, G., Ghiribelli, B., Giorgetti, G. & Palmeri, R. 2001: Evidence of a close link between petrology and isotope records; constraints from SEM, EMP, TEM and in situ ^{40}Ar - ^{39}Ar laser analyses on multiple generations of white micas (Lanternman Range, Antarctica). *Earth and Planetary Science Letters*, 192, 389-405.
- Di Vincenzo, G., Viti, C. & Rocci, S. 2003: The effect of chlorite interlayering on ^{40}Ar - ^{39}Ar biotite dating: an ^{40}Ar - ^{39}Ar laser probe and TEM investigations of variably chloritised biotites. *Contrib. Mineral. Petrol.*, 145, 643-658.
- Dodson, M. H. 1973: Closure temperature in cooling geochronological and petrological systems. *Contrib. Mineral. Petrol.*, 259-274.
- Droop, G. T. R., Lombardo, B. & Pognante, U. 1990: Formation and distribution of eclogite facies rocks in the Alps. In: *Eclogite facies rocks* (edited by D. A. Carswell). Blackie, Glasgow and London, 225-259.
- Duchêne, S., Bilchert-Toft, J., Luais, B., Télouk, P., Lardeaux, J. M. & Albarède, F. 1997: The Lu-Hf dating of garnets and the ages of Alpine high-pressure metamorphism. *Nature*, 387, 586-589.
- Dunlap, W. J. 1997: Neocrystallization or cooling? $^{40}\text{Ar}/^{39}\text{Ar}$ ages of white micas from low grade mylonites. *Chem. Geol.*, 143, 181-203.
- Ellenberger, F. 1958: *Étude géologique du pays de Vanoise*. *Mém. Serv. Carte géol. Fr.*, 561 pp.
- Elter, G. 1960: La zona pennidica dell'alta e media Val d'Aosta e le unità limitrofe. *Mem. Ist. Geol. Univ. Padova*, 22, 113.
- 1972: Contribution à la connaissance du Briançonnais interne et de la bordure piémontaise dans les Alpes Graies nord-orientales et considérations sur les rapports entre les zones du Briançonnais et des Schistes Lustrés. *Mém. Ist. Geol. Univ. Padova*, 28, 19.
- Elter, G. & Elter, P. 1965: Carta geologica della regione del Piccolo San Bernardo (vesante italiano). Note illustrative. Consiglio Nazionale delle Ricerche.
- Elter, P. & Elter, G. 1954: Sull'esistenza, nei dintorni del Piccolo San Bernardo, di un elemento tettonico riferibile al ricoprimento del Pas du Roc. *dell' Acad. Naz. dei Lincei*, 22, 181-187.
- Engi, M., C.N., S. & Burri, T. 2001a: Metamorphic evolution of pelitic rocks of the Monte Rosa nappe: Constraints from petrology and single grain monazite age data. *Schweiz. Mineral. Petrogr. Mitt.*, 81, 305-328.
- Engi, M., Scherrer, N. & Burri, T. 2001b: Metamorphic evolution of pelitic rocks of the Monte Rosa Nappe; constraints from petrology and single grain monazite age data. *Schweiz. Mineral. Petrogr. Mitt.*, 81, 305-328.
- Escher, A. & Beaumont, C. 1997: Formation, burial and exhumation of basement nappes at crustal scale: a geometric model based on the Western Swiss-Italian Alps. *J. Struct. Geol.*, 19, 955-1074.
- Escher, A., Masson, H. & Steck, A. 1993: Nappe geometry in the Western Swiss Alps. *J. Struct. Geol.*, 7, 955-974.
- Evans, B. E. 1990: Phase relations of epidote-blueschists. *Lithos*, 25, 3-23.
- Fabre, J. 1961: Contribution à l'étude de la Zone Houillère Briançonnaise en Maurienne et en Tarentaise

- (Alpes Savoie). Mém. BRGM, 2, 315 pp.
- Feys, R. 1963. Étude géologique du Carbonifère briançonnais (Hautes-Alpes). Mém. Bur. Rech. Géol. Min., 6, 387 pp.
- Foland, K. A. 1979: Limited mobility of argon in metamorphic terrain. *Geochim. cosmochi. Acta*, 43, 793-801.
- Freeman, S. R., Butler, R. W. H. & Cliff, R. A. 1998a: Direct dating of mylonite evolution: a multi-disciplinary geochronological study from the Moine Thrust Zone, NW Scotland. *J. Geol. Soc.*, 155, 745-758.
- Freeman, S. R., Butler, R. W. H., Cliff, R. A., Inger, S. & Barnicoat, A. C. 1998b: Deformation migration in an orogen-scale shear zone array: an example from the Basal Briançonnais Thrust, internal Franco-Italian Alps. *Geol. Mag.*, 135, 349-367.
- Freeman, S. R., Inger, S., Butler, R. W. H. & Cliff, R. A. 1997: Dating deformation using Rb-Sr in white mica: Greenschist facies deformation ages from the Entrelor shear zone, Italian Alps. *Tectonics*, 16, 57-76.
- Frey, M., Desmons, J. & Neubauer, F. 1999a: *Metamorphic Maps of the Alps*. CNRS (Paris), Swiss N.S.F (Berne), BMfWFV and FWF (Vienna).
- 1999b: The new metamorphic map of the Alps: Introduction. *Schweiz. Mineral. Petrogr. Mitt.*, 77, 1-4.
- Frisch, W. 1979: Tectonic progradation and plate tectonics of the Alps. *Tectonophysics*, 60, 121-139.
- Froitzheim, N. 1992: Formation of recumbent folds during synorogenic crustal extension (Austroalpine nappes, Switzerland). *Geology*, 20, 923-926.
- 2001: Origin of the Monte Rosa Nappe in the Pennine Alps; a new working hypothesis. *Geol. Soc. Am. Bull.*, 113, 604-614.
- Froitzheim, N., Schmid, S. M. & Frey, M. 1996: Mesozoic paleogeography and timing of eclogite-facies metamorphism in the Alps: A working hypothesis. *Eclog. geol. Helv.*, 89, 81-110.
- Fudral, S. 1998: Etude géologique de la structure téthysienne dans les Alpes franco-italiennes nord-occidentales de la doire Ripaire (Italie) à la région de Bourg Saint-Maurice (France). Laboratoire de Géologie de l'Université de Grenoble, Mémoire HS n°29,306.
- Fügenschuh, B., Loprieno, A., Ceriani, S. & Schmid, S. 1999: Structural analysis of the Subbriançonnais and Valais units in the area of Moûtiers (Savoy, Western Alps): paleogeographic and tectonic consequences. *Int. J. Earth Sci.*, 88, 201-218.
- Fügenschuh, B. & Schmid, S. M. 2003: Late stages of deformation and exhumation of an orogen constrained by fission-track data: a case study in the Western Alps. *Geol. Soc. Am. Bull.*, 115, 1425-1440.
- Gebauer, D. 1999: Alpine geochronology of the Central and Western Alps: new constraints for a complex geodynamic evolution. *Schweiz. Mineral. Petrogr. Mitt.*, 79, 191-208.
- Gerber, C. 1965: Flore et stratigraphie du Carbonifère des Alpes françaises. *Bur Rech Mem Géol Min*, 21, 380 pp.
- Giorgis, D., Thélin, P., Stampfli, G. M. & Bussy, F. 1999: The Mont-Mortt metapelites: Variscan metamorphism and geodynamic context (Briançonnais basement, Western Alps, Switzerland). *Schweiz. Mineral. Petrogr. Mitt.*, 79, 381-398.
- Goffé, B. & Bousquet, R. 1997: Ferrocapholite, chloritoïde et lawsonite dans les métapelites des unités du Versoyen et du Petit St Bernard (zone valaisanne, Alpes occidentales). *Schweiz. Mineral. Petrogr. Mitt.*, 77, 137-147.
- Goffé, B. C., C. 1986: High-pressure metamorphism in the Western Alps: zoneography of metapelites, chronology and consequences. *Schweiz. Mineral. Petrogr. Mitt.*, 66, 41-52.
- Gouffon, Y. 1993: Géologie de la «nappe» du Grand St-Bernard entre la Doire Baltée et la frontière suisse (Vallée d'Aoste- Italie). *Mémoires de Géologie (Lausanne)*, 12, 147.
- Graham, C. M. 1981: Experimental Hydrogen Isotope Studies III: Diffusion of Hydrogen in Hydrous Minerals, and Stable Isotope Exchange in Metamorphic Rocks. *Contrib. Mineral. Petrol.*, 76, 216-228.
- Guillot, F., Schaltegger, U., Bertrand, J. M., Deloule, E. & Baudin, T. 2002: Zircon U-Pb geochronology of

- Ordovician magmatism in the polycyclic Ruitor Massif (Internal W Alps). *Int. J. Earth Sci.*, 9, 964-978.
- Hames, W. E. & Cheney, J. T. 1997: On the loss of $^{40}\text{Ar}^*$ from muscovite during polymetamorphism. *Geochim. cosmoch. Acta*, 61, 3863-3872.
- Hammerschmidt, K. & Frank, E. 1991: Relics of high pressure metamorphism in the Lepontine Alps (Switzerland) - $^{40}\text{Ar}/^{39}\text{Ar}$ and microprobe analyses on white K-micas. *Schweiz. Mineral. Petrogr. Mitt.*, 71, 261-274.
- Henry, C., Michard, A. & Chopin, C. 1993: Geometry and structural evolution of ultra-high-pressure and high-pressure rocks from the Dora-Maira massif, Western Alps, Italy. *J. Struct. Geol.*, 18, 965-981.
- Holdaway, M. J., Mukhopadhyay, B., Dyar, M. D., Guidotti, C. V. & Dutrow, B. L. 1997: Garnet-biotite geothermometry revised; new Margules parameters and a natural specimen data set from Maine. *Am. Mineral.*, 82, 582-595.
- Holland, T. J. B. & Powell, R. 1998: An internally consistent data set for petrological interest. *J. Metamorph. Geol.*, 16, 309-343.
- Hurford, A.-J. & Hunziker, J. C. 1989: A revised thermal history for the Gran Paradiso massif. *Schweiz. Mineral. Petrogr. Mitt.*, 69, 319-329.
- Jäger, E. 1967a: Die Bedeutung der Biotit Alterswerte. In: *Altersbestimmungen an Glimmern in den Zentralalpen* (edited by E. Jäger, E. Niggli and E. Wenk) 134. *Beitr. Geol. Karte, NF*, 11-21.
- 1967b: Die Bedeutung der Biotit-Alterswerte. In: *Altersbestimmungen an Glimmern der Zentralalpen* (edited by E. Jäger, Niggli, E. and Wenk E.) *Beitr. Geol. Karte Schweiz, NF*.
- 1973: Die alpine Orogenese im Lichte der radiometrischen Altersbestimmungen. *Eclog. geol. Helv.*, 66, 11-21.
- Jagoutz, E. 1993: Das radiometrische Datieren metamorpher Gesteine: Sein und Schein. Abstract Volume DMG 1993, München.
- Jaillard, E. 1989: La transition Briançonnais externe - Briançonnais interne en Savoie. *L'Aiguille des Aimesy, le Roc du Bourgerat et le massif d'Ambin. Géol. Alpine*, 65, 105-134.
- 1990. Lithostratigraphie et paléogéographie des séries briançonnaises internes de Haute-Tarentaises (Savoie) : conséquences paleogeographiques et structurales, *Géologie de la France 1990*, 1, 33-44.
- Jolivet, L., Faccenna, C., Goffé, B., Mattei, M., Rossetti, F., Brunet, C., Storti, F., Funicello, R., Cadet, J. P., d'Agostino, N. & Parra, T. 1998a: Midcrustal shear zones in postorogenic extension: Example from the northern Tyrrhenian Sea. *Journal of Geophysical Research*, 103, 12123-12161.
- Jolivet, L., Goffé, B., Bousquet, R., Oberhänsli, R. & Michard, A. 1998b: Detachements in high-pressure mountain belts, Tethyan examples. *Earth and Planetary Science Letters*, 160, 31-47.
- Keller, L. M., Abart, R., Stünitz, H. & De Capitani, C. in press: Deformation, mass transfer and reactions in an eclogite facies shear zone in a polymetamorphic metapelite, (Monte Rosa, Western Alps).
- Keller, L. M., De Capitani, C. D. & Abart, R. submitted: The phengite-paragonite solvus I: A quarternary solution model for white micas based on natural coexisting phengite-paragonite pairs.
- Keller, L. M. & Schmid, S. M. 2001: On the kinematics of shearing near the top of the Monte Rosa nappe and the nature of the Furgg zone in Val Loranco (Antrona valley, N. Italy): Tectono-metamorphic and paleogeographical consequence. *Schweiz. Mineral. Petrogr. Mitt.*, 81, 347-367.
- Kelly, S. P. 2002: Excess argon in K-Ar and Ar-Ar geochronology. *Chem. Geol.*, 188, 1-22.
- Kleinhanns, I. C., Kreissig, K., Kamber, B. S., Meisel, T., Nägler, T. F. & Kramers, J. D. 2002: Combined Chemical Separation of Lu, Hf, Sm, Nd and REEs from a Single Rock Digest: Precise and Accurate Isotope Determinations of Lu-Hf and Sm-Nd Using Multicollector-ICPMS. *Anal. Chem.*, 74, 67-73.
- Lapen, T. H., Johnson, C. M., Baumgartner, L. P., Mahlen, J. N., Bread, L. B. & Amato, J. M. 2003: Burial rates during prograde metamorphism of an ultra-high-pressure terrane: an example from Lago di Cigana, Western Alps, Italy. *Earth and Planetary Science Letters*, 215, 52-72.
- Lemoine, M. 1961: Le Briançonnais interne et la zone des Schistes Lustrés dans les vallées du Guil et de l'Ubaye (Hautes et Basses Alpes) (Schéma structural). *Trav. Lab. Géol. Fac. Sci. Grenoble*, 47, 181-201.
- Lickorish, W. H. & Ford, M. 1998: Sequential restoration of the external Alpine Digne Thrust System, SE

- France, constrained by Kinematic data and Synorogenic sediments. In: Cenozoic Foreland Basins of Western Europe (edited by A. Mascle, C. Puigdefàbregas, H. P. Luterbacher and M. Fernández) 134. Geological Society Special Publications, 189-211.
- Loprieno, A. 2001: A combined structural and sedimentological approach to decipher the evolution of the Valaisan domain in Savoy, (Western Alps), Basel, 285 pp.
- Luais, B., Duchêne, S. & de Sigoyer, J. 2001: Sm-Nd disequilibrium in high-pressure, low-temperature Himalayan and Alpine rocks. *Tectonophysics*, 342, 1-22.
- Ludwig, K. R. 2001: User's manual for Isoplot/Ex erv. 2.49, a geochronological toolkit for Microsoft Excel. Berkley Geochronological Center Spec. Publ. 1a, 55 pp.
- Macaya, J., González-Lodeiro, F., Martínez-Catalán, J. R. & Alvarez, F. 1991: Continuous deformation, ductile thrusting and backfolding of cover and basement in the Sierra de Guadamarrama, Hercynian orogen of central Spain. *Tectonophysics*, 191, 291-309.
- Mancktelow, N. 1992: Neogene lateral extension during convergence in the Central Alps: Evidence from interrelated faulting and backfolding around the Simplonpass (Switzerland). *Tectonophysics*, 215, 295-317.
- Marion, R. 1984: Contribution à l'étude géologique de la Vanoise. Le massif de la Grande Sassièrre et la région de Tignes-Val d'Isère. Unpublished PhD thesis, Université de Savoie, 172 pp.
- Markley, M. J., Teyssier, C. & Caby, R. 1999: Re-examining Argand's view of the Siviez-Mischabel nappe. *J. Struct. Geol.*, 21, 1119-1124.
- Markley, M. J., Teyssier, C. & Cosca, M. A. 2002: The relation between grain size and $^{40}\text{Ar}/^{39}\text{Ar}$ date of the Alpine white mica from the Siviez-Mischabel Nappe, Switzerland. *J. Struct. Geol.*, 24, 1937-1955.
- Markley, M. J., Teyssier, C., Cosca, M. A., Caby, R., Hunziker, J. C. & Sartori, M. 1998: Alpine deformation and $^{40}\text{Ar}/^{39}\text{Ar}$ geochronology of synkinematic white mica in the Siviez-Mischabel Nappe, western Pennine Alps, Switzerland. *Tectonics*, 17, 407-425.
- Massonne, H.-J. & Szpurka, Z. 1997: Thermodynamic properties of white micas on the basis of high-pressure experiments in the systems $\text{K}_2\text{O}-\text{MgO}-\text{Al}_2\text{O}_3-\text{SiO}_2-\text{H}_2\text{O}$ and $\text{K}_2\text{O}-\text{FeO}-\text{Al}_2\text{O}_3-\text{SiO}_2-\text{H}_2\text{O}$. *Lithos* 41 229-250.
- Mayer, A., Abouchamin, W. & Dal Piaz, G. V. 1999: Eocene Sm-Nd age for the eclogitic metamorphism of the Zermatt-Saas ophiolite in Ays Valley, Western Alps. *Eur. Union Geosci.*, 10, Abstr. 809.
- Mercier, D. & Beaudoin, B. 1987: Révision du Carbonifère Briançonnais: Stratigraphie et évolution du bassin. *Geol. Alpine*, 13, 25-31.
- Merle, O. & Guillier, B. 1989: The building of the Central Swiss Alps: an experimental approach. *Tectonophysics*, 165, 41-56.
- Michard, A., Goffé, B., Chopin, C. & Henry, C. 1996: Did the Western Alps develop through an Oman-type stage? The geotectonic setting of high-pressure metamorphism in two contrasting Tethyan transects. *Eclog. geol. Helv.*, 89, 43-80.
- Milnes, A. G. 1974a: Post-Nappe folding in the Western Lepontine. *Eclog. geol. Helv.*, 67, 333-348.
- 1974b: Structure of the Pennine Zone (Central Alps): New Working Hypothesis. *Geol. Soc. Am. Bull.*, 85, 1727-1732.
- Milnes, A. G., Gfeller, M. & Müller, R. 1981: Sequence and style of major post-nappe structures, Simplon-Pennine Alps. *J. Struct. Geol.*, 3, 411-420.
- Monié, P. 1985: La méthode $^{39}\text{Ar}-^{40}\text{Ar}$ appliquée au métamorphisme alpin dans le massif du Mon-Rose (Alpes Occidentales). *Chronologie détaillée depuis 110 Ma. Eclog. Geol. Helv.*, 78, 487-516.
- 1990: Preservation of Hercynian $^{40}\text{Ar}/^{39}\text{Ar}$ ages through high-pressure low-temperature Alpine metamorphism in the Western Alps. *Eur. J. of Mineral.*, 2, 343-361.
- Mugnier, J. L., Bergerat, F., Damotte, B., Guellec, S., Nicolas, A., Polino, R., Roure, F., Tardy, M. & Truffert, C. 1996: Crustal structure of the western Alps and their forelands. *Mém. Soc. Géol. France.*, 170, 73-97.
- Mugnier, J.-L., Guellec, S., Menard, G., Roure, F., Tardy, M. & Vialon, P. 1990: Crustal balanced cross-sections through the external Alps deduced from ECORS profile. In: Deep structure in the Alps

- (edited by P. Heitzman, F. Roure and R. Polino). Mémoire de la Société géologique de France.
- Mulch, A., Cosca, M. A. & Handy, M. R. 2001: In-situ UV-laser $^{40}\text{Ar}/^{39}\text{Ar}$ geochronology of a micaeous mylonite: an example of defect enhanced argon loss. *Contrib. Mineral. Petrol.*
- Müller, R. 1983: Die Struktur der Mischabelfalte (Penninische Alpen). *Eclog. geol. Helv.*, 76, 391-416.
- Müller, W. 2003: Strengthening the link between geochronology, textures and petrology. *Earth and Planetary Science Letters*, 206, 237-251.
- Müller, W., Kelly, S. P. & I.M., V. 2002: Dating fault-generated pseudotachylytes: comparison of $^{39}\text{Ar}/^{39}\text{Ar}$ stepwise-heating, laser ablation and Rb-Sr microsampling analyses. *Contrib. Mineral. Petrol.*, 144, 57-77.
- Nagel, T., de Capitani, C. & Frey, M. 2002a: Isograds and PT evolution in the eastern Lepontine Alps, Switzerland. *J. Metamorph. Geol.*, 20, 309-324.
- Nagel, T., De Capitani, C., Frey, M., Froitzheim, N., Stünitz, H. & Schmid, S. M. 2002b: Structural and metamorphic evolution in the lepontine dome. *Eclog. geol. Helv.*, 95, 301-322.
- Nägler, T. F., Holzer, L. & Frei, R. 1995: Nd and Pb in Monazite Inclusions within Polymetamorphic Garmets: Hell or Heaven? AGU fall meeting, supplements to EOS, November 7.
- Nicolas, A., Hirn A., Polino, R., R. Nicolich and ECORS-CROP Working Group. 1990: Lithospheric wedging in the Western Alps inferred from the ECORS-CROP traverse. *Geology*, 18, 587-590.
- Nicolas, A., Polino, R., Hirn, A. & Nicolich, R. a. E.-C. W. G. 1990: ECORS-CROP traverse and deep structures of the western Alps: a synthesis. *Mém. Soc. géol. France*, 170, 15-27.
- Parra, T., Vidal, O. & Agard, P. 2002a: A thermodynamic model for Fe-Mg dioctahedral K white micas using data from phase equilibrium experiments and natural pelitic assemblages. *Contrib. Mineral. Petrol.*, 143, 706-732.
- Parra, T., Vidal, O. & Jolivet, L. 2002b: Relation between intensity of deformation and retrogression in blueschist metapelites of Tinos Island (greece) evidenced by chlorite-mica local equilibria. *Lithos*, 63, 41-66.
- Pfiffner, O. A., Ellis, S. & Beaumont, C. 2000: Collision tectonics in the Swiss Alps: Insight from geodynamic modelling. *Tectonics*, 19, 1065-1094.
- Pfiffner, O. A., Lehner, P., Heitzmann, P. & Mueller, S. 1997: Deep Structures of the Alps: Results from NRP 20 (edited by O. A. e. a. Pfiffner). Birkhäuser, Basel, 73-114.
- Philippot, P. 1988: Déformation et éclogitisation progressives d'une croûte océanique subductée: Le Monviso, Alpes occidentales. Contraintes cinématiques durant la collision alpine. Unpublished PhD, Montpellier, 269 pp.
- 1990: Opposite vergence of nappes and crustal extension in the French-Italian Western Alps. *Tectonics*, 9, 1143-1164.
- Philippot, P., Blichert-Toft, J., Perchuk, A., Costa, S. & Gerasimov, V. 2001: Lu-Hf and Ar-Ar chronometry supports extreme rate of subduction zone metamorphism deduced from geospeedometry. *Tectonophysics*, 342, 22-38.
- Platt, J. P., Lister, G., Cunningham, P., Weston, P., Peel, F., Baudin, T. & Dondey, H. 1989: Thrusting and backthrusting in the Briançonnais domain of the Western Alps. In: *Alpine Tectonics* (edited by M. Coward and M. P. P. Dietrich, R.G.). *Geol. Soc. Spec. Publ. London*, 135-152.
- Platt, J. P. & Lister, G. S. 1985: Structural evolution of a nappe complex, southern Vanoise massif, French Penninic Alps. *J. Struct. Geol.*, 7, 145-160.
- Polino, R. & Dal Piaz, G. V. 1978: Geologia dell'Alta Val d'Isère e del Bacino del lago Serrù. *Mem. Ist. Geol. Univ. Padova*, 22, 1-20.
- Ramsay, J. G. & Huber, M. I. 1987. *The Techniques of Modern Structural Geology, V.2: Folds and Fractures*: San Diego, Academic Press, London, 391pp.
- Reddy, S. M. & Potts, J. P. 1999: Constraining absolute deformation ages: the relationship between deformation mechanisms and isotopic systematics. *J. Struct. Geol.*, 21, 1255-1265.
- Reddy, S. M., Wheeler, J., Butler, R. W. H., Cliff, R. A., Freeman, S., Inger, S., Pickles, C. & Kelly, S. P. 2003: Kinematic reworking and exhumation within the convergent Alpine Orogen. *Tectonophysics*, 365, 77-102.

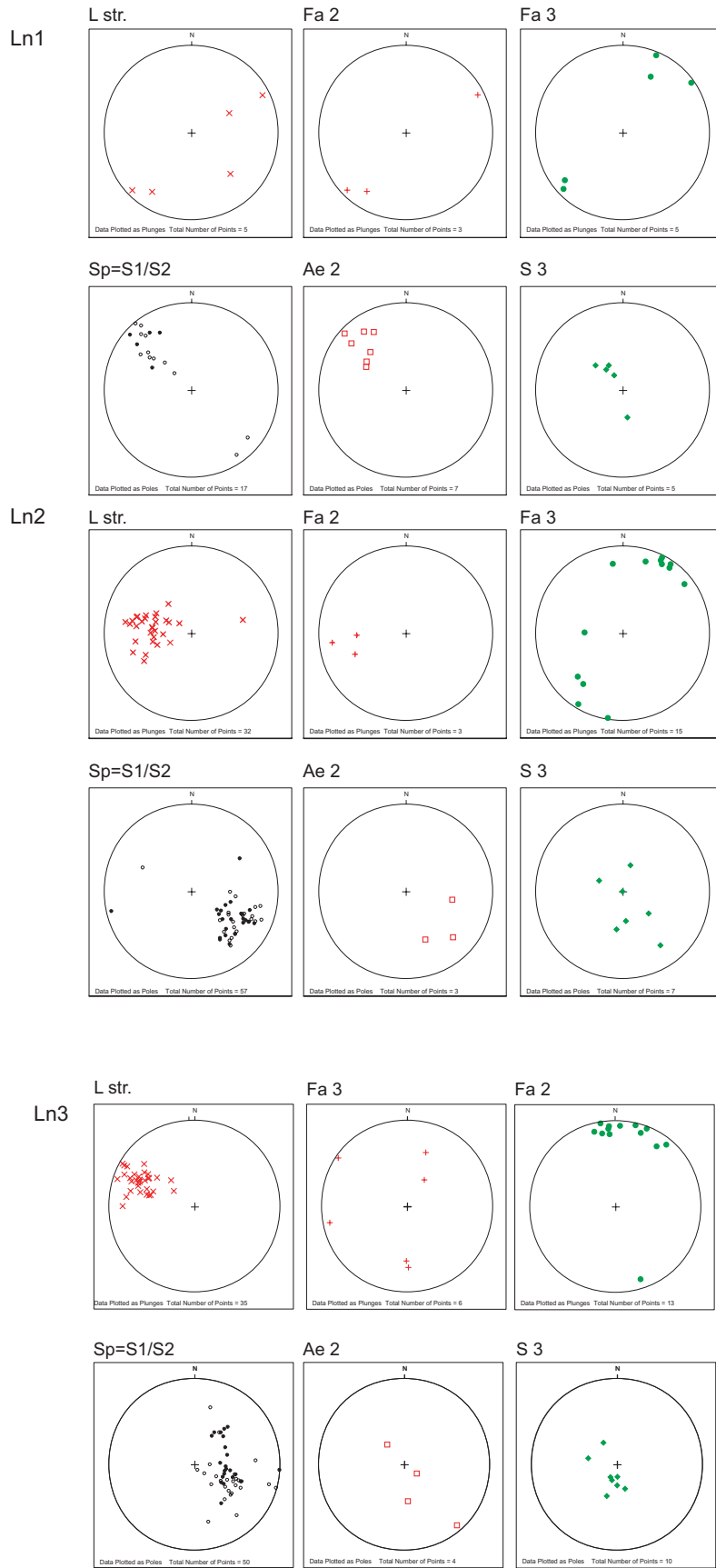
- Reddy, S. M., Wheeler, J. & Cliff, R. A. 1999: The geometry and timing of orogenic extension: an example from the Western Italian Alps. *J. Metamorph. Geol.*, 17, 573-589.
- Ricou, L. E. & Siddans, A. W. B. 1986: Collision tectonics in the Western Alps. *Geol. Soc. London Spec. Publ.*, 19, 229-244.
- Ring, U. & Merle, O. 1992: Forethrusting, backfolding, and lateral gravitational escape in the northern part of the Western Alps (Monte Rosa region). *Geol. Soc. Am. Bull.*, 104, 901-914.
- Rolland, Y., Lardeaux, J. M., Guillot, S. & Nicollet, C. 2000: Extension syn.convergence, poïçonnement vertical et unités métamorphiques contrastées en bordure ouest du Grand Paradis (Alpes Franco-Italiennes). *Geodyn. Acta*, 13, 133-148.
- Roure, F., Bergerat, F., Damotte, B., Mugnier, J.-L. & Polino, R. 1996: The ECORS-CROP Alpine seismic traverse. *Mém. Soc. Geol. France*, 170, 113pp.
- Saadi, M. 1992: Géologie du haut Val di Rhêmes (Vallée d'Aoste). Unpublished diploma thesis, Genève, 120 pp.
- Scaillet, S. 1996: Excess ^{40}Ar transport scale and mechanism in high-pressure phengites: A case study from eclogitized metabasites of the Dora-Maira nappe, western Alps. *Geochim. cosmochi. Acta*, 60, 1075-1090.
- Scaillet, S., Feraud, G., Ballèvre, M. & Amouric, M. 1992: Mg/Fe and [(Mg,Fe)Si-Al₂] compositional control on argon behaviour in high-pressure white micas: A $^{40}\text{Ar}/^{39}\text{Ar}$ continuous laser-probe study from the Dora_Maira nappe of the internal western Alps, Italy. *Geochim. cosmochi. Acta*, 56, 2851-2872.
- Scherer, E. E., Cameron, K. L. & Bilchert-Toft, J. 2000: Lu-Hf garnet geochronology: Closure temperature relative to the Sm-Nd system and the effects of trace element inclusions. *Geochim. cosmochi. Acta*, 64, 3413-3432.
- Scherer, E. E., Münker, C. & Mezger, K. 2001: Calibration of the lutetium-hafnium clock. *Science*, 293, 683-686.
- Schmid, S. M., Aebli, H. R., Heller, F. & Zingg, A. 1989: The role of the Periadriatic Line in the tectonic evolution of the Alps. In: *Alpine Tectonics* (Coward, M., et al., eds.). *Geol. Soc. London Spec. Publ.*, 45, 153-157.
- Schmid, S. M. & Kissling, E. 2000: The arc of the Western Alps in the light of new data on deep crustal structure. *Tectonics*, 19, 62-85.
- Schmid, S. M., Pfiffner, O. A., Froitzheim, N., Schönborn, G. & Kissling, E. 1996: Geophysical-geological transect and tectonic evolution of the Swiss-Italian Alps. *Tectonics*, 15, 1036-1064.
- Schmid, S. M., Rùck, P. & Schreurs, G. 1990a: The significance of the Schams nappes for reconstruction of the paleotectonic and orogenic evolution of the Penninic zone along the NFP-20 East traverse (Grisons, eastern Switzerland). In: *Deep structure of the Alps* (edited by F. Roure, P. Heitzmann and R. Polino) 156. *Mémoire de la Société géologique de France*, Paris, 263-287.
- 1990b: The significance of the Schams nappes for the reconstruction of the paleotectonic and orogenic evolution of the Pennine zone along the NFP 20 East traverse (Grisons, eastern Switzerland). *Mém. soc. géol. France*, 156; *Mém. Soc. géol. suisse*, 1; *Vol. spec. Soc. Geol. It.*, 1, 263-287.
- Schmid, S. M., Zingg, A. & Handy, M. R. 1987: Kinematics of movements along the Insubric Line and the emplacement of the Ivera Zone. *Tectonophysics*, 135, 47-66.
- Schreurs, G. 1990: Structural analysis of the Schams nappes and adjacent tectonic units: implications for the orogenic evolution of the Penninic zone in the eastern Switzerland. In: *Deep structure of the Alps* (edited by F. Roure, P. Heitzmann and R. Polino) 156. *Mém. Soc. Géol. France*, Paris, 415-435.
- 1993: Structural analysis of the Schams nappes and adjacent tectonic units: implications for the orogenic evolution of the Pennine zone in eastern Switzerland. *Bull. Soc. Géol. France*, 164, 415-435.
- Schürch, M. L. 1987: Les ophiolites de la zone du Versoyen: témoin d'un bassin à évolution métamorphique complexe. Unpublished PhD, Genève, 157 pp.
- Schwartz, S., Lardeaux, J. M., Guillot, S. & Tricart, P. 2000: Diversité du métamorphisme éclogitique dans

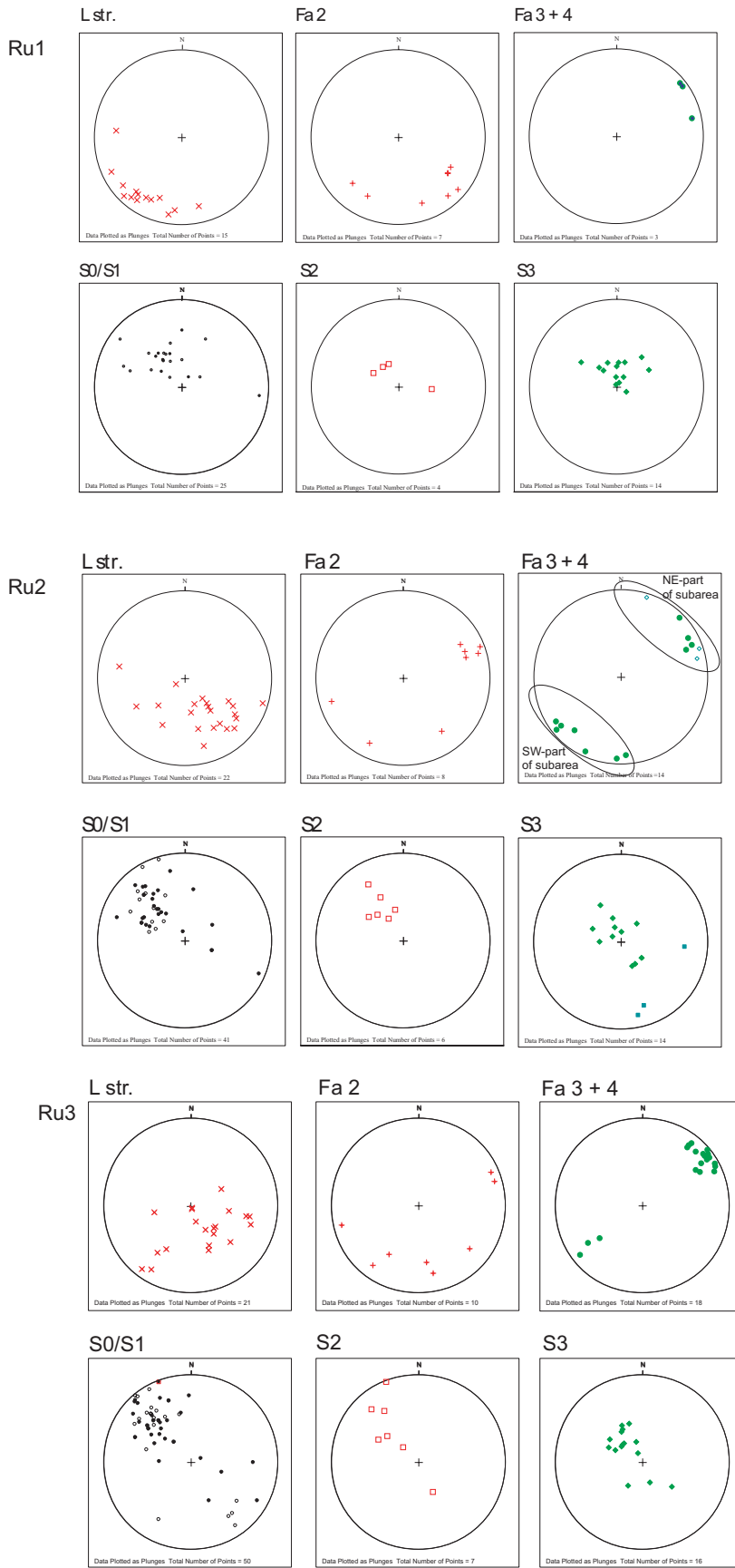
- le massif ophiolotique du Montviso (Alpes occidentales, Italie). *Geodyn. Acta*, 169-188.
- Scott, D. J. & St Onge, M. R. 1995: Constraints on Pb closure temperature in titanite based on rocks from the Ungava Orogen, Canada; implications for U-Pb geochronology and P-T-t path determinations. *Geology*, 23, 1123-1126.
- Seward, D., Ford, M., Bürgisser, J., Lickorish, H., Williams, E. A. & Meckel III, W. L. D. 1999: Preliminary results of fission-track analyses in the Southern Pelvoux area, SE France. *Mem. Sci. Geol.*, 51, 25-31.
- Sherlock, S. C. & Arnaud, N. O. 1999: Flat plateau and impossible isochrons: Apparent ^{40}Ar - ^{39}Ar geochronology in high-pressure terrain. *Geochim. cosmochim. Acta*, 63, 2835-2838.
- Simpson, C. & Schmid, S. M. 1983: An evolution of criteria to deduce the sense of movement in sheared rocks. *Geol. Soc. Am. Bull.*, 94, 1281-1288.
- Soom, M. A. 1990: Abkühlungs- und Hebungsgeschichte der Externmassive beidseits der Simplon-Rhone-Linie seit dem Oligozän: Spaltspurdaterungen an Apatit/Zirkon und K-Ar-Datierungen an Biotit/Muskowit (westliche Zentralalpen, Bern, 64 pp.
- Spear, F. S. 1993: *Metamorphic Phase Equilibria and Pressure-Temperature-Time Paths*. Mineralogical Society of America, Washington, D. C., 799.
- Stampfli, G. M. 1993: Le Briançonnais, terrain exotique dans les Alpes? *Eclog. geol. Helv.*, 86, 1-45.
- Thöni, M. 2002: Sm-Nd isotope systematics in garnet from different lithologies (Eastern Alps): age results, and an evolution of potential problems for Sm-Nd chronology. *Chem. Geol.*, 185, 255-281.
- Thöni, M. & Lagoutz, E. 1992: Some new aspects of dating eclogites in orogenic belts; Sm/Md, Rb/Sr and Pb-Pb isotopic results from the Austroalpine Saualpe and Koralpe type-locality (Canrinthia/Syria, southeastern Austria). *Geochim. cosmochim. Acta*, 56, 347-368.
- Todd, C. S. & Engi, M. 1997: Metamorphic field gradients in the Central Alps. *J. Metamorph. Geol.*, 15, 513-530.
- Tricart, P. 1984: From passive margin to continental collision: A tectonic scenario for the Western Alps. *Am. J. Sci.*, 284, 97-120.
- Trümpy, R. 1955: Remarques sur la corrélation des unités penniques externes entre Savoie et Valais et sur l'origine des nappes préalpines. *Bull. Soc. Géol. de France*, 6ème série, 217-231.
- 1966: Considérations générales sur le «Verrucano» des Alpes Suisses. *Atti del symposium sul Verrucano*, Pisa 1966. *Soc. Toscana Sci. Nat.*, 212-232.
- Ulardic, C. 2001: *Strukturgeologische und petrographische Untersuchungen im Valgrisenche (Briançonnais der italienischen Alpen)*. Unpublished diploma work, Freiburg, Germany, 100 pp.
- Vearncombe, J. R. 1985: The structure of the Gran Paradiso basement massif and its envelope, Western Alps. *Eclog. geol. Helv.*, 78, 49-72.
- Vidal, O., Goffé, B., Bousquet, R. & Parra, T. 1999a: Calibration and testing of an empirical chloritoid-chlorite Mg-Fe exchange thermometer and thermodynamic data for daphnite. *J. Metamorph. Geol.*, 17, 25-39.
- Vidal, O., Goffé, B., R., B. & Parra, T. 1999b: Calibration and testing of an empirical chloritoid-chlorite exchange thermometer and thermodynamic data for daphnite. *J. Metamorph. Geol.*, 17, 25-39.
- Vidal, O. & Parra, T. 2000: Exhumation of high pressure metapelites obtained from local equilibria for chlorite phengite assemblage. *Geol. Mag.*, 35, 139-161.
- Vidal, O., Parra, T. & Trotet, F. 2001: A thermodynamic model for Fe-Mg aluminous chlorite using data from phase equilibrium experiments and natural pelitic assemblages in the 100-600°C, 1-25 kbar range. *Am. J. Sci.*, 301, 557-592.
- Vidal, O., Theye, T. & Chopin, C. 1994: Experimental study of chloritoid stability at high pressure and various $f\text{O}_2$ conditions. *Contrib. Mineral. Petrol.*, 118, 256-270.
- Villa, I. M. 1998: Isotopic closure. *Terra Nova*, 10, 42-47.
- 2001: Radiogenic isotopes in fluid inclusions. *Lithos*, 55, 115-124.
- Villa, I. M., Grobéty, B., Kelly, S. P., Trigila, R. & Wieler, R. 1996: Assessing Ar transport paths and mechanisms for Mc Clure Mountains Hornblende. *Contrib. Mineral. Petrol.*, 126, 67-80.
- Villa, I. M., Hermann, J. & Müntener, O. 2000: ^{39}Ar - ^{40}Ar dating of multiply zoned amphibole generations

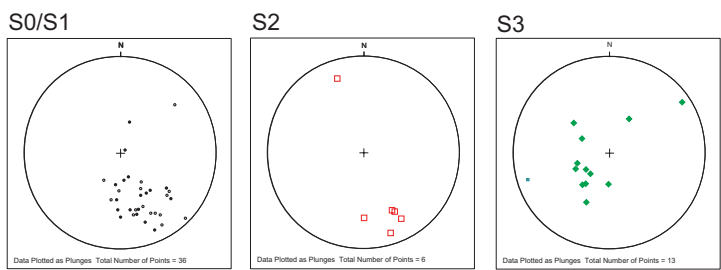
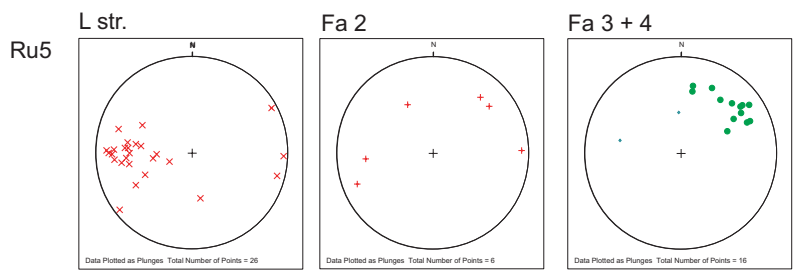
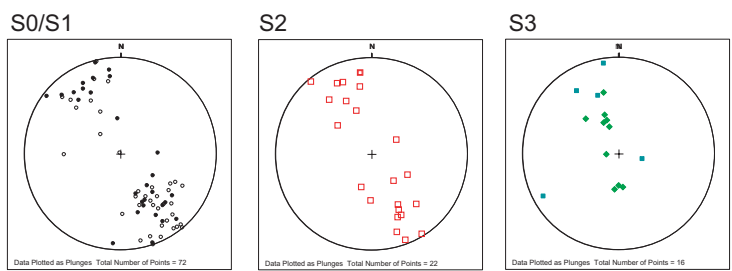
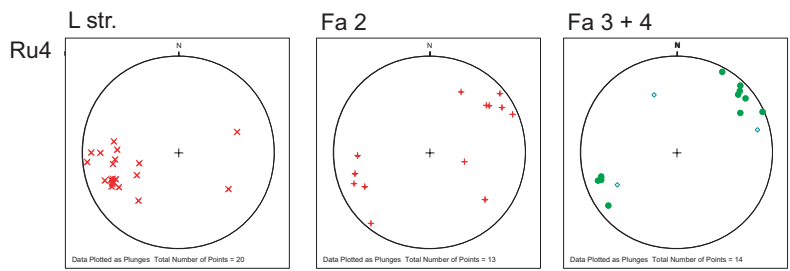
- (Malenco, Italian Alps). *Contrib. Mineral. Petrol.*, 140, 363-381.
- Villa, I. M. & Puxeddu, M. 1994: Geochronology of the Larderello geothermal field; new data and the “closure temperature” issue. *Contrib. Mineral. Petrol.*, 115, 415-426.
- Villa, I. M., Ruggieri, G. & Puxeddu, M. 1997: Petrological and geochronological discrimination of two white-mica generations in a granite cored from the Larderello-Travale geothermal field (Italy). *Eur. J. of Mineral.*, 9, 563-568.
- Vogl, J. J. 2002: Late orogenic backfolding and extension in the Brooks Range collisional orogen, northern Alaska. *J. Struct. Geol.*, 24, 1753-1776.
- Wheeler, J. 1991: Structural evolution of a subducted continental sliver: the northern Dora Maira massif, Italian Alps. *J. Geol. Soc.*, 148, 1101-1113.
- Wheeler, J. & Butler, R. W. H. 1994: Criteria to identify crustal extension. *J. Struct. Geol.*, 16, 1023-1027.
- Wijbrans, J. R. & McDougall, I. 1986: $^{39}\text{Ar}/^{39}\text{Ar}$ dating of white micas from an Alpine high-pressure metamorphic belt on Naxos: the resetting of the argon isotopic system. *Contrib. Mineral. Petrol.*, 93, 187-194.

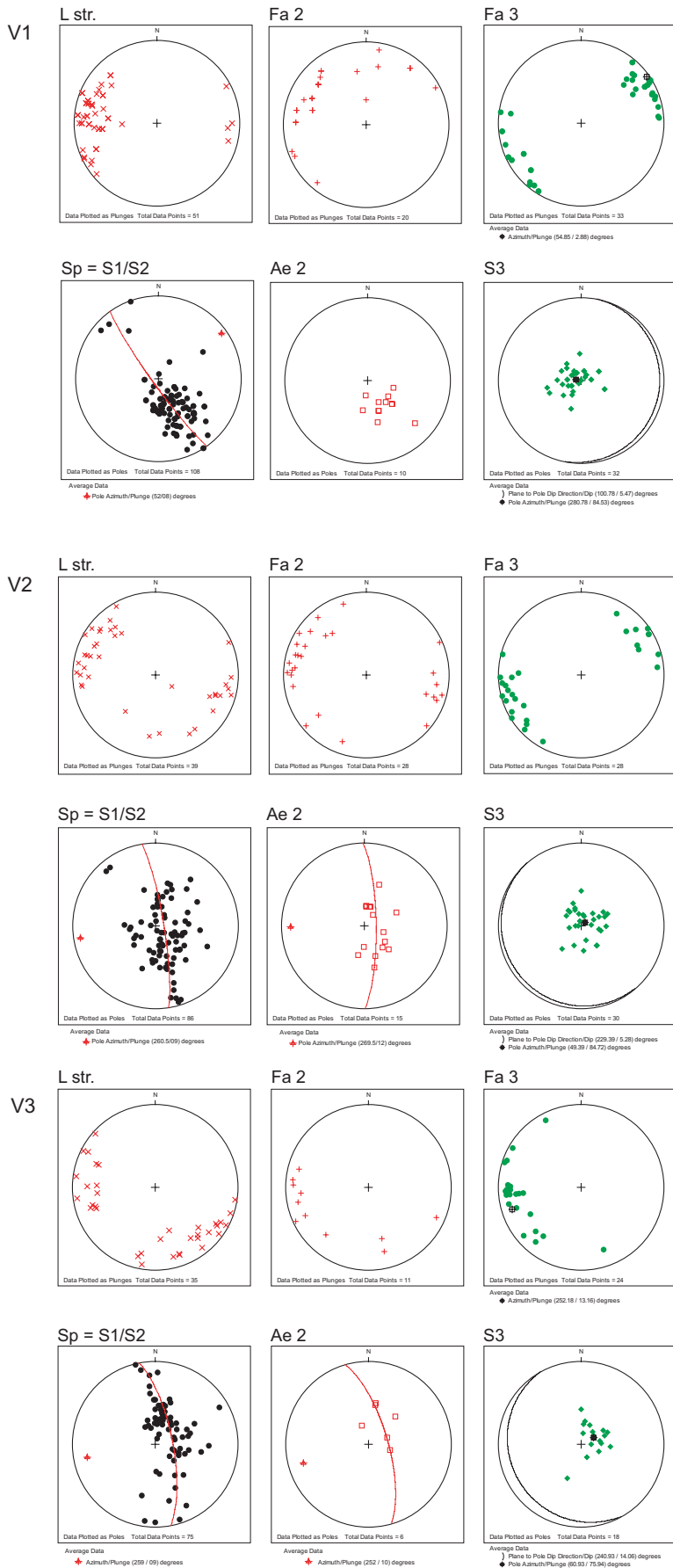
Appendix

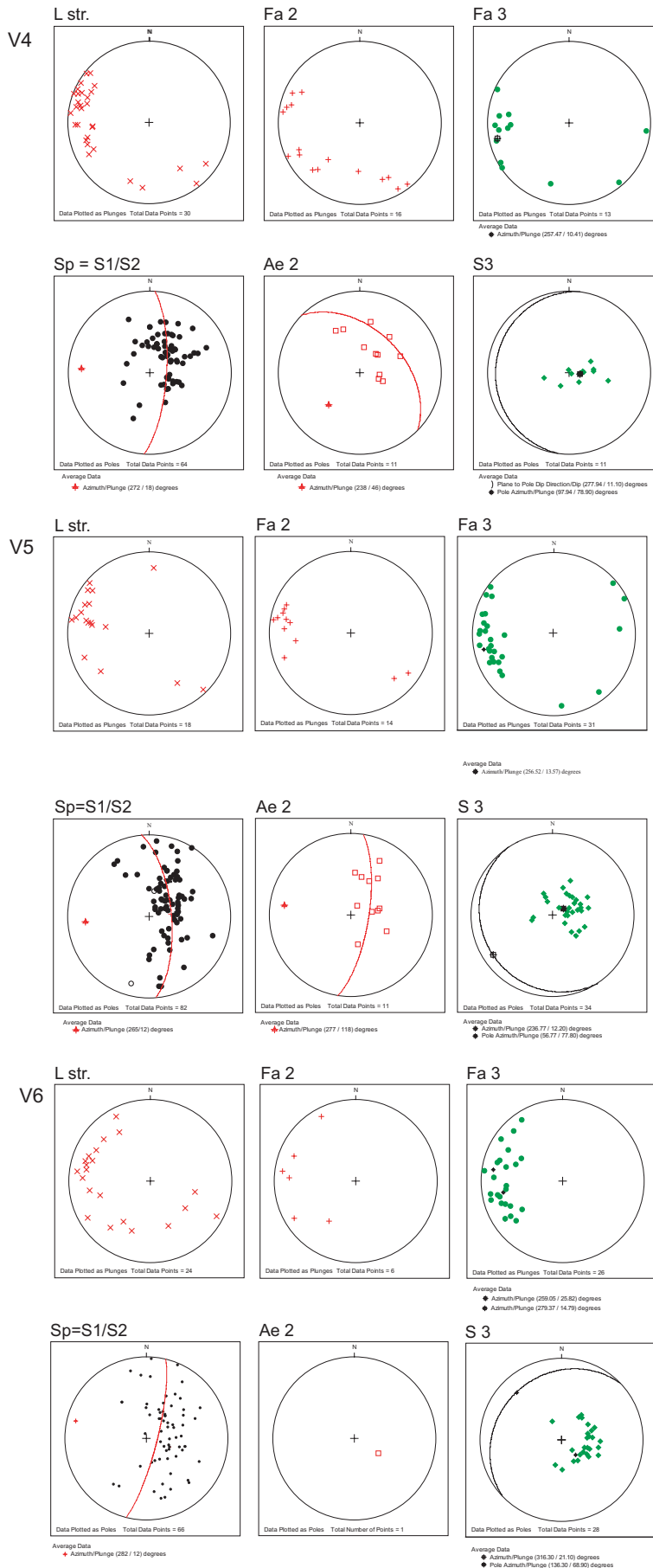
Appendix I: Structural data
Appendix II: Deformation table
Appendix III: Ar-Ar geochronology

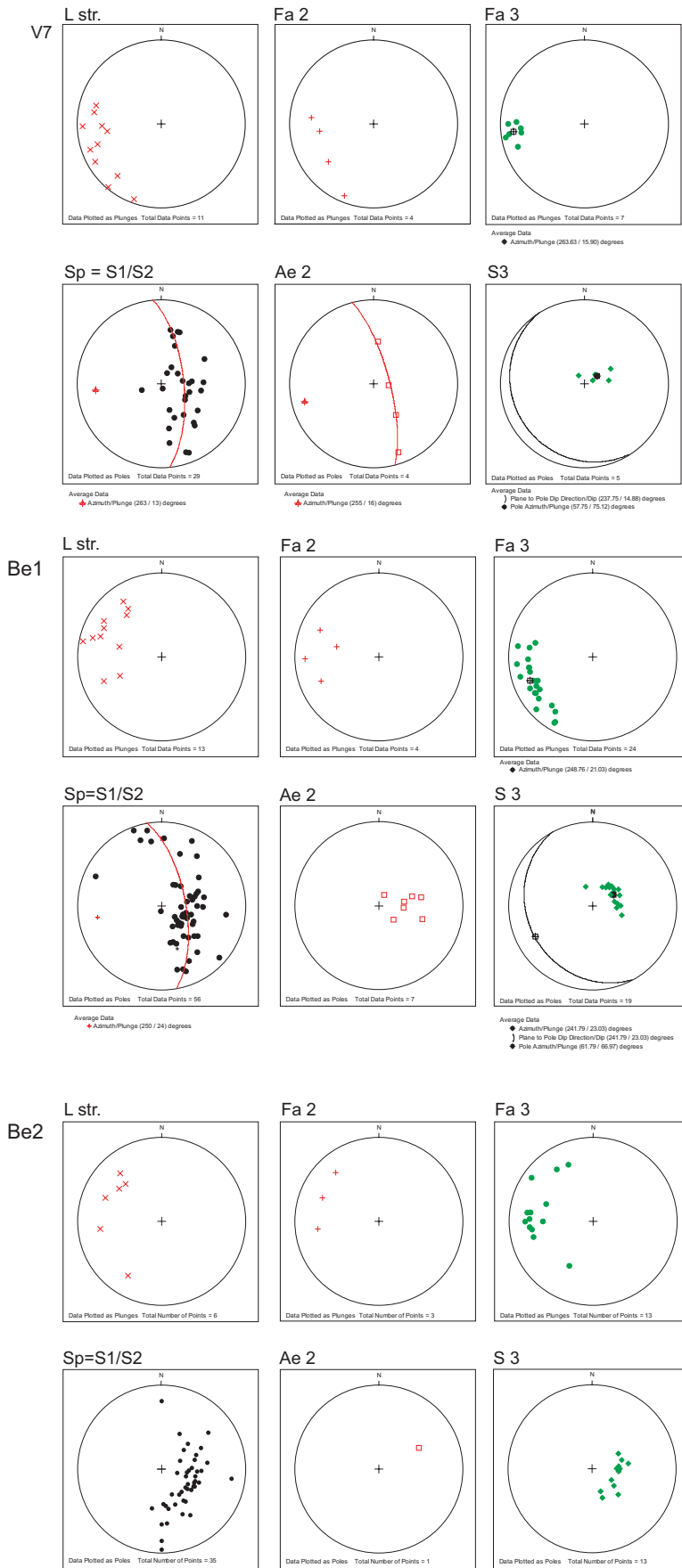












Appendix II: Deformation Table

An attempt to correlate the deformation phases across the entire Western Alps

Tectonic evolution of the Western Alps: an attempt to correlate deformation events

Stefan Bucher, Stefano Ceriani, Bernhard Fügenschuh, Stefan Schmid

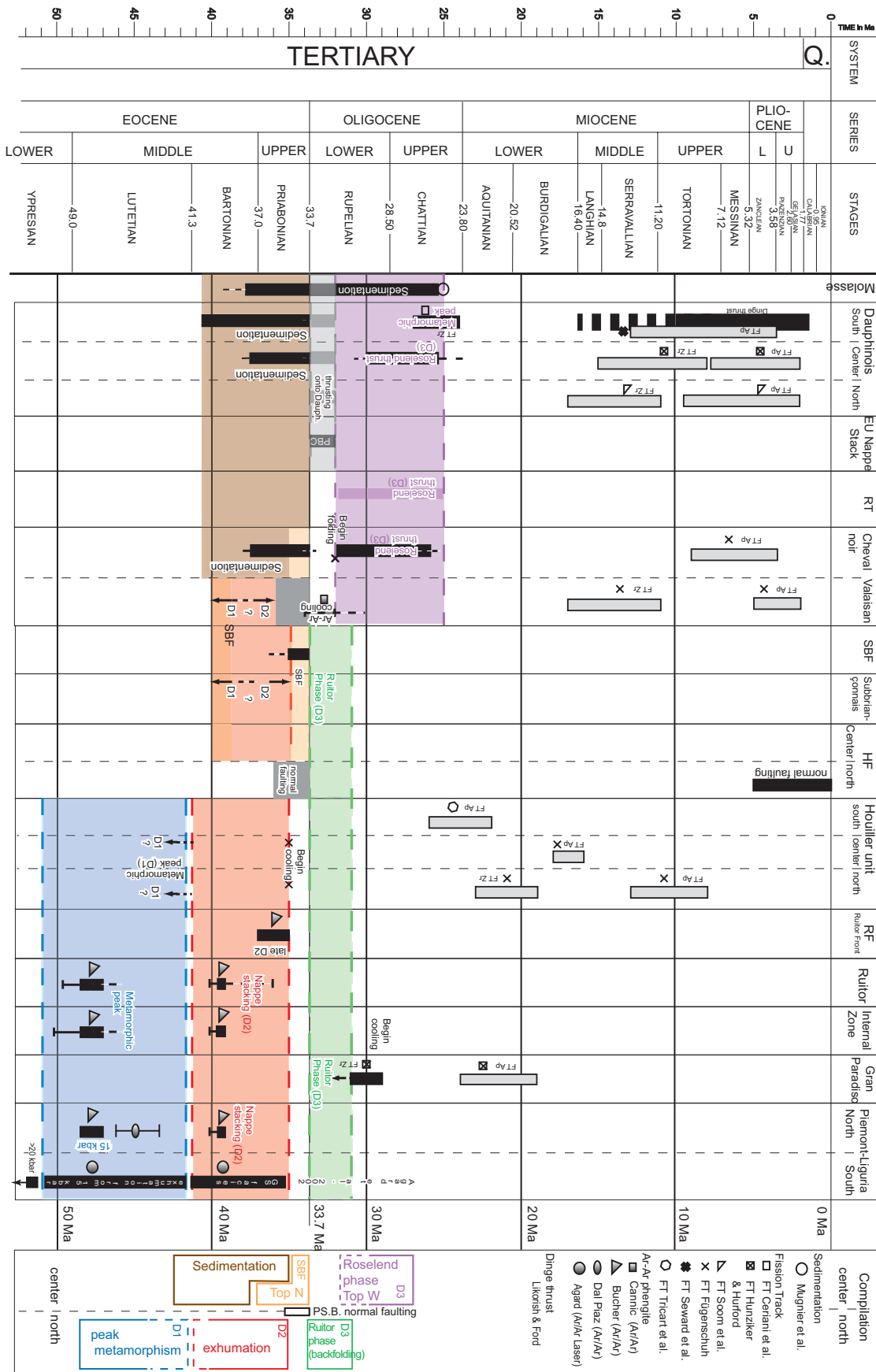
Department of Earth Sciences, Basel University, Bernoullistr. 32, Basel, Switzerland

Different processes, such as subduction, HP-metamorphism, exhumation, multistage thrusting and folding, contributed to the formation of the Alpine orogen. Quite commonly, not all of these stages are recorded in a single tectonic unit. Correlation is often based on geochronological data from medium- to high-grade metamorphosed units. In our contribution we try to correlate the deformation stages recorded in the low-grade metamorphic external units with those observed in the high-grade internal units. HP-metamorphism, exhumation and nappe refolding are the major tectono-metamorphic events in the Penninic units. The relevant geochronological data (Agard et al. 2002 and references therein; Bucher & Villa, same volume) are: HP- conditions are recorded during D1 at 47 ± 1 Ma; exhumation and nappe stacking takes place under greenschist facies condition between 43-39 Ma and is related to D2. The last movements attributed to nappe stacking are recorded at the tectonic contact between the Zone Houillère and the Rutor unit (late D2) at around 35 Ma. Note that there is a major difference regarding peak pressure conditions of about 7 kbar between these two units. All these stages take place prior to collision between Adriatic and European plates and in a north-south directed compressive regime.

The collisional evolution started with large-scale nappe refolding, observed in the Penninic units throughout the entire western Alps. Age data suggest an age of 34-32 Ma for this late-stage deformation event.

Unfortunately the pre-collision stages (D1 and D2) are not recorded in the external units and therefore a direct correlation is not possible. Presumably, the external zones remained undeformed, except for local folding during the “Pyrenean” phase. The Zone Houillère, which is continuous along the arc of the Western Alps and is in direct contact with the external units in the south, plays a key role for the correlation of the deformation phases. South of the Pelvoux massif the Embrunais-Ubaye nappes were emplaced onto the Dauphinois coevally with nappe refolding observed in the internal units. Around 32 Ma top-WNW thrusting affected the whole western Alps. First a major thrust, i.e. the Roselend thrust, carried the internal units on top of the external units. Then deformation migrated into the Dauphinois domain and reached the Subalpine molasse at about 25 Ma ago. From 25 Ma to present tectonic activity became less intense in the whole Western Alps. During this time cooling to near-surface temperatures can be observed for the entire western Alps, starting in the internal Penninic units and progressively migrating outwards into the Dauphinois domain. During Miocene-Pliocene times top-SW directed thrusting initiated in the area south of the Pelvoux massif, postdating the WNW directed thrusting phase.

The correlation proposed indicates that the internal Penninic units share a common evolution from north to south during the pre-collisional as well as the beginning of the post-collisional stage (Oligocene). From Miocene times onwards, however, a distinct evolution can be observed between the areas north and the south of the Pelvoux massif.



Most important references used to constrain the deformation table:

Sedimentation:

(Mugnier et al., 1996)

Fission Track:

(Hurford & Hunziker, 1989)

(Soom, 1990)

(Seward et al., 1999)

(Fügenschuh & Schmid, 2003)

Ar-Ar phengite:

(Cannic, 1996)

(Agard et al., 2002) and references therein

(Dal Piaz et al., 2001)

Bucher & Villa, submitted and refereneces therein

Dinge Thrust:

(Lickorish & Ford, 1998)

References:

- Agard, P., Monié, P., Jolivet, L. & Goffé, B., 2002. Exhumation of the Schistes Lustrés complex: in situ laser probe $^{40}\text{Ar}/^{39}\text{Ar}$ constraints and implications for the Western Alps. *Journal of Metamorphic Geology*, **20**, 599-618.
- Cannic, S. 1996. L'évolution magmatique et tectono-métamorphique du Substratum du Domaine Valaisan (Complexe Versoyen, Alpes Occidentales): implication dans l'histoire alpine), Thésis; Université Joseph Fourier-Grenoble 1 et Université de Lausanne.
- Dal Piaz, G. V., Cortiana, G., Del Moro, A., Martin, S., Pennacchioni, G. & Tartarotti, P., 2001. Tertiary age and paleostructural inferences of the eclogitic imprint in the Austroalpine outliners and Zermatt-Saas ophiolite, western Alps. *International Journal of Earth Sciences*, **90**, 668-684.
- Fügenschuh, B. & Schmid, S. M., 2003. Late stages of deformation and exhumation of an orogen constrained by fission-track data: a case study in the Western Alps. *GSA Bulletin*, **115**.
- Hurford, A.-J. & Hunziker, J. C., 1989. A revised thermal history for the Gran Paradiso massif. *Schweizerische Mineralogische und Petrographische Mitteilungen*, **69**, 319-329.
- Lickorish, W. H. & Ford, M. 1998. Sequential restoration of the external Alpine Digne Thrust System, SE France, constrained by Kinematic data and Synorogenic sediments. In: *Cenozoic Foreland Basins of Western Europe* (edited by Fernández, M.) **134**. Geological Society Special Publications, 189-211.
- Mugnier, J. L., Bergerat, F., Damotte, B., Guellec, S., Nicolas, A., Polino, R., Roure, F., Tardy, M. & Truffert, C., 1996. Crustal structure of the western Alps and their forelands. *Mémoire de la Société géologique de France*, **170**, 73-97.
- Seward, D., Ford, M., Bürgisser, J., Lickorish, H., Williams, E. A. & Meckel III, W. L. D., 1999. Preliminary results of fission-track analyses in the Southern Pelvoux area, SE France. *Mem. Sci. Geol.*, **51**, 25-31.
- Soom, M. A. 1990. Abkühlungs- und Hebungsgeschichte der Externmassive beidseits der Simplon-Rhone-Linie seit dem Oligozän: Spaltspurdaterungen an Apatit/Zirkon and K-Ar-Datierungen an Biotit/Muskowit (westliche Zentralalpen, Bern).

Appendix III: Geochronology
Ar/Ar incremental heating on micas

Rui9958, 125-160 µm, integrated age of all steps: 51,7 ± 0.3 Ma

Step	Temp. °C	³⁹ Ar %	³⁹ Ar total (m)	1 σ (abs.) (m)	⁴⁰ Ar* (m)	³⁹ Ar (m)	1 σ (abs.) (m)	³⁹ Ar (m)	1 σ (abs.) (m)	Cl (m)	³⁷ Ar (m)	1 σ (abs.) (m)	³⁹ Ar (m)	1 σ (abs.) (m)	ClK	Age (Ma)	1 σ (abs.) (Ma)	³⁹ Ar/ ⁴⁰ Ar	1 σ (abs.)	³⁹ Ar/ ⁴⁰ Ar	1 σ (abs.)	
1	481	2.9	6.90E-09 ± 5.80E-13	3.97E-09	2.50E-10 ± 2.70E-13	1.01E-11 ± 2.80E-13	9.18E-12 ± 2.90E-13	6.34E-12 ± 2.90E-13	2.97E-12 ± 5.24E-13	9.93E-12 ± 2.20E-13	0.0046654256 ± 36.01 ± 0.59	3.62E-02 ± 3.62E-02	4.39E-05 ± 4.39E-05	1.44E-03 ± 3.20E-05								
2	551	2.1	4.00E-09 ± 1.10E-12	2.99E-09	1.80E-10 ± 1.80E-13	9.18E-11 ± 9.40E-13	2.88E-11 ± 2.38E-11	2.38E-11 ± 3.63E-12	5.39E-13 ± 5.39E-13	4.04E-12 ± 1.10E-13	0.0152447774 ± 37.20 ± 0.61	4.52E-02 ± 4.52E-02	5.08E-04 ± 1.10E-04	4.10E-05 ± 4.10E-05								
3	613	4.1	7.95E-09 ± 1.50E-11	6.78E-09	3.59E-10 ± 6.30E-13	2.88E-11 ± 9.40E-13	2.88E-11 ± 2.90E-13	2.21E-12 ± 4.30E-12	3.79E-13 ± 3.79E-13	4.55E-12 ± 1.80E-13	0.00564222 ± 44.18 ± 0.11	4.82E-02 ± 4.82E-02	1.95E-04 ± 7.80E-06	8.80E-06 ± 8.80E-06								
4	671	12.8	2.32E-08 ± 1.70E-12	2.18E-08	1.12E-09 ± 10.00E-13	1.87E-11 ± 2.90E-13	1.87E-11 ± 2.90E-13	2.21E-12 ± 3.79E-13	4.15E-13 ± 4.15E-13	2.39E-12 ± 1.30E-13	0.007968983 ± 48.07 ± 0.14	4.48E-02 ± 4.50E-02	1.67E-04 ± 8.80E-06	5.11E-05 ± 5.11E-05								
5	725	7.3	1.43E-08 ± 8.70E-13	1.36E-08	6.39E-10 ± 6.40E-13	1.02E-11 ± 1.80E-13	1.89E-11 ± 1.80E-13	3.74E-12 ± 8.88E-12	2.94E-12 ± 3.49E-13	2.94E-12 ± 1.40E-13	0.000801983 ± 51.11 ± 0.10	4.28E-02 ± 4.28E-02	1.17E-04 ± 5.60E-06	5.61E-05 ± 5.61E-05								
6	838	17.7	3.88E-08 ± 3.10E-12	3.73E-08	1.54E-09 ± 1.40E-12	2.04E-11 ± 1.10E-13	1.86E-12 ± 1.86E-12	1.57E-11 ± 1.92E-13	4.11E-12 ± 1.40E-13	0.000280197 ± 54.61 ± 0.07	4.00E-02 ± 3.80E-05	1.07E-04 ± 3.00E-06	5.62E-05 ± 5.62E-05									
7	910	20.6	4.53E-08 ± 2.50E-12	4.43E-08	1.80E-09 ± 1.70E-12	2.31E-11 ± 1.80E-13	1.39E-12 ± 1.39E-12	5.95E-11 ± 2.87E-13	3.38E-12 ± 1.40E-13	0.0001779958 ± 55.62 ± 0.07	3.98E-02 ± 3.90E-05	7.45E-05 ± 7.45E-05	5.17E-05 ± 5.17E-05									
8	971	15.1	3.09E-08 ± 2.70E-12	3.02E-08	1.32E-09 ± 1.20E-12	1.90E-11 ± 1.80E-13	1.90E-11 ± 2.20E-13	3.02E-12 ± 3.02E-12	2.27E-12 ± 2.17E-13	0.0001277596 ± 57.70 ± 0.08	4.28E-02 ± 3.90E-05	7.80E-05 ± 4.50E-06	5.87E-05 ± 5.87E-05									
9	1050	4.1	9.81E-09 ± 10.00E-13	9.39E-09	3.60E-10 ± 3.60E-13	5.52E-12 ± 1.80E-13	1.03E-12 ± 1.03E-12	5.12E-11 ± 4.50E-13	1.43E-12 ± 1.70E-13	0.0006580811 ± 58.78 ± 0.30	3.67E-02 ± 3.70E-05	1.44E-04 ± 1.70E-05	1.87E-05 ± 1.87E-05									
10	1340	0.9	4.19E-09 ± 8.80E-13	2.93E-09	7.88E-11 ± 1.90E-13	1.29E-12 ± 1.50E-13	-4.27E-13 ± 3.84E-13	4.30E-12 ± 1.50E-13			0 ± 83.33 ± 1.20	1.87E-02 ± 4.50E-05	1.02E-03 ± 3.60E-05									
total (m)			2.103E-07		1.978E-07	8.705E-09	1.612E-10	5.070E-11	2.275E-10	9.155E-05	3.289E-03	4.334E-11	3.197E-02									
K(g)			6.832E-02																			
J=																						
mass=			0.001268 g																			

Rui 9978, 125-160 µm, integrated age of all steps: 260 ± 0.4 Ma

Step	Temp. °C	³⁹ Ar %	³⁹ Ar total (m)	1 σ (abs.) (m)	⁴⁰ Ar* (m)	³⁹ Ar (m)	1 σ (abs.) (m)	³⁹ Ar (m)	1 σ (abs.) (m)	Cl (m)	³⁷ Ar (m)	1 σ (abs.) (m)	³⁹ Ar (m)	1 σ (abs.) (m)	ClK	Age (Ma)	1 σ (abs.) (Ma)	³⁹ Ar/ ⁴⁰ Ar	1 σ (abs.)	³⁹ Ar/ ⁴⁰ Ar	1 σ (abs.)	
1	2.6	1.58E-08 ± 2.10E-12	8.59E-09 ± 1.63E-10	2.80E-13	1.14E-11 ± 2.40E-13	5.22E-12 ± 1.92E-11	5.37E-13	2.27E-11 ± 1.90E-13	0.0073891682 ± 116.88 ± 0.77	1.06E-02 ± 1.80E-05	1.48E-03 ± 1.20E-05											
2	553	4.0	9.17E-09 ± 1.50E-12	8.60E-09 ± 1.44E-10	2.80E-13	4.63E-12 ± 2.50E-13	2.92E-12 ± 1.91E-11	5.47E-13	1.99E-12 ± 2.10E-13	0.0056809822 ± 164.30 ± 1.20	1.28E-02 ± 3.10E-05	2.12E-04 ± 2.30E-05										
3	616	4.0	2.25E-08 ± 8.60E-12	2.11E-08 ± 2.40E-13	9.85E-12 ± 2.00E-13	6.07E-12 ± 5.37E-12	4.12E-13	4.50E-12 ± 1.80E-13	0.005592949 ± 183.92 ± 0.47	1.11E-02 ± 1.20E-05	2.00E-04 ± 7.90E-06											
4	671	7.3	4.74E-08 ± 1.40E-11	4.64E-08 ± 4.60E-10	4.40E-10 ± 4.50E-13	1.12E-11 ± 4.70E-13	5.08E-12 ± 1.83E-12	3.91E-13	3.58E-12 ± 1.50E-13	0.002539472 ± 217.08 ± 0.29	9.70E-03 ± 9.00E-06	7.51E-05 ± 3.20E-06										
5	729	15.3	1.18E-07 ± 2.40E-11	1.17E-07 ± 9.59E-10	9.20E-13 ± 9.20E-13	1.84E-11 ± 2.00E-13	6.44E-12 ± 6.16E-12	3.43E-12 ± 5.76E-13	3.43E-12 ± 5.76E-13	0.001543853 ± 259.62 ± 0.26	8.12E-03 ± 8.00E-06	2.90E-05 ± 1.60E-06										
6	780	18.3	1.48E-07 ± 3.10E-11	1.48E-07 ± 1.15E-09	1.10E-12 ± 1.10E-12	1.70E-11 ± 2.40E-13	2.92E-12 ± 4.62E-12	5.40E-13	2.97E-12 ± 1.70E-13	0.000584819 ± 272.43 ± 0.26	7.73E-03 ± 7.40E-06	2.00E-05 ± 1.20E-06										
7	882	17.1	1.40E-07 ± 1.80E-11	1.08E-09 ± 9.70E-13	1.89E-11 ± 1.60E-13	5.97E-12 ± 4.75E-12	4.75E-12 ± 3.88E-13	3.05E-12 ± 1.20E-13	0.001212435 ± 273.72 ± 0.24	7.69E-03 ± 6.90E-06	2.18E-05 ± 8.30E-07											
8	913	10.1	8.21E-08 ± 9.90E-12	8.16E-08 ± 6.32E-10	5.80E-13	1.01E-11 ± 1.70E-13	2.29E-12 ± 6.87E-13	4.42E-13	1.82E-12 ± 1.40E-13	0.000833021 ± 273.39 ± 0.27	7.70E-03 ± 7.00E-06	2.22E-05 ± 1.80E-06										
9	970	11.7	6.39E-08 ± 5.10E-12	6.37E-08 ± 4.81E-10	5.30E-13	7.38E-12 ± 1.70E-13	1.39E-12 ± 1.60E-13	1.20E-12 ± 2.88E-13	7.93E-13 ± 2.10E-13	0.000741575 ± 279.79 ± 0.38	7.53E-03 ± 8.20E-06	1.24E-05 ± 3.20E-06										
10	1080	14.7	1.02E-07 ± 1.40E-11	1.01E-07 ± 7.37E-10	6.90E-13 ± 6.90E-13	1.38E-11 ± 1.80E-13	4.88E-12 ± 1.80E-13	1.42E-12 ± 2.00E-13	1.42E-12 ± 2.00E-13	0.001459781 ± 289.06 ± 0.29	7.24E-03 ± 6.90E-06	2.45E-05 ± 1.80E-06										
11	1333	4.2	3.72E-08 ± 1.90E-12	3.66E-08 ± 2.64E-10	2.70E-13	4.91E-12 ± 2.10E-13	1.42E-12 ± 2.10E-13	1.42E-12 ± 2.10E-13	8.68E-12 ± 4.89E-13	2.03E-12 ± 1.70E-13	0.0012861783 ± 292.22 ± 0.45	7.10E-03 ± 7.20E-06	5.44E-05 ± 4.40E-06									
total (m)			7.860E-07		6.322E-07	6.269E-09	1.273E-10	4.417E-11	6.510E-11	1.020E-04	1.183E-03	4.925E-11	2.881E-02									
K(g)			6.203E-02																			
J=																						
mass=			0.001268 g																			

Cere0035, 125-160 µm, integrated age of all steps: 93.5 ± 0.6 Ma

Sample	Temp. (°C)	⁴⁰ Ar %	⁴⁰ Ar total (ml)	1 σ (abs.) (ml)	⁴⁰ Ar* (ml)	³⁹ Ar (ml)	1 σ (abs.) (ml)	³⁹ Ar (ml)	1 σ (abs.) (ml)	Cl (ml)	³⁷ Ar (ml)	1 σ (abs.) (ml)	³⁹ Ar (ml)	1 σ (abs.) (ml)	Cl/K	1 σ (abs.) (ml)	Age (Ma)	1 σ (abs.) (Ma)	³⁹ Ar/ ⁴⁰ Ar	1 σ (abs.)	³⁹ Ar/ ⁴⁰ Ar	1 σ (abs.)	
1	500	1.2	6.92E-09 ± 3.10E-11	5.14E-09	7.52E-11 ± 9.80E-13	6.38E-13	± 2.10E-13	-1.38E-12	9.92E-12	± 7.52E-13	6.04E-12	± 1.50E-13	-0.004270227 ±	65.17 ± 1.00	1.09E-02 ± 1.50E-04	8.72E-04 ± 2.20E-05							
2	573	3.3	1.87E-08 ± 6.70E-12	1.73E-08	1.98E-10 ± 2.90E-13	5.67E-12	± 2.00E-13	2.48E-12	4.87E-12	± 7.95E-13	4.71E-12	± 2.00E-13	0.002900713 ±	83.47 ± 0.31	1.05E-02 ± 1.60E-05	2.92E-04 ± 1.10E-05							
3	640	7.7	4.72E-08 ± 2.40E-11	4.21E-08	4.69E-10 ± 5.30E-13	1.03E-11	± 1.80E-13	1.70E-12	-2.02E-12	± 5.70E-13	1.71E-11	± 1.70E-13	0.0009428463 ±	86.31 ± 0.15	9.81E-03 ± 1.20E-05	3.82E-04 ± 3.80E-06							
4	703	13.0	8.17E-08 ± 1.30E-11	7.52E-08	7.87E-10 ± 7.30E-13	1.54E-11	± 1.70E-13	2.02E-12	3.89E-12	± 1.14E-12	2.21E-11	± 2.10E-13	0.0005916703 ±	90.47 ± 0.11	9.63E-03 ± 9.00E-06	2.71E-04 ± 2.80E-06							
5	761	22.7	1.40E-07 ± 8.90E-12	1.36E-07	1.37E-09 ± 1.30E-12	2.11E-11	± 1.70E-13	2.30E-12	-1.39E-12	± 8.93E-13	1.39E-11	± 2.10E-13	0.0003032458 ±	93.35 ± 0.09	9.84E-03 ± 9.00E-06	9.98E-05 ± 1.50E-06							
6	810	16.4	9.73E-08 ± 9.20E-12	9.43E-08	9.94E-10 ± 9.30E-13	1.67E-11	± 2.10E-13	3.04E-12	3.84E-12	± 8.94E-13	1.03E-11	± 2.10E-13	0.000703368 ±	89.86 ± 0.10	1.02E-02 ± 9.60E-06	1.20E-04 ± 2.20E-06							
7	860	19.6	1.08E-07 ± 1.40E-11	1.05E-07	1.18E-09 ± 1.10E-12	1.80E-11	± 1.50E-13	2.30E-12	-1.32E-12	± 1.12E-12	9.88E-12	± 2.00E-13	0.000448412 ±	84.30 ± 0.09	1.09E-02 ± 1.00E-06	9.15E-05 ± 1.80E-06							
8	925	11.1	6.88E-08 ± 5.20E-12	6.51E-08	6.69E-10 ± 6.40E-13	1.03E-11	± 2.30E-13	1.42E-12	8.35E-13	± 1.31E-12	5.53E-12	± 1.80E-13	0.000466839 ±	92.09 ± 0.11	1.00E-02 ± 9.60E-06	8.28E-05 ± 2.70E-06							
9	983	2.9	2.71E-08 ± 3.90E-12	2.61E-08	1.75E-10 ± 2.80E-13	2.53E-12	± 1.70E-13	-1.58E-13	-1.78E-12	± 7.07E-13	3.39E-12	± 1.50E-13	-0.000205421 ±	139.78 ± 0.32	6.43E-03 ± 1.00E-05	1.25E-04 ± 5.60E-06							
10	1111	1.8	2.84E-08 ± 2.40E-12	2.75E-08	1.09E-10 ± 2.40E-13	3.44E-12	± 2.10E-13	1.60E-12	-2.32E-12	± 7.66E-13	2.98E-12	± 1.70E-13	0.0033676376 ±	229.38 ± 0.81	3.85E-03 ± 8.30E-06	1.05E-04 ± 6.00E-06							
11	1366	0.3	4.88E-09 ± 1.40E-12	3.60E-09	1.80E-11 ± 4.40E-14	-2.89E-12	± -1.10E-13	-3.71E-12	-9.04E-12	± -3.99E-14	4.32E-12	± 1.90E-13	-0.0475183912 ±	184.61 ± 2.80	3.69E-03 ± 9.10E-06	8.87E-04 ± 3.80E-05							
Total			6.27E-07	5.97E-07	6.04E-09	1.07E-10		1.16E-11	4.80E-12			1.00E-10	-0.042209058										
K(g)					0.06245			2.78E-05	9.14E-05														
J=	0.00053824																						
Mass=	0.0275																						

Cere0033, 125-160 µm, integrated age of all steps: 69.3 ± 0.8 Ma

Sample	Temp. (°C)	⁴⁰ Ar %	⁴⁰ Ar total (ml)	1 σ (abs.) (ml)	⁴⁰ Ar* (ml)	³⁹ Ar (ml)	1 σ (abs.) (ml)	³⁹ Ar (ml)	1 σ (abs.) (ml)	Cl (ml)	³⁷ Ar (ml)	1 σ (abs.) (ml)	³⁹ Ar (ml)	1 σ (abs.) (ml)	Cl/K	1 σ (abs.) (ml)	Age (Ma)	1 σ (abs.) (Ma)	³⁹ Ar/ ⁴⁰ Ar	1 σ (abs.)	³⁹ Ar/ ⁴⁰ Ar	1 σ (abs.)	
1	576	2.3	1.89E-08 ± 4.30E-11	8.64E-09	1.44E-10 ± 7.10E-13	1.42E-11	± 2.20E-13	7.90E-12	1.67E-11	± 9.38E-13	2.79E-11	± 6.30E-13	0.0116378276 ±	56.57 ± 1.20	8.55E-03 ± 4.30E-05	1.65E-03 ± 3.80E-05							
2	647	4.9	3.45E-08 ± 1.50E-11	2.22E-08	3.09E-10 ± 2.90E-13	1.43E-11	± 3.90E-13	6.09E-12	± 1.00E-12	4.16E-11	± 3.80E-13	0.0021663323 ±	67.84 ± 0.34	8.94E-03 ± 9.20E-06	1.29E-03 ± 1.10E-05								
3	705	11.4	7.10E-08 ± 2.10E-11	5.15E-08	7.12E-10 ± 7.00E-13	2.50E-11	± 9.40E-14	4.30E-12	10.00E-12	± 1.07E-12	6.89E-11	± 3.20E-13	0.0013939847 ±	68.10 ± 0.14	1.00E-02 ± 1.00E-05	9.29E-04 ± 4.60E-06							
4	761	18.7	1.07E-07 ± 4.30E-11	8.58E-08	1.17E-09 ± 1.20E-12	3.08E-11	± 2.20E-13	3.75E-12	2.15E-12	± 1.09E-12	7.09E-11	± 3.00E-13	0.0007359705 ±	68.99 ± 0.10	1.10E-02 ± 1.20E-05	6.84E-04 ± 2.80E-06							
5	809	22.7	1.39E-07 ± 8.60E-12	1.05E-07	1.48E-09 ± 1.30E-12	3.56E-11	± 1.70E-13	3.73E-12	6.18E-12	± 8.55E-13	8.08E-11	± 3.40E-13	0.000602516 ±	69.64 ± 0.09	1.10E-02 ± 1.00E-05	6.29E-04 ± 2.60E-06							
6	858	23.8	1.34E-07 ± 1.80E-11	1.11E-07	1.49E-09 ± 1.40E-12	3.50E-11	± 2.30E-13	2.91E-12	3.72E-12	± 1.27E-12	7.56E-11	± 3.10E-13	0.0004822722 ±	70.49 ± 0.12	1.12E-02 ± 1.00E-05	5.79E-04 ± 2.30E-06							
7	924	12.5	7.50E-08 ± 6.00E-12	5.88E-08	7.81E-10 ± 7.40E-13	2.13E-11	± 2.70E-13	1.64E-12	-3.28E-13	± 1.13E-12	5.89E-11	± 2.80E-13	0.0004822722 ±	69.77 ± 0.09	1.12E-02 ± 1.00E-05	5.79E-04 ± 2.30E-06							
8	981	2.2	2.41E-08 ± 2.70E-12	1.09E-08	1.39E-10 ± 2.20E-13	1.09E-11	± 1.10E-13	9.72E-13	-5.63E-12	± -1.25E-12	4.45E-11	± 2.80E-13	0.001601537 ±	73.51 ± 0.55	5.88E-03 ± 9.10E-06	1.85E-03 ± 1.10E-05							
9	1113	1.2	1.71E-08 ± 2.00E-12	5.97E-09	7.41E-11 ± 1.40E-13	8.07E-12	± 1.60E-13	1.58E-13	-7.47E-12	± -1.58E-12	3.77E-11	± 1.90E-13	0.000488913 ±	75.64 ± 0.69	4.34E-03 ± 6.20E-06	2.20E-03 ± 1.10E-05							
10	1383	0.3	1.18E-08 ± 2.80E-12	1.27E-09	1.65E-11 ± 1.30E-13	6.97E-12	± 1.60E-13	8.52E-14	-1.40E-12	± -7.44E-13	3.98E-11	± 3.00E-13	0.001165748 ±	72.22 ± 4.90	1.40E-03 ± 1.10E-05	3.02E-03 ± 2.50E-05							
total			6.20E-07	4.61E-07	6.27E-09	2.02E-10		2.78E-11	3.00E-11			5.38E-10	0.0207422565										
K(g)					0.05249			5.35E-05	4.62E-04														
J=	0.000531891																						
Mass=	0.0321																						

PT2, 125-160 μm , integrated age of all steps: 60.8 \pm 0.2 Ma

Sample	PT2	Temp. (°C)	³⁹ Ar %	³⁹ Ar total (nmol)	1 σ (abs.) (nmol)	³⁹ Ar* (nmol)	³⁹ Ar (nmol)	1 σ (abs.) (nmol)	³⁹ Ar (nmol)	1 σ (abs.) (nmol)	Cl (nmol)	³⁷ Ar (nmol)	1 σ (abs.) (nmol)	³⁹ Ar (nmol)	1 σ (abs.) (nmol)	CIK	1 σ (abs.) (nmol)	Age (Ma)	1 σ (abs.) (Ma)	³⁹ Ar/ ³⁹ Ar	1 σ (abs.)	³⁹ Ar/ ³⁹ Ar	1 σ (abs.)
1	579	1.3	1.34E-08	± 2.93E-11	9.99E-09	1.90E-10	± 1.70E-13	7.85E-12	± 5.30E-13	3.28E-12	2.22E-11	± 8.44E-13	1.16E-11	± 1.50E-13	0.003858665	± 49.97	± 0.24	1.42E-02	± 3.00E-05	8.64E-04	± 1.10E-05		
2	644	3.2	3.42E-08	± 4.30E-11	2.70E-08	4.63E-10	± 1.10E-12	1.03E-11	± 4.20E-13	4.46E-13	7.05E-12	± 1.19E-12	2.45E-11	± 3.90E-13	0.0002219875	± 55.38	± 0.28	1.35E-02	± 3.60E-05	7.16E-04	± 1.20E-05		
3	640	7.6	7.78E-08	± 2.00E-11	6.82E-08	1.09E-09	± 9.70E-11	1.90E-11	± 4.30E-14	2.72E-13	1.93E-11	± 8.75E-13	3.16E-11	± 4.60E-13	0.0000571987	± 59.14	± 0.13	1.41E-02	± 1.30E-05	4.08E-04	± 6.00E-06		
4	703	11.1	1.22E-07	± 2.95E-11	1.02E-07	1.60E-09	± 1.50E-12	3.29E-11	± 2.40E-13	1.11E-12	1.18E-11	± 8.80E-13	6.93E-11	± 3.10E-13	0.0001588847	± 60.31	± 0.08	1.31E-02	± 1.30E-05	5.66E-04	± 2.80E-06		
5	761	15.2	1.72E-07	± 1.40E-10	1.43E-07	2.19E-09	± 2.60E-12	4.89E-11	± 3.20E-13	3.03E-12	1.05E-12	± 9.42E-13	9.68E-11	± 5.40E-13	0.0003165799	± 61.97	± 0.11	1.28E-02	± 1.90E-05	5.82E-04	± 2.70E-06		
6	806	19.4	2.17E-07	± 1.90E-11	1.80E-07	2.79E-09	± 2.50E-12	5.69E-11	± 3.20E-13	6.07E-12	-2.26E-12	± -1.35E-12	1.08E-10	± 5.40E-13	0.0008012079	± 61.41	± 0.08	1.32E-02	± 1.20E-05	4.99E-04	± 2.80E-06		
7	855	22.0	2.47E-07	± 1.20E-10	2.08E-07	3.16E-09	± 3.20E-12	6.82E-11	± 1.80E-13	5.17E-12	-2.77E-12	± -1.04E-12	1.38E-10	± 5.20E-13	0.0007843545	± 61.82	± 0.08	1.28E-02	± 1.40E-05	5.60E-04	± 2.10E-06		
8	917	11.0	1.24E-07	± 1.70E-11	1.02E-07	1.88E-09	± 1.40E-12	3.79E-11	± 1.90E-13	5.38E-12	9.13E-12	± 1.59E-12	7.45E-11	± 5.50E-13	0.0007843545	± 61.02	± 0.11	1.28E-02	± 1.10E-05	6.03E-04	± 4.40E-06		
9	979	4.4	4.52E-08	± 5.40E-12	4.04E-08	6.28E-10	± 5.80E-13	1.22E-11	± 1.40E-13	1.83E-12	-5.16E-12	± -1.16E-12	1.60E-11	± 1.60E-13	0.0006738034	± 61.20	± 0.09	1.39E-02	± 1.30E-05	3.55E-04	± 3.80E-06		
10	1122	2.4	2.97E-08	± 5.60E-12	2.27E-08	3.45E-10	± 3.20E-13	6.85E-12	± 1.60E-13	7.86E-13	2.81E-12	± 9.65E-12	8.17E-12	± 1.60E-13	0.0005129842	± 62.45	± 0.14	1.37E-02	± 1.30E-05	3.25E-04	± 6.30E-06		
11	1123	1.8	1.95E-08	± 1.90E-11	1.71E-08	2.62E-10	± 4.10E-13	5.34E-12	± 1.80E-13	7.76E-13	-8.33E-13	± -1.06E-12	7.95E-12	± 1.60E-13	0.0008822025	± 62.12	± 0.20	1.34E-02	± 2.40E-05	4.08E-04	± 8.10E-06		
12	1124	0.6	6.75E-09	± 5.70E-12	5.28E-09	9.00E-11	± 5.50E-13	3.86E-12	± 1.4	10.00E-12	1.68E-12	± -5.24E-13	-8.56E-13	± 1.40E-13	0.0042839878	± 55.70	± 0.55	1.39E-02	± 8.20E-05	7.85E-04	± 2.10E-05		
total (nmol)			1.10E-08		9.24E-07	1.44E-08		3.89E-10		2.99E-11	6.69E-11		5.89E-10		0.0125290774								
K(g)						0.06109				2.91E-05	5.18E-04												
Mass=	0.063																						

PT1, 160-500 μm , integrated age of all steps: 61.6 \pm 0.3 Ma

Sample	PT1	Temp. (°C)	³⁹ Ar %	³⁹ Ar total (nmol)	1 σ (abs.) (nmol)	³⁹ Ar* (nmol)	³⁹ Ar (nmol)	1 σ (abs.) (nmol)	³⁹ Ar (nmol)	1 σ (abs.) (nmol)	Cl (nmol)	³⁷ Ar (nmol)	1 σ (abs.) (nmol)	³⁹ Ar (nmol)	1 σ (abs.) (nmol)	CIK	1 σ (abs.) (nmol)	Age (Ma)	1 σ (abs.) (Ma)	³⁹ Ar/ ³⁹ Ar	1 σ (abs.)	³⁹ Ar/ ³⁹ Ar	1 σ (abs.)
1	579	1.2	7.04E-09	± 1.90E-11	4.00E-09	8.10E-11	± 1.90E-13	3.45E-12	± 1.10E-13	5.78E-13	2.31E-11	± 2.63E-12	1.10E-11	± 2.20E-13	0.0016394504	± 46.91	± 0.78	1.15E-02	± 4.10E-05	1.48E-03	± 3.20E-05		
2	644	2.1	1.10E-08	± 1.70E-11	7.52E-09	1.50E-10	± 5.60E-12	± 1.10E-13	1.66E-12	6.42E-12	± 1.20E-23	± 1.82E-12	1.16E-11	± 7.70E-13	0.0026557674	± 47.75	± 0.04	1.36E-02	± 3.90E-01	1.00E-03	± 7.30E-05		
3	640	4.8	2.57E-08	± 2.20E-11	2.12E-08	3.38E-10	± 4.40E-13	8.31E-12	± 3.10E-13	1.53E-12	-2.13E-12	± -2.52E-12	1.51E-11	± 1.70E-13	0.001046308	± 59.74	± 0.17	1.31E-02	± 2.10E-05	5.88E-04	± 6.70E-06		
4	703	33.0	1.81E-07	± 6.40E-11	1.52E-07	2.30E-09	± 2.30E-12	4.85E-11	± 2.10E-13	4.40E-12	1.03E-11	± 1.94E-12	9.82E-11	± 4.00E-13	0.0004935417	± 62.55	± 0.08	1.27E-02	± 1.30E-05	5.32E-04	± 2.20E-06		
5	761	28.4	1.34E-07	± 1.90E-11	1.21E-07	1.84E-09	± 1.70E-12	3.35E-11	± 1.30E-13	3.46E-12	-3.05E-12	± -3.32E-12	2.24E-11	± 2.30E-13	0.0004319995	± 62.22	± 0.07	1.37E-02	± 1.30E-05	3.33E-04	± 2.20E-06		
6	806	12.4	6.34E-08	± 3.20E-12	5.68E-08	8.63E-10	± 7.90E-13	1.54E-11	± 1.40E-13	1.01E-12	-1.07E-11	± -3.07E-12	2.24E-11	± 1.90E-13	0.0002894026	± 62.23	± 0.08	1.36E-02	± 1.30E-05	3.55E-04	± 2.90E-06		
7	855	9.3	4.60E-08	± 3.90E-12	4.19E-08	6.47E-10	± 6.20E-13	1.31E-11	± 3.00E-13	1.10E-12	1.20E-12	± 2.49E-12	1.39E-11	± 2.20E-13	0.0003987991	± 61.24	± 0.10	1.41E-02	± 1.40E-05	3.02E-04	± 4.50E-06		
8	917	3.9	1.92E-08	± 2.80E-12	1.78E-08	2.72E-10	± 2.90E-13	4.07E-12	± 1.80E-13	1.10E-13	-1.10E-13	± -1.99E-12	5.21E-12	± 1.80E-13	-0.000826239	± 61.31	± 0.19	1.42E-02	± 1.50E-05	2.72E-04	± 9.30E-06		
9	979	2.6	1.30E-08	± 3.60E-12	1.20E-08	1.82E-10	± 2.40E-13	3.38E-12	± 1.50E-13	5.55E-13	-7.81E-12	± -2.82E-12	3.66E-12	± 2.10E-13	0.0007006038	± 62.17	± 0.33	1.40E-02	± 1.90E-05	2.80E-04	± 1.60E-05		
10	1122	3.4	1.89E-08	± 3.90E-12	1.51E-08	2.34E-10	± 2.50E-13	3.30E-12	± 1.70E-13	5.40E-13	-1.33E-12	± -3.04E-12	5.70E-12	± 1.70E-13	-0.0005298912	± 61.10	± 0.21	1.39E-02	± 1.50E-05	3.44E-04	± 1.00E-05		
11	1388	0.8	5.32E-09	± 2.90E-12	4.19E-09	5.85E-11	± 1.80E-13	8.17E-13	± 1.70E-13	-5.90E-13	-7.78E-12	± -2.57E-12	3.84E-12	± 2.20E-13	-0.0023223097	± 67.65	± 1.00	1.10E-02	± 3.50E-05	7.22E-04	± 4.00E-05		
total (nmol)			5.23E-07		4.54E-07	6.97E-09		1.39E-10		1.31E-11	1.01E-11		2.33E-10		0.0045280377								
K(g)						0.01483				6.39E-06	3.97E-05												
Mass=	0.126																						

Rdl009, 125-160 μm , integrated age of all steps: $50.1 \pm 0.3 \text{ Ma}$

Sample	Rdl009	Temp. (°C)	$^{40}\text{Ar}/^{39}\text{Ar}$ %	^{40}Ar total (ml)	1σ (abs.) (ml)	^{39}Ar (ml)	^{39}Ar (ml)	1σ (abs.) (ml)	^{39}Ar (ml)	1σ (abs.) (ml)	Cl (ml)	^{37}Ar (ml)	1σ (abs.) (ml)	^{39}Ar (ml)	1σ (abs.) (ml)	ClK	1σ (abs.) (ml)	Age (Ma)	1σ (abs.) (Ma)	$^{39}\text{Ar}/^{37}\text{Ar}$	1σ (abs.)	$^{39}\text{Ar}/^{40}\text{Ar}$	1σ (abs.)	
1	506	0.9	5.55E-09	$\pm 4.20E-12$	$\pm 2.08E-09$	5.68E-11	$\pm 2.40E-13$	$\pm 3.32E-12$	3.80E-14	$\pm 4.62E-13$	2.47E-12	$\pm 7.95E-13$	$\pm 1.17E-11$	$\pm 1.80E-13$	0.001872821	± 35.28	± 0.89	1.02E-02	$\pm 4.40E-05$	2.11E-03	$\pm 3.20E-05$			
2	579	2.9	1.09E-08	$\pm 5.90E-12$	$\pm 7.50E-09$	1.76E-10	$\pm 1.70E-13$	$\pm 1.49E-12$	1.49E-12	$\pm 2.29E-12$	8.26E-12	$\pm 8.26E-13$	$\pm 1.00E-11$	$\pm 1.80E-13$	0.001946465	± 40.96	± 0.30	1.88E-02	$\pm 9.77E-04$	9.57E-04	$\pm 1.80E-05$			
3	640	6.4	2.47E-08	$\pm 3.00E-12$	$\pm 1.76E-08$	3.99E-10	$\pm 3.80E-13$	$\pm 3.00E-12$	2.29E-12	$\pm 1.18E-12$	2.29E-12	$\pm 1.18E-12$	$\pm 2.41E-11$	$\pm 2.30E-13$	0.000689343	± 42.89	± 0.17	1.99E-02	$\pm 1.80E-05$	9.77E-04	$\pm 9.50E-06$			
4	699	11.1	3.79E-08	$\pm 8.60E-12$	$\pm 3.32E-08$	6.82E-10	$\pm 6.60E-13$	$\pm 1.21E-11$	1.06E-12	$\pm 4.26E-12$	-6.82E-13	$\pm 6.82E-13$	$\pm 1.59E-11$	$\pm 2.10E-13$	0.000353919	± 46.58	± 0.10	1.80E-02	$\pm 1.80E-05$	4.20E-04	$\pm 5.60E-06$			
5	761	15.2	5.37E-08	$\pm 2.60E-11$	$\pm 4.99E-08$	9.35E-10	$\pm 9.10E-13$	$\pm 1.06E-13$	1.23E-12	$\pm 3.14E-12$	$\pm 6.56E-13$	$\pm 1.28E-11$	$\pm 2.10E-13$	0.0003013838	± 51.11	± 0.08	1.74E-02	$\pm 1.30E-05$	2.36E-04	$\pm 3.80E-06$				
6	812	14.5	5.49E-08	$\pm 3.80E-12$	$\pm 4.61E-08$	9.87E-10	$\pm 8.10E-13$	$\pm 1.42E-11$	9.45E-13	$\pm 5.85E-13$	$\pm 1.12E-12$	$\pm 7.89E-13$	$\pm 1.70E-13$	0.0002110554	± 50.71	± 0.07	1.80E-02	$\pm 1.70E-05$	1.62E-04	$\pm 4.20E-06$				
7	866	16.0	4.88E-08	$\pm 3.50E-12$	$\pm 4.61E-08$	8.94E-10	$\pm 8.10E-13$	$\pm 1.80E-13$	6.82E-13	$\pm 5.85E-13$	$\pm 7.21E-12$	$\pm 1.11E-12$	$\pm 8.18E-12$	$\pm 2.00E-13$	0.000175354	± 49.41	± 0.08	1.94E-02	$\pm 1.70E-05$	1.68E-04	$\pm 4.20E-06$			
8	921	18.9	6.12E-08	$\pm 2.70E-12$	$\pm 5.33E-08$	1.16E-09	$\pm 10.00E-13$	$\pm 1.88E-11$	1.22E-12	$\pm 2.71E-12$	-7.21E-12	$\pm 1.11E-12$	$\pm 9.93E-12$	$\pm 2.50E-13$	0.000241054	± 47.90	± 0.07	1.90E-02	$\pm 1.70E-05$	1.62E-04	$\pm 4.10E-06$			
9	983	10.6	3.38E-08	$\pm 1.80E-12$	$\pm 3.25E-08$	6.51E-10	$\pm 6.10E-13$	$\pm 9.08E-12$	1.90E-13	$\pm 2.02E-12$	$\pm 1.40E-12$	$\pm 1.40E-12$	$\pm 3.80E-12$	$\pm 2.00E-13$	0.000251533	± 47.83	± 0.10	1.94E-02	$\pm 1.80E-05$	1.13E-04	$\pm 5.80E-06$			
10	1122	3.0	1.89E-08	$\pm 2.20E-12$	$\pm 1.72E-08$	1.86E-10	$\pm 2.50E-13$	$\pm 4.04E-12$	1.17E-12	$\pm 1.28E-12$	$\pm 1.30E-12$	$\pm 1.30E-12$	$\pm 3.67E-12$	$\pm 2.40E-13$	0.001445195	± 87.78	± 0.37	1.02E-02	$\pm 1.40E-05$	2.00E-04	$\pm 1.30E-05$			
11	1382	0.5	7.28E-09	$\pm 2.20E-12$	$\pm 5.23E-09$	3.04E-11	$\pm 1.30E-13$	$\pm 2.31E-12$	6.71E-13	$\pm 4.81E-12$	$\pm 7.89E-13$	$\pm 6.87E-12$	$\pm 1.70E-13$	0.0036810734	± 159.82	± 1.60	4.18E-03	$\pm 1.80E-05$	9.48E-04	$\pm 2.30E-05$				
Total															0.0125824676	$\pm 1.16E-10$								
K(g)															0.04884									
J=	0.00033939														1.97E-05									
Mass	0.0335														-1.06E-05									

Bez0033, 125-160 μm , integrated age of all steps: $54.0 \pm 0.4 \text{ Ma}$

Sample	Bez0033	Temp. (°C)	^{40}Ar %	^{40}Ar total (ml)	1σ (abs.) (ml)	^{39}Ar (ml)	^{39}Ar (ml)	1σ (abs.) (ml)	^{39}Ar (ml)	1σ (abs.) (ml)	Cl (ml)	^{37}Ar (ml)	1σ (abs.) (ml)	^{39}Ar (ml)	1σ (abs.) (ml)	ClK	1σ (abs.) (ml)	Age (Ma)	1σ (abs.) (Ma)	$^{39}\text{Ar}/^{37}\text{Ar}$	1σ (abs.)	$^{39}\text{Ar}/^{40}\text{Ar}$	1σ (abs.)	
1	579	2.8	1.53E-08	$\pm 2.50E-11$	$\pm 5.20E-09$	1.39E-10	$\pm 1.80E-13$	$\pm 1.02E-11$	2.80E-13	$\pm 2.18E-12$	1.33E-11	$\pm 1.25E-12$	$\pm 3.41E-11$	$\pm 6.70E-13$	0.0039215403	± 36.03	± 1.40	9.07E-03	$\pm 1.90E-05$	2.23E-03	$\pm 4.40E-05$			
2	644	5.7	2.79E-08	$\pm 3.40E-13$	$\pm 1.31E-08$	2.87E-10	$\pm 2.60E-13$	$\pm 1.28E-11$	8.22E-11	$\pm 5.40E-14$	-1.06E-12	$\pm 1.18E-12$	$\pm 5.02E-11$	$\pm 2.40E-13$	0.0004432072	± 43.60	± 0.24	1.02E-02	$\pm 9.40E-06$	1.80E-03	$\pm 8.70E-06$			
3	703	13.0	5.85E-08	$\pm 2.70E-11$	$\pm 3.42E-08$	6.55E-10	$\pm 5.90E-13$	$\pm 2.30E-13$	3.50E-12	$\pm 4.92E-13$	$\pm 9.17E-13$	$\pm 8.22E-11$	$\pm 3.30E-13$	0.0012291663	± 49.90	± 0.15	1.13E-02	$\pm 1.10E-05$	1.41E-03	$\pm 5.70E-06$				
4	761	16.3	6.83E-08	$\pm 4.80E-12$	$\pm 4.60E-08$	8.18E-10	$\pm 7.60E-13$	$\pm 2.94E-11$	2.40E-13	$\pm 2.68E-12$	$\pm 2.97E-14$	$\pm 9.41E-13$	$\pm 7.55E-11$	$\pm 3.30E-13$	0.000465972	± 53.73	± 0.12	1.20E-02	$\pm 1.10E-05$	1.1E-03	$\pm 4.80E-06$			
5	865	21.1	8.01E-08	$\pm 5.70E-12$	$\pm 5.98E-08$	1.06E-09	$\pm 9.70E-13$	$\pm 1.20E-13$	4.34E-12	$\pm 4.56E-12$	$\pm 1.12E-12$	$\pm 6.88E-11$	$\pm 2.80E-13$	0.0009381887	± 53.74	± 0.09	1.33E-02	$\pm 1.20E-05$	8.56E-04	$\pm 3.60E-06$				
6	865	17.6	6.63E-08	$\pm 4.80E-12$	$\pm 4.92E-08$	8.34E-10	$\pm 8.20E-13$	$\pm 2.17E-11$	3.07E-12	$\pm 2.88E-12$	$\pm 6.46E-12$	$\pm 8.40E-13$	$\pm 2.60E-13$	0.0007451671	± 53.20	± 0.10	1.31E-02	$\pm 1.20E-05$	8.73E-04	$\pm 3.90E-06$				
7	839	15.4	5.90E-08	$\pm 8.50E-12$	$\pm 4.38E-08$	7.73E-10	$\pm 7.10E-13$	$\pm 1.40E-13$	3.07E-12	$\pm 6.91E-13$	$\pm 1.28E-12$	$\pm 5.12E-11$	$\pm 2.30E-13$	0.0009143267	± 54.18	± 0.10	1.33E-02	$\pm 1.20E-05$	8.68E-04	$\pm 3.90E-06$				
8	991	5.0	3.02E-08	$\pm 3.40E-12$	$\pm 1.79E-08$	2.51E-10	$\pm 3.20E-13$	$\pm 1.70E-13$	1.09E-15	$\pm 3.41E-12$	$\pm 9.03E-13$	$\pm 9.03E-13$	$\pm 4.30E-11$	$\pm 2.60E-13$	0.000009399	± 66.55	± 0.29	8.30E-03	$\pm 1.10E-05$	1.42E-03	$\pm 8.50E-06$			
9	1120	2.5	2.48E-08	$\pm 1.80E-12$	$\pm 1.24E-08$	1.24E-10	$\pm 2.20E-13$	$\pm 9.97E-12$	1.80E-13	$\pm 4.49E-13$	$\pm 1.30E-12$	$\pm 1.30E-12$	$\pm 4.20E-11$	$\pm 2.10E-13$	0.001258805	± 95.00	± 0.49	4.98E-03	$\pm 8.70E-06$	1.69E-03	$\pm 8.40E-06$			
10	1384	0.7	1.90E-08	$\pm 1.30E-12$	$\pm 7.81E-09$	3.51E-11	$\pm 1.80E-13$	$\pm 1.35E-11$	6.04E-12	$\pm 8.69E-13$	$\pm 7.73E-13$	$\pm 3.79E-11$	$\pm 2.60E-13$	0.039573573	± 203.75	± 2.10	1.85E-03	$\pm 9.50E-06$	1.99E-03	$\pm 1.40E-05$				
Total															0.0480715864									
K(g)															1.07E-04									
J=	0.00053763																							
Mass	0.032																							

Vaud003.3, 250-300 μm, integrated age of all steps: 47.0 ± 0.3 Ma

Sample	EKL03	⁴⁰ Ar	⁴⁰ Ar total	1 σ (abs.)	⁴⁰ Ar*	³⁹ Ar	1 σ (abs.)	³⁹ Ar	1 σ (abs.)	Cl	³⁷ Ar	1 σ (abs.)	³⁹ Ar	1 σ (abs.)	Cl/K	1 σ (abs.)	Age (Ma)	1 σ (abs.)	³⁹ Ar/ ⁴⁰ Ar	1 σ (abs.)	³⁹ Ar/ ⁴⁰ Ar	1 σ (abs.)
1	579	1.2	5.04E-09 ± 2.30E-11	3.88E-09	8.38E-11 ± 2.40E-13	7.44E-12	3.70E-13	5.68E-12	1.99E-11 ± 3.02E-12	4.11E-12	± 3.02E-12	1.17E-11	1.80E-13	0.0156274686 ±	43.80 ± 0.64	1.68E-02 ± 8.90E-05	8.15E-04 ± 3.80E-05					
2	644	2.7	1.20E-08 ± 1.40E-11	8.57E-09	1.92E-10 ± 2.90E-13	6.83E-12	1.30E-13	2.40E-12	8.50E-12 ± 2.38E-12	1.77E-11	± 3.30E-13	0.028822499 ±	42.91 ± 0.49	1.58E-02 ± 3.00E-05	9.77E-04 ± 2.70E-05							
3	703	12.8	6.10E-08 ± 1.20E-12	4.30E-08	8.95E-10 ± 1.20E-12	2.53E-11	2.50E-13	3.6E-12	5.58E-12 ± 2.33E-12	5.98E-11	± 2.70E-13	0.000330652 ±	46.48 ± 0.10	1.47E-02 ± 2.00E-05	9.77E-04 ± 4.40E-06							
4	761	49.2	2.08E-07 ± 9.50E-11	1.71E-07	3.45E-09 ± 3.40E-12	6.28E-11	3.30E-13	-2.80E-13	-1.28E-10 ± -2.07E-12	1.19E-10	± 4.70E-13	-0.000196868 ±	47.36 ± 0.06	1.68E-02 ± 1.80E-05	5.78E-04 ± 2.30E-06							
5	806	19.1	7.74E-08 ± 3.40E-11	6.59E-08	1.34E-09 ± 4.40E-13	8.57E-12	2.00E-13	3.7E-12	-2.87E-12 ± -1.66E-12	1.28E-11	± 2.50E-13	0.000491598 ±	46.90 ± 0.07	1.73E-02 ± 1.70E-05	4.78E-04 ± 9.80E-06							
6	855	6.5	2.98E-08 ± 9.90E-13	2.23E-08	4.55E-10 ± 4.40E-13	4.18E-12	3.20E-13	7.08E-14	-1.60E-11 ± -1.91E-12	6.98E-12	± 2.10E-13	0.000681284 ±	47.50 ± 0.25	1.72E-02 ± 2.20E-05	5.02E-04 ± 1.50E-06							
7	917	3.4	1.39E-08 ± 1.30E-12	1.18E-08	2.38E-10 ± 3.70E-13	4.18E-12	1.90E-13	2.37E-13	1.68E-11 ± 1.62E-12	5.11E-12	± 1.80E-13	0.000868325 ±	47.25 ± 0.38	1.67E-02 ± 4.30E-05	6.04E-04 ± 2.20E-05							
8	979	2.0	8.48E-09 ± 1.30E-12	6.98E-09	1.41E-10 ± 3.70E-13	2.85E-12	1.90E-13	2.37E-13	1.68E-11 ± 1.62E-12	5.11E-12	± 1.80E-13	0.000868325 ±	48.35 ± 0.40	1.66E-02 ± 2.50E-05	5.92E-04 ± 2.30E-05							
9	1122	2.1	8.83E-09 ± 2.70E-12	7.39E-09	1.48E-10 ± 2.20E-13	3.53E-12	2.10E-13	8.99E-13	1.67E-12 ± 2.85E-12	4.88E-12	± 2.10E-13	0.001415457 ±	48.76 ± 0.70	1.49E-02 ± 4.10E-05	7.28E-04 ± 3.70E-05							
10	1388	1.1	5.28E-09 ± 1.80E-12	4.10E-09	7.88E-11 ± 2.10E-13	2.16E-12	8.60E-14	4.88E-13	-8.78E-12 ± -1.79E-12	4.01E-12	± 1.30E-13	0.001415451 ±	49.76 ± 0.20	1.49E-02 ± 4.10E-05	7.28E-04 ± 3.70E-05							
total			4.21E-07		3.44E-07	7.02E-09		1.50E-10	1.79E-11	-1.09E-10		2.88E-10	0.0238231333									
K(g)	0.000537931				0.06204				3.62E-05	-1.78E-03												
J=	0.0508																					
Mass=	0.0321																					

Vaud003.2, 125-160 μm, integrated age of all steps: 46.7 ± 0.3 Ma

Sample	EKL02	⁴⁰ Ar	⁴⁰ Ar total	1 σ (abs.)	⁴⁰ Ar*	³⁹ Ar	1 σ (abs.)	³⁹ Ar	1 σ (abs.)	Cl	³⁷ Ar	1 σ (abs.)	³⁹ Ar	1 σ (abs.)	Cl/K	1 σ (abs.)	Age (Ma)	1 σ (abs.)	³⁹ Ar/ ⁴⁰ Ar	1 σ (abs.)	³⁹ Ar/ ⁴⁰ Ar	1 σ (abs.)
1	579	1.2	6.78E-09 ± 2.30E-11	5.09E-09	9.38E-11 ± 4.10E-13	4.77E-12	1.80E-13	2.56E-12	2.22E-12 ± 7.51E-13	5.90E-12	± 4.10E-13	0.0062815459 ±	51.08 ± 1.20	1.38E-02 ± 7.20E-05	8.70E-04 ± 6.00E-05							
2	644	3.0	1.82E-08 ± 1.00E-11	1.08E-08	2.35E-10 ± 5.30E-13	8.79E-12	1.20E-13	1.22E-12	3.19E-13 ± -1.01E-12	2.57E-11	± 2.00E-13	0.0011977528 ±	43.12 ± 0.26	1.29E-02 ± 3.00E-05	1.41E-03 ± 1.10E-05							
3	703	16.2	8.11E-08 ± 10.00E-12	6.23E-08	1.28E-09 ± 1.20E-12	2.93E-11	1.60E-13	2.38E-12	6.26E-12 ± 1.02E-12	6.37E-11	± 3.30E-13	0.0004273845 ±	46.39 ± 0.08	1.58E-02 ± 1.50E-05	7.88E-04 ± 4.00E-06							
4	761	43.0	2.11E-07 ± 2.70E-11	1.67E-07	3.04E-09 ± 3.00E-12	7.14E-11	2.40E-13	1.88E-12	1.48E-10 ± 5.60E-13	0.0002760256 ±	46.94 ± 0.06	1.61E-02 ± 1.40E-05	6.99E-04 ± 3.70E-06									
5	865	17.4	7.94E-08 ± 8.30E-12	6.71E-08	1.37E-09 ± 1.20E-12	2.58E-11	1.60E-13	1.86E-12	3.06E-12 ± 7.55E-13	4.18E-11	± 1.80E-13	0.0003109898 ±	46.57 ± 0.07	1.73E-02 ± 1.80E-05	5.24E-04 ± 2.70E-06							
6	865	7.6	3.47E-08 ± 8.00E-12	2.93E-08	6.03E-10 ± 5.60E-13	1.15E-11	1.50E-13	9.94E-13	2.81E-12 ± 7.94E-13	1.81E-11	± 1.80E-13	0.0003789754 ±	46.30 ± 0.09	1.74E-02 ± 1.70E-05	5.29E-04 ± 5.10E-06							
7	839	4.3	2.00E-08 ± 1.50E-12	1.68E-08	3.43E-10 ± 3.70E-13	6.24E-12	2.10E-13	1.87E-13	5.98E-14 ± 7.55E-13	1.08E-11	± 1.60E-13	0.0001251557 ±	46.62 ± 0.14	1.72E-02 ± 1.80E-05	5.40E-04 ± 8.20E-06							
8	991	3.2	1.52E-08 ± 4.30E-12	1.28E-08	2.58E-10 ± 3.10E-13	4.79E-12	1.50E-13	1.15E-13	5.98E-14 ± 6.92E-13	8.88E-12	± 1.80E-13	0.0001632289 ±	46.72 ± 0.21	1.69E-02 ± 2.20E-05	5.34E-04 ± 1.20E-05							
9	1120	3.3	1.33E-08 ± 2.50E-12	1.28E-08	2.60E-10 ± 3.30E-13	5.08E-12	1.70E-13	4.83E-13	6.11E-13 ± -7.54E-13	8.24E-12	± 2.20E-13	0.0004271937 ±	47.35 ± 0.24	1.69E-02 ± 2.20E-05	5.37E-04 ± 1.40E-05							
10	1384	0.7	4.31E-09 ± 9.30E-14	2.69E-09	5.69E-11 ± 1.70E-13	2.20E-12	2.00E-13	5.08E-13	1.30E-13 ± 1.50E-12	5.49E-12	± 1.70E-13	0.0020644558 ±	45.19 ± 0.86	1.32E-02 ± 3.90E-05	1.27E-03 ± 4.00E-05							
total			4.88E-07		3.87E-07	7.90E-09		1.70E-10	1.44E-11	2.27E-11		3.33E-10	0.0115886781									
K(g)	0.000536026				0.06573				2.75E-05	3.47E-04												
J=	0.0321																					
Mass=	0.0321																					

Trajo05 unpicked

Sample	Traq005	unpick	³⁹ Ar total	1 σ (gbs)	³⁹ Ar*	³⁹ Ar	1 σ (gbs)	Q	³⁷ Ar	1 σ (gbs)	³⁹ Ar	1 σ (gbs)	CKK	1 σ (gbs)	Age (Ma)	1 σ (gbs)	³⁹ Ar/ ³⁹ Ar	1 σ (gbs)	³⁹ Ar/ ³⁹ Ar	1 σ (gbs)
1	560	0.72	1.55E-09 ± 0.0	6.65E-10	2.96E-11 ± 0.0	1.12E-12 ± 0.0	2.19E-13	8.43E-12 ± 3.70E-13	2.98E-12 ± 0.0	0.001703723 ± 0.0014400108 ± 0.0018796627 ± 0.0003938123 ± 0.0003034189 ± 0.000462762 ± 0.0001684245 ± 0.0004390633 ± 0.00010871842 ± 0.004330635 ± 0.0072374895 ± 0.0001	2.163 ± 40.17 ± 37.51 ± 44.68 ± 47.50 ± 43.48 ± 40.74 ± 38.74 ± 39.37 ± 51.99 ± 108.32 ± 10.00	1.50 ± 0.50 ± 0.81 ± 0.68 ± 0.34 ± 0.23 ± 0.21 ± 0.32 ± 0.63 ± 2.00 ± 10.00	0.019 ± 0.022 ± 0.025 ± 0.032 ± 0.035 ± 0.038 ± 0.019 ± 0.036 ± 0.030 ± 0.006 ± 0.001	3.90E-04 ± 0.0019 ± 9.50E-05 ± 6.80E-05 ± 4.5200E-05 ± 4.80E-05 ± 4.00E-05 ± 1.8800E-05 ± 1.4000E-05 ± 2.7800E-05 ± 3.6800E-05 ± 2.90E-05 ± 5.40E-05 ± 0.0028 ± 5.1000E-05	6.8000E-05 ± 6.8000E-05 ± 4.8000E-05 ± 4.5200E-05 ± 2.4700E-05 ± 1.8800E-05 ± 1.4000E-05 ± 2.7800E-05 ± 3.6800E-05 ± 2.90E-05 ± 5.40E-05 ± 0.0028 ± 5.1000E-05					
2	630	3.189	7.66E-08 ± 0.0	5.54E-08	1.32E-09 ± 1.8E-12	3.54E-11 ± 0.0	6.55E-12	5.31E-11 ± 5.24E-12	7.14E-11 ± 0.0	0.0014400108 ± 0.0018796627 ± 0.0003938123 ± 0.0003034189 ± 0.000462762 ± 0.0001684245 ± 0.0004390633 ± 0.00010871842 ± 0.004330635 ± 0.0072374895 ± 0.0001	40.17 ± 37.51 ± 44.68 ± 47.50 ± 43.48 ± 40.74 ± 38.74 ± 39.37 ± 51.99 ± 108.32 ± 10.00	0.50 ± 0.81 ± 0.68 ± 0.34 ± 0.23 ± 0.21 ± 0.32 ± 0.63 ± 2.00 ± 10.00	0.019 ± 0.022 ± 0.025 ± 0.032 ± 0.035 ± 0.038 ± 0.019 ± 0.036 ± 0.030 ± 0.006 ± 0.001	3.90E-04 ± 0.0019 ± 9.50E-05 ± 6.80E-05 ± 4.5200E-05 ± 4.80E-05 ± 4.00E-05 ± 1.8800E-05 ± 1.4000E-05 ± 2.7800E-05 ± 3.6800E-05 ± 2.90E-05 ± 5.40E-05 ± 0.0028 ± 5.1000E-05	6.8000E-05 ± 6.8000E-05 ± 4.8000E-05 ± 4.5200E-05 ± 2.4700E-05 ± 1.8800E-05 ± 1.4000E-05 ± 2.7800E-05 ± 3.6800E-05 ± 2.90E-05 ± 5.40E-05 ± 0.0028 ± 5.1000E-05					
3	700	3.13	1.38E-08 ± 0.0	5.07E-09	1.30E-10 ± 0.0	7.04E-12 ± 0.0	-3.66E-14	8.47E-13 ± 9.72E-13	2.97E-11 ± 0.0	0.0014400108 ± 0.0018796627 ± 0.0003938123 ± 0.0003034189 ± 0.000462762 ± 0.0001684245 ± 0.0004390633 ± 0.00010871842 ± 0.004330635 ± 0.0072374895 ± 0.0001	40.17 ± 37.51 ± 44.68 ± 47.50 ± 43.48 ± 40.74 ± 38.74 ± 39.37 ± 51.99 ± 108.32 ± 10.00	0.50 ± 0.81 ± 0.68 ± 0.34 ± 0.23 ± 0.21 ± 0.32 ± 0.63 ± 2.00 ± 10.00	0.019 ± 0.022 ± 0.025 ± 0.032 ± 0.035 ± 0.038 ± 0.019 ± 0.036 ± 0.030 ± 0.006 ± 0.001	3.90E-04 ± 0.0019 ± 9.50E-05 ± 6.80E-05 ± 4.5200E-05 ± 4.80E-05 ± 4.00E-05 ± 1.8800E-05 ± 1.4000E-05 ± 2.7800E-05 ± 3.6800E-05 ± 2.90E-05 ± 5.40E-05 ± 0.0028 ± 5.1000E-05	6.8000E-05 ± 6.8000E-05 ± 4.8000E-05 ± 4.5200E-05 ± 2.4700E-05 ± 1.8800E-05 ± 1.4000E-05 ± 2.7800E-05 ± 3.6800E-05 ± 2.90E-05 ± 5.40E-05 ± 0.0028 ± 5.1000E-05					
4	760	14.83	4.06E-08 ± 0.0	2.87E-08	6.15E-10 ± 0.0	1.98E-11 ± 0.0	5.02E-12	4.69E-12 ± 9.64E-13	4.03E-11 ± 0.0	0.0014400108 ± 0.0018796627 ± 0.0003938123 ± 0.0003034189 ± 0.000462762 ± 0.0001684245 ± 0.0004390633 ± 0.00010871842 ± 0.004330635 ± 0.0072374895 ± 0.0001	44.68 ± 47.50 ± 43.48 ± 40.74 ± 38.74 ± 39.37 ± 51.99 ± 108.32 ± 10.00	0.68 ± 0.34 ± 0.23 ± 0.21 ± 0.32 ± 0.63 ± 2.00 ± 10.00	0.032 ± 0.035 ± 0.038 ± 0.019 ± 0.036 ± 0.030 ± 0.006 ± 0.001	4.5200E-05 ± 4.80E-05 ± 4.00E-05 ± 1.8800E-05 ± 1.4000E-05 ± 2.7800E-05 ± 3.6800E-05 ± 2.90E-05 ± 5.40E-05 ± 0.0028 ± 5.1000E-05	4.5200E-05 ± 4.80E-05 ± 4.00E-05 ± 1.8800E-05 ± 1.4000E-05 ± 2.7800E-05 ± 3.6800E-05 ± 2.90E-05 ± 5.40E-05 ± 0.0028 ± 5.1000E-05					
5	820	17.19	4.35E-08 ± 0.0	3.54E-08	7.13E-10 ± 0.0	1.47E-11 ± 0.0	1.22E-12	-4.30E-13 ± -5.70E-13	2.75E-11 ± 0.0	0.0003938123 ± 0.0003034189 ± 0.000462762 ± 0.0001684245 ± 0.0004390633 ± 0.00010871842 ± 0.004330635 ± 0.0072374895 ± 0.0001	47.50 ± 43.48 ± 40.74 ± 38.74 ± 39.37 ± 51.99 ± 108.32 ± 10.00	0.34 ± 0.23 ± 0.21 ± 0.32 ± 0.63 ± 2.00 ± 10.00	0.035 ± 0.038 ± 0.019 ± 0.036 ± 0.030 ± 0.006 ± 0.001	4.80E-05 ± 4.00E-05 ± 1.8800E-05 ± 1.4000E-05 ± 2.7800E-05 ± 3.6800E-05 ± 2.90E-05 ± 5.40E-05 ± 0.0028 ± 5.1000E-05	4.80E-05 ± 4.00E-05 ± 1.8800E-05 ± 1.4000E-05 ± 2.7800E-05 ± 3.6800E-05 ± 2.90E-05 ± 5.40E-05 ± 0.0028 ± 5.1000E-05					
6	860	18.52	4.11E-08 ± 0.0	3.49E-08	7.68E-10 ± 0.0	1.40E-11 ± 0.0	1.01E-12	-1.92E-12 ± -7.29E-13	2.09E-11 ± 0.0	0.0003034189 ± 0.000462762 ± 0.0001684245 ± 0.0004390633 ± 0.00010871842 ± 0.004330635 ± 0.0072374895 ± 0.0001	43.48 ± 40.74 ± 38.74 ± 39.37 ± 51.99 ± 108.32 ± 10.00	0.23 ± 0.21 ± 0.32 ± 0.63 ± 2.00 ± 10.00	0.038 ± 0.019 ± 0.036 ± 0.030 ± 0.006 ± 0.001	4.00E-05 ± 1.8800E-05 ± 1.4000E-05 ± 2.7800E-05 ± 3.6800E-05 ± 2.90E-05 ± 5.40E-05 ± 0.0028 ± 5.1000E-05	4.00E-05 ± 1.8800E-05 ± 1.4000E-05 ± 2.7800E-05 ± 3.6800E-05 ± 2.90E-05 ± 5.40E-05 ± 0.0028 ± 5.1000E-05					
7	890	6.40	1.39E-08 ± 0.0	1.13E-08	2.65E-10 ± 0.0	4.74E-12 ± 0.0	-5.34E-14	-1.27E-12 ± -1.14E-12	8.96E-12 ± 0.0	0.0001684245 ± 0.0004390633 ± 0.00010871842 ± 0.004330635 ± 0.0072374895 ± 0.0001	40.74 ± 38.74 ± 39.37 ± 51.99 ± 108.32 ± 10.00	0.21 ± 0.32 ± 0.63 ± 2.00 ± 10.00	0.019 ± 0.036 ± 0.030 ± 0.006 ± 0.001	1.90E-05 ± 0.0008 ± 1.4000E-05 ± 2.7800E-05 ± 3.6800E-05 ± 2.90E-05 ± 5.40E-05 ± 0.0028 ± 5.1000E-05	1.90E-05 ± 0.0008 ± 1.4000E-05 ± 2.7800E-05 ± 3.6800E-05 ± 2.90E-05 ± 5.40E-05 ± 0.0028 ± 5.1000E-05					
8	940	4.18	1.00E-08 ± 0.0	7.07E-09	1.73E-10 ± 0.0	4.09E-12 ± 0.0	1.27E-13	2.10E-12 ± 2.00E-02	1.03E-11 ± 0.0	0.0001684245 ± 0.0004390633 ± 0.00010871842 ± 0.004330635 ± 0.0072374895 ± 0.0001	38.74 ± 39.37 ± 51.99 ± 108.32 ± 10.00	0.32 ± 0.63 ± 2.00 ± 10.00	0.036 ± 0.030 ± 0.006 ± 0.001	3.80E-05 ± 0.0016 ± 2.7800E-05 ± 3.6800E-05 ± 2.90E-05 ± 5.40E-05 ± 0.0028 ± 5.1000E-05	3.80E-05 ± 0.0016 ± 2.7800E-05 ± 3.6800E-05 ± 2.90E-05 ± 5.40E-05 ± 0.0028 ± 5.1000E-05					
9	1000	1.80	5.85E-09 ± 0.0	3.07E-09	7.48E-11 ± 0.0	2.28E-12 ± 0.0	-3.53E-13	3.24E-11 ± 2.10E-02	9.41E-12 ± 0.0	0.00010871842 ± 0.004330635 ± 0.0072374895 ± 0.0001	39.37 ± 51.99 ± 108.32 ± 10.00	0.63 ± 2.00 ± 10.00	0.030 ± 0.006 ± 0.001	4.90E-05 ± 0.0024 ± 3.6800E-05 ± 2.90E-05 ± 5.40E-05 ± 0.0028 ± 5.1000E-05	4.90E-05 ± 0.0024 ± 3.6800E-05 ± 2.90E-05 ± 5.40E-05 ± 0.0028 ± 5.1000E-05					
10	1100	0.70	4.58E-09 ± 0.0	1.57E-09	2.89E-11 ± 0.0	2.78E-12 ± 0.0	5.44E-13	3.41E-11 ± 2.80E-02	1.02E-11 ± 0.0	0.00010871842 ± 0.004330635 ± 0.0072374895 ± 0.0001	51.99 ± 108.32 ± 10.00	2.00 ± 10.00	0.006 ± 0.001	2.90E-05 ± 0.0022 ± 4.6000E-05 ± 3.20E-05 ± 6.00E-05	2.90E-05 ± 0.0022 ± 4.6000E-05 ± 3.20E-05 ± 6.00E-05					
11	1234	0.12	3.41E-09 ± 0.0	5.62E-10	4.88E-12 ± 0.0	1.77E-12 ± 0.0	-1.53E-13	4.38E-12 ± 2.80E-02	9.65E-12 ± 0.0	0.00010871842 ± 0.004330635 ± 0.0072374895 ± 0.0001	108.32 ± 10.00	10.00	0.001 ± 0.0028 ± 5.1000E-05	5.40E-05 ± 0.0028 ± 5.1000E-05	5.40E-05 ± 0.0028 ± 5.1000E-05					
total			2.55E-07	1.84E-07	4.12E-09	1.08E-10	1.41E-11	1.28E-10	0.000000002	0.001485463										
K(g)	0.000537																			
±	0.0399																			

Trajo05 picked

Sample	Traq005	picked	³⁹ Ar total	1 σ (gbs)	³⁹ Ar*	³⁹ Ar	1 σ (gbs)	Q	³⁷ Ar	1 σ (gbs)	³⁹ Ar	1 σ (gbs)	CKK	1 σ (gbs)	Age (Ma)	1 σ (gbs)	³⁹ Ar/ ³⁹ Ar	1 σ (gbs)	³⁹ Ar/ ³⁹ Ar	1 σ (gbs)
1	575	0.838916	5.99E-10 ± 1.80E-11	1.59E-09	5.16E-11 ± 3.90E-13	-3.20E-11 ± -5.00E-13	3.19E-11	7.65E-12 ± 7.75E-13	-3.35E-12 ± -1.10E-13	-0.142279894 ± 0.0018722475 ± 0.000638019 ± 0.0005958985 ± 0.0003947109 ± 0.0003379633 ± 0.0004123107 ± 0.0004639728 ± 0.0004634093 ± 0.0128226419 ± 0.000537278	29.51 ± 39.56 ± 43.80 ± 48.51 ± 48.30 ± 47.53 ± 44.17 ± 40.09 ± 39.05 ± 37.70 ± 39.38 ± 32.14 ± 10.00	1.10 ± 0.22 ± 0.10 ± 0.07 ± 0.12 ± 0.12 ± 0.12 ± 0.13 ± 0.30 ± 0.43 ± 2.50 ± 10.00	8.62E-02 ± 2.70E-03 ± 3.60E-05 ± 7.86E-04 ± 1.40E-05 ± 1.79E-02 ± 1.50E-05 ± 6.22E-04 ± 1.50E-06 ± 1.61E-02 ± 1.80E-05 ± 6.02E-04 ± 1.70E-02 ± 1.80E-05 ± 5.21E-04 ± 6.50E-06 ± 1.87E-02 ± 1.80E-05 ± 4.71E-04 ± 7.80E-06 ± 2.20E-02 ± 2.20E-05 ± 5.49E-04 ± 8.40E-06 ± 1.97E-02 ± 2.30E-05 ± 6.75E-04 ± 2.10E-05 ± 1.60E-02 ± 3.20E-05 ± 1.26E-03 ± 2.40E-05 ± 8.27E-03 ± 3.20E-05 ± 3.20E-03 ± 6.00E-05	8.62E-02 ± 2.70E-03 ± 3.60E-05 ± 7.86E-04 ± 1.40E-05 ± 1.79E-02 ± 1.50E-05 ± 6.22E-04 ± 1.50E-06 ± 1.61E-02 ± 1.80E-05 ± 6.02E-04 ± 1.70E-02 ± 1.80E-05 ± 5.21E-04 ± 6.50E-06 ± 1.87E-02 ± 1.80E-05 ± 4.71E-04 ± 7.80E-06 ± 2.20E-02 ± 2.20E-05 ± 5.49E-04 ± 8.40E-06 ± 1.97E-02 ± 2.30E-05 ± 6.75E-04 ± 2.10E-05 ± 1.60E-02 ± 3.20E-05 ± 1.26E-03 ± 2.40E-05 ± 8.27E-03 ± 3.20E-05 ± 3.20E-03 ± 6.00E-05						
2	646	7.03751	2.04E-08 ± 3.10E-11	1.60E-08	3.87E-10 ± 4.60E-13	1.05E-11 ± 3.30E-13	3.15E-12	1.48E-11 ± 1.01E-12	1.50E-11 ± 2.80E-13	0.0018722475 ± 0.000638019 ± 0.0005958985 ± 0.0003947109 ± 0.0003379633 ± 0.0004123107 ± 0.0004639728 ± 0.0004634093 ± 0.0128226419 ± 0.000537278	39.56 ± 43.80 ± 48.51 ± 48.30 ± 47.53 ± 44.17 ± 40.09 ± 39.05 ± 37.70 ± 39.38 ± 32.14 ± 10.00	0.22 ± 0.10 ± 0.07 ± 0.12 ± 0.12 ± 0.12 ± 0.13 ± 0.30 ± 0.43 ± 2.50 ± 10.00	2.70E-03 ± 3.60E-05 ± 7.86E-04 ± 1.40E-05 ± 1.79E-02 ± 1.50E-05 ± 6.22E-04 ± 1.50E-06 ± 1.61E-02 ± 1.80E-05 ± 6.02E-04 ± 1.70E-02 ± 1.80E-05 ± 5.21E-04 ± 6.50E-06 ± 1.87E-02 ± 1.80E-05 ± 4.71E-04 ± 7.80E-06 ± 2.20E-02 ± 2.20E-05 ± 5.49E-04 ± 8.40E-06 ± 1.97E-02 ± 2.30E-05 ± 6.75E-04 ± 2.10E-05 ± 1.60E-02 ± 3.20E-05 ± 1.26E-03 ± 2.40E-05 ± 8.27E-03 ± 3.20E-05 ± 3.20E-03 ± 6.00E-05	2.70E-03 ± 3.60E-05 ± 7.86E-04 ± 1.40E-05 ± 1.79E-02 ± 1.50E-05 ± 6.22E-04 ± 1.50E-06 ± 1.61E-02 ± 1.80E-05 ± 6.02E-04 ± 1.70E-02 ± 1.80E-05 ± 5.21E-04 ± 6.50E-06 ± 1.87E-02 ± 1.80E-05 ± 4.71E-04 ± 7.80E-06 ± 2.20E-02 ± 2.20E-05 ± 5.49E-04 ± 8.40E-06 ± 1.97E-02 ± 2.30E-05 ± 6.75E-04 ± 2.10E-05 ± 1.60E-02 ± 3.20E-05 ± 1.26E-03 ± 2.40E-05 ± 8.27E-03 ± 3.20E-05 ± 3.20E-03 ± 6.00E-05						
3	707	15.9986	4.93E-08 ± 5.90E-11	4.02E-08	8.80E-10 ± 1.30E-12	1.73E-11 ± 3.90E-14	3.04E-12	8.07E-12 ± 1.28E-12	3.06E-11 ± 1.70E-13	0.000638019 ± 0.0005958985 ± 0.0003947109 ± 0.0003379633 ± 0.0004123107 ± 0.0004639728 ± 0.0004634093 ± 0.0128226419 ± 0.000537278	43.80 ± 46.98 ± 48.51 ± 48.30 ± 47.53 ± 44.17 ± 40.09 ± 39.05 ± 37.70 ± 39.38 ± 32.14 ± 10.00	0.10 ± 0.07 ± 0.12 ± 0.12 ± 0.12 ± 0.12 ± 0.13 ± 0.30 ± 0.43 ± 2.50 ± 10.00	3.50E-05 ± 6.22E-04 ± 1.50E-06 ± 1.61E-02 ± 1.80E-05 ± 6.02E-04 ± 1.70E-02 ± 1.80E-05 ± 5.21E-04 ± 6.50E-06 ± 1.87E-02 ± 1.80E-05 ± 4.71E-04 ± 7.80E-06 ± 2.20E-02 ± 2.20E-05 ± 5.49E-04 ± 8.40E-06 ± 1.97E-02 ± 2.30E-05 ± 6.75E-04 ± 2.10E-05 ± 1.60E-02 ± 3.20E-05 ± 1.26E-03 ± 2.40E-05 ± 8.27E-03 ± 3.20E-05 ± 3.20E-03 ± 6.00E-05	3.50E-05 ± 6.22E-04 ± 1.50E-06 ± 1.61E-02 ± 1.80E-05 ± 6.02E-04 ± 1.70E-02 ± 1.80E-05 ± 5.21E-04 ± 6.50E-06 ± 1.87E-02 ± 1.80E-05 ± 4.71E-04 ± 7.80E-06 ± 2.20E-02 ± 2.20E-05 ± 5.49E-04 ± 8.40E-06 ± 1.97E-02 ± 2.30E-05 ± 6.75E-04 ± 2.10E-05 ± 1.60E-02 ± 3.20E-05 ± 1.26E-03 ± 2.40E-05 ± 8.27E-03 ± 3.20E-05 ± 3.20E-03 ± 6.00E-05						
4	760	19.1633	6.46E-08 ± 6.60E-12	5.17E-08	1.05E-09 ± 9.60E-13	2.38E-11 ± 2.30E-13	3.04E-12	4.44E-12 ± 1.00E-12	4.34E-11 ± 2.30E-13	0.000638019 ± 0.0005958985 ± 0.0003947109 ± 0.0003379633 ± 0.0004123107 ± 0.0004639728 ± 0.0004634093 ± 0.0128226419 ± 0.000537278	46.98 ± 48.51 ± 48.30 ± 47.53 ± 44.17 ± 40.09 ± 39.05 ± 37.70 ± 39.38 ± 32.14 ± 10.00	0.07 ± 0.12 ± 0.12 ± 0.12 ± 0.12 ± 0.12 ± 0.13 ± 0.30 ± 0.43 ± 2.50 ± 10.00	1.50E-05 ± 6.22E-04 ± 1.50E-06 ± 1.61E-02 ± 1.80E-05 ± 6.02E-04 ± 1.70E-02 ± 1.80E-05 ± 5.21E-04 ± 6.50E-06 ± 1.87E-02 ± 1.80E-05 ± 4.71E-04 ± 7.80E-06 ± 2.20E-02 ± 2.20E-05 ± 5.49E-04 ± 8.40E-06 ± 1.97E-02 ± 2.30E-05 ± 6.75E-04 ± 2.10E-05 ± 1.60E-02 ± 3.20E-05 ± 1.26E-03 ± 2.40E-05 ± 8.27E-03 ± 3.20E-05 ± 3.20E-03 ± 6.00							

Danksagung

Zum Gelingen dieser Arbeit haben die verschiedensten Leute beigetragen. Stefan Schmid, der diese Arbeit initiiert und betreut hat half durch seine Ideen und Kenntnisse einen roten Faden durch das Thema zu legen. Dabei waren die vielen gemeinsamen Feldbegehungen besonders fruchtbar. Für die gute Zusammenarbeit und die aktive Unterstützung möchte ich ihm ganz besonders danken. Von Romain Bousquet habe ich in zahlreichen Diskussionen und auf gemeinsamen Feldbegehungen u.a. das nötige Rüstzeug für die Petrologie gelernt, wofür ich mich bei ihm vielmals bedanken möchte.

Besonders bedanken möchte ich mich auch bei Igor Villa, der mir die Grundlagen der Isotopengeologie beigebracht hat, was einen grossen Teil dieser Arbeit überhaupt erst ermöglichte. Zudem haben seine brillanten Kommentare die Wissenschaft von unerwarteten Seiten beleuchtet. Vielmals bedanken möchte ich mich auch bei Ilka Kleinhanns. Nicht zuletzt war es die perfekte Teamarbeit bezüglich der Lu-Hf Datierungen, die zu einem erfolgreichen Abschluss des Projektes beigetragen hat.

Ein grosses Dankeschön gebührt Bernhard Fügenschuh, der mir die Grundlagen der Feldgeologie beigebracht und damit und in vielen konstruktiven Diskussionen einen wesentlich Teil zum Gelingen der vorliegenden Arbeit beigetragen hat.

Ganz herzlich bedanken möchte ich mich auch bei Stefano Ceriani, nicht zuletzt für die vielen semi- und nicht-geologischen Diskussionen, die auch geologische Früchte getragen haben.

Besonders bedanken möchte ich mich auch bei der ganzen Isotopengeologie-Crew von Bern, bei der ich mich – nicht nur als Geologe – sehr wohl gefühlt habe.

Auch ein grosses Dankeschön an alle vom Westalpen-Team (Ghislain Trullenque, Christina Ulardic, Andrea Loprieno)

Weiterer Dank geht an alle, die mir bei den technischen Analysen und Problemen zur Seite standen: Willem Stern, Heinz Hürlimann und Ralf Milke vom geochemischen Labor Basel, die ganze Mikrosonden-Crew, besonders Christian De Capitani, dessen Erklärungen sich selten auf das Technische beschränkten, was meine Kenntnisse in Petrologie sehr bereicherte. Diskussionen mit Rainer Abart haben diese noch zusätzlich vertieft. Auch bei Willi Tschudin möchte ich mich bedanken für die schnelle Ausführung der Dünnschliffpräparationen. Hans Ruedi Rüegg sei gedankt für die technische Hilfe, auch für die nicht geologische. Joëlle Glanzmann möchte ich für ihre Hilfe danken.

Zudem möchte ich meine Kollegen erwähnen, die bei Diskussionen immer wieder neue Ideen beitrugen und meine Manuskripte korrigierten (Lukas Keller, Michael Stipp, Thorsten Nagel, Katy Waite). Schliesslich möchte ich mich bei allen Bernoullianer bedanken, deren freundschaftliche Hilfe ich in den letzten Jahren in Anspruch nehmen durfte.

Besonders erwähnen möchte ich auch all jene Personen, die für mein Wohl im Aosta Tal gesorgt haben: Die ganze Crew vom Rif. Bezzi, allen von der Bar du Lac, von der Albergo Frassi, dem Hotel Perret, dem Rif. L'Epée, dem Rif. Deffayes und dem Rif. Benevolo.

Ohne einen ruhigen Gegenpol wären die verschiedenen Hochs und Tiefs der Doktorarbeit wohl kaum zu ertragen gewesen. Meiner Freundin Ricarda Gerosa möchte ich für die viele Geduld, die sie aufbrachte, und die gemeinsam verbrachte Zeit herzlich danken. Für ihre Unterstützung und ihr Interesse spreche ich meinen Eltern einen ganz besonderen Dank aus.

CURRICULUM VITAE

Name: **Stefan Bucher**

Geburtstag: 3. Februar 1972

Geburtsort: Zürich

Nationalität: Schweiz

Seit 1999

Dissertation in Geologie

Institut: Geologisch-Paläontologisches Institut

Ort: Universität Basel, Schweiz

Dissertation: **“The Briançonnais units along the ECORS-CROP transect (Italian-French Alps): structures, metamorphism and geochronology**

1995 – 1999

Hauptstudium Geologie/Paläontologie

Abschluss: Diplom in Erdwissenschaften

Institut: Geologisch-Paläontologisches Institut

Ort: Universität Basel, Schweiz

Spezialisierung: Strukturgeologie, Tektonik, Sedimentologie

Diplomarbeit: „Strukturgeologische und petrographische Untersuchungen am kleinen St. Bernard Pass (Aostatal/Savoien)“ (1999): 73pp.

Kartierung: Geologische Kartierung der Unité du Pt. S. Bernard und der Unité du Versoyen, kleiner St. Bernard Pass, Aostatal, Italien

1992 – 1995

Grundstudium Geologie/Paläontologie

Universität: Eidgenössisch-Technische Hochschule (ETH) Zürich

Ort: Zürich, Schweiz

1987 – 1991

Kantonale Mittelschule Zürich Enge

1985 – 1987

Sekundarschule in Richterswil

1979 – 1985

Primarschule in Richterswil